Volume 72 • Issue 3 • July-September 2023

ISSN : 0003-2778

Scopus
Indexed

JOURNAL OF THE ANATOMICAL SOCIETY OF INDIA

An International Journal

An Official Publication of Anatomical Society of India

Full text online at **https://journals.lww.com/joai**
Submit articles online at **https://review.jow.medknow.com/jasi**

Editor-in-Chief
Dr. Vishram Singh

Wolters Kluwer

Medknow

Journal of the Anatomical Society of India

Print ISSN: 0003-2778

GENERAL INFORMATION

About the Journal

Journal of the Anatomical Society of India (ISSN: Print 0003-2778) is peer-reviewed journal. The journal is owned and run by Anatomical Society of India. The journal publishes research articles related to all aspects of Anatomy and allied medical/surgical sciences. Pre-Publication Peer Review and Post-Publication Peer Review Online Manuscript Submission System Selection of articles on the basis of MRS system Eminent academicians across the globe as the Editorial board members Electronic Table of Contents alerts Available in both online and print form. The journal is published quarterly in the months of January, April, July and October.

Scope of the Journal

The aim of the *Journal of the Anatomical Society of India* is to enhance and upgrade the research work in the field of anatomy and allied clinical subjects. It provides an integrative forum for anatomists across the globe to exchange their knowledge and views. It also helps to promote communication among fellow academicians and researchers worldwide. The Journal is devoted to publish recent original research work and recent advances in the field of Anatomical Sciences and allied clinical subjects. It provides an opportunity to academicians to disseminate their knowledge that is directly relevant to all domains of health sciences.

The Editorial Board comprises of academicians across the globe.

JASI is indexed in Scopus, available in Science Direct.

Abstracting and Indexing Information

The journal is registered with the following abstracting partners:

Baidu Scholar, CNKI (China National Knowledge Infrastructure), EBSCO Publishing's Electronic Databases, Ex Libris – Primo Central, Google Scholar, Hinari, Infotrieve, Netherlands ISSN center, ProQuest, TdNet, Wanfang Data

The journal is indexed with, or included in, the following:

SCOPUS, Science Citation Index Expanded, IndMed, MedInd, Scimago Journal Ranking, Emerging Sources Citation Index.

Impact Factor® as reported in the 2022 Journal Citation Reports® (Clarivate Analytics, 2023): 0.4

Information for Authors

Article processing and publication charges will be communicated by the editorial office. All manuscripts must be submitted online at https://review.jow.medknow.com/jasi.

Subscription Information

A subscription to JASI comprises 4 issues. Prices include postage. Annual Subscription Rate for non-members-

Rates of Membership (with effect from 1.1.2022)		
	India	**International**
Ordinary membership	INR 1500	US $ 100
Couple membership	INR 2250	
Life membership	INR 8000	US $ 900
Subscription Rates (till 31st August)		
Individual	INR 6000	US $ 650
Library/Institutional Trade discount of 10% for agencies only	INR 12000	US $ 1000
Subscription Rates (after 31st August)		
Individual	INR 6500	US $ 700
Library/Institutional	INR 12500	US $ 1050

The Journal of Anatomical Society of India (ISSN: 0003-2778) is published quarterly **Subscriptions** are accepted on a prepaid basis only and are entered on a calendar year basis. Issues are sent by standard mail Priority rates are available upon request.

Information to Members/Subscribers

All members and existing subscribers of the Anatomical Society of India are requested to send their membership/existing subscription fee for the current year to the Treasurer of the Society on the following address: Prof (Dr.) Punit Manik, Treasurer, ASI, Department of Anatomy, KGMU, Lucknow - 226003. Email: punitamanik@yahoo.co.in. All payments should be made through an account payee bank draft drawn in favor of the **Treasurer, Anatomical Society of India,** payable at **Lucknow** only, preferably for **Allahabad Bank, Medical College Branch, Lucknow.** Outstation cheques/drafts must include INR 70 extra as bank collection charges.

All complaints regarding non-receipt of journal issues should be addressed to the Editor-in-Chief, JASI at editorjasi@gmail.com. The new subscribers may, please contact wkhlrpmedknow_subscriptions@wolterskluwer.com.

Requests of any general information like travel concession forms, venue of next annual conference, etc. should be addressed to the General Secretary of the Anatomical Society of India.

For mode of payment and other details, please visit www.medknow.com/subscribe.asp

Claims for missing issues will be serviced at no charge if received within 60 days of the cover date for domestic subscribers, and 3 months for subscribers outside India. Duplicate copies cannot be sent to replace issues not delivered because of failure to notify publisher of change of address. The journal is published and distributed by Wolters Kluwer India Pvt. Ltd. Copies are sent to subscribers directly from the publisher's address. It is illegal to acquire copies from any other source. If a copy is received for personal use as a member of the association/society, one cannot resale or give-away the copy for commercial or library use.

The copies of the journal to the subscribers are sent by ordinary post. The editorial board, association or publisher will not be responsible for non receipt of copies. If any subscriber wishes to receive the copies by registered post or courier, kindly contact the publisher's office. If a copy returns due to incomplete, incorrect or changed address of a subscriber on two consecutive occasions, the names of such subscribers will be deleted from the mailing list of the journal. Providing complete, correct and up-to-date address is the responsibility of the subscriber.

Nonmembers: Please send change of address information to subscriptions@medknow.com.

Advertising Policies

The journal accepts display and classified advertising. Frequency discounts and special positions are available. Inquiries about advertising should be sent to Wolters Kluwer India Pvt. Ltd, advertise@medknow. com.

The journal reserves the right to reject any advertisement considered unsuitable according to the set policies of the journal.

The appearance of advertising or product information in the various sections in the journal does not constitute an endorsement or approval by the journal and/or its publisher of the quality or value of the said product or of claims made for it by its manufacturer.

Addresses

Editorial Office

Dr. Vishram Singh, Editor-in-Chief, JASI
B5/3 Hahnemann Enclave, Plot No. 40, Sector 6, Dwarka Phase – 2,
New Delhi - 110 075, India.
Email: editorjasi@gmail.com

Published by

Wolters Kluwer India Pvt. Ltd
A-202, 2nd Floor, The Qube,
C.T.S. No.1498A/2 Village Marol, Andheri (East),
Mumbai - 400 059, India.
Phone: 91-22-66491818
Website: www.medknow.com

Printed at

Nikeda Art Printers Pvt. Ltd.,
Building No. C/3 - 14,15,16, Shree Balaji Complex, Vehele Road,
Village Bhatale, Taluka Bhiwandi, District Thane - 421302, India.

Journal of the Anatomical Society of India

Print ISSN: 0003-2778

EDITORIAL BOARD

Journal of the Anatomical Society of India

Volume 72 | Issue 3 | July-September 2023

CONTENTS

continued...

CASE REPORTS

Parkinson's Disease Revisited

Parkinson's disease (PD) is a brain disorder that causes unintended/uncontrollable movements such as shaking/tremors, stiffness, and difficulty in balance and coordination. It was named so by an eminent neurologist, Dr. Jean-Martin Charcot, in 1817 after the name of a London Doctor, James Parkinson after his death, who had published a detailed essay on Shaking Palsy. Although James Parkinson himself had suggested the name "*paralysis agitans,"* it was "PD" that struck, as given by Charcot.

PD is responsible for parkinsonism in about 85% of the cases; hence, it is also called "primary *parkinsonism.*" Parkinsonism is an umbrella term used for all neurological disorders that produce signs and symptoms more or less similar to PD.[1]

PD is the most common neurological disorder, second only to Alzheimer's disease. It is a chronic progressive disease that causes major disability and untimely death. PD is not as fatal as the condition itself; however, the complications that arise from it, namely, infection (pneumonia) and falls (fractures), can be fatal.

It affects about 1.2 million Americans yearly in the U.S. and rising both in incidence and prevalence. It affects more males than females above the age of 65 years.

Etiology

It is well-known that PD occurs due to neurodegeneration of pigmented dopaminergic nerve cells of the pars compacta of the substantia nigra of the midbrain – the site of maximus production of dopamine in the brain.[2]

This, in turn, leads to a deficiency of dopamine in the corpus striatum, a cluster of nuclei, namely, the caudate nucleus, putamen, and globus pallidus, which form part of the *basal nuclei of the cerebral cortex*.[3]

As we all know, dopamine is a neurotransmitter that transmits messages between nerves, which not only control muscle movements but are also involved in the pleasure and reward centers of the brain. The decreased level of dopamine in the corpus striatum leads to various signs and symptoms of PD.

There is no definitive cause of PD known so far; hence, it is also called "*idiopathic parkinsonism*." However, some factors are linked to it as under:

Age

As we age, it is normal for nerve cells of the substantia nigra to die, but normally it happens at a very slow rate; however, in some people, it occurs at a faster rate, and once 50%–60% of nerve cells die, the symptoms of PD begin, which progress with age. PD usually affects people above 65 years of age.

Genetic factors

These are either autosomal dominant or autosomal recessive. Individuals with a parent or sibling, who is affected with PD, have more chances to suffer from it. About 10%–20% of PD cases are linked to genetic causes.

Environmental factors

These include exposure to pesticides, heavy metals, and detergents.

Head trauma

Repeated head trauma may also be a cause of PD; for example, the world-famous boxer, Mr. Mohammed Ali, suffered from PD.

Gender

Men are more likely to suffer from PD than women.

Clinical Presentation

The PD presents the following MAIN signs and symptoms:[4]

- *Resting tremors* | Shaking of hands; often associated with pill-rolling movements of the opposed thumb and index fingertip
- *Lead pipe or cog wheel type of muscular rigidity* associated with stiff scuffling gait and *stooped posture*
- *Bradykinesia* leading to a general slowing down of movements and absence of associated movements like arm-swinging during walking and difficulty in getting up from the chair
- *Postural instability and fall* due to loss of balance.

Additional symptoms: these may include:

- Depression, dissatisfaction, and anxiety
- Insomnia (sleeping problems)
- Erectile dysfunction
- Hyperhidrosis (excessive sweating)
- Dysphagia (difficulty in swallowing)
- Excessive drooling of saliva
- Urinary incontinence
- Dementia
- Cognitive amnesia.

Investigations

There are no laboratories or imaging tests for a definitive diagnosis of PD. However, earlier DaTscan, single-photon emission computed tomography, and magnetic resonance imaging of the brain were done to rule out the diseases that mimic PDs such as corticobasal syndrome, Lewy bodies, essential tremor, multiple system atrophy, and arteriosclerotic parkinsonism.

Recently, a new laboratory test analyzing the brain and spinal cord cerebrospinal fluid for clumps of protein called alpha-synuclein can accurately detect PD.

Diagnosis

PD is usually diagnosed based on medical history, performing medical examination and investigation.

Treatment

Currently, there is no cure for PD; however, treatments are available to relieve the symptoms and maintain the quality of life to a certain extent.[5]

Drug therapy

There are many drugs given to relieve the symptoms of PD; however, the following drugs are most commonly given.

Levodopa

It is most effective as it is a natural chemical, which passes into neurons, where it is converted into dopamine. Levodopa is usually given in combination with carbidopa to prevent nausea that levodopa may cause.

Dopamine agonists

They do not change into dopamine. Instead, they mimic dopamine effects in the brain.

Monoamine oxidase-B inhibitors

They help prevent the breakdown of dopamine.

Surgical Treatment, i.e., Deep brain stimulation

In this, the surgeon implants a pulse generator in the chest wall akin to a heart pacemaker to stimulate the part of the brain affected by PD. The DBS is considered in patients who are levodopa responsive; however, their levodopa-related motor complications are not managed adequately.

Stem cell therapy

In this, the stem cells are administered in the body through an intravenous route. These cells reach the areas of inflammation and damage in the brain through a process called *homing*.

Gene therapy

It consists of the creation of new gene-coded cells that produce specific neurotransmitters, namely, dopamine; so far, it is under trial.

In addition to the above treatment, some supportive therapies are given to help patients.

These include:
- Physiotherapy
- Occupation therapy
- Speech therapy
- Psychotherapy
- Speech therapy.

Finally, since the cause of PD is unknown, there are no proven ways to prevent the disease. However, some research has shown that changing lifestyle and doing aerobic exercise might reduce the risk of PD.

Vishram Singh, Rashi Singh[1], Gaurav Singh[2]

Department of Anatomy, Kasturba Medical College, Mangalore, Manipal Academy of Higher Education, Manipal, Karnataka, [1]Department of Pediatric and Preventive Dentistry, Santosh Dental College and Hospital, Ghaziabad, [2]Clinical Editor, British Medical Journal (BMJ), Noida, NCR Delhi, India

Address for correspondence: *Prof. Vishram Singh, B5/3 Hahnemann Enclave, Plot No. 40, Sector 6, Dwarka Phase – 2, New Delhi - 110 075, India.*
E-mail: drvishramsingh@gmail.com

References

1. Goetz CG. The history of Parkinson's disease: Early clinical descriptions and neurological therapies. Cold Spring Harb Perspect Med 2011;1:a008862.
2. Trist BG, Hare DJ, Double KL. Oxidative stress in the aging substantia nigra and the etiology of Parkinson's disease. Aging Cell 2019;18:e13031.
3. Singh V. Textbook of Clinical Neuroanatomy. 4th ed. New Delhi: Elsevier; 2020. p. 162-3.
4. Bloem BR, Okun MS, Klein C. Parkinson's disease. Lancet 2021;397:2284-303.
5. Stoker TB, Barker RA. Recent developments in the treatment of Parkinson's disease. F1000Res 2020;9:v1000-862.

Article Info

Received: 04 September 2023
Accepted: 05 September 2023
Available online: 28 September 2023

Access this article online	
Quick Response Code:	**Website:** https://journals.lww.com/joai
	DOI: 10.4103/jasi.jasi_95_23

How to cite this article: Singh V, Singh R, Singh G. Parkinson's disease revisited. J Anat Soc India 2023;72:185-6.

Original Article

Gender Determination of Scapula by Computed Tomography Scan Measurement

Abstract

Introduction: Gender is the most vital segment of the biological characteristics which can be evaluated from the skeleton because of the marked sexual dimorphism of bone segments. The aim of this study is to evaluate the effect of gender on the scapula measure for healthy sedentary subjects. The parameters used in the present study were different from the previous research. Hence, the current work was designed to measure gender differences of the scapula in the Iranian population. The aim of this study is to evaluate the effect of gender on the scapula measure for healthy sedentary subjects. The design of this research has been done with the coordination and activity of all authors to examine the effect of gender in scapula characters. **Material and Methods:** This study was performed on scapula computed tomography in 68 patients. These characters in this bone: acromion glenoid distance, length of the acromion, width of acromion, acromion coracoid distance, length of scapula, width of scapula, length of coracoid (LC), length of glenoid (LG), and width of glenoid. With the help of the SPSS software, the logistical regression equation was derived from the stepwise method. By multiplying the value of each dimension with its corresponding coefficient (β coefficient) and adding the products together along with the appropriate constant, the sex of a specimen can be determined. For the regression equation incorporating all for scapular dimensions, the logistic regression score (Y) is calculated as follows: Y = (−0.003× Width of scapula (WS)) + (0.006 × LC) + (−0.14 × height of glenoid [HG]) + 2.098. **Results:** This study shows the scapular bone characteristic comparison between the two sexes, which statistically significant difference in the width of the bone scapula (P = 0.02) and the coracoid length (P = 0.04) and LG (P = 0.01). In males, significant positive correlation was found between Height of scapula (HS), and height of glenoid (HG) (0.884) and in females, significant positive correlation was maximum the relationship between the HS and LC (0.904**). **Discussion and Conclusion:** Due to the small number of our samples, it would be better to study more widely so that other differences such as the length of the scapula and the glenoid width can be achieved, and more confidently, that these two attributes do not play a role in determining the sex.

Keywords: *Gender, glenoid cavity, radiography, scapula*

Mahdi Hamzehtofigh, Razieh Mokhtari[1], Fatemeh Seif[2], Parvindokht Bayat[3]

Department of Nursing, Students Research Committee, Arak University of Medical Sciences, Arak, Iran, [1]Department of Nursing, Faculty of Nursing, Arak University of Medical Sciences, Arak, Iran, [2]Department of Medical Physics and Radiotherapy, Arak University of Medical Sciences and Khansari Hospital, Arak, Iran, [3]Department of Anatomy, Faculty of Medicine, Arak University of Medical Sciences, Arak, Iran

Introduction

Gender is the most vital segment of the biological characteristics which can be evaluated from the skeleton because of the marked sexual dimorphism of bone segments.[1] A few skeletal components have been considered in this field, for example, skull, tibia, humerus, foramen magnum, hyoid, etc.[1]

The bone which was examined in the present study was a flat bone: the scapula. The decision to concentrate on the scapula was because of its negligible morphological changes throughout life after the development is complete. Furthermore, in the situation that frequently appears in case of acts of disaster victim identification, where flat and short bones appear to be secured over long bones, long bones are frequently broken and scattered.[2] Knowledge of the normal behavior of the scapula is of paramount importance to assess clinical pathologies, physiological adaptations, treatment, or rehabilitation program effects.

Furthermore, studies in the literature provide the scapular motion of healthy controls for several motions, and it has been shown that some characteristics such as age, gender, and shoulder dominance induce variations in the shoulder motion, It has been shown that some characteristics such as age and shoulder dominance induce

How to cite this article: Hamzehtofigh M, Mokhtari R, Seif F, Bayat P. Gender determination of scapula by computed tomography scan measurement. J Anat Soc India 2023;72:187-92.

Article Info

Received: 07 April 2019
Accepted: 08 February 2020
Available online: 28 September 2023

Address for correspondence:
Dr. Parvindokht Bayat, Department of Anatomy, Faculty of Medicine, Arak University of Medical Sciences, Arak, Iran. E-mail: bayat.parvindokht@gmail.com

Access this article online

Website: https://journals.lww.com/joai

DOI: 10.4103/JASI.JASI_9_19

Quick Response Code:

variations in the shoulder motion.[3-7] Also studied the effect of gender on the shoulder range of motion and measured a significantly greater range of motion for female subjects.

In some research, the acromial shape varied significantly with the sexes. Men are more likely to have Type III and women tend to have Type I.[8] However when other authors considered the relationship between the acromial types and sexes, there was a greater percentage of Type II in both men and women; therefore, they reported that the acromial shape also does not vary significantly with the sexes; therefore, there was no relationship between acromial types and the sexes.[8]

The effects of scapular gender on glenohumeral (GH) proprioception were investigated. The results of previous studies indicate that GH proprioception in the asymptomatic shoulder is independent of hand dominance and gender.[9,10]

However recently, some studies reported, scapular fixation produced a more consistent response in groups, gender influenced GH proprioception, irrespective of scapular fixation and the age of the subject, males were more accurate in reproducing all angles compared to females.[11-13] In previous studies on either healthy or pathological subjects, it has been concluded that the population is composed of different proportions of men and women. Sex has no significant effect on sudden motion.[11-13]

The aim of this study is to evaluate the effect of gender on the scapula measure for healthy sedentary subjects. The parameters used in the present study were different from the previous research. Hence, the current work was designed to measure gender differences of the scapula in the Iranian population.

Material and Methods

This study was performed on scapula computed tomography (CT) in 68 patients. All patients were imaged with a Spiral CT performed using the HiSpeed Advantage System (OFTiMa, RT580; General Electric, USA) with a scanning technique of 120 KV and 200 mA. Three-dimensional (3D) images were reconstructed with a slice thickness of 3 mm at increments of 2 mm by the Advantage Windows 3D Analysis Package release 2.1 (GE Medical Systems). Three-millimeter-thick slices were used, from which surface-shaded display CT models were generated on an online workstation (Advantage Windows; General Electric, Milwaukee, Wisc., USA). The 2D maximum-intensity projection reconstructions included coronal and sagittal images which were viewed on bone window settings. In assessing each modality separately, only hardcopy printed films were used. Each modality was independently and blindly assessed by two senior radiologists with experience in musculoskeletal radiology. Further diagnostic consensus was reached using all modalities at the same time with all the authors together to get an accurate diagnosis as possible for each patient. That bone was entered into the study with normal scapula and no recognizability of the fracture. With the upper limbs held up beside the head with inspiratory breath-hold, imaging was done between the upper borders of the clavicles and the kidneys. Characters are as follows:

1. Length of scapula: the length between the highest point of the superior angle and the lowest point of the inferior angle [Figure 1.A]
2. Width of scapula: from the middle of the dorsal border of the glenoid fossa to the end of the spinal axis on the vertebral border [Figure 1.B]
3. Length of glenoid (LG): length between the most superior and the most inferior point of the acromion process – The axis of this dimension varies from individual to individual [Figure 1.C]
4. Width of glenoid: maximum breadth of the articular margin of the glenoid cavity perpendicular to the glenoid cavity height [Figure 1.D]
5. Acromio-coracoid distance: maximum distance between the ventral portion of the coracoid process and the most dorsal portion of the acromion [Figure 2.E]
6. Acromio-glenoidal distance: the distance between the tip of acromion process and supraglenoid tubercle [Figure 2.F]
7. Length of acromion: is the distance between tip and midpoint of posterior border of acromion process [Figure 2.G].
8. Width of acromion: the distance between the lateral and medial borders at the midpoint of the acromion process [Figure 2.H]
9. Length of coracoid (LC): measured from the base to the tip of the coracoid process [Figure 3.I]
10. The thickness of the acromion: 1 cm posterior to the anterior border and 1 cm medially to the lateral border
11. Type of inferior surface of the anterior third of the acromion according to appearance: (1) rough (2) smooth
12. The shape of the acromion according to the Bigliani classification: (1) flat (2) curve (3) hook.

Results

In this study, 68 scans of scapula were used for study, of which 50% were female and the rest were male, and similarly, Table 1 shows the scapular bone profile completely (including minimum and maximum mean, mean, and standard deviation). Table 2 shows the scapular bone characteristic comparison between the two sexes, which shows the statistically significant difference in the width of the bone scapula ($P = 0.02$) and the coracoid length ($P = 0.04$) and LG ($P = 0.01$). The comparison of the types of the inferior surface of acromion process in the two sexes is a statistically significant difference ($P = 0.02$) [Graphs 1and 2].

A significant positive correlation was found between the characters' values in scapula bone male [Table 3] which was most the relationship between the height of

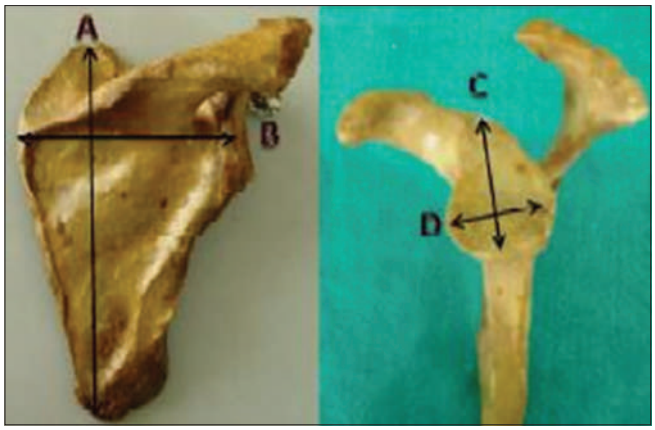

Figure 1: Osteometric measurements of scapula.[2] A-Length of scapula, B-Width of scapula,C-Length of glenoid, D-Width of glenoid

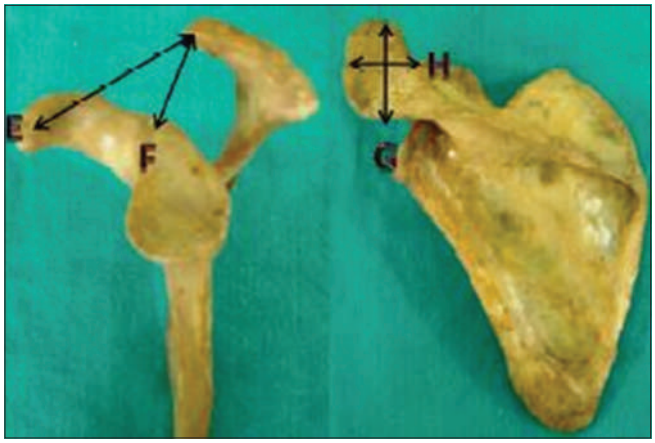

Figure 2: Osteometric measurements of scapula (contd).[2] E-Acromio-coracoid distance, F-Acromio-glenoidal distance, G-Length of acromion, H-Width of acromion

Figure 3: Osteometric measurements of scapula (contd).[2] I-Length of coracoid

Table 1: The scapular bone characteristic (including minimum and maximum mean, mean, and standard deviation) is shown in Iranian population

Characters	*n*	Minimum	Maximum	Mean±SD
Age	60	22.00	80.00	52.25±16.21
AGD	47	7.39	51.41	27.21±9.13
LA	47	17.35	153.26	54.71±23.43
WA	55	13.49	65.22	28.58±10.82
ACD	49	10.92	78.72	38.08±15.91
WS	66	32.16	167.93	98.79±30.59
HS	65	61.99	249.77	146±43.43
LC	60	15.64	77.57	43.82±14.34
WG	60	12.95	54.52	29.42±10.30
HG	64	18.67	63.00	37.54±10.16

AGD: Acromion glenoid distance, LA: Length of acromion, WA: Width of acromion, ACD: Acromion coracoid distance, WS: Width of scapula, HS: Height of scapula, LC: Length of coracoid, WG: Width of glenoid, HG: Height of glenoid, SD: Standard deviation

Table 2: Comparison of scapular characteristics in men and female

Characters	Gender	*n*	Mean±SD	*P*
AGD	Male	23	26.6117±7.58079	0.67
	Female	23	27.7851±10.78438	
LA	Male	25	58.5273±19.33029	0.31
	Female	21	51.5145±27.31422	
WA	Male	26	29.8188±11.02155	0.43
	Female	29	27.4841±10.72482	
ACD	Male	23	41.0980±17.49112	0.27
	Female	25	36.0494±14.10688	
WS	Male	32	107.88±30.52853	0.02
	Female	33	91.1940±28.39504	
HS	Male	33	1.5679E2±45.19975	0.07
	Female	31	1.3791E2±38.04940	
LC	Male	31	47.3539±14.81253	0.04
	Female	29	40.0552±13.03830	
WG	Male	31	31.6559±10.58798	0.83
	Female	29	27.0478±9.60503	
HG	Male	32	40.6667±10.32657	0.01
	Female	31	34.8065±8.98467	
Age	Male	27	54.6667±17.72656	0.27
	Female	32	50.0625±15.02672	

AGD: Acromion glenoid distance, LA: Length of acromion, WA: Width of acromion, ACD: Acromion coracoid distance, WS: Width of scapula, HS: Height of scapula, LC: Length of coracoid, WG: Width of glenoid, HG: Height of glenoid, SD: Standard deviation

scapula (HS) and height of glenoid (HG) (0.884**) In addition, a significant positive correlation was also found between the characters' values in scapula bone in female which was maximum the relationship between the HS and LC (0.904**) [Table 4]. Moreover, in general, there was a higher correlation between the characters of the scapula in women. In our tables, we only consider a significant correlation >0.600**.

With the help of (SPSS Statistics) SPSS version 22, SPSS, Chicago 1989, the logistical regression equation was derived from the stepwise method which is shown in Table 2. By multiplying the value of each dimension with

Table 3: Correlation in male

	AGD	LA	WA	ACD	WS	HS	LC	WG	HG
AGD									
LA					0.761	0.866	0.680	0.769	0.826
WA						0.641	0.623		
ACD					0.600	0.663	0.749		0.648
WS		0.761		0.600		0.878	0.861	0.774	0.826
HS		0.866	0.641	0.663	0.878		0.851	0.852	0.884
LC		0.680	0.623	0.749	0.861	0.851		0.702	0.839
WG		0.769			0.774	0.852	0.702		0.835
HG		0.826		0.648	0.826	0.884	0.839	0.835	

AGD: Acromion glenoid distance, LA: Length of acromion, WA: Width of acromion, ACD: Acromion coracoid distance, WS: Width of scapula, HS: Height of scapula, LC: Length of coracoid, WG: Width of glenoid, HG: Height of glenoid

Table 4: Correlation in female

	AGD	LA	WA	ACD	WS	HS	LC	WG	HG
AGD		0.823	0.709	0.741	0.824	0.875	0.842	0.705	0.728
LA	0.823		0.884				0.706		
WA	0.709	0.884		0.734			0.792		
ACD	0.741		0.734		0.640	0.622	0.816	0.698	0.738
WS	0.824			0.640		0.630	0.546	0.512	0.634
HS	0.875			0.622	0.630		0.904	0.892	0.832
LC	0.842	0.706	0.792	0.816		0.904		0.893	0.781
WG	0.705			0.698		0.892	0.893		0.631
HG	0.728			0.738	0.634	0.832	0.781	0.631	

AGD: Acromion glenoid distance, LA: Length of acromion, WA: Width of acromion, ACD: Acromion coracoid distance, WS: Width of scapula, HS: Height of scapula, LC: Length of coracoid, WG: Width of glenoid, HG: Height of glenoid

Table 5: Logistic regression equation and stepwise function analysis

Variable	β coefficient	SE	Significance	Significance Exp (B)	95.0% CI for Exp (B)
WS	−0.003	0.004	0.353	0.992	0.754-1.130
LC	0.006	0.009	0.504	1.010	0.809-1.451
HG	−0.014	0.012	0.269	0.937	0.17-1.857
Constant	2.098	0.259	0.000	10.79	

WS: Width of scapula, HG: Height of glenoid, LC: Length of coracoid, SE: Standard error, CI: Confidence interval

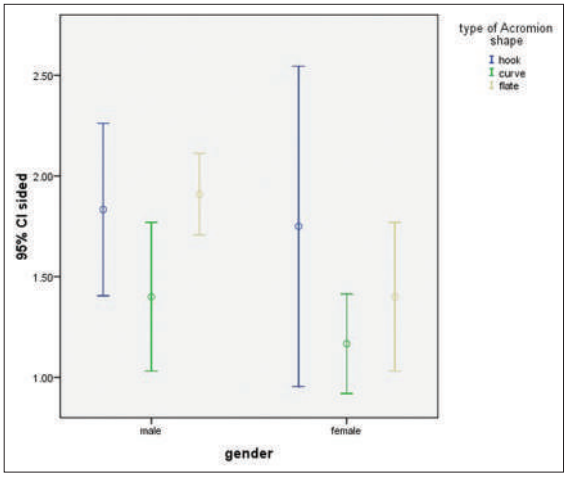

Graph 1: The represents of the types of acromion process, both male and female

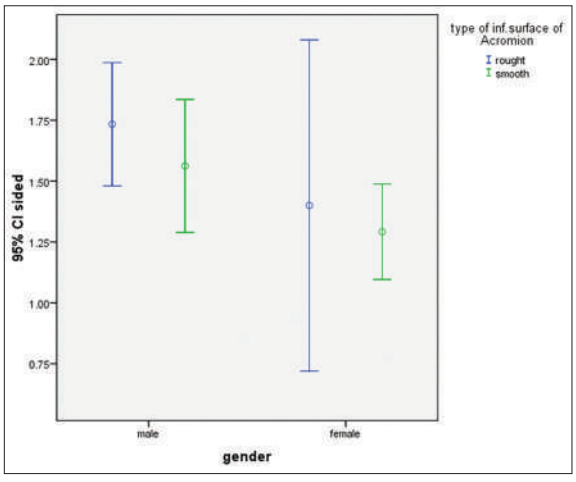

Graph 2: The represents of the types of inferior surface of acromion process, both male and female

its corresponding coefficient (β coefficient) and adding the products together along with the appropriate constant, the sex of a specimen can be determined. For the regression equation incorporating all for scapular dimensions, the

logistic regression score (Y) is calculated as follow: Y = (−0.003 × WS) + (0.006 × LC) + (−0.14 × HG) + 2.098 Table 5.

Discussion

In the present study, the descriptive statistics of 11 variables were reported which shows mean and standard deviation for both sexes. The overall mean value collected from the scapula of males was larger than the females, but some of the parameters have a significant difference between both the groups. The present study demonstrated higher values of measurements of male compared to female scapula bones. These results corroborate with data already reported in the literature for other types of populations.

There was a significant difference between female and male specimens for each dimension measured ($P < 0.05$). Height-to-width ratios were also significantly different comparing men to women ($P < 0.05$). These differences resulted in a rounder male glenoid and more oval female glenoid.[14]

Seventy-four cadaveric shoulder CT scans (37 males and 37 females with statistically equivalent age and body mass index) were reconstructed using Mimics® to create 3D models of the humerus and scapula. After 3D reconstruction, each CT bone model was analyzed in Rapidform® to quantify the morphology of the humerus, scapula, and the spatial relationship between the two to better understand the role of gender on the morphological variability of the GH joint.[15]

Dynamic analysis of the shoulder joint during arm elevation has been investigated under various conditions and in various types of subjects with the development of analytical devices, but there has been no report describing sex differences. Therefore, the current study was performed, and it clarified that scapular upward rotation and internal rotation angles during arm elevation were different for each sex.

The upward rotation angle was significantly greater in males, and the internal rotation angle was significantly greater in females. Ogston and Ludewig[16] compared scapular movement during 10°–120° scapular plane arm elevation between multidirectional instability (MDI) patients and control subjects, and they observed that the scapular upward rotation angle was significantly smaller, and the scapular internal rotation angle was greater in all MDI patients during the elevation phase. In the current study, the upward rotation angle was smaller in females at all elevation angles, excluding 120°, and the internal rotation angle was greater in females at all elevation angles, which is similar to their findings.

No person with shoulder instability was included in the present study, but a higher incidence of generalized joint laxity in females was reported.[17,18]

In addition, in a survey of Asians of the same age group as our subjects, the incidence of generalized joint laxity was 25.4% and 38.5% in males and females, respectively, suggesting that the presence or absence of this laxity was involved in the current results.[19] A follow-up study with a generalized joint laxity test and electromyographic evaluation is necessary.

This paper considers that the reason for the shoulder scapula bones of men is generally larger than the female could be due to the physical effort performed by male ancestors. This justification was also adopted by Costa OA *et al*. This fact is due to the greater development of the muscles of the upper limbs of male individuals, and hence that bone growth accompanies this structure to ensure the support of the muscle tissue attached.[20]

The discrepancies between the current work and previous studies could be due to structural differences of scapula between different populations as a result of the growth hormone which is affected by genes and environmental factors.[21] Furthermore, due to different methods used for measurements, as El Morsi DA *et al*. applied the measurements directly from the bone, while in the present work, the measurements were taken from CT.[21]

Conclusion

The length of the scapula and the glenoid width do not play a role in determining the sex.

Acknowledgement

This work was supported by the Research Council of Arak University of Medical Sciences [Grant Number 2101, Ethical code:93-175-19].

Financial support and sponsorship

This study was funded by the Vice-chancellor of research at the Arak University of Medical Sciences.

Conflicts of interest

There are no conflicts of interest.

References

1. Decoster LC, Vailas JC, Lindsay RH, Williams GR. Prevalence and features of joint hypermobility among adolescent athletes. Arch Pediatr Adolesc Med 1997;151:989-92.
2. Lingamdenne PE, Marapaka P. Measurement and analysis of anthropometric measurements of the human scapula in Telangana region, India. Int J Anat Res 2016;4:2677-83.
3. Barnes CJ, Van Steyn SJ, Fischer RA. The effects of age, sex, and shoulder dominance on range of motion of the shoulder. J Shoulder Elbow Surg 2001;10:242-6.
4. Dayanidhi S, Orlin M, Kozin S, Duff S, Karduna A. Scapular kinematics during humeral elevation in adults and children. Clin Biomech (Bristol, Avon) 2005;20:600-6.
5. Matsuki K, Matsuki KO, Mu S, Yamaguchi S, Ochiai N, Sasho T, *et al*. *In vivo* 3-dimensional analysis of scapular kinematics: Comparison of dominant and nondominant shoulders. J Shoulder Elbow Surg 2011;20:659-65.
6. McClure PW, Michener LA, Sennett BJ, Karduna AR. Direct 3-dimensional measurement of scapular kinematics

during dynamic movements *in vivo*. J Shoulder Elbow Surg 2001;10:269-77.
7. van Andel CJ, Wolterbeek N, Doorenbosch CA, Veeger DH, Harlaar J. Complete 3D kinematics of upper extremity functional tasks. Gait Posture 2008;27:120-7.
8. Natsis K, Tsikaras P, Totlis T, Gigis I, Skandalakis P, Appell HJ, *et al*. Correlation between the four types of acromion and the existence of enthesophytes: A study on 423 dried scapulas and review of the literature. Clin Anat 2007;20:267-72.
9. Blasier RB, Carpenter JE, Huston LJ. Shoulder proprioception. Effect of joint laxity, joint position, and direction of motion. Orthop Rev 1994;23:45-50.
10. Lephart SM, Warner JJ, Borsa PA, Fu FH. Proprioception of the shoulder joint in healthy, unstable, and surgically repaired shoulders. J Shoulder Elbow Surg 1994;3:371-80.
11. Borstad JD. Resting position variables at the shoulder: Evidence to support a posture-impairment association. Phys Ther 2006;86:549-57.
12. Ludewig PM, Reynolds JF. The association of scapular kinematics and glenohumeral joint pathologies. J Orthop Sports Phys Ther 2009;39:90-104.
13. Yano Y, Hamada J, Tamai K, Yoshizaki K, Sahara R, Fujiwara T, *et al*. Different scapular kinematics in healthy subjects during arm elevation and lowering: Glenohumeral and scapulothoracic patterns. J Shoulder Elbow Surg 2010;19:209-15.
14. Merrill A, Guzman K, Miller SL. Gender differences in glenoid anatomy: An anatomic study. Surg Radiol Anat 2009;31:183-9.
15. Jacobson A, Gilot GJ, Hamilton MA, Greene A, Flurin PH, Wright TW, *et al*. Glenohumeral anatomic study. A comparison of male and female shoulders with similar average age and BMI. Bull Hosp Jt Dis (2013) 2015;73 Suppl 1:S68-78.
16. Ogston JB, Ludewig PM. Differences in 3-dimensional shoulder kinematics between persons with multidirectional instability and asymptomatic controls. Am J Sports Med 2007;35:1361-70.
17. Forléo LH, Hilário MO, Peixoto AL, Naspitz C, Goldenberg J. Articular hypermobility in school children in Sao Paulo, Brazil. J Rheumatol 1993;20:916-7.
18. Larsson LG, Baum J, Mudholkar GS. Hypermobility: Features and differential incidence between the sexes. Arthritis Rheum 1987;30:1426-30.
19. Al-Rawi ZS, Al-Aszawi AJ, Al-Chalabi T. Joint mobility among university students in Iraq. Br J Rheumatol 1985;24:326-31.
20. Costa OA, de Albuquerque AP, de Albuquerque PV, de Oliveira RB, de Albuquerque LY, Caiaffo V. Morphometric analysis of the scapula and their differences between females and males. Int j morphol 2016;34:1164-8.
21. El Morsi DA, Gaballah G, Mahmoud W, Tawfik AI. Sex determination in Egyptian population from scapula by computed tomography. J Forensic Res 2017;8:2-4.

Original Article

Three-dimensional Evaluation of the Nasolacrimal Duct and Maxillary Sinus Ostium in Patients with Cleft Lip and Palate

Esin Bozdemir, Özlem Yarbasi[1]

Department of Oral and Maxillofacial Radiology, Faculty of Dentistry, University of Süleyman Demirel, Isparta, [1]Düzce Oral and Dental Health Center, Düzce, Turkey

Abstract

Objective: Cleft lip and/or palate (CLP) is one of the most common congenital craniofacial anomalies. Individuals with CLP experience numerous problems including lack of nutrition, impaired speech, hearing loss, obstruction of nasolacrimal duct, poor dentition and facial morphology, and sinusitis. This study aimed to compare the nasolacrimal canal morphometry (nasolacrimal duct [NLD]), maxillary sinus ostium (MSO) localization, and presence of the accessory maxillary ostium (AMO) in patients with unilateral or bilateral CLP with healthy controls. **Materials and Methods:** The transversal and anteroposterior diameters and the length of the NLD were measured in 33 patients with unilateral CLP and 30 patients with bilateral CLP using cone-beam computed tomography. There were 16 (53.3%) males and 14 females (46.7%) in the bilateral CLP group and 18 males and 15 females in the unilateral CLP group. The mean ages of the patients were 17.36 ± 5.27 in patients with unilateral CLP and 18.6 ± 5.66 in patients with bilateral CLP. The anteroposterior location of the MSO and AMO was evaluated. **Results:** The transversal (P = 0.003) and anteroposterior (P = 0.002) diameters of NLD were found to be significantly different between the patients with bilateral CLP and the control group. The NLD length was found to be significantly different between the control group and the affected sides in the unilateral CLP group (P = 0.02). The MSO was found more in the middle region in the control group compared to the unilateral CLP group (P = 0.004). The AMO was found in 66.7% of the patients with bilateral CLP and 62.1% of the patients with unilateral CLP. The AMO was found more in the control group than in the bilateral CLP group (P = 0.01). **Conclusions:** Cleft lip and palate is an anomaly that can affect both the diameter and the length of the NLD and MSO localization.

Keywords: *Cleft lip and palate, cone-beam computed tomography, maxillary sinus ostium, nasolacrimal duct*

Introduction

Cleft lip and/or palate (CLP) is one of the most common congenital craniofacial anomalies, constituting 15% of all congenital anomalies.[1,2] These defects occur due to the failed fusion of bony and soft tissue growth elements of the cranial and maxillofacial bones *in utero* caused by a complex interaction of genetic and environmental factors.[3]

The incidence of CLP varies according to ethnicity, country, and socioeconomic status. Between the 4th and 8th weeks of the intrauterine period, CLP deformities may occur due to a defect that occurs during facial structure formation.[1] Individuals with CLP experience numerous problems including lack of nutrition, impaired speech, hearing loss, the obstruction of nasolacrimal duct (NLD), sinusitis, chronic upper respiratory tract infections, poor dentition and facial morphology, and psychological problems.[4]

Radiological examination plays a crucial role in the diagnosis, treatment planning, and follow-up of patients with CLP.[1] Multiple radiographic imaging is performed throughout childhood and adolescence. These may include two-dimensional imaging methods such as panoramic, periapical, occlusal, and frontal or lateral cephalometric radiographs. The most frequently used three-dimensional (3D) techniques are computed tomography (CT), cone-beam CT (CBCT), magnetic resonance imaging, stereophotogrammetry, and laser surface scanning.[3]

CBCT could be the preferred method because it has a lower radiation dose than CT. Being addicted to low radiation doses

How to cite this article: Bozdemir E, Yarbasi Ö. Three-dimensional evaluation of the nasolacrimal duct and maxillary sinus ostium in patients with cleft lip and palate. J Anat Soc India 2023;72:193-8.

Article Info

Received: 27 October 2022
Revised: 01 April 2023
Accepted: 14 May 2023
Available online: 28 September 2023

Address for correspondence:
Dr. Esin Bozdemir, Department of Oral and Maxillofacial Radiology, Faculty of Dentistry, University of Süleyman Demirel, Isparta, Turkey.
E-mail: dtesin@hotmail.com

Access this article online

Website: https://journals.lww.com/joai
DOI: 10.4103/jasi.jasi_153_22
Quick Response Code:

had many advantages compared to CT, such as low cost, easy handling, and providing a more detailed 3D view of craniofacial structures.[4,5]

The maxillary sinus, which is one of the most important structures of the midface, is morphologically affected in patients with CLP.[4] The maxillary sinus ostium (MSO) is located at the highest part of the medial wall of the sinus and opens into the narrow ethmoidal infundibulum.[6,7] The accessory maxillary ostium (AMO) is located in the medial maxillary wall, between the uncinate process and the inferior concha.[8]

Sinusitis is commonly observed in patients with CLP; however, its cause remains unknown. Malposition of the MSO and the presence of AMO are thought to play a role in the formation of chronic maxillary sinusitis by disrupting the mucociliary clearance of the maxillary sinus.[6,7] The NLD runs along the lateral wall of the nasal cavity and enters the inferior nasal meatus behind the anterior end of the inferior nasal concha.[9]

Although a study related to the NLD of patients with unilateral CLP is present in the literature,[10] there are no studies on patients with bilateral CLP. Furthermore, no previous study has investigated the localization of the MSO in patients with CLP. Therefore, this study aimed to compare the nasolacrimal canal morphometry, MSO localization, and presence of AMO in patients with unilateral or bilateral CLP with healthy controls.

Materials and Methods

Subjects

A total of 63 (33 – unilateral and 30 – bilateral) CLP patients who applied to the division of oral and maxillofacial radiology for CBCT scanning from July 2012 to November 2020 were included in this study. The CBCT images of the patients with unilateral and bilateral CLP as well as the controls were retrospectively evaluated. The control group comprised 41 age- and sex-matched individuals who were randomly selected for comparison with the 33 and 30 patients with unilateral and bilateral CLP, respectively. There were 16 (53.3%) males and 14 females (46.7%) in the bilateral CLP group and 18 males and 15 females in the unilateral CLP group. The mean ages of the patients were 17.36 ± 5.27 in patients with unilateral CLP and 18.6 ± 5.66 in patients with bilateral CLP.

The study was approved by the university-local ethics committee (Number: 72867572-050.01.04). Written informed consent was obtained from each patient who is >18 years of age and parent for patients aged <18 years. CBCT was performed for the diagnosis and treatment planning in the CLP groups and due to various reasons, such as an impacted tooth, missing teeth, and orthodontic treatment, in the control group. Thirty-two of the patients were excluded from the study due to reasons such as pathological lesions, such as cysts and tumors, affecting the examined area, insufficient image quality, and inability to observe the region to be examined in any cross-section.

Cone-beam computed tomography technique

All CBCT images were acquired by ProMax 3D Mid (Planmeca, Helsinki, Finland) with a field of view of 200 mm × 170 mm, 0.04 mm^3 voxel size, and approximately 20 s of acquisition time at 90 kV and 10 mA. CBCT images were evaluated in the Digital Imaging and Communications in Medicine format using the Romexis software program (Planmeca Oy, Helsinki, Finland).

Measurements

All images were assessed by a single maxillofacial radiologist in the darkroom. All the measurements were made in 1 week, and 10% (n = 11) of the measurements were repeated to determine the intra-observer agreement.

The narrowest anteroposterior and transverse diameters were measured at the level of the infraorbital margin in the axial section. NLD length was measured in the sagittal section between the most proximal and distal points visible [Figure 1].[11]

The anteroposterior location of the MSO was divided into the following three categories in the coronal section: (a) the anterior region: from the mesial aspect of the maxillary first premolar to that of the first molar; (b) the middle region: from the mesial aspect of the maxillary first molar to the distal aspect of the maxillary second molar; and (c) the posterior region: from the distal aspect of the maxillary second molar to the posterior of the tuber maxillae.[6]

AMO was examined radiographically as present/absent. NLD obstruction was evaluated as present/absent in all three sections.

Statistical analyses

The Shapiro–Wilk test was used to evaluate the normality of the distributions. Normal distribution was observed in all the groups. The Chi-square test was used to compare categorical variables between the control and CLP groups. $P < 0.05$ was considered statistically significant. The Student's t-test was used to compare numerical measurement values. Intraclass correlation coefficient (ICC) was used to determine the intra-observer agreement of the NLD measurements.

Results

A total of 192 NLDs of 96 patients (33 patients with unilateral CLP, 30 patients with bilateral CLP, and 33 control patients) were examined. There was no difference among the four groups according to age [Table 1] ($P > 0.05$). The ICCs were perfect and calculated as 0.98 for the transversal diameter, 0.92 for the anteroposterior diameter, and 0.99 for the duct length.

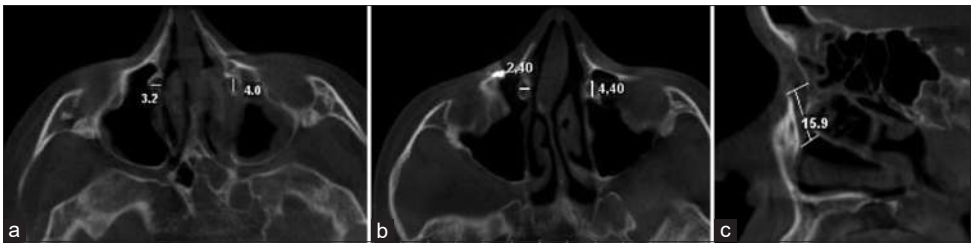

Figure 1: Axial CBCT scan shows transversal (a) and anteroposterior (b) diameter measurement of the nasolacrimal duct in a patient with unilateral CLP. Sagittal CBCT scan shows nasolacrimal duct length measurement (c). CBCT: Cone-beam computed tomography, CLP: Cleft lip and/or palate

Table 1: The mean ages of the patients in the study groups

	The mean age±SD (minimum–maximum)	*P*
Unilateral CLP group	17.36±5.27 (10–32)	0.60
Control group I	17.87±2.30 (14–22)	
Bilateral CLP group	18.6±5.66 (10–28)	0.92
Control group II	18.47±2.36 (14–23)	

CLP: Cleft lip and/or palate, SD: Standard deviation

The mean transversal NLD diameter was narrower in female patients compared to that in male patients in both the unilateral and bilateral CLP groups. A wider anteroposterior NLD diameter was found in female patients in both the unilateral and bilateral CLP groups. There was no significant difference between sex in the groups ($P > 0.05$).

The study population was divided into two age groups (10–19 years and >19 years). Patients with CLP over 19 years of age had wider transversal and anteroposterior NLD diameters. The difference between age groups was statistically significant ($P < 0.05$).

The mean transversal NLD diameter was 3.26 ± 0.80 mm (minimum: 2, maximum: 5.20) for the affected side and 3.96 ± 0.60 mm (minimum: 2.83, maximum: 5.20) for the unaffected side in the unilateral CLP group, and 4.19 ± 0.78 mm (minimum: 2.4, maximum: 6.2) in the control group. There was a significant difference between the affected and unaffected sides in the unilateral CLP group ($P < 0.001$). The difference between the unaffected side and the control group was not significant. The narrowest mean anteroposterior NLD diameter was 5.04 ± 0.58 mm on the affected side. There was a significant difference between the control group and the affected and unaffected sides of the unilateral CLP group in terms of anteroposterior NLD diameter ($P < 0.001$).

The mean NLD length was 15.58 ± 1.48 mm and 15.88 ± 2.20 mm for the affected and unaffected sides, respectively, and 16.65 ± 2.22 mm for the control group. There was a significant difference between the control group and the unaffected sides in the unilateral CLP group [$P = 0.02$, Table 2].

The mean transversal NLD diameter was 3.67 ± 0.87 mm in the patients with the bilateral CLP and 4.16 ± 0.91 mm in the control group. The difference between the patients with bilateral CLP and the control group was significant with respect to the transversal and anteroposterior diameters of the NLD. However, there was no significant difference in terms of the NLD length between both the groups [Table 3].

The MSO localization was detected mostly in the anterior region in the unilateral and bilateral CLP groups and the control group. The MSO was localized more in the middle region in patients in the control group compared to that of patients in the unilateral CLP group. The difference between the patients with unilateral CLP and the control group was statistically significant ($P = 0.004$). The AMO was found in 66.7% of the patients with bilateral CLP and 62.1% of the patients with unilateral CLP. The AMO was found more in the control group than in the bilateral CLP group ($P = 0.01$). Mucosal thickening in the maxillary sinus was detected more in patients with CLP compared to that in the control group ($P = 0.002$). There were 11 patients with sinusitis (five patients with bilateral CLP, two patients with unilateral CLP, and four patients in the control group). The incidence of NLD obstruction was 71.7% in the bilateral CLP group and 74.2% in the unilateral CLP group. The difference between the patients with CLP and the control group was not statistically significant ($P > 0.05$).

However, although there was a significant difference between NLD obstruction and NLD diameter in patients with bilateral CLP, there was no difference in the unilateral CLP group [Table 4]. In the study population, smaller means of nasolacrimal transversal and anteroposterior diameters in the side with NLD obstruction was determined ($P \leq 0.001$ and $P < 0.01$, respectively).

Discussion

Because CLP affects the midface, the NLD in this area may also be affected. NLD obstruction or narrowing may occur secondary to patients with facial clefts such as CLP.[12] However, patients with CLP may have congenital defects of the nasolacrimal apparatus, such as agenesis or stenosis of the canaliculi, lacrimal sac, and NLD.[13] Therefore, having the knowledge of the morphometry of the lacrimal drainage system in facial clefts is vital for avoiding potential recalcitrant epiphora and infections during primary cleft repair.[12] Epiphora is a commonly

Table 2: Measurements of the transversal and anteroposterior diameters and length of nasolacrimal duct in patients with unilateral cleft lip-palate

Groups	*n*	Nasolacrimal transversal diameter, mean±SD	*P*	Nasolacrimal anteroposterior diameter, mean±SD	*P*	NLD length, mean±SD	*P*
UCLP cleft side group	33	3.26±0.80	0.00*	5.04±0.58	0.71	15.58±1.48	0.51
UCLP noncleft side group	33	3.96±0.60		5.10±0.76		15.88±2.20	
UCLP cleft side group	33	3.26±0.80	0.00*	5.04±0.58	0.00**	15.58±1.48	0.02*
Control group	66	4.19±0.78		5.88±0.80		16.65±2.22	
UCLP noncleft side group	33	3.96±0.60	0.15	5.10±0.76	0.00**	15.88±2.20	0.16
Control group	66	4.19±0.78		5.88±0.80		16.65±2.22	

*P<0.05, **P<0.001. UCLP: Unilateral cleft lip and/or palate, SD: Standard deviation, NLD: Nasolacrimal duct

Table 3: Measurements of the transversal and anteroposterior diameters and length of nasolacrimal duct in bilateral cleft lip-palate patients

Groups	*n*	Nasolacrimal transversal diameter, mean±SD	*P*	Nasolacrimal anteroposterior diameter, mean±SD	*P*	NLD length, mean±SD	*P*
BCLP group	60	3.67±0.87	0.003*	5.37±1.15	0.002*	16.68±2.24	0.85
Control group	60	4.16±0.91		5.99±0.91		16.61±1.86	

*P<0.01. BCLP: Bilateral cleft lip and /or palate, SD: Standard deviation, NLD: Nasolacrimal duct

Table 4: Measurements of the transversal and anteroposterior diameters of the nasolacrimal duct according to the presence of nasolacrimal duct obstruction in patients with cleft lip-palate

	Mean±SD		*P*
	With NLD obstruction	Without NLD obstruction	
UCLP cleft side group			
Nasolacrimal transversal diameter	3.26±0.76	3.34±0.91	0.82
Nasolacrimal anteroposterior diameter	4.97±0.59	5.26±0.58	0.28
BCLP			
Nasolacrimal transversal diameter	3.34±0.56	4.52±0.96	0.00**
Nasolacrimal anteroposterior diameter	5.14±1.08	5.95±1.17	0.01*

*P<0.05, **P<0.001. BCLP: Bilateral cleft lip and /or palate, UCLP: Unilateral cleft lip-palate, NLD: Nasolacrimal duct

observed lacrimal drainage system disease that may reduce visual acuity. Obstruction or narrowing of the NLD system may cause Epiphora.

There was a study conducted on the NLD in patients with CLP. This study investigated the morphometric changes in the NLD of the side affected by the cleft in the unilateral CLP group. In our study, we examined patients with unilateral and bilateral CLP. Comparisons were made between the primary acquired nasolacrimal duct obstruction (PANDO) group and the control group in the previous studies related to the NLD morphometry.[14-17] In addition, previous studies have evaluated NLD morphometry according to different age groups, ethnic groups, and sex.[18-24]

In comparative studies, a smaller NLD diameter was found in patients with the obstructed NLD compared to that in the control groups. Hence, it has been reported that the small diameter of the NLD may increase the risk of PANDO and be one of the etiologic factors. Similar to these studies, the mean nasolacrimal diameter was smaller means of nasolacrimal transversal and anteroposterior diameters in the side with NLD obstruction in the study population in our study.

Previous studies reported that the NLD diameter was narrower in females compared to that in male patients and no significant difference between sex groups was observed, which agrees with our study ($P > 0.05$).[19,23,24] However, we found that the mean anteroposterior NLD diameter was slightly wider in females than in males ($P > 0.05$).

Similar to our study, a narrow NLD diameter was determined in those under the age of 20 in a study by Zhang *et al*.[19] In a study by Lee *et al*., which also included the pediatric population, a narrow NLD diameter in children under the age of 10 was found.[22] An inverse relationship has been observed between age and the NLD diameter in patients with PANDO. The older the patient, the narrower the NLD diameter; however, no relationship was observed in the control group in the study conducted by Janssen *et al*.[14] In the present study, we found that NLD diameter increased with age; however, the study population consisted of patients with CLP with ages ranging from 10 to 32 years. The differences among studies may result from the differences in the method used for the measurement of the NLD diameter or the study population.

CBCT is an imaging method that uses a lower radiation dose and has a lower cost than CT. It is used for

diagnosis and treatment planning in all areas of medicine and dentistry, including oral and maxillofacial surgery, ear, nose, throat, orthopedics, interventional radiology, orthodontics, periodontology, and forensic dentistry. Since CLP is a true 3D deformity, it must be evaluated using 3D imaging methods to provide a better insight into the anatomical condition for treatment planning. However, there are a great number of previous morphological studies related to NLD that used CT;[12,15,17-19,21,22] however, CBCT has only been used in few previous studies.[10,20,25]

Only one study has been conducted by Altun *et al*.[10] on the NLD morphometry in patients with CLP[11] in which the study population consisted of patients with unilateral CLP and the control group. Our study is the first to evaluate the morphology of the NLD in patients with both unilateral CLP and bilateral CLP. Altun *et al*.[10] reported that the transversal NLD diameter was narrower on the affected side than the unaffected side and there were no statistically significant differences between the control group and the affected and unaffected sides in the unilateral CLP group. In our study, there was a statistically significant difference between the control group and the affected side in the unilateral CLP group in terms of both the transversal and anteroposterior NLD diameters. In addition, a statistically significant difference was found between the control group and the bilateral CLP group.

Altun *et al*.[10] evaluated the NLD length in the study that examined the NLD morphometry in unilateral CLP patients using CBCT. It was reported that NLD length was not affected by unilateral CLP presence in this study.[10] In our study, NLD length was shorter in the affected side of patients with unilateral CLP than that in the control group and this difference was statistically significant. However, there was no statistically significant difference between the bilateral CLP group and the control group. The difference related to the length between the two studies might have resulted from the difference in the measurement technique.

Maxillary sinusitis is commonly observed in patients with CLP and its reasons are not completely understood. The maxillary accessory ostium is one of the anatomical variations that may play a role in the development of chronic maxillary sinusitis.[26-28] However, the differential location of the MSO may be a cause of chronic sinusitis.[6,7] Mucosal thickening and maxillary sinusitis in patients with unilateral CLP in which the MSO was found in the anterior region was found to be more than that in the control group in our study. However, the relationship between the presence of the MSO and sinusitis was not determined.

Conclusions

Based on the results of our study, the diameter of the transversal NLD was significantly narrower in patients with unilateral CLP compared with that in the control group. Both the transversal and anteroposterior NLD diameters were found to be narrower in patients with bilateral CLP. These results show that NLD was affected on these patients due to narrower NLD diameter in patients with CLP compared with that in the control group. There is a higher risk of development of PANDO in these patients. Because patients with CLP may have a defect of nasolacrimal apparatus such as stenosis of the NLD, it is important to know the morphometry of the lacrimal system to avoid potential recalcitrant epiphora and infections during the primary cleft repair. However, the inflammatory disease of maxillary sinuses was detected more in patients with CLP than in the control group. The AMO was found more in the control group than in the bilateral CLP group. Therefore, AMO may not be a cause for the development of chronic maxillary sinusitis in patients with CLP. The location of the MSO was significantly different in unilateral CLP patients compared to the control group.

Financial support and sponsorship

Nil.

Conflicts of interest

There are no conflicts of interest.

References

1. Gezgin O, Botsali MS. Evaluation of teeth development in unilateral cleft lip and palate patients in mixed dentition by using medical image control systems. Niger J Clin Pract 2018;21:156-62.
2. Lelertsirivorakul J, Kajornchaivut N, Pungchanchaikul P, Jinaporntham S. Dental caries experience, treatment needs, dental anomalies and malocclusion in preschool children with cleft lip and/or palate. J Med Assoc Thai 2017;100:S109-16.
3. Santaella GM, Azevedo BC, Scarfe WC. Cone beam imaging in orofacial cleft therapy. Decis Dent 2020;6:36-9.
4. Erdur O, Ucar FI, Sekerci AE, Celikoglu M, Buyuk SK. Maxillary sinus volumes of patients with unilateral cleft lip and palate. Int J Pediatr Otorhinolaryngol 2015;79:1741-4.
5. Parveen S, Husain A, Mascarenhas R, Reddy SG. Clinical utility of cone-beam computed tomography in patients with cleft lip palate: Current perspectives and guidelines. J Cleft Lip Palate Craniofac Anomal 2018;5:74-87.
6. Şimşek Kaya G, Daltaban Ö, Kaya M, Kocabalkan B, Sindel A, Akdağ M. The potential clinical relevance of anatomical structures and variations of the maxillary sinus for planned sinus floor elevation procedures: A retrospective cone beam computed tomography study. Clin Implant Dent Relat Res 2019;21:114-21.
7. Souza AD, Rajagopal KV, Ankolekar VH, Souza AS, Kotian SR. Anatomy of maxillary sinus and its ostium: A radiological study using computed tomography. CHRISMED J Health Res 2016;3:37-40.
8. Yeung AW, Colsoul N, Montalvao C, Hung K, Jacobs R, Bornstein MM. Visibility, location, and morphology of the primary maxillary sinus ostium and presence of accessory Ostia: A retrospective analysis using cone beam computed tomography (CBCT). Clin Oral Investig 2019;23:3977-86.
9. Maliborski A, Różycki R. Diagnostic imaging of the nasolacrimal drainage system. Part I. Radiological anatomy of lacrimal pathways. Physiology of tear secretion and tear outflow. Med Sci Monit 2014;20:628-38.

10. Altun O, Dedeoğlu N, Avci M. Examination of nasolacrimal duct morphometry using cone beam computed tomography in patients with unilateral cleft lip/palate. J Craniofac Surg 2017;28:e725-8.
11. Altinkaynak H, Gunes H. Anatomical parameters of the nasolacrimal duct in healthy children measured with computed tomography. Beyoglu Eye J 2019;4:86-91.
12. Ali MJ, Paulsen F. Syndromic and nonsyndromic systemic associations of congenital lacrimal drainage anomalies: A major review. Ophthalmic Plast Reconstr Surg 2017;33:399-407.
13. Anchlia S, Rao KS, Bonanthaya K, Anupama B, Nayak IV. Ophthalmic considerations in cleft lip and palate patients. J Maxillofac Oral Surg 2011;10:14-9.
14. Janssen AG, Mansour K, Bos JJ, Castelijns JA. Diameter of the bony lacrimal canal: Normal values and values related to nasolacrimal duct obstruction: Assessment with CT. AJNR Am J Neuroradiol 2001;22:845-50.
15. Takahashi Y, Nakata K, Miyazaki H, Ichinose A, Kakizaki H. Comparison of bony nasolacrimal canal narrowing with or without primary acquired nasolacrimal duct obstruction in a Japanese population. Ophthalmic Plast Reconstr Surg 2014;30:434-8.
16. Park JH, Huh JA, Piao JF, Lee H, Baek SH. Measuring nasolacrimal duct volume using computed tomography images in nasolacrimal duct obstruction patients in Korean. Int J Ophthalmol 2019;12:100-5.
17. Bulbul E, Yazici A, Yanik B, Yazici H, Demirpolat G. Morphometric evaluation of bony nasolacrimal canal in a Caucasian population with primary acquired nasolacrimal duct obstruction: A multidetector computed tomography study. Korean J Radiol 2016;17:271-6.
18. Fasina O, Ogbole GI. CT assessment of the nasolacrimal canal in a black African population. Ophthalmic Plast Reconstr Surg 2013;29:231-3.
19. Zhang S, Cheng Y, Xie J, Wang Z, Zhang F, Chen L, *et al.* Anatomical study and locating nasolacrimal duct on computed topographic image. J Craniofac Surg 2017;28:275-9.
20. Okumuş Ö. Investigation of the morphometric features of bony nasolacrimal canal: A cone-beam computed tomography study. Folia Morphol (Warsz) 2020;79:588-93.
21. Lin Z, Kamath N, Malik A. Morphometric differences in normal bony nasolacrimal anatomy: Comparison between four ethnic groups. Surg Radiol Anat 2021;43:179-85.
22. Lee H, Ha S, Lee Y, Park M, Baek S. Anatomical and morphometric study of the bony nasolacrimal canal using computed tomography. Ophthalmologica 2012;227:153-9.
23. McCormick A, Sloan B. The diameter of the nasolacrimal canal measured by computed tomography: Gender and racial differences. Clin Exp Ophthalmol 2009;37:357-61.
24. Takahashi Y, Nakamura Y, Nakano T, Asamoto K, Iwaki M, Selva D, *et al.* The narrowest part of the bony nasolacrimal canal: An anatomical study. Ophthalmic Plast Reconstr Surg 2013;29:318-22.
25. Kolsuz ME, Bilecenoğlu B, Kurt MH, Bozkurt P, Orhan K. Morphometric evaluation of nasolacrimal canal diameters using cone beam computed tomography: A cross-sectional study. Turk Klin J Dent Sci 2019;25:169-74.
26. Sahin C, Ozcan M, Unal A. Relationship between development of accessory maxillary sinus and chronic sinusitis. Med J DY Patil Univ 2015;8:606-8.
27. Ghosh P, Kumarasekaran P, Sriraman G. Incidence of accessory Ostia in patients with chronic maxillary sinusitis. Int J Otorhinolaryngol Head Neck Surg 2018;4:443-7.
28. Bani-Ata M, Aleshawi A, Khatatbeh A, Al-Domaidat D, Alnussair B, Al-Shawaqfeh R, *et al.* Accessory maxillary Ostia: Prevalence of an anatomical variant and association with chronic sinusitis. Int J Gen Med 2020;13:163-8.

Original Article

Electron Microscopic Observation of Normal and 2,4,5-Trihydroxyl Phenylethylamine (6-hydroxydopamine) Lesioned Corpus Striatum in Wistar Albino Rats

Ravisankar P[1,2], Ravishankar P[1], Ravindran R[3], Sridevi G[4], Mathew J[5]

Departments of [1]Anatomy and [4]Physiology, SRM Dental College and Hospital, SRMIST, Ramapuram Campus, Departments of [2]Anatomy and [3]Physiology, Dr. A. L. Mudaliar Post Graduate Institute of Basic Medical Sciences, University of Madras, Taramani Campus, Chennai, Tamil Nadu, India, [5]Department of Physiology, Ibn Sina National College for Medical Studies, Jeddah, Saudi Arabia

Abstract

Background: The prevalence and incidence of Parkinson's disease (PD) is increasing due to a prolonged life expectancy. The cardinal features of PD include resting tremor, rigidity, bradykinesia, and postural instability. In rodents the 2,4,5-trihydroxyphenylethylamine [6-hydroxydopamine (6-OHDA)] induced lesion of the nigrostriatal system showed retrograde degeneration and structural changes in the corpus striatum under transmission the electron microscope (TEM). **Aim and Objectives:** To study the ultra-structure of normal and 6-OHDA lesioned corpus striatum in Wistar albino rats under the transmission electron microscope. **Material and Methods:** Wistar albino male adult rats received unilateral stereotaxical injection of 6-OHDA on the right side of striatum and were sacrificed after 120 days. The following stereotaxic co-ordinates were used to target the dorsolateral part of the striatum: AP = 0.2 mm, ML = 3.2 mm, DV = 4.5 mm from the bregma. Another target was the dorsomedial part of striatum: AP = 1.1 mm, ML = 2.4 mm and DV = 3.5 mm.The motor behavior was monitored in cylinder which was counted for a period of 60 min. **Results and Conclusion:** Our TEM finding in the control rats demonstrated that nucleus was round and comparatively large in proportion to the cell body and lies in the centre of the nerve cell in the striatum. Occasionally one or two dense nucleoli were located eccentrically in the nucleoplasm. Additionally, in the cytoplasm around the nucleus, the conspicuous organelles along with the numerous ribosomes which were mostly free and appear as rosettes or clusters, some of which were attached to the endoplasmic reticulum. Furthermore, few short of granular endoplasmic reticula were seen. Interestingly, the lesioned rats showed neuronal and glial cells damage at the ultra-structural level in striatum under TEM observation.

Keywords: *6-hydroxydopamine lesion, apomorphine-induced rotation, corpus striatum, Parkinson's disease, transmission electron microscope, ultra-structure*

Introduction

Parkinson's disease (PD) is characterized by an extensive loss of dopamine (DA) neurons in the substantia nigra (SN), pars campacta, and their terminals in the striatum.[1,2] In addition to neuronal loss, PD is accompanied by the formation of intra-neural inclusions such as Lewy bodies and the protein α-synuclein.[3] The nigrostriatal projection to the globus pallidus and striatum from the SN contains DA. The degeneration of nigro-striatal system due to loss of neurons in the SN and consequent loss of DA in striatum are the underlying causes of PD. The symptoms of PD can be reproduced by the blockade of DA D_2 receptors in the basal ganglia. This is commonly seen secondary to the use of typical antipsychotic medication.[4]

The anatomical and functional changes in PD may be classified into a three phase model: (1) Mesencephalic (dopaminergic neuronal loss), (2) basal ganglia (dopaminergic differentiation), and (3) cortical (functional reorganization).[5] When the SN and caudate putamen are lesioned, the ipsilateral dopaminergic fibers are lost. In response to this loss, the denervated striatum becomes more sensitive to DA. DA transporters (DATs) are expressed in dopaminergic neurons and their expression may be a significant marker of dopaminergic nerve cells. The disruption of DA transmission in the striatum is likely to be an important component of the pathophysiology of schizophrenia. The striatum is rich in DA receptors and all the known effective antipsychotic medications are known to block DA receptors.[6-8]

How to cite this article: Ravisankar P, Ravishankar P, Ravindran R, Sridevi G, Mathew J. Electron microscopic observation of normal and 2,4,5-trihydroxyl phenylethylamine (6-hydroxydopamine) lesioned corpus striatum in Wistar albino rats. J Anat Soc India 2023;72:199-204.

Article Info

Received: 28 March 2023
Revised: 03 July 2023
Accepted: 23 July 2023
Available online: 28 September 2023

Address for correspondence:
Prof. Ravisankar P, Department of Anatomy, SRM Dental College and Hospital, SRMIST, Bharathi Salai, Ramapuram Campus, Chennai - 600 089, Tamil Nadu, India.
E-mail: ravi_anat@yahoo.com

Access this article online

Website: https://journals.lww.com/joai
DOI: 10.4103/jasi.jasi_30_23
Quick Response Code:

It is known that DATs in nigrostriatal system may take part in the pathogenic mechanism of PD. The mRNA expression of DATs was decreased markedly in brain of animal model induced by 1-methyl-4-phenyl-1,2,3,6-tetrahydropyridine and in PD patients.[9,10] The administration of 2,4,5-trihydroxyphenylethylamine (6-hydroxydopamine [6-OHDA]) into the brain of the rat induces a well-established model of PD.[11-14] The loss of DA after the 6-OHDA lesionn has been established as an index of nigro-striatal damage with the apomorphine-induced rotational behavior.[15-17] In the present study, the corpus striatum of Wistar albino rats were lesioned with 6-OHDA stereotaxically and the retrograde degeneration was studied under the transmission electron microscope (TEM). We have determined the effect of 6-OHDA-induced lesion on structural changes in the striatal and extra-nigral regions in adult Wistar albino rats.

Materials and Methods

Animals

The adult Wistar albino rats weighing 180–220 g body weight were used. They were housed in pairs and allowed for 7–15 days to acclimatize to the animal care facility before the behavioral tests and surgery. The animals were maintained in an air-conditioned animal house with constant 12-h light and 12-h dark cycle. Animals were allowed *ad libitum* access to food and water when not undergoing behavioral tests and surgery. The experiments were conducted in accordance with the standard procedures of the Institutional Animal Ethical Committee (IAEC) and carried out in the department of anatomy, Dr. A. L. M. PGIBMS, University of Madras, Chennai - 600 113. The project approval number is IAEC No 01/008/03.

Experimental groups

For this experiment, the rats were randomly divided into three groups; each group consists of six male Wistar albino rats. Group-I: Control, Group-II: Sham Control in which 0.2% ascorbic acid in 0.9% saline was injected, Group-III: Lesioned in which 0.2% ascorbic acid in 0.9% saline with 6-OHDA was injected.

Stereotaxic co-ordinates

The rats were anesthetized by intra-peritoneal administration of Pentothal sodium at the dose of 40 mg/kg body weight. Incisors bars were set at – 3.3 and 1.0. The rats were immobilized in a stereotaxic frame in the flat skull position and mid-sagittal skin incision was made on the scalp for 2 cm length to expose the skull. An infusion set was prepared, consisting of a sterilized 26-gaugestainless steel cannula and hypodermic tube, which in turn, was connected to a 10 µl Hamilton micro syringe (P/N: 80300/00 Hamilton Bonaduz AG, CH-7402, Switzerland).

The following stereotaxic co-ordinates were used to target the dorsolateral part of the striatum: anteroposterior (AP) = 0.2 mm, mediolateral (ML) = 3.2 mm, and dorsoventral (DV) = 4.5 mm from the bregma. Another target was the dorsomedial part of striatum: AP = 1.1 mm, ML = 2.4 mm and DV = 3.5 mm. These targets of lesions were reached using the stereotaxic atlas of Paxinos and Watson.[18] After making the AP and ML co-ordinates, a hole (1.6 mm diameter) was made on the skull with dental drill. Then the cannula (1.5 mm diameter) was placed through the holes drilled in the skull and DV co-ordinates were used to target the area of striatum from the duramater [Figure 1a-d].

Drug and dosage

The 2,4,5-trihydroxyphenylethylamine (6-OHDA) is a selective catecholaminergic neurotoxin, which has been widely used to investigate the pathogenesis and progression of PD. The specificity of 6-OHDA neurotoxicity has been associated with its uptake and accumulation by transport mechanism specific for catecholaminergic neurons. One mg of 6-OHDA was dissolved in 0.5 ml of ascorbate saline (0.02 g of ascorbic acid was dissolved in 10 ml of sterile normal saline, to prepare ascorbate saline). The normal saline was prepared by dissolving 0.9 g of sodium chloride in 100 ml of deionized water. It was autoclaved and used to prepare ascorbate saline. Just 30 min before the 6-OHDA injection, the desipraminehydrochlordie (25 mg/kg of body weight) was injected intra-peritoneally to prevent the uptake of toxin by other neurons. In each site with the concentration of 20 µg in10 µl at the rate of 0.5–1 µl/minute of 6-OHDA was manually injected [Figure 2].

Postoperative care

Care was taken to revive the animals from anesthesia and was monitored till completely recovered. The antibiotic (Gentamycin = 0.5 mg/kg body weight) was given two times a day for 3 days to prevent the infection of surgical wound. Seven days after the surgery, the animals were continued with the behavioral studies. To record the

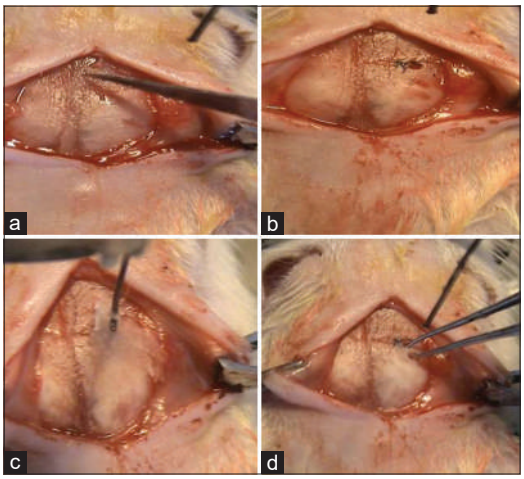

Figure 1: Rat skull has been exposed after fixing in stereotaxic frame. (a) Skull has been exposed after making skin incision, (b) After making first coordinate (right side), (c) Injection of 6-hydroxydopamine on the right side of corpus striatum, (d) After making second coordinate

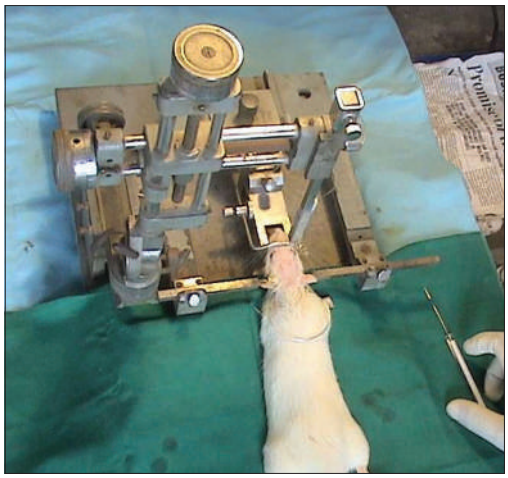

Figure 2: Rat fixed in stereotaxic frame and 6-hydroxydopamine (6-OHDA) injection. Injection of 6-OHDA with the help of 10 μl Hamilton syringe, 20 μg in 10 μl ascorbate saline was injected at the rate of 0.5–1 μl/min

behavioral activity, the videos and photographs were taken periodically for all the groups till the end of the period.

Apomorphine-induced rotation

Nonselective DA agonist apomorphine hydrochloride (A4393, sigma Aldrich, US) (0.05 mg/kg/bw) was injected subcutaneously in the neck region between 7 and 30 days after the 6-OHDA lesion. We followed the basic principles of rotational behavior study described by Ungerstedt; Olsson *et al*.[15,17] Since we could not design the "automatic" rat rotometer; we simplified the observation on rotational behaviour. Each animal was placed in a glass cylinder measuring 30 cm height and 22 cm diameter and the number of contralateral rotation of the animals in cylinder were counted for a period of 60 min.

Tissue preparation for transmission electron microscope

Animals from Group I and Group III after 120 days of survival were sacrificed for the ultra-structural investigation of corpus striatum. The animals were anesthetized with Pentothal sodium using an over dose of 120 mg/kg of body weight, through intra peritoneal route. Transcardially, the animals were perfused with normal saline followed by the 4% glutaraldehyde for 20 min period, then the brains were removed and fixed for an additional 4 days in 3% glutaraldehyde and washed in buffer. Post fixation by 1% Osmium tetroxide and washed in buffer. This double fixation gives stability during dehydration, embedding and electron bombardment during transmission in TEM. Further, it also provides staining contrast, decreased distortion and fixes fine cellular ultra-structure which is suitable for brain tissue. Then, the tissue was dehydrated by the ascending series in graded alcohol (50%–100%) and clearing by propylene oxide and infiltrated by propylene oxide and epoxy resin. Finally, tissues were embedded in siliconized rubber mold with epoxy resin kept in at 60°C for 48 h, cool down to the room temperature. Blocks were taken for sectioning and polymerization.

Sectioning

One micron thick sections were cut through ultra-microtome (Leica ultracut-UCT) with glass knife and stained by toludine blue. Light microscopic observation was extremely useful when sections are needed to give a general idea of the orientation of the tissue and for making the areas of (able to cut ultrathin section) interest in the block face prior to further trimming of blocks for ultra microtomy. Ultrathin section (<100 nm) was cut through ultra-microtome (Leica) with diamond knife (Diatome). Ultrathin sections were taken on copper grid and stained (double metallic) with uranyl acetate and Reynolds solution (sodium citrate + lead nitrate) which gives a good contrast. Then, the sections were transmitted in TEM (Phillips, Netherland) and photographed.

Results

Apomorphine-induced rotations

In this study, the sham lesioned animals (Group II) did not show any abnormal rotation after the apomorphine injection in all the duration of rotational behaviour test. In group III animals, there was significant increase in the controlateral rotation (1st week = 26.60 folds; 2nd week = 27.04 folds; 3rd week = 25.75 folds, and 4th week = 25.72 folds) when compared with the nonlesioned control animals in all the period [Table 1].

Electron microscopic observation

Numerous small cells in the striatum showed a simple cytoplasmic structure, while the large cells possess a complicated fine structure. Under the electron microscope, two kinds of cell can be differentiated in this region in preparations fixed with glutaraldehyde-osmium. The cells with large round nucleiin a light cytoplasm resemble the light-nucleated cell. The cells with smaller and denser nucleus with deep indentations, and a more densely packed cytoplasmmay coincide with the dark-nucleated cells. Transverse section of normal nerve fibers with varying size having few mitochondria in axons was observed [Figure 3a and b]. White matter adjacent to corpus striatum can also be observed, shows thick and thinly myelinated nerve fibers. The neuropil area showed a few axo-dendritic synapses with type 1 synaptic vesicle [Figure 3c and d]. The glial cells such as oligodendrocytes and astrocytes with few nerve fibers were also seen around [Figure 4a-c].

The6-OHDA lesioned corpus striatum showed that the degenerating nigro-striatal axon terminals which were fragmented and easily recognized in the area of striatum. Most of the neuropil area of striatum observed a similar stage of degeneration, being highly electron dense and containing few recognizable organelles other than swollen mitochondria and some vesicular elements. The axo-dendritic synapses which were primarily with spines were identified by the presence of a wide

Table 1: Rotation for 60 min after apomorphine induced in 6-hydroxydopamine lesion and human amniotic epithelial cells transplantation from the 1st week to 4th week

Group	1st week	2nd week	3rd week	4th week
Group I	9.00±1.29	10.50±0.42	11.50±0.95	11.33±1.22
Group II	9.00±0.81	7.50±0.95	6.83±0.40	6.66±0.66
Group III	255.66±18.17[a,***]	305.00±19.76[a,***]	319.33±26.77[a,***]	314.16±20.92[a,***]

***$P \leq 0.001$, [a]Comparison between Group I versus III. Values were measured in the number of rotation for 50 min after 0.05 mg/kg/sc apomorphine. Each value represents mean±SE of six rats. Group I: Control, Group II: Sham control, Group III: 6-OHDA lesioned. 6-OHDA: 6-hydroxydopamine, SE: Standard error

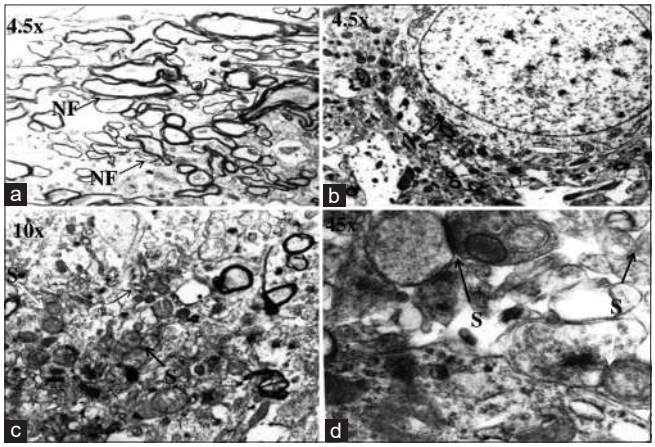

Figure 3: Normal corpus striatum. Electron microscopic view of normal corpus striatum in different magnifications. (a) Transverse section of normal nerve fibers under lower magnification (×4.5), (b) Nucleus of normal nerve cell (×4.5), (c) Neuropil area showing axo-dendritic synapses (S) (×10), (d) Neuropil area showing few axo-denditic synapses (S) (×45). NF: Nerve fibres, S: Synapses, NC: Normal neuronal cell

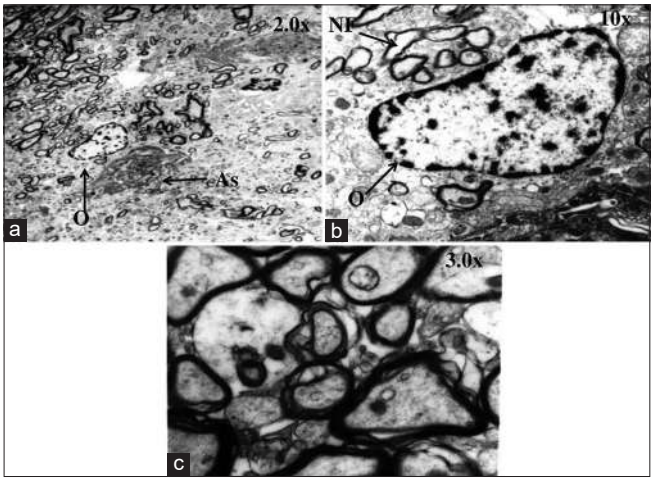

Figure 4: Normal corpus striatum. Electron microscopic view of normal corpus striatum in different magnifications. (a) Oligodendrocytes and Astrocyte with it process (×2.0), (b) Oligodendroglia with nerve fibers (×10), (c) Transverse section of normal nerve fibers under lower magnification (×3.0). O: Oligodendrocytes, As: Astrocyte, NF: Nerve fibres,

spread synaptic clefts with post synaptic density. The axons were thick and thinly myelinated nerve fibers showed loosening or separation of myelin lamellate in 6-OHDA lesioned corpus striatum [Figure 5a]. The glial cells such as astrocytes showed similar to nerve cells with dense electron nucleolus and few nerve fibers around it [Figure 5b]. The oligodendroglia contains few stalks of rER, few mitochondria and part of astrocytic cytoplasm showed dilated Golgi complex [Figure 5c]. The fragmentation of glial cells and few swollen mitochondria surrounding cytoplasmic process have been observed [Figure 5d].

Numerous axon terminals, which belong to striatal nerve cells or other nuclei of glial cells, have been demarcated. A few types of synaptic vesicles were distinguished by their size or by presences of dense granules on their membranes, which seems to be specific to corpus striatum. The neuropil area showed few unclear axo-dendritic synapses with swollen mitochondria in the neuronal process under higher magnification [Figure 6a-c].

The present work demonstrates the effects of 6-OHDA in degeneration of striatal neurons as well as the degree of apomorphine hydrochloride-induced stereotyped rotational behavioral in experimental rats. Subsequently, changes in glial cells, such as astroglia, oligodendroglia, and microglial activation following the dopaminergic neuron lesion were observed [Figure 6d].

Discussion

We assessed the motor function using apomorphine-induced rotation test, considered as reliable objective and closely related to the degree of nigrostriatal dysfunction, as well as DA depletion. Previous studies have demonstrated that the intra-striatal injection of 6-OHDA causes retrograde degeneration of SN dopaminergic neurons, resulting in the depletion of the striatal DA.[19,20]

The 6-OHDA is a neurotoxin taken up into dopaminergic neurons through the DAT, where the compound is autooxidized to form semiquinone and superoxide anions that subsequently are converted to hydroxyl radicals through interaction with H_2O_2. Injection of the toxin into striato-nigral projections results in selective damage to dopaminergic neurons and has been used to create widely used models of PD in rats.[21] Ingham *et al*. found that loss of asymmetric synapses, remarkably same as the decrease or loss in dendritic spine density found on medium sized spiny neurons 26 days after the 6-OHDA lesion.[22,23] Medium sized spine and synapses loss complement with each other and consistent with the suggestion that loss of spine after the 6-OHDA lesion is accompanied by loss of a symmetric

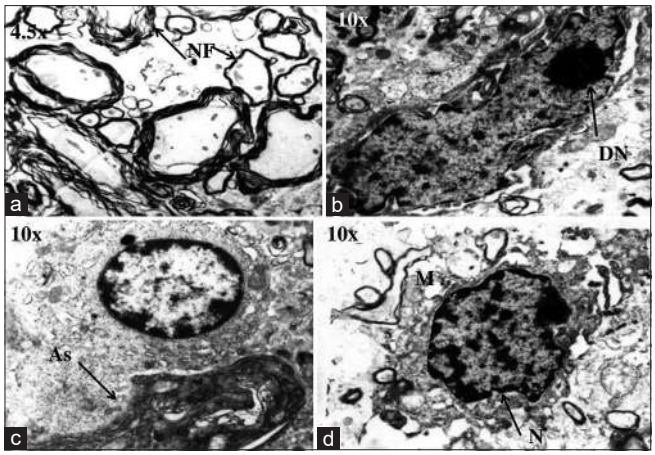

Figure 5: 6-hydroxydopamine (6-OHDA) lesioned corpus striatum. Electron microscopic view of 6-OHDA lesioned corpus striatum in different magnifications, (a) Thick and thinly myelinated nerve fibers showing loosening or separation of myelin lamellae (NF) (×4.5), (b) Astrocyte with electron dense nucleus with few nerve fibers around (DN) (×10), (c) Oligodendrocytes and part of astrocyte. Oligodendrocytes contains few stalks of unfixed rER and a few Mitochondria-Part of astrocytic cytoplasm shows dilated Golgi complexes (×10), (d) Uneven shaped nucleus probably astrocyte and a few swollen mitochondria (M) surrounding cytoplasmic processes (×10). NF: Nerve fibers, As: Astrocytes, DN: Dense nucleolus, M: Mitochondria

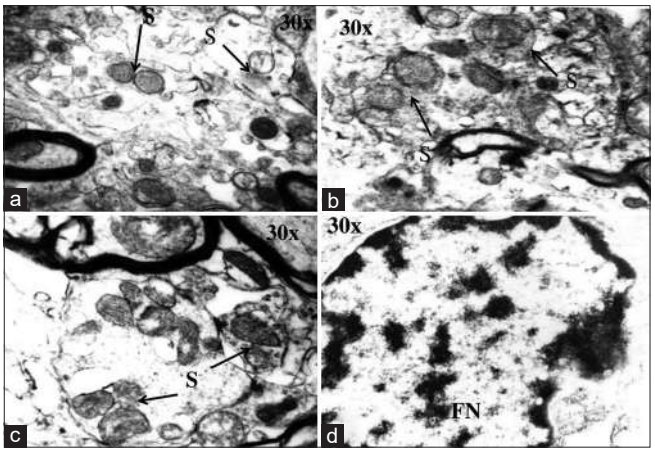

Figure 6: 6-hydroxydopamine (6-OHDA) lesioned corpus striatum. Electron microscopic view of 6-OHDA lesioned corpus striatum in different magnifications, (a) Neuropil area showing a few unclear axo-dendritic synapses (×30), (b) Neuropil area showing unclear axo-dendritic synapses and swollen mitochondria in neuronal processes (×30), (c) Unclear axo-dendritic synapses in an neuropil area (×30), (d) Fragmented nucleus of the nerve cell (×30). S: Synapses, FN: Fragmented nucleus

synapses on these spines. Morphological plasticity has been shown to occur in enkephalin-immunoreactive axons collateral and terminal bouton of medium sized spiny neurons in the rat neostriatum and globus pallidus after unilateral 6-OHDA lesion of the nigrostriatal pathway.[24-26]

We suggest that there are at least three possibilities for spine and synapse to disappear, first, spine and synapses may be lost from a specific neuronal subtypes; second, there may be a specific origin of the presynaptic synapses that are lost, and third, the loss of DA may have a generalized action that is independent of presynaptic or post synaptic origins of the lost synapses.

We have recently reported that the changes and recovery of antioxidants and the level of DA and its metabolites changes in 6-OHDA lesioned and HAE cells transplanted brain region in corpus striatum.[27,28]

Conclusion

The present findings confirm the utility of this staining protocol for TEM. The ultra-structural changes in corpus striatum show that the reduction of different types of synapses, neuronal, and glial cells damage in the striatal neurons and correlated with the apomorphine-induced rotations. Furthermore, these findings suggest that decreased neuronal volume as well as number contributes to the functional deficits observed after unilateral 6-OHDA lesion may also play a role in PD. The present study provides further ultra-structural view on corpus striatum in normal and 6-OHDA-induced PD rats. Further molecular studies are needed to authenticate the 6-OHDA lesion in corpus striatum.

Acknowledgments

The authors would like to thank the Department of Gastroenterology, Christian Medical College and Hospital, Vellore - 632 004, Tamil Nadu, India, for providing the facility to use Electron Microscopic studies. We also thank Dr. BK. Chandrasekhar Sagar, Professor of Electron Microscopy, Officer in-charge, Electron Microscopy-Common Research Facility, Department of Neuropathology NIMHANS, Bangaluru-560029, Karnataka, India, for his interpretation of images of normal and 6-OHDA lesioned corpus striatum. We furthermore thank the Department of Anatomy, Dr. A. L. M. PGIBMS, University of Madras for providing the animal house facility and financial support in the form of Tamil Nadu Junior Research Fellowship (TNJRF).

Financial support and sponsorship

Nil.

Conflicts of interest

There are no conflicts of interest.

References

1. Hornykiewicz O. Parkinson's disease: From brain homogenate to treatment. Fed Proc 1973;32:183-90.
2. Calne DB. Progress in Parkinson's disease. N Engl J Med 1984;310:523-4.
3. Spillantini MG, Schmidt ML, Lee VM, Trojanowski JQ, Jakes R, Goedert M. Alpha-synuclein in lewy bodies. Nature 1997;388:839-40.
4. Lingford-Hughes A, Kalk N. Core Psychiatry E-book. 3rd ed. London: Elsevier; 2012.
5. Péran P, Cherubini A, Assogna F, Piras F, Quattrocchi C, Peppe A, *et al.* Magnetic resonance imaging markers of Parkinson's disease nigrostriatal signature. Brain 2010;133:3423-33.

6. Seeman P, Chau-Wong M, Tedesco J, Wong K. Brain receptors for antipsychotic drugs and dopamine: Direct binding assays. Proc Natl Acad Sci U S A 1975;72:4376-80.
7. Creese I, Burt DR, Snyder SH. Dopamine receptor binding predicts clinical and pharmacological potencies of antischizophrenic drugs. Science 1976;192:481-3.
8. Lahti AC, Holcomb HH, Weiler MA, Medoff DR, Tamminga CA. Functional effects of antipsychotic drugs: Comparing clozapine with haloperidol. Biol Psychiatry 2003;53:601-8.
9. Miller GW, Gainetdinov RR, Levey AI, Caron MG. Dopamine transporters and neuronal injury. Trends Pharmacol Sci 1999;20:424-9.
10. Counihan TJ, Penney JB Jr. Regional dopamine transporter gene expression in the substantia nigra from control and Parkinson's disease brains. J Neurol Neurosurg Psychiatry 1998;65:164-9.
11. Kirik D, Rosenblad C, Björklund A. Characterization of behavioral and neurodegenerative changes following partial lesions of the nigrostriatal dopamine system induced by intrastriatal 6-hydroxydopamine in the rat. Exp Neurol 1998;152:259-77.
12. Blum D, Torch S, Lambeng N, Nissou M, Benabid AL, Sadoul R, *et al.* Molecular pathways involved in the neurotoxicity of 6-OHDA, dopamine and MPTP: Contribution to the apoptotic theory in Parkinson's disease. Prog Neurobiol 2001;65:135-72.
13. Betarbet R, Sherer TB, Greenamyre JT. Animal models of Parkinson's disease. Bioessays 2002;24:308-18.
14. Deumens R, Blokland A, Prickaerts J. Modeling Parkinson's disease in rats: An evaluation of 6-OHDA lesions of the nigrostriatal pathway. Exp Neurol 2002;175:303-17.
15. Ungerstedt U. Stereotaxic mapping of the monoamine pathways in the rat brain. Acta Physiol Scand Suppl 1971;367:1-48.
16. Arbuthnott G, Fuxe K, Ungerstedt U. Central catecholamine turnover and self-stimulation behaviour. Brain Res 1971;27:406-13.
17. Olsson M, Nikkhah G, Bentlage C, Björklund A. Forelimb akinesia in the rat Parkinson model: Differential effects of dopamine agonists and nigral transplants as assessed by a new stepping test. J Neurosci 1995;15:3863-75.
18. Paxinos G, Watson C. The Rat Brain in Sterotaxic Coordinates. 2nd ed. New York: Academic Press; 1986.
19. Schwarting RK, Bonatz AE, Carey RJ, Huston JP. Relationships between indices of behavioral asymmetries and neurochemical changes following mesencephalic 6-hydroxydopamine injections. Brain Res 1991;554:46-55.
20. Singh S, Kumar P. Neuroprotective potential of curcumin in combination with piperine against 6-hydroxy dopamine induced motor deficit and neurochemical alterations in rats. Inflammopharmacology 2017;25:69-79.
21. Schwarting RK, Huston JP. The unilateral 6-hydroxydopamine lesion model in behavioral brain research. Analysis of functional deficits, recovery and treatments. Prog Neurobiol 1996;50:275-331.
22. Ingham CA, Hood SH, Arbuthnott GW. Spine density on neostriatal neurones changes with 6-hydroxydopamine lesions and with age. Brain Res 1989;503:334-8.
23. Ingham CA, Hood SH, van Maldegem B, Weenink A, Arbuthnott GW. Morphological changes in the rat neostriatum after unilateral 6-hydroxydopamine injections into the nigrostriatal pathway. Exp Brain Res 1993;93:17-27.
24. Ingham CA, Hood SH, Arbuthnott GW. A light and electron microscopical study of enkephalin-immunoreactive structures in the rat neostriatum after removal of the nigrostriatal dopaminergic pathway. Neuroscience 1991;42:715-30.
25. Ingham CA, Hood SH, Mijnster MJ, Baldock RA, Arbuthnott GW. Plasticity of striatopallidal terminals following unilateral lesion of the dopaminergic nigrostriatal pathway: A morphological study. Exp Brain Res 1997;116:39-49.
26. Ingham CA, Hood SH, Taggart P, Arbuthnott GW. Plasticity of synapses in the rat neostriatum after unilateral lesion of the nigrostriatal dopaminergic pathway. J Neurosci 1998;18:4732-43.
27. Ravisankar P, Ravishankar P, Prithviraj E, Ravindran R. Evaluation of antioxidants in discrete regions of brain after the transplantation of human amniotic epithelial cells in 2,4,5-trihydroxyphenylethylamine-lesioned Wistar albino rats. Int J Appl Basic Med Res 2022;12:103-10.
28. Ravisankar P, Ramesh Kumar R, Ravindran R, Omprakash KV. Neurochemical observations after the transplantation of human amniotic epithelial cells in 2, 4, 5-trihydroxyphenylethylamine (6-OHDA) induced Parkinsonism disease model in Wistar albino rats. Int J Anat Appl Physiol 2021;07:164-73.

Original Article

Investigation of Intrathoracic Morphology in Computed Tomography Images of Individuals with Anterior Chest Wall Deformity

Mustafa Ozturk, Harun Ulger[1], Ibrahim Ethem Ozsoy[2], Mehmet Akif Tezcan[2], Ahmet Savranlar[3]

Kayseri Health Practice and Research Center, University of Health Sciences Turkey, [1]Department of Anatomy, University of Erciyes, School of Medicine, Departments of [2]Thoracic Surgery and [3]Radyology, Kayseri Health Practice and Research Center, University of Health Sciences Turkey, Kayseri, Turkey

Abstract

Objective: Morphological determination of the location, position, and level of the intrathoracic organs in relation to the thoracic vertebrae of individuals with anterior chest wall deformity using computed tomography (CT) images. **Study Design:** Retrospective study. **Place and Duration of Study:** Kayseri Health Practice and Research Center, University of Health Sciences Turkey, Kayseri, Turkey, January 2020–January 2022. **Subjects and Methods:** In the study, clinical and morphological measurements of intrathoracic organs were performed on thorax CT images of 80 patients with pectus excavatum (PE) and 70 pectus carinatum (PC) diagnose. **Results:** The mean Haller index (HI) of patients with PE was measured at the highest T11 (Female: 3.79 cm, Male: 3.67 cm) and lowest at T7 (Female: 3.41 cm, Male: 3 cm). The mean HI at all levels (T5-T11) was higher than healthy individuals ($P < 0.05$). PE severity was higher in women than men. Due to the increase in the severity of PE, it was determined that the heart was displaced in the left anterior, left posterior and downward directions, and the cardiothoracic ratio (CTR) increased. In severe cases, it was seen that the aorta was located on the left side of the corpus vertebrae in the left posterior region. In patients with PC, the most severe HI value was measured at the T7 level (1.54 cm) in women and at the T9 level (1.42 cm) in men. There was no significant difference between the CTRs of patients with PC and healthy individuals. **Conclusion:** We think that knowing the location, position, and levels of the organs in cases with anterior chest wall deformity will shed light on clinical studies.

Keywords: *Cardiothoracic ratio, Haller index, pectus carinatum, pectus excavatum, thorax morphology*

Introduction

Anterior chest wall deformities include many congenital diseases. The most common (80%–90%) type of deformity in the community is pectus excavatum (PE) and develops with posterior depression of the sternum and cartilage costal. Pectus carinatum (PC), on the other hand, is the second most common (15%–16%) type in the community, and it is the type of deformity in which the anterior chest wall protrudes forward excessively. Other deformities account for approximately 3%–4% of anterior chest wall deformities.[1-3]

Anterior chest wall deformities begin to appear from birth and become more evident during childhood and adolescence when bone development continues rapidly.[1,2] Today, although there are many indices for measuring pectus severity and deciding on surgery, the Haller index (HI) is the most commonly used index in the clinic.[4-6]

Knowing the location of the intrathoracic organs is important in surgery, especially when corrective surgery is applied for anterior chest wall deformities.[7-9] Depending on the severity of the deformity, many morphological changes such as cardiac rotation, right ventricular compression, and sternum torsion may occur in the intrathoracic organs and formations in patients with PE.[10,11]

In the literature review on anterior chest wall deformities, it is seen that studies are generally the ones for the diagnosis and treatment of the disease or indexing studies for surgical applications. However, there are very limited studies on the position, location, and levels of the organs in the chest cavity due to these deformities.[4-6]

In this study, we aimed to morphologically determine the location, position, and level of the intrathoracic organs of the individuals with anterior chest wall deformity according to the thoracic vertebrae using computed tomography (CT) images.

How to cite this article: Ozturk M, Ulger H, Ozsoy IE, Tezcan MA, Savranlar A. Investigation of intrathoracic morphology in computed tomography images of individuals with anterior chest wall deformity. J Anat Soc India 2023;72:205-10.

Article Info

Received: 03 October 2022
Accepted: 23 July 2023
Available online: 28 September 2023

Address for correspondence:
Dr. Mustafa Ozturk, Kayseri Health Practice and Research Center, University of Health Sciences Turkey, Kayseri, Turkey.
E-mail: mustafa2013@gmail.com

Access this article online

Website: https://journals.lww.com/joai
DOI: 10.4103/jasi.jasi_138_22
Quick Response Code:

Subjects and Methods

This study was planned retrospectively, and ethics committee approval was obtained (Date: March 02, 2020, Decision No. 2020/28).

Within the scope of the study, the data of individuals who applied to the Kayseri City Training and Research Hospital Thoracic Surgery Polyclinic between January 1, 2010, and December 31, 2020, and who had a thorax CT scan were retrospectively scanned in digital environment in the presence of a thoracic surgeon and radiology specialist, and the patients with detected anterior chest wall deformity were evaluated for deformity, type, age, and gender were included in the study.

Within the scope of the clinical evaluation, the PACS module was opened in the Hospital Information Management System and the thorax CT images of the patients and healthy individuals with PE deformity were found at the lower levels of the T5-T11 vertebrae in the axial section, and the vertebrae with the highest sternum protrusion on the axial section of the patients with PC deformity. HI measurements were performed at the lower level [Figure 1a]. HI value; on the axial section of the thorax CT image, the transverse length with the widest inside of the chest was found by dividing the length with the shortest intrathoracic anterior-posterior distance [Figure 1a].

The HI value is also an indicator of the severity of the deformity. Pectus severity values were evaluated as mild if they were 2.5–3.2 cm, moderate if they were between 3.2 and 3.5 cm, and severe deformities if they were >3.5 cm.

The cardiothoracic ratio (CTR) was calculated by dividing the transverse length of the heart by the transverse length of the thorax to determine the intrathoracic location of the heart [Figure 1b]. The inside of the chest was divided into four regions (left anterior region, left posterior region, right anterior region, and right posterior region) on the axial sections at the levels where PE and PC were most severe, and the localization of the intrathoracic organs was examined morphologically and morphometrically [Figure 1c]. In addition, it was determined what percentage of the heart was in the thorax to the right of the midline or the left of the midline. The obtained values were compared with the values of healthy individuals.

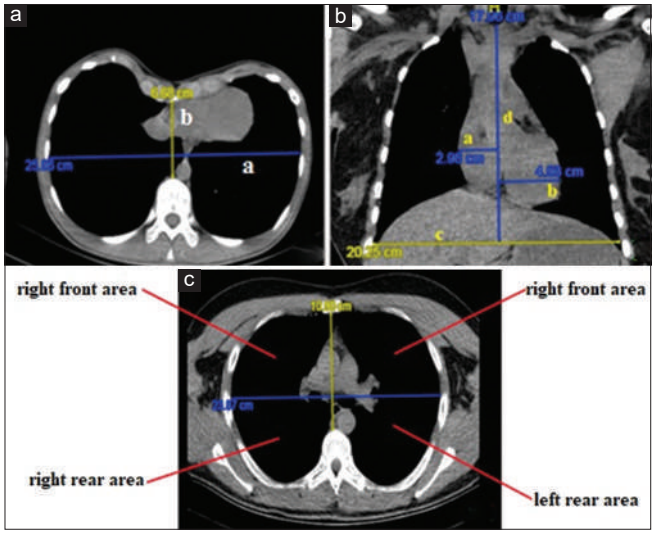

Figure 1: (a) Haller index measurement (a/b), (b) Calculation of cardiothoracic ratio, and (c) Division of the inside of the chest into four regions in the axial section

Results

In the study, 6000 patient files were scanned and 1112 cases with anterior chest wall deformity were found. Of these cases, approximately 50% (554 cases; 475 men, 79 women) were PE, 47% (520 cases; 433 men, 87 women) were PC, and 3% were cases with other deformities (sternal deformities in 3 male and 1 female patients, pectoral muscle deficiency in 1 male patient, and other rib deformities in 10 female and 23 male patients).

Eighty PE (20 women and 60 men), 70 PC (18 women and 52 men), and 110 healthy individuals were included in the study. Most of the patients with PE and PC deformities (75%) were men. The highest and lowest HI values and thoracic levels of PE and healthy individuals are given in Figure 2.

When the mean HI values of T5-T11 levels of patients with PE and healthy individuals without deformity were compared [Table 1], the values of patients with PE were found to be higher ($P < 0.05$).

Six (30%) of 20 female patients with PE were mild, 3 (15%) were moderate, 11 (55%) were severe, 25 (41%) of 60 male patients with PE were mild, 13 (21%) were moderately severe and 22 (37%) were severe. Although men constituted approximately 75% of the total number of patients with PE, the severity of pectus was higher in female patients than in males.

According to the thoracic vertebral levels (T5-T11), the mean pectus severity values are 4.44 cm at the highest T9 level in female patients, 2.85 cm at the lowest T11 level,

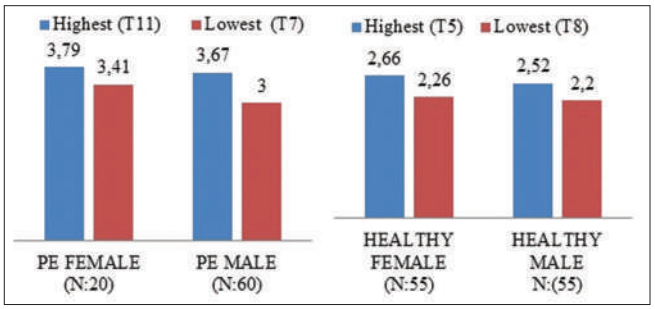

Figure 2: The highest and lowest values of haller index (cm) in patients with pectus excavatum and healthy individuals

and 3.95 cm at the highest T11 level in male patients, and 3.45 cm at the lowest T9 and T10 levels.

In the calculation for the intrathoracic location of the heart in patients with PE, the mean CTR was found to be 0.49 in female patients, 0.45 in healthy women, 0.46 in male patients, and 0.43 in healthy men. When patients with PE and healthy individuals were compared according to gender, the difference between the mean CTR ratios of male and female patients with PE and healthy females and males was found to be statistically significant [$P < 0.05$, Table 2].

The results show that the heart shifts slightly to the left due to the increase in pectus severity in patients compared to the control group [Figure 3].

Considering the location of the heart in the mean chest cavity in patients with PE [Table 2], there was no difference between women with PE and healthy women, but the difference between the ratio of heart placement to both the right and left between men with PE and healthy men was found remarkable [$P < 0.05$, Table 2].

In the CT images of healthy individuals at T8 and T9 levels, the heart is located in the 2/3 left anterior region, the aorta is located in the left posterior region, in the left anterior of the corpus vertebrae, and the esophagus is located in front of the aorta, and the intra-abdominal organs are located in the sections at T10 and T11 levels [Figure 4].

In patients with mild PE at T8-T11 levels, 1/3 of the heart is in the right anterior region, 2/3 is in the left anterior region, in moderately severe cases, almost the entire part of the heart is in the left anterior region, in severe cases, it was observed that the heart was located 1/2 in the left anterior region and 1/2 in the left posterior region. In severe cases at the T9 level, it was seen that the aorta was located in the left posterior region and on the left side of the corpus vertebrae, and the esophagus was located in front of the left posterior region of the aorta. The most striking finding at the T10 level was that the heart and lungs could still be seen in this section in mild, moderate, and severe cases. However, in the image of the healthy individual, intra-abdominal organs were seen at the same levels.

In the study, it was observed that the morphological changes in the T8-T11 levels, where PE is most severe, generally shifted to the left anterior region, and then to the left posterior region as the severity of the deformity increased, depending on the increase in pectus severity. In addition, it was determined that the inferior vena cava was located between the sternum and the corpus vertebra due to the increase in the severity of the pectus. It was remarkable that the heart was still visible at the T10 level, especially in PE patients. This showed that, depending on the pectus severity, the heart not only displaced left anteriorly and posteriorly, but also displaced downwards.

Of the 70 patients with PC, 74% were males and 26% were females. When PC patients were classified according to their subtypes, it was observed that 62 patients (44 males and 18 females) (85.5%) were chondrogladiolar type; on the other hand, chondromanumbrial deformity was detected in 4 male patients and mixed type deformity in 4 male patients. The level where the deformity was most severe

Table 1: Haller index averages of T5–T11 levels of individuals with pectus excavatum and healthy individuals

Gender	Thoracic levels	$\bar{X}$±SS		*t-test**	*P*
		PE (*n*=80)	Healthy individuals (*n*=110)		
Female	T5	3.78±0.75	2.72±0.48	5.847	<0.05
	T6	3.48±0.83	2.46±0.35	5.331	<0.05
	T7	3.41±0.88	2.34±0.31	5.313	<0.05
	T8	3.56±1.20	2.31±0.28	4.599	<0.05
	T9	3.70±1.10	2.38±0.31	5.243	<0.05
	T10	3.67±0.90	2.47±0.33	5.158	<0.05
	T11	3.79±0.80	2.65±0.38	3.125	<0.05
Male	T5	3.33±0.70	2.56±0.38	7.438	<0.05
	T6	3.09±0.64	2.37±0.37	7.416	<0.05
	T7	3.00±0.60	2.28±0.34	8.106	<0.05
	T8	3.07±0.61	2.23±0.33	9.285	<0.05
	T9	3.28±0.75	2.32±0.37	8.788	<0.05
	T10	3.46±0.79	2.42±0.37	8.056	<0.05
	T11	3.67±1.19	2.42±0.33	3.345	<0.05

t-test*: Independent Groups *t*-Test. PE: Pectus excavatum, $\bar{X}$: Arithmetic mean, SS: Standard deviation

Table 2: Cardiothoracic ratio and percentage location of the heart in the thorax in healthy individuals and the ones with pectus excavatum deformity

	Gender	Patients with PE (*n*=80)		Healthy individuals (*n*=110)		*t-test**	*P*
		$\bar{X}$±SS	Median (minimum–maximum)	$\bar{X}$±SS	Median (minimum–maximum)		
CTR average	Female	0.49±0.52	0.49 (0.39–0.58)	0.45±0.52	0.45 (0.35–0.59)	2.957	<0.05
CTR average	Male	0.46±0.06	0.45 (0.36–0.59)	0.43±0.05	0.41 (0.33–0.60)	2.892	<0.05
Right-sided placement rate of the heart	Female	31.65±7.69	32.25 (16.98–48.08)	34.02±5.27	34.27 (19.17–44.91)	−1.276	0.213
Left-sided placement rate of the heart	Female	68.35±7.69	67.75 (51.92–83.02)	65.98±5.27	65.73 (55.09–80.83)	1.276	0.213
Right-sided placement rate of the heart	Male	32.80±7.86	33.86 (13.18–46.70)	35.61±5.79	34.57 (25.64–46.45)	−2.191	<0.05
Left-sided placement rate of the heart	Male	67.19±7.86	66.14 (53.30–86.82)	64.39±5.79	65.43 (53.55–74.36)	2.191	<0.05

t-test*: IndependentGroups t-Test, CTR: Cardiothoracic ratio, PE: Pectus excavatum, $\bar{X}$: Arithmetic mean, SS: Standard deviation

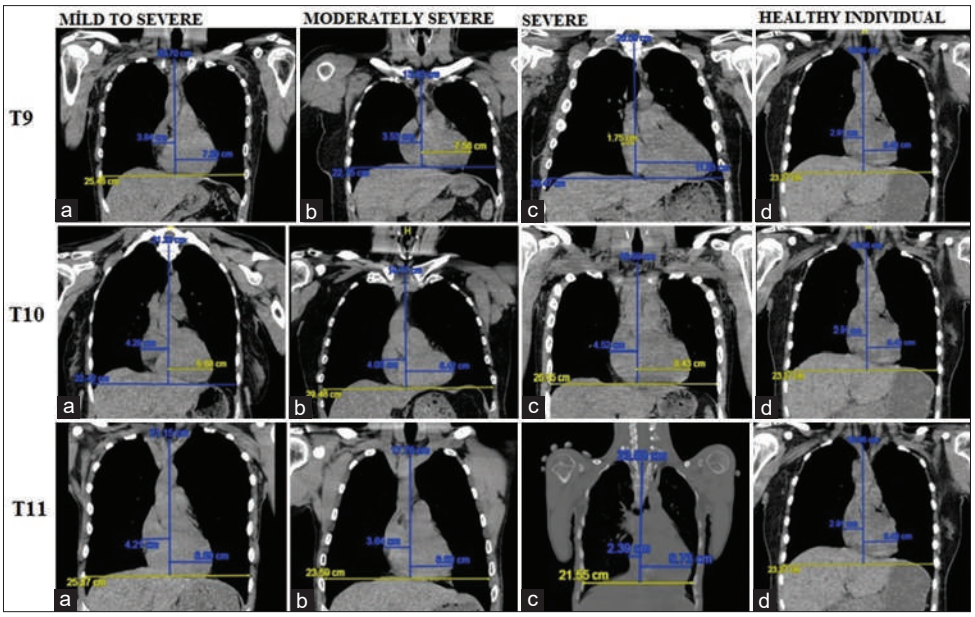

Figure 3: Cardiothoracic ratio calculations according to pectus severity at T9-T11 levels of patients with pectus excavatum

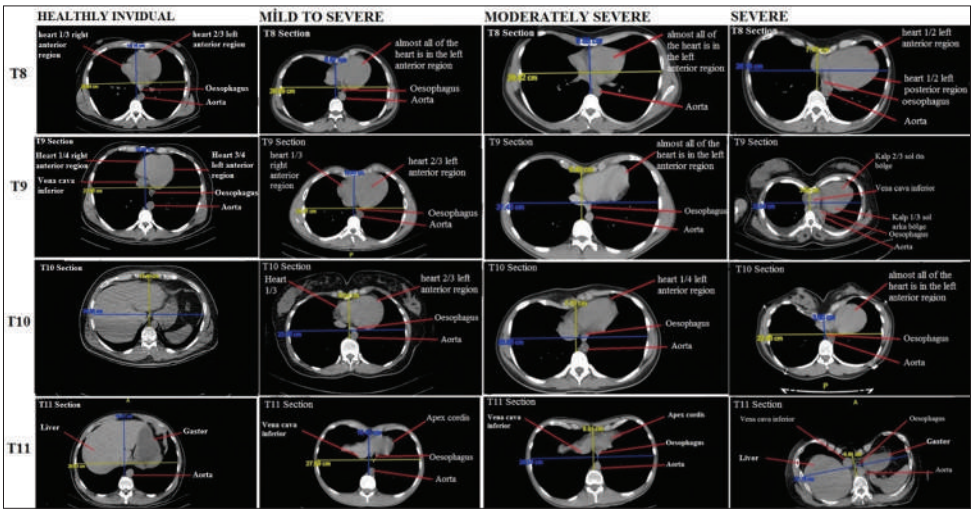

Figure 4: Changes in intrathoracic morphology at T8-T11 levels of pectus excavatum (mild, moderate and severe) and healthy individuals

was observed to be T8 level (18 patients) and then T9 level (15 patients). According to gender, the most severe level of deformity was measured at the T7 level (1.54 cm) in the female patient and the T9 level (1.42 cm) in the male patient. While there were no serious morphological changes in the chest in T5-T7 sections of patients with PC and healthy individuals, in T8-T10 sections it was observed that the distance between the heart and the corpus vertebrae particularly increased, the chest was compressed from the sides, and protruded forward, and the anterior-posterior distance increased.

The CTR was 0.42 in female patients with PC, 0.45 in healthy women, 0.42 in male patients with PC, and 0.43 in healthy men. According to these results, there was no significant difference between male and female patients with PC and healthy female and male individuals.

The location of the heart in the mean thoracic cavity in female patients with PC was 63.86% on the left, 65.98% on the left in healthy women, 64.43% on the left in male patients, and 64.39% on the left in healthy men. According to these results, the location of the heart in the thorax due to PC deformity did not change in male patients, while a decrease in favor of the left side and an increase in favor of the right side were detected in female patients.

Discussion

In the community, PE is seen more frequently than PC. In many studies conducted in student and patient groups, the number of patients with PE was found to be higher than the number of patients with PC.[12-15] In two different studies conducted on primary and secondary school students in Turkey in 2016 and 2018, the number of PC patients was

found to be higher than the number of PE patients.[16,17] In our study, although the rate of PE (49.8%) was slightly higher in 1112 cases with chest deformity, it was found to be close to the rate of PC (46.8%).

HI is an important index used to measure the severity of the deformity and this measurement is made at the thoracic level where the deformity is most severe. However, studies on HI measurements at other thoracic vertebral levels where deformity is seen are limited. In a study in which the HI value at the T3-T11 level of healthy individuals between the ages of 8 and 18 years was calculated, the mean value was 2.74 in 203 female individuals and 2.56 in 230 male individuals.[18] In our study, the mean HI at T5-T11 levels was measured as 2.42 in 55 healthy female individuals and 2.37 in healthy male individuals.

In a study on the prevalence of PE, in 297 (231 male, 66 female) patients, pectus severity values were found to be higher in female patients than male patients, although the number of male patients was higher than the number of female patients, according to the results of HI measurements made from T6, T8, processus xiphoideus, and maximum depression levels.[19] In our study, the mean HI at T6-T11 levels was measured as 3.56 in female patients with PE and 3.17 in male patients. Similarly, pectus severity values at T6-T11 levels of female patients were found to be higher than male patients in our study.

In studies in which pectus severity was reported as mild, moderate, and severe in patients with PE, it was reported that the number of patients with "severe" deformities was higher than the number of mild and moderate patients.[20-22] In our study, a total of 80 patients with PE were found to be mild in 39%, moderate in 20%, and severe in 41%. In our study and other studies, the number of patients with "severe" deformities was found to be higher than the number of "mild" and "moderate" patients.

In some studies conducted on patients with PC, the mean value of HI is seen to vary between 1.90 and 2.20.[19,23,24] In our study, the mean pectus severity at T5-T10 levels of 70 (18 women, 52 men) PC patients was measured as 2.01. It is seen that the HI results determined in our study and the HI results in other studies are similar.

When pectus deformities are examined morphologically, more morphological changes are observed in PE patients compared to PC patients depending on collapse.

The anatomical location of the heart in the thorax may change due to the increase in compression on the heart, especially due to the severity of the PE deformity.

CTR is a ratio that reveals the size of the heart in the thorax. Although knowing the CTR in pectus patients does not give information about the true size or volume of the heart, it gives information about the displacement of the heart in the chest depending on the severity of the deformity.

In studies conducted to determine the location of the heart in the chest in patients with PE, it has been reported that CTR is increased in patients with PE and this increase is mostly localized to the left side.[25,26] In our study, CTR was calculated as 0.47 in the patient group with PE and 0.44 in the healthy group. In addition, in our study, the rate of the left placement of the heart in the female patient group was 68.35%, 66.70% in female healthy individuals, 67.19% in the male patient group, and 64.39% in female healthy individuals.

In some studies, it has been reported that cardiac findings increase depending on the severity of the deformity, especially right ventricular changes and that the heart is displaced as a result of the rotation of the sternum to the right or left depending on the severity of the deformity.[9,10]

In our study, it was observed that the heart moved to the left anterior region due to the increase in pectus severity at T8-T11 levels, where PE was most severe, and then to the left posterior region as the severity of the deformity increased. It was remarkable that the heart was still visible at T10 level, especially in PE patients. This showed that the heart did not only shift to the left anterior and left posterior direction depending on the severity of the pectus, but also shifted downward depending on the severity of the deformity.

Conclusion

We think that knowing the location, position, and thoracic vertebra levels of the organs in cases with anterior chest wall deformity will shed light on clinical studies.

This study has several limitations. First, the study includes retrospective and single-center results. Second, the sample size was relatively limited.

Financial support and sponsorship

Nil.

Conflicts of interest

There are no conflicts of interest.

References

1. Rea G, Sezen CB. Chest wall deformities. In: StatPearls. Treasure Island (FL): StatPearls Publishing; 2022. Available from: https://pubmed.ncbi.nlm.nih.gov/31971714/. [Last accessed on 2022 Aug 25].
2. Kutluk AC, Metin M. Congenital chest wall deformities. J. Turk Spinal Surg 2017;28:195-204.
3. Zeybek A, Tosun K, Gencer C, Kalemci S, Öz N, Çalişkan S, *et al.* Association between the pectoral muscles and rib anomalies in Poland syndrome. J Anat Soc India 2020;69:81-90.
4. Sujka JA, St Peter SD. Quantification of pectus excavatum: Anatomic indices. Semin Pediatr Surg 2018;27:122-6.
5. Sesia SB, Heitzelmann M, Schaedelin S, Magerkurth O, Kocher GJ, Schmid RA, *et al.* Standardized Haller and asymmetry index combined for a more accurate assessment of pectus excavatum. Ann Thorac Surg 2019;107:271-6.
6. Haller JA Jr., Kramer SS, Lietman SA. Use of CT scans in

selection of patients for pectus excavatum surgery: A preliminary report. J Pediatr Surg 1987;22:904-6.
7. Ito Y, Suzuki H, Sasahara Y, Mitsukawa N, Yoshino I. Can surgical repair for pectus excavatum contribute to lung growth? Interact Cardiovasc Thorac Surg 2021;33:928-34.
8. Hoffmann T, Katballe N, Stokholm Nørlinger T, Vincenzo de Paoli F. Surgical correction of pectus carinatum. Multimed Man Cardiothorac Surg 2020;2020. [Doi: 10.1510/mmcts. 2020.050].
9. Ortiz JA, Abrego BV. Surgical correction of recurrent pectus excavatum of an adult patient, case report, and review of literature. Indian J Thorac Cardiovasc Surg 2020;36:226-30.
10. Capunay C, Martinez-Ferro M, Carrascosa P, Bellia-Munzon G, Deviggiano A, Nazar M, *et al.* Sternal torsion in pectus excavatum is related to cardiac compression and chest malformation indexes. J Pediatr Surg 2020;55:619-24.
11. Rodriguez-Granillo GA, Raggio IM, Deviggiano A, Bellia-Munzon G, Capunay C, Nazar M, *et al.* Impact of pectus excavatum on cardiac morphology and function according to the site of maximum compression: Effect of physical exertion and respiratory cycle. Eur Heart J Cardiovasc Imaging 2020;21:77-84.
12. Biavati M, Kozlitina J, Alder AC, Foglia R, McColl RW, Peshock RM, *et al.* Prevalence of pectus excavatum in an adult population-based cohort estimated from radiographic indices of chest wall shape. PLoS One 2020;15:e0232575.
13. Westphal FL, Lima LC, Lima Neto JC, Chaves AR, Santos Júnior VL, Ferreira BL. Prevalence of pectus carinatum and pectus excavatum in students in the city of Manaus, Brazil. J Bras Pneumol 2009;35:221-6.
14. Rajabi-Mashhadi MT, Ebrahimi M, Mobarhan MG, Moohebati M, Boskabady MH, Kazemi-Bajestani SM. Prevalence of chest wall deformities in a large sample of Iranian children aged 7-14 years. Iran J Pediatr 2010;20:221-4.
15. Işık H, Çaylak H, Sapmaz E, Karataş O, Kavaklı K, Şengül İnan M, *et al.* Demographic characteristics of pectus deformities across Turkey. Turk Gogus Kalp Damar Cerrahisi Derg 2019;28:322-30.
16. Tokur M, Demiröz ŞM, Sayan M, Tokur N, Arpağ H. Chest wall deformities and coincidence of additional anomalies, screening results of the 25.000 Turkish children with the review of the literature. Curr Thorac Surg 2016;1:21.
17. Akkaş Y, Gülay Peri N, Koçer B, Gülbahar G, Baran Aksakal FN. The prevalence of chest wall deformity in Turkish children. Turk J Med Sci 2018;48:1200-6.
18. Archer JE, Gardner A, Berryman F, Pynsent P. The measurement of the normal thorax using the Haller index methodology at multiple vertebral levels. J Anat 2016;229:577-81.
19. Fonkalsrud EW. Surgical correction of pectus carinatum: Lessons learned from 260 patients. J Pediatr Surg 2008;43:1235-43.
20. Zhang DK, Tang JM, Ben XS, Xie L, Zhou HY, Ye X, *et al.* Surgical correction of 639 pectus excavatum cases via the Nuss procedure. J Thorac Dis 2015;7:1595-605.
21. Gürsu AH, Karagün BS, Korkmaz O, Gürsu SS, Uçar MA. Correlation between Haller index and echocardiographic and spirometric findings in children with pectus excavatum. Turk Kardiyol Dern Ars 2014;42:259-64.
22. Sarioglu FC, Gezer NS, Odaman H, Sarioglu O, Ulusoy O, Ates O, *et al.* Lung density analysis using quantitative computed tomography in children with pectus excavatum. Pol J Radiol 2021;86:e372-9.
23. Stephenson JT, Du Bois J. Compressive orthotic bracing in the treatment of pectus carinatum: The use of radiographic markers to predict success. J Pediatr Surg 2008;43:1776-80.
24. Jung J, Chung SH, Cho JK, Park SJ, Choi H, Lee S. Brace compression for treatment of pectus carinatum. Korean J Thorac Cardiovasc Surg 2012;45:396-400.
25. Saleh RS, Finn JP, Fenchel M, Moghadam AN, Krishnam M, Abrazado M, *et al.* Cardiovascular magnetic resonance in patients with pectus excavatum compared with normal controls. J Cardiovasc Magn Reson 2010;12:73.
26. Simşek Z, Günay E, Aksakal E, Kutucularoğlu MG, Güneren G. Evaluation of cardiopulmonary findings of young adult patients with isolated pectus excavatum. Anadolu Kardiyol Derg 2011;11:77-8.

Original Article

Morphometric Variations of the Suprascapular Notch using Three-dimensional Computed Tomography Scans in a Group of Jordanian Population

Islam Altarawneh[1], Darwish Badran[1,2], Osama Samara[3], Amjad Shatarat[1,4], Mohamed Kharabsheh[3], Tamer Abuelsamen[1], Amro Akkash[1], Hala Alzaghloul[1]

[1]Department of Anatomy and Histology, School of Medicine University of Jordan, [2]Ibin Sina University for Medical Sciences, [3]Department of Radiology, University of Jordan Hospital, [4]Aqaba Medical Sciences University, Amman, Jordan

Abstract

Aim: The study was performed to understand the morphological anatomical variations of suprascapular notch (SSN) among Jordanian population and to explore the correlation between the morphological measurements according to gender, age, weight, and height. **Materials and Methods:** A total of 182 computed tomography scans of scapulae were analyzed for 91 patients. The type of SSN was determined using a classification based on the following three geometrical measurements: superior transverse diameter, middle transverse diameters, and maximal depth. **Results:** The most common type predominated in the sample was Type III with percentages on the right and left, respectively (89% and 84%), 4% for Type II, 7% for Type I, and 8% were having a foramen, whereas absent SSN cases were 4%. On the left side, 1% for Type II, 15% who have Type I, and about 7% of the patients have foramen, whereas absent SSN cases were 7%. **Conclusion:** Knowledge of the anatomical variations of the SSN described in this study should be helpful in endoscopic and open procedures of the suprascapular region and also may increase the safety of operative decompression of the suprascapular nerve.

Keywords: *Entrapment, foramen, scapular, shoulder, variation*

Introduction

The superior border of the scapula runs from the superior angle to the lateral angle where a notch presents at the root of the coracoid process called the suprascapular notch (SSN).[1,2] The SSN is an alternative varying to a foramen through the attachment of the superior transverse scapular ligament which can be ossified in certain instances.[3,4] The foramen serves as a route for the suprascapular nerve to pass through.[1] The suprascapular area is well-renowned for the occurrence of a number of anatomical variations in the morphology of the notch specifically. To many authors, the morphology of the SSN is recognized as one of the causes of suprascapular nerve entrapment.[5-7] The morphology was classified to three main shapes of being J, U, and V shaped.[3,5] Other coexisting or associated anatomical pathologies of the notch that tends to result in this neuropathy come to be the ossification of the superior transverse scapular ligament, narrowed V-shaped SSN, hypertrophied subscapular muscle but mainly and most importantly, the narrow notch of the osteofibrous tunnel of the path of the suprascapular nerve.[4] Data of the morphology of the SSN are critical for analyzing the incidence of suprascapular nerve entrapment, reducing its injury, and approaching most effective treatment.[5,8] Although the morphology of the notch and its relation to nerve entrapment has been reported in many populations, data in the Middle East specifically Jordan are very much not present. This study aims to determine the prevalence of various morphological types of the SSN in the Jordanian population in mention of the presence or absence of sexual dimorphism in the further goal of building ground for the understanding of the pathophysiology and treatment of suprascapular nerve entrapment all based on new imaging techniques.

Materials and Methods

In this study, high-resolution three-dimensional chest computed tomography (CT) scans (*Siemens Somation*

How to cite this article: Altarawneh I, Badra D, Samara O, Shatarat A, Kharabsheh M, Abuelsamen T, *et al.* Morphometric variations of the suprascapular notch using three-dimensional computed tomography scans in a group of Jordanian population. J Anat Soc India 2023;72:211-6.

Article Info

Received: 16 April 2023
Accepted: 31 July 2023
Available online: 28 September 2023

Address for correspondence:
Dr. Amjad Shatarat, Department of Anatomy and Histology, School of Medicine University of Jordan, Amman, Jordan, Aqaba Medical Sciences University Aqaba, Jordan.
E-mail: a.shatarat@ju.edu.jo

Access this article online

Website: https://journals.lww.com/joai
DOI: 10.4103/jasi.jasi_38_23
Quick Response Code:

Definition Dual Source) performed for 91 individuals who come to the university of Jordan hospital. The sample has 50.5% males (n = 46) and 49.5% females (n = 45). The sample was categorized according to gender, age, height, and weight. First, the scapular region for each individual was inspected to ensure that there are no kind of bruising, fracture, trauma, and any sort of limitations in movement, after those measurements were taken by radiology specialist using the software built in CT scan system (Synapse 3D Fujifilm). The classification of SSN types was based on the classification used by Polguj *et al*.[8] Imaginary lines were drawn to get measurements to study the SSN, as shown in Figure 1.

1- The superior transverse diameter (STD): value of the horizontal measurements taken in the horizontal plane between the corners of the SSN
2- The maximal depth (MD): maximum value of the longitudinal measurements taken in the vertical plane from the STD to the deepest point of the SSN
3- The middle transverse diameter (MTD): value of the horizontal measurements taken in the horizontal plane between opposite walls of the SSN at half distance of the MD. According to the previous measurements, the shape of the SSN classified into:
    1. Type I the superior transverse distance less than the MD distance
    2. Type II the superior transverse distance equals the MD distance
    3. Type III the superior transverse distance more than the MD distance
    4. Type IV foramen
    5. Type V absent notch or foramen.

The Results

All analysis was performed using IBM SPSS Statistics for Windows, version 25.0. (Armonk, NY:IBM Corp). $P < 0.05$ was considered statistically significant. The test was used for nonparametric data such as Mann–Whitney test (MW) and Kruskal–Wallis test (KW), and the Student's *t*-test to get the means and standard deviations for each measurement.

Variations in the types of the supra-scapular notch

The results in Table 1 show the percentages of the different types or shapes of SSN; the highest percentage on both the right and left sides was for Type III, the least percentage was for Type II, as shown in Figure 2.

Variations of the suprascapular notch according to gender dimorphism on both sides

For the nonnormally distributed data, MW test as a nonparametric test was used to explore the differences between the measurements on both sides and if there is any difference between males and females as shown in Table 2. In Figure 3, different types of SSN were found on both sides for the same individual.

Superior transverse distance

The results in Table 2 show the mean rank of the males' STD (MR = 44.94, 44.89) is greater than the mean ranks of the females (MR = 39.00, 36.11) on both sides, respectively, with a nonsignificant value of MW test (Sig. = 0.263), (Sig. = 0.091) between males and females on both sides.

Middle transverse distance

The results in Table 2 show the mean rank of males' MTD (MR = 48.27) on the right side is higher than the mean

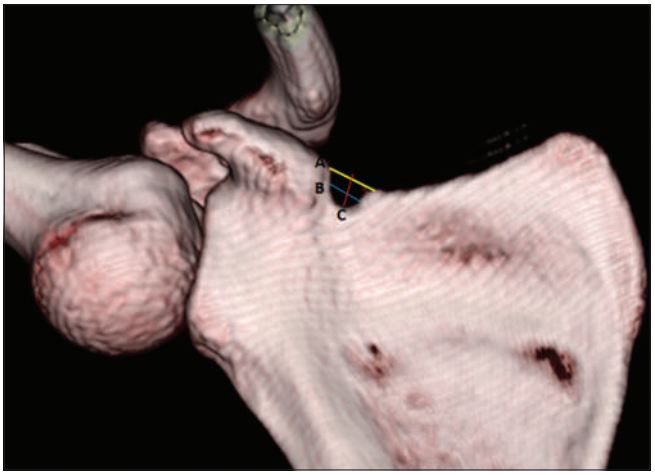

Figure 1: Dimensions of the suprascapular notch: A is superior transverse distance (yellow), B is middle transverse distance (blue), C is maximal depth distance (red)

Table 1: Percentages of suprascapular notch types

Type	Right frequency	Percentage	Left frequency	Percentage
Type I	6 (n=83)	7.23	12 (n=80)	15.00
Type II	3 (n=83)	3.61	1 (n=80)	1.25
Type III	74 (n=83)	89.15	67 (n=80)	83.75
Type IV	7 (n=91)	7.69	6 (n=91)	6.95
Type V	4 (n=91)	4.39	6 (n=91)	6.95

Table 2: Variations in suprascapular notch measurements according to gender

	Male	Female	Significant	MW
Right side	n=42	n=41		
STD	44.93	39.00	0.263	738
MTD	48.27	35.57	0.016	597
MDD	53.16	30.54	0.001	391
Left side	n=40	n=40		
STD	44.89	36.11	0.091	624
MTD	47.65	33.35	0.006	514
MDD	42.03	38.98	0.557	739

MW test used. STD: Right side mean=8.11, SD=3.06, Left side mean=6.04, SD=2.43, MTD: Right side mean=6.30, SD=2.54, Left side mean=4.16, SD=2.48, MDD: Right side mean=4.05, SD=2.58, Left side mean=7.41, SD=2.92. STD: Superior transverse distance, MTD: Middle transverse distance, MDD: Maximal depth distance, MW: Mann–Whitney, SD: Standard deviation

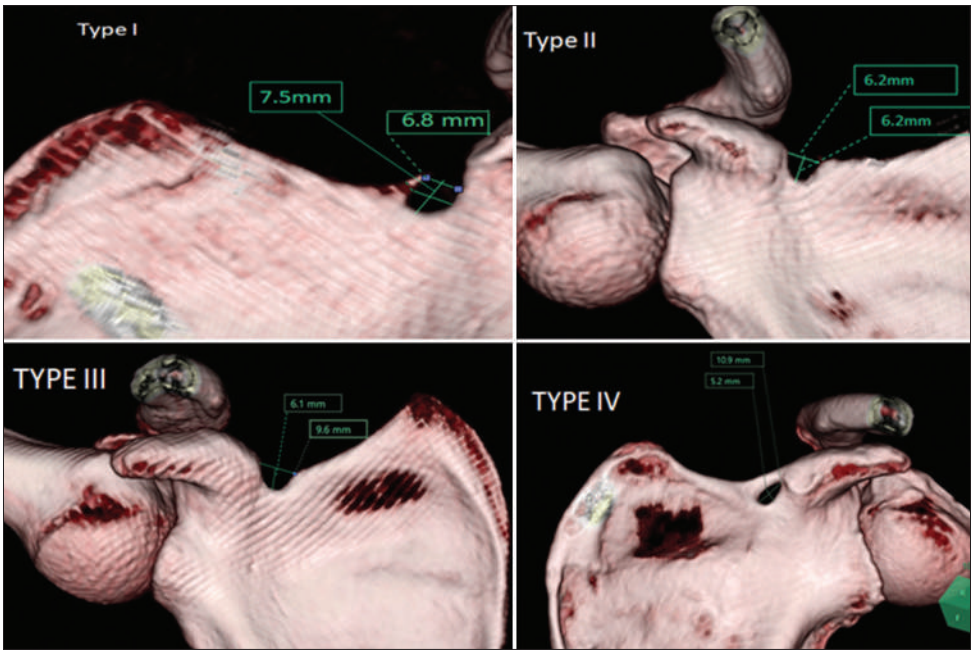

Figure 2: Types of the suprascapular notch by 3D CT scanning

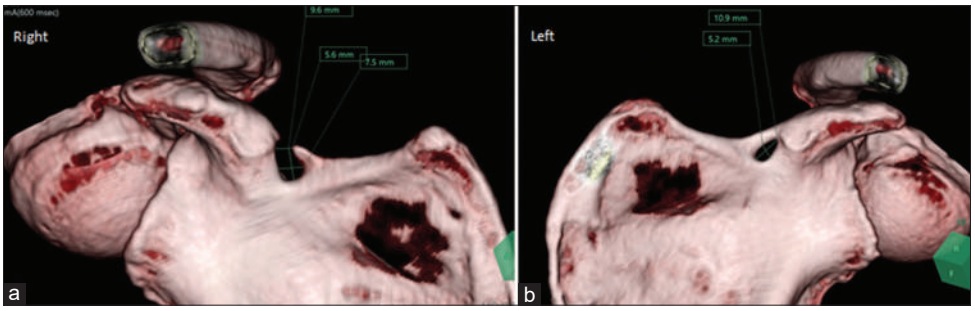

Figure 3: (a and b) suprascapular notch on right and left sides for one individual, (a) right side type I notch, (b) left side with a foramen type IV

rank of females' MTD (MR = 35.57) with a statistically significant value of MW test (Sig. = 0.016). Moreover, the results reveal that the mean rank of males' MTD on the left side (MR = 47.65) is higher than the mean rank of females' MTD (MR = 33.35) with a statistically significant value of MW (Sig. = 0.006). These results suggest significant differences between patients' right (MTD) and left (MTD) measurements due to gender and in favor of males.

Maximal depth distance

It was found, as shown in Table 2, that the mean rank of males' MD on the right side (MR = 53.16) is more than the mean rank of females' MD on the right side (MR = 30.54) with a significant difference (Sig. = 0.0001) in favor of males. In contrast, no significant differences between males' and females' measurements on the left side (Sig. = 0.557) were found.

Variations of the suprascapular notch according to age

KW test was used. To conduct such a test, patients' ages are categorized into four percentiles, which are 1 (ages ≤43.00), 2 (ages ≤58.00), 3 (ages ≤71.00), and 4 (ages ≤88.00). The results in Table 3 confirm that there are no significant differences between patients measurements on both sides. The significance values were (superior transverse distance on the right and left (Sig. = 0.812 and 0.492) middle transverse distance on the right and left (Sig. = 0.875 and 0.470, respectively) MD (Sig. = 0.746 and 0.646) according to their ages.

Variations in suprascapular notch according to height

Four ranges were used to classify patients based on their heights, which are: 1 (heights ≤160.00), 2 (161≤ heights ≤167), 3 (168≤ heights ≤174), and 4 (175≤ heights ≤186.00).

The results in Table 4 show that the highest mean rank of superior transverse distance values on the right side and left side was for patients with heights more than 160 and <167 (right side $n = 83$, $n = 18$), (left side $n = 83$, $n = 16$).

It should be noted that the highest mean ranks of superior transverse distance on both sides for patients

Table 3: Variations in suprascapular notch according to age

	Age ≤43	Age ≤58	Age ≤71	Age ≤88	Significant	KW (df)
Right side measurements	*n*=21	*n*=24	*n*=20	*n*=18		
ST	44.05	41.38	38.05	44.83	0.812	0.954 (3)
MT	44.14	39.48	40.55	44.47	0.85	0.690 (3)
MD	43.81	37.42	44.25	43.35	0.746	1.231 (3)
Left side measurements	*n*=20	*n*=22	*n*=21	*n*=17		
ST	45.6	37.84	35.86	43.68	0.492	2.41 (3)
MT	41.95	38.7	35.62	47.15	0.47	2.53 (3)
MD	43.2	42.32	34.95	41.82	0.646	1.658 (3)

KW test was used. KW: Kruskal–Wallis, ST: Superior transverse, MT: Middle transverse, MD: Maximal depth

Table 4: Variations in supra-scapular notch according to height/Kruskal–Wallis test

	Height 1	Height 2	Height 3	Height 4	Significant	KW (df)
Right side measurements	*n*=25	*n*=18	*n*=39	*n*=1		
ST	34.28	45.03	44.9	67.5	0.309	4.53 (3)
MT	32.12	47.17	45.08	76	0.054	7.66 (3)
MD	29.26	42.17	49.35	71	0.007	12.06 (3)
Left side measurements	*n*=23	*n*=16	*n*=40	*n*=1		
ST	34.02	47.88	40.34	78	0.111	6.00 (3)
MT	32.26	46.13	42.4	64	0.163	5.12 (3)
MD	38.43	42.56	39.93	78	0.401	2.94

KW: Kruskal–Wallis, ST: Superior transverse, MT: Middle transverse, MD: Maximal depth

with a height >174 were excluded because there is one patient with such a height. In terms of the differences between these groups, the results reveal that there are no significant differences between patients' STD on both sides, respectively, Sig. = 0.309 and 0.111).

The middle transverse distance values indicate that patients with heights more than 160 and <168 have the highest middle transverse distance on the right side mean rank (MR = 47.17) on the left side (MR = 46.13). The results show nonsignificant variations according to height (right side Sig. = 0.054) and (left side, Sig. = 0.163).

As shown in Table 4, the majority of the patients (n = 39) with heights ranged between 168 and 175 have the highest mean rank of the MD distance on the right side (MR = 49.35), whereas patients with heights range from 161 to 167 (n = 16) have the highest mean rank on the left side (MR = 42.56). Notably, the results underline significant differences between patients' MD on the right side due to height (KW = 12.06, Sig. = 0.007) and there are no significant differences between patients' MD on the left side due to height (KW = 2.94, Sig. = 0.401).

Variations in suprascapular notch according to weight

Patients are categorized based on their weights into four groups: Group 1 (n = 23, weight ≤64), Group 2 (n = 23) (64< weight ≤78), Group 3 (n = 24), (78< weight ≤92.00), and Group 4 (n = 21), (92< weight ≤115). Differences between these groups are tested using KW test. As shown in Table 5, the results reveal no significant differences between patients' measurements.

Discussion

Well awareness of the SSN anatomy may help to avoid and accurately evaluate any impending case with signs of pathology related to suprascapular nerve and vasculature.

This study was conducted to explore the different morphological parameters of the SSN and its prevalence in Jordan throughout a sample of 91 individuals and to explore the possible presence of dimorphism between both genders due to different reasons such as body habitus as it was explored by previous studies that the suprascapular nerve entrapment is more prevalent among males than females.[9]

The morphology of SSN was classified in many studies in the literature; the oldest classifications, as mentioned by Polguj,[9] were taken by Hrdricka in 1942 and Olivier in 1960. Who described the notch by observations and then the most cited classification was formed by Rengachary *et al.* into which the SSN classified into six types.[10] In the present study, the quantitative classification by Polguj *et al.* was used and classified the types of SSN into five types by measuring three distances on both sides: (1) The STD, (2) The MD, and (3) The MTD.[8]

The sample types in the prior studies were implemented using either dried cadaveric specimens[2,6,11-13] or using the radiological techniques such as MRI,[5] CT scans,[4,9,14] and ultrasonography.[1]

The present study revealed that the predominating type of the SSN in the Jordanian population was type III and by scanning the previous studies, numerous studies described

Table 5: Variations in suprascapular notch according to weight

	Weight 1	Weight 2	Weight 3	Weight 4	Significant	KW (df)
Right side measurements	*n*=21	*n*=21	*n*=23	*n*=18		
ST	41.98	40.1	47.41	37.33	0.579	1.96 (3)
MT	38.55	40.02	49.13	39.22	0.419	2.83 (3)
MD	34.76	48.67	43.5	40.75	0.303	3.64 (3)
Left side measurements	*n*=21	*n*=19	*n*=21	*n*=19		
ST	36.9	40.21	45.18	38.89	0.638	1.69 (3)
MT	34.69	48.39	41.24	38.12	0.294	3.71 (3)
MD	36.14	39.71	43.95	42.29	0.72	1.34 (3)

KW test was used. KW: Kruskal–Wallis, ST: Superior transverse, MT: Middle transverse, MD: Maximal depth

the variations in the morphometric dimensions of the SSN in several populations; type III which is a symmetrical U-shaped notch in Rengachary *et al*. and polji[8,10] was found to be the most common type in many studies in different population such as in Kenyan population (29%) and the least common was the type IV (foramen),[11] this is in match with Ugandan 51% for type III and the least common was type V which is incomplete ossification of the suprascapular ligament, but notably that the prevalence of completely ossified STSL is moderately high (8.2%) in the Ugandan population compared to other populations.[15] In studying 423 scapulae in Germany also, Type III was having the percentage that is the highest (41.8%).[13] As well in India two different studies showed that the presence of SSN was superior to the foramen with type III; was the most common in the samples studied 32% and 48%, respectively,[6,16] this finding was not in consistent with the study by Kumar *et al.,* in which type II was founded to have the highest percentages over the other types.[12]

Another study in Malawian population showed that type I was the most common which is wide, shallow, and V-shaped (36.8%).[17] In china, one study mentioned that type II was the most common type observed in Chinese in 171 scapulae (58.16%),[18] another more recent study showed that type I (44.8%) was dominated over type II.[19] Type IV which is, small V-shaped notch, was the most common type in Italy observed in 156 scapulae (31.1%).[20]

Some rare types were reported in the literature such as the coexistence of both the suprascapular foramen and SSN, which mentioned two Caucasian cases retrospectively studied their CT scans and they found the presence of a foramen separated with a bony bridge from a SSN,[4] as well as in a study by Natsis *et al.* three scapulae were found to have a notch accompanied with a bony foramen,[13] comparing the present study in Jordanian, the coexistence of a foramen with the SSN was not contained within this study, but there were four cases who have a foramen on one side and a notch on the other side, and just two cases have a symmetrical foramina on both sides. In Brazilian study, it was noticed that the presence of an ossified transverse scapular ligament was common in a study indicating that the foramen is the predominating type over the SSN.[21] On discussing the effect of age, in a study showed that the foramen and narrow notch formed from a wide notch before and by the aging effect the SSN changed in a way that become ossified to be a foramen.[14] This is in contest to a study by Albino *et al.* who mentioned a significant effect of age on increasing the depth of notch in age group above 73 years old.[20] In this study, the effect of age was not that significant and this could be related to somehow to the sample count number of the CT scans of scapulae and the age groups in the sample were restricted to ages above 40s.

Interestingly, the core of this study was to explore the sexual dimorphism effect on the morphology of the SSN as well as the symmetry between both sides in each individual, and the results showed that the middle transverse distance was clearly more in males than females with a significant values, especially on the left side, also the MD distance was more in males compared to females with a significant variation on the right side compared to the left side, and this study one of the leading studies that accurately perform a comparisons between males and females with a correlation with symmetrical analysis for both sides**.**

Conclusion

The SSN morphology is of clinical significance and anatomical importance. This is due to the effect it can pursue on the suprascapular nerve entering through it causing its entrapment and compression, which leads to complications related to the shoulder immovability and its weakness. Thus, being one of the causatives to what is known as suprascapular neuropathy.

Financial support and sponsorship

Nil.

Conflicts of interest

There are no conflicts of interest.

References

1. Jezierski H, Podgórski M, Stefańczyk L, Kachlik D, Polguj M. The influence of suprascapular notch shape on the visualization of structures in the suprascapular notch region: Studies based on a new four-stage ultrasonographic protocol. Biomed Res Int 2017;2017:5323628. [doi: 10.1155/2017/5323628].
2. Pawar KD, Chavan SK, Joshi MM. Morphometric study of suprascapular notch and its variations in dried human scapulae. EJMED 2020;2. [doi: 10.24018/ejmed.2020.2.6.473].

3. Saikia R, Baishya RJ, Deka B. Variations in the shape of the suprascapular notch in dry human scapula: An anatomical study. Int J Sci Res 2017;5:187-90.
4. Polguj M, Jędrzejewski K, Majos A, Topol M. Coexistence of the suprascapular notch and the suprascapular foramen – A rare anatomical variation and a new hypothesis on its formation based on anatomical and radiological studies. Anat Sci Int 2013;88:156-62.
5. Farhan TM, Kamoona HR. MRI-evaluation of suprascapular notch morphometry and its clinical applications. J Med Res Surg 2021;2:1-6.
6. Daripelli S, Tolupunoori B, Vinodini L. Morphometric study of suprascapular notch and its safe zone in Indian population. Maedica (Bucur) 2020;15:461-7.
7. Sangam MR, Sarada Devi SS, Krupadanam K, Anasuya K. A study on the morphology of the suprascapular notch and its distance from the glenoid cavity. J Clin Diagn Res 2013;7:189-92.
8. Polguj M, Jędrzejewski K, Podgórski M, Topol M. Morphometric study of the suprascapular notch: Proposal of classification. Surg Radiol Anat 2011;33:781-7.
9. Polguj M, Sibiński M, Grzegorzewski A, Grzelak P, Majos A, Topol M. Variation in morphology of suprascapular notch as a factor of suprascapular nerve entrapment. Int Orthop 2013;37:2185-92.
10. Rengachary SS, Burr D, Lucas S, Hassanein KM, Mohn MP, Matzke H. Suprascapular entrapment neuropathy: A clinical, anatomical, and comparative study. Part 2: Anatomical study. Neurosurgery 1979;5:447-51.
11. Sinkeet SR, Awori KO, Odula PO, Ogeng'o JA, Mwachaka PM. The suprascapular notch: Its morphology and distance from the glenoid cavity in a Kenyan population. Folia Morphol (Warsz) 2010;69:241-5.
12. Kumar A, Sharma A, Singh P. Anatomical study of the suprascapular notch: Quantitative analysis and clinical considerations for suprascapular nerve entrapment. Singapore Med J 2014;55:41-4.
13. Natsis K, Totlis T, Tsikaras P, Appell HJ, Skandalakis P, Koebke J. Proposal for classification of the suprascapular notch: A study on 423 dried scapulas. Clin Anat 2007;20:135-9.
14. Yamakado K. The suprascapular notch narrows with aging: A preliminary solution of the old conjecture based on a 3D-CT evaluation. Surg Radiol Anat 2016;38:693-7.
15. Adewale AO, Segun OO, Usman IM, Monima AL, Kegoye ES, Kasozi KI, *et al.* Morphometric study of suprascapular notch and scapular dimensions in Ugandan dry scapulae with specific reference to the incidence of completely ossified superior transverse scapular ligament. BMC Musculoskelet Disord 2020;21:733.
16. Kannan U, Kannan NS, Anbalagan J, Rao S. Morphometric study of suprascapular notch in Indian dry scapulae with specific reference to the incidence of completely ossified superior transverse scapular ligament. J Clin Diagn Res 2014;8:7-10.
17. Kaledzera T, Matundu B, Adefolaju GA, Manda J, Mwakikunga A. Morphometric study of the suprascapular notch and scapular dimensions in adult Malawian cadavers and implications of completely ossified superior transverse scapular ligament. Pan Afr Med J 2022;41:324.
18. Wang HJ, Chen C, Wu LP, Pan CQ, Zhang WJ, Li YK. Variable morphology of the suprascapular notch: An investigation and quantitative measurements in Chinese population. Clin Anat 2011;24:47-55.
19. Zhang L, Wei HR, Guo XG, Fu SJ, Xu YX, Zhong SZ, *et al.* Variable morphology of the suprascapular notch: A proposal for classification in Chinese population. Ann Anat 2019;221:173-8.
20. Albino P, Carbone S, Candela V, Arceri V, Vestri AR, Gumina S. Morphometry of the suprascapular notch: Correlation with scapular dimensions and clinical relevance. BMC Musculoskelet Disord 2013;14:172.
21. Silva J, Abidu-Figueiredo M, Fernandes RM, Aureliano-Rafael F, Sgrott E, Silva S, *et al*. High incidence of complete ossification of the superior transverse scapular ligament in Brazilians and its clinical implications. Int J Morphol 2007;25:855-9.

Original Article

Anatomical Study and Clinical Significance of Basivertebral Foramen of S1 Vertebra

Abstract

Background: Chronic low-back pain affects majority of the population worldwide. A paucity of data on the morphology of basivertebral foramen of S1 vertebra hampers the understanding of vertebrogenic cause of chronic low-back pain. The aim of the study was to investigate normal adult basivertebral foramen (S1) morphometry and discuss its clinical significance. **Materials and Methods:** One hundred sacra that consisted of dry bone and computed tomography scans were included in the study. All the morphometric analyses on dry sacra were performed using sliding caliper. Topographic location of the basivertebral foramen was studied based on its distance from the upper rim of the S1 body and the closest distance from the nearest point of origin of pedicles. Shape, number, height, and depth of the basivertebral foramen were noted. The data collected were subjected to statistical analysis was done using GraphPad Prism version 7 for Windows, (GraphPad Software, Boston, Massachusetts, USA). **Results:** The basivertebral foramina was found in the posterior aspect of the body of the S1 vertebra. The shape of the foramina varied from round, tear-shaped, slit-like, and comma-shaped. The mean depth of the foramen correlated with the anterior-posterior diameter of the body of the S1 vertebra. **Conclusions:** Detailed knowledge of these foramen could be important for medical education because they could cause changing operation techniques during surgeries and in the treatment of chronic low-back pain.

Keywords: *Basivertebral, morphometry, pain, sacrum, treatment*

Roshni Sadashiv, Suresh Managutti, Anil Bargale[1], Pooja Nimbal[2], Preetam Patil[2]

Departments of Anatomy, [1]Biochemistry and [2]Radiodiagnosis and Imaging, SDM College of Medical Sciences and Hospital, Shri Dharmasthala Manjunatheshwara University, Dharwad, Karnataka, India

Introduction

The anatomy of the topmost first sacral vertebra is clinically important as it constitutes the lumbosacral region along with the fifth lumbar vertebra.[1] The lumbosacral region is particularly vulnerable to wear and tear, injury, misalignment, and congenital and pathological derangement. The stability of this region largely depends on the morphometry of the constituent bones, connecting ligaments, and neurovascular integrity.[1] The first sacral vertebra consists of large body with cruciate arrangement of high-density trabeculae and a prominent anterosuperior lip called the promontory.[2] The basivertebral foramina are located at the posterior wall of the body of the first sacral vertebra (centrum) leading to the basivertebral canal. This canal is traversed by basivertebral nerves and vessels furnishing the blood supply and transmitting pain signals.[3]

Chronic low-back pain affects majority of the population worldwide. Although several causes are delineated, two models of pain are suggested. Although several causes are delineated, two models of pain are suggested: Discogenic and Vertebrogenic pain. The former arises due to disc derangement and the latter arises from the vertebra specifically involving the basivertebral nerve.[4] New modality of treatment of such vertebral end plate nerve dysfunction comprises basivertebral nerve ablation procedures.

The basivertebral foramens are well-known entities with respect to cervical, thoracic, and lumbar vertebrae. However, the anatomic data of S1 with respect to morphological description of basivertebral foramen have rarely been described in the literature.[3,5]

Thus, the current study aimed to describe the morphology and topography of basivertebral foramen and discuss its clinical implications.

Materials and Methods

A descriptive study was designed after obtaining approval from the institutional ethical committee. Forty dry sacra of Indian origin available in the archives of the

How to cite this article: Sadashiv R, Managutti S, Bargale A, Nimbal P, Patil P. Anatomical study and clinical significance of basivertebral foramen of S1 vertebra. J Anat Soc India 2023;72:217-21.

Article Info

Received: 27 January 2023
Revised: 28 May 2023
Accepted: 31 July 2023
Available online: 28 September 2023

Address for correspondence:
Dr. Roshni Sadashiv, Department of Anatomy, SDM College of Medical Sciences and Hospital, Shri Dharmasthala Manjunatheshwara University, Dharwad, Karnataka, India. E-mail: drroshnisadashiv@gmail.com

Access this article online

Website: https://journals.lww.com/joai
DOI: 10.4103/jasi.jasi_8_23
Quick Response Code:

osteology library department of anatomy were collected. The age of the sacrum ranged from 55 to 75 years. Sex of the sacrum as analyzed by sacral index consisted of 22 female and 18 male sacra. All the morphometric analysis was performed using sliding digital caliper accurate to 0.01 mm. The S1 morphometric was analyzed with respect to the anterior-posterior and transverse diameter of sacral plateau aiming to detect any possible correlation of sacral slope to the basivertebral foramen morphometry. Topographic location of the basivertebral foramen was studied based on its distance from the upper rim of the S1 body and the closest distance from the nearest point of origin of pedicles. Shape, number, and horizontal and vertical height of the basivertebral foramen were noted.[3] The patency of the foramen was studied by introducing an orthodontic wire (thickness – 0.2 mm) into the basivertebral canal.[6] The depth of the basivertebral canal was measured by passing the orthodontic wire through the foramen till a point of resistance and marked. The wire was later removed to measure the distance traveled using metallic measuring scale. Vowing to the limitation of precise measurements in the dried sacra, the morphometry was also measured in the computed tomography (CT) scans.

Imaging through computed tomography scans

The study included a retrospective analysis of CT scans conducted on patients who had a pelvic or sacral CT in the hospital from 2021 to 2022. Sixty sacral vertebrae of patients of different age groups and either gender referred to the department of radiodiagnosis of multispecialty hospital for CT abdomen and pelvis were chosen. They were examined for evaluation of other pathologies (such as ureteric calculi, pain abdomen, pancreatitis, appendicitis, and liver pathologies). Patients having spinal/vertebral lesions, spine fractures, trauma history, and pathological deformity due to tumor or infection were excluded from the study. Somatom Definition as Plus (Siemens) 128-slice thickness CT scanner was used for imaging. Images were reconstructed in bone window with a thickness of 0.6 mm using appropriate filters. Multiplanar reformation was used to discern the morphology of basivertebral foramen (BVF) based on the imaging, and the basivertebral foramen morphology and shapes (BVF) shapes were classified into circular, elliptical, coma, teardrop, and pinhead. Various measurements such as diameter of the foramen (transverse and vertical), interforamen distance, distance from either of the pedicles, promontory, and posterior border of the body of the S1 vertebra were taken in axial and coronal sections, whereas the depth of the foramen was taken in sagittal view. Statistical analysis was done using GraphPad Prism version 7 for Windows, (GraphPad Software, Boston, Massachusetts, USA).

Results

In the dry sacra, the mean anteroposterior S1 vertebral body measured 28.85 mm (standard deviation [SD] = 2.97 mm), and the mean transverse diameter measured 44.90 mm (SD = 3.93 mm). The male mean values were found to be greater than female values. Out of the total 40 sacra studied, 38 (95%) cases presented with basivertebral foramina. These foramina were found in the posterior aspect of the body of the S1 vertebra closer to the midsagittal plane [Figure 1a-f]. Thirty-three cases presented with double foramina. Five cases showed multiple foramina >3 of unequal size, varying

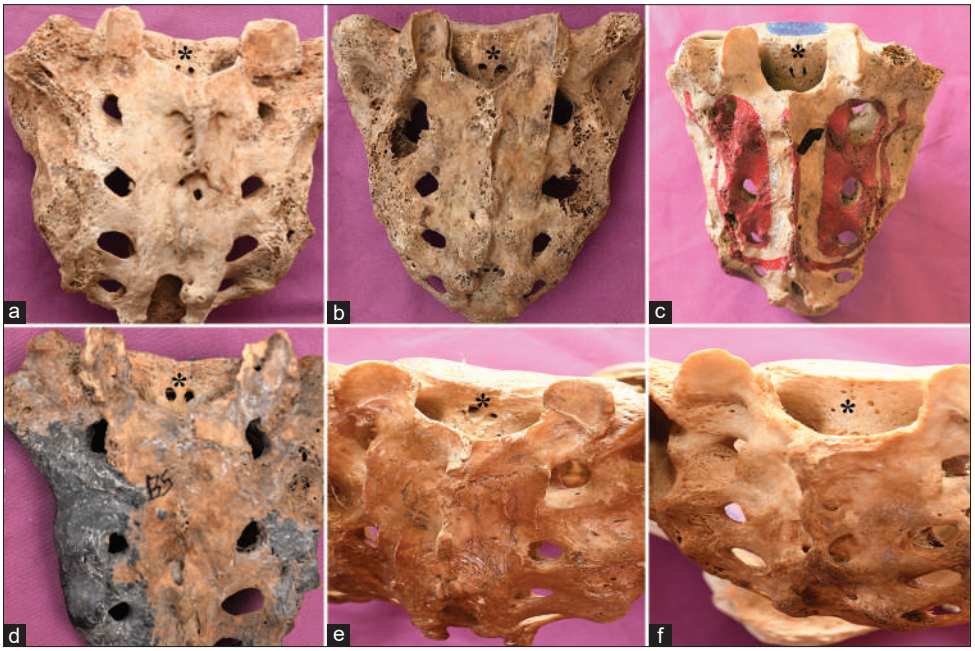

Figure 1: (a) Double basivertebral foramina* <1 mm diameter, (b) Double basivertebral foramina* >1 mm diameter, (c) Slit-shaped basivertebral foramina*, (d) Trabeculated basivertebral foramina*, (e) Bony spicule dividing left-sided basivertebral foramen, (f) Multiple basivertebral foramina*

Table 1: Morphometry of the basivertebral foramina of the first sacral vertebra

Side	Mean±SD					
	Diameter (mm)		Depth (mm)	Distance between foramina (mm)	Distance from upper rim S1 body (mm)	Distance from pedicle (mm)
	Vertical	Transverse				
Right	3.1±1.7	2.4±1.7	7.1±3.03	3.35±0.77	9.47±2.42	15.35±2.41
Left	3.5±1.7	2.6±1.6	7.0±2.60		9.41±1.78	15.65±2.53

SD: Standard deviation

Table 2: Computed tomography scan measurements of basivertebral foramen

Side	Mean±SD				
	Diameter (mm)		Distance between foramina (mm)	Distance from promontory S1 body (mm)	Distance from pedicle (mm)
	Vertical	Transverse			
Right	1.48±0.58	1.38±0.34	0.64±0.22	13.83±1.87	13.85±1.69
Left	1.29±0.34	1.38±0.80		12.40±2.51	13.85±1.96

SD: Standard deviation

shapes, and depth, as shown in Figure 1f. Symmetrical foramina with respect to shape and size were observed in eight cases although the depth differed. In 85% of cases with double foramina, approximately equal sizes were identified. The mean vertical height of the foramina on the right side was 3.1 mm (SD = 1.7 mm), and the mean vertical height on the left measured 3.5 mm (SD = 1.7). The mean transverse diameter on the right and the left measured 2.4 mm (SD = 1.7 mm) and 2.6 mm (SD = 1.6 mm), respectively. The mean distance of the foramina from the upper rim of the vertebral body on the right was 9.47 mm (SD = 2.42 mm) and on the left was 9.41 mm (SD = 1.78 mm). The mean distance from the pedicle to the foramen on the right side measured 15.35 mm (SD = 2.41 mm) and from the left measured 15.65 mm (SD = 2.53 mm). The shape of the foramina was circular [Figures 1a and b], teardrop, slit-like [Figure 1c], elliptical, comma and pinhead shape [Figure 1a]. An osseous septum dividing most often a right-sided foramen and duplicating it was seen in 1% of cases [Figure 1e]. In majority of cases, the foramina were equidistant with a mean distance of 3.35 mm (SD = 0.77 mm). The interior of the foramina were trabeculated in fewer cases [Figure 1d]. The mean depth of the foramen on the right side measured 7.1 mm (SD = 3.03 mm) and on the left side measured 7 mm (SD = 2.60 mm). A positive correlation was observed with respect to the depth of the foramina and the AP diameter of the body of the S1 vertebra (right depth and AP = 0.936, $P < 0.01$; left depth and AP = 0.757, $P < 0.01$). The summary of the findings is tabulated in Tables 1 and 2.

CT scan examination revealed basivertebral canal location and morphometry [Table 2]. Around 35%–40% of cases showed hypoplastic foramen (mostly on the right side), as shown in Figure 2. In 25%–30% of cases, the basivertebral foramina were found closer to the promontory, as illustrated in Figure 3. In 10%–15% of cases, the foramina were closely placed to each other. There was no significant difference in the measurements observed in the dry sacra to radiological findings detected.

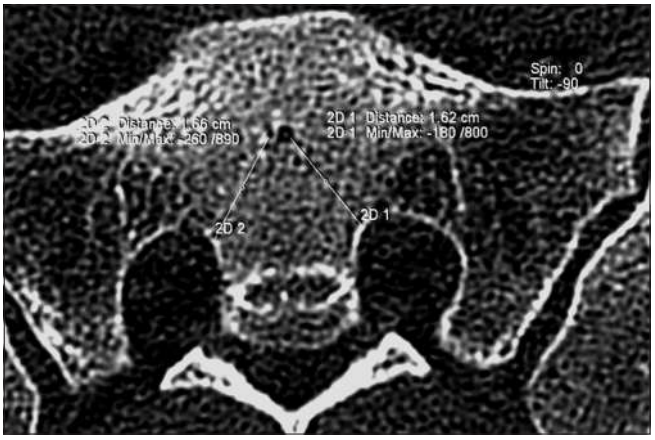

Figure 2: Computed tomography view of the right-sided hypoplastic foramen and decreased interforaminal distance (<0.5 mm)

Discussion

Chronic low-back pain

Chronic low-back pain affects a large population globally, and it is considered a leading cause of disability. The lifetime prevalence of low-back pain is reported to be 49%–70% with at least one episode of pain in one's lifetime.[7] Low-back pain is seen in those <45 years of age and is largely attributed to occupation risks. The modern technological advancement has led to prolonged sitting hours in workspace, and it is one of the causes of low-back pain.[8] However, aging, obesity, and occupations requiring heavy labor and weight lifting are other risk factors associated.[4,8]

Diagnosis of chronic low-back pain is complex. Specific causes include pathological rearrangements of hernia nuclei pulposi, infections, osteoporosis, rheumatoid arthritis, compression fractures, and tumors. About 90% of patients complain of nonspecific low-back pain, the cause of which remains unknown.[7,9]

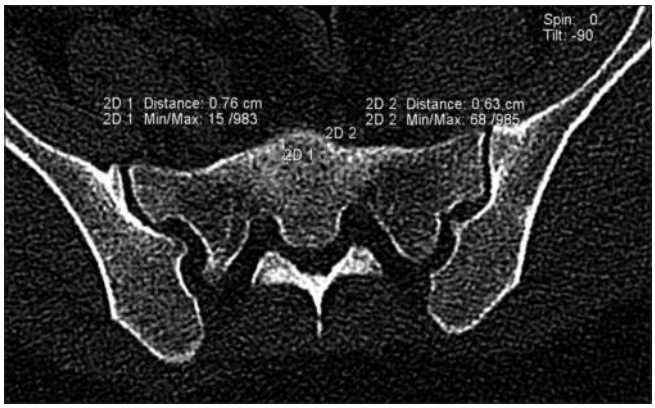

Figure 3: Computed tomography view of the basivertebral foramina with >3 mm interforaminal Distance

Sacral anatomy and low-back pain

The sacrum, located at the base of the vertebral column, helps in the transmission of the body weight through its fused bony elements. The first sacral vertebra is usually associated with a wide range of morphological variations. In the case of lumbarization of the sacral vertebra, the first sacral vertebra behaves as the sixth lumbar vertebra and thus behaves as a separate entity. On the contrary, the L5 vertebra could fuse to the sacrum partially or completely. These are characterized as lumbosacral vertebra transitions which are attributed to low-back pain conditions.[10] The discogenic pain is thought to be due to the sensitive nociceptors in the annulus fibrosis of degenerating disc. Contrary to this theory, recent evidence mark the injury to the basivertebral nerve that innervates the vertebral end plates suggestive of vertebrogenic low-back pain.[4]

The basivertebral nerve

The basivertebral foramen on the posterior aspect of the vertebral body is recognized using imaging modalities such as magnetic resonance imaging and CT scans. The basivertebral nerve traverses along with the nutrient artery through this foramen which is least explored.[11] The paired nerve is a branch of the sinuvertebral nerve which in turn is formed by a somatic root and autonomic root of the ventral rami and gray rami, respectively.[4] It ramifies to supply the vertebral end plate after traversing one-third the distance of the vertebral body.[12] Apart from the lumbar vertebra, vertebrogenic pain is thought to have a role in the pathogenesis of vertebrogenic pain due to the change in vertebral curvature at L5 and SI and subjected to biomechanical load.[4] The S1 morphology is considered to be largely varied among population and is associated with the sacral slope and pelvic tilt. According to a study, the basivertebral nerve of S1 vertebral body showed a variation when compared with lumbar bodies. Here, the entry point was along the lateral border with a lateral medial path and clustering of nerves located at the vertebral center unlike the posterior-anterior path taken in L5 vertebra.[13] However, in our study, we found that the foramen leading into the canal traversed posteroanteriorly almost more than one-third body of the vertebra. In certain cases, as seen through the CT, they were close to the promontory. However, it was difficult to discern the depth of the foramen radiologically.

A recent modality of treatment of chronic low-back pain is a minimally invasive nerve ablation technique. This method has resulted in effectively reducing the symptoms of chronic low-back pain of vertebral origin. However, researchers are still unraveling the anatomy of vertebral column to use this technique effectively.[4,13] The procedure is done under CT guidance prerequisites that involve the location of the nerve entry through transpedicular approach. Initially, a cannula is placed through the pedicle into the posterior aspect of the vertebral body to create a channel followed by the placement of radiofrequency probe and activated for a specified temperature and time. In our study, the approximate distance of the foramen from the pedicles was found to be 15 mm.

Other clinical considerations

In the present study, we found that the depth of the basivertebral canal positively correlated with the AP diameter of the body of the S1 vertebra. This basivertebral foramen should not be confused for vertebral body fractures. On the contrary, these foramina have been largely attributed to vertebral body fractures when found in the midline with larger diameter that can weaken the posterior aspect and the axial plane of the vertebral body.[3] Two cases out of the 40 cases studied showed bilateral large foramina with a maximum depth of >1 cm.

Road traffic accidents and trauma due to fall endanger the sacrum for fractures in young individuals, whereas osteoporotic changes are other causes of sacral fractures in the elderly. The conventional method in the stabilization of the lumbosacral region (posterior pelvic ring) includes sacroiliac screw fixation and techniques. The limitation of this technique is that displacement of the screws by 10 mm or more can endanger surrounding neuronal foramina.[14] While placing the screws, several factors are taken into consideration such as the density of bone, screw length, various trajectories, bony corridors, or neurovascular and alimentary anatomy. The current study showed that their distance from the pedicle on either side was approximately 15 mm and from that of the upper rim of vertebral body was 9 mm.

These landmarks may guide the clinicians in sacral screw insertion from several entry points as in case of S1 pedicle screw placement or sacroiliac screw placement, thus ensuring patient safety pre- and postoperatively.[15] Further, the basivertebral foramens are thought to communicate with intravertebral clefts and are attributed to leakage of cement during percutaneous kyphoplasty for vertebral body compression fractures due to osteoporotic changes. The depth and extent of the canal should be kept in mind while

performing such procedures to minimize complications such as neurogenic deficit, adjacent vertebral body fractures, or pulmonary embolisms.[11]

A variety of neoplasms are known to affect the sacrum, especially involving the sacral canal such as schwannomas, neurofibromas, and ependymomas. They are known to compress adjacent neuronal structures or pelvic organs. The patient initially experiences low-back pain that can go unnoticed. A rare cavernous hemangioma is thought to involve adjacent neuronal foramina of the sacrum. The basivertebral foramina could be involved in metastasis. It is imperative that radiologists familiarize with such conditions and their extent for better diagnosis and contribute toward the treatment.[2]

Conclusion

The current study may provide an anatomical guide for clinical practice and research, thus designing therapeutical modalities in the treatment of chronic low-back pain of vertebral origin. This study may help spine surgeons or pain management physicians in exact location, morphometric of the basivertebral foramen for surgical access to this region, and thus optimize the treatment of low-back pain. The authors also suggest that the morphology of the basivertebral foramen of the S1 vertebra be taken into account for surgical fixation of sacral fractures by screw placements to minimize postoperative complications due to the involvement of neurovascular structures traversing the canal.

Financial support and sponsorship

Nil.

Conflicts of interest

There are no conflicts of interest.

References

1. Mitchell GA. The lumbosacral junction. J Bone Joint Surg 1934;16:233-54.
2. Diel J, Ortiz O, Losada RA, Price DB, Hayt MW, Katz DS. The sacrum: Pathologic spectrum, multimodality imaging, and subspecialty approach. Radiographics 2001;21:83-104.
3. Tzika M, Paraskevas GK, Piagkou M, Papatolios AK, Natsis K. Basivertebral foramina of true vertebrae: Morphometry, topography and clinical considerations. Surg Radiol Anat 2021;43:889-907.
4. Urits I, Noor N, Johal AS, Leider J, Brinkman J, Fackler N, *et al*. Basivertebral nerve ablation for the treatment of vertebrogenic pain. Pain Ther 2021;10:39-53.
5. Xu R, Ebraheim NA, Yeasting RA, Wong FY, Jackson WT. Morphometric evaluation of the first sacral vertebra and the projection of its pedicle on the posterior aspect of the sacrum. Spine (Phila Pa 1976) 1995;20:936-40.
6. Chaisuksunt V, Kwathai L, Namonta K, Rungruang T, Apinhasmit W, Chompoopong S. Occurrence of the foramen of Vesalius and its morphometry relevant to clinical consideration. Scientific World Journal 2012;2012:817454.
7. Koes BW, van Tulder MW, Thomas S. Diagnosis and treatment of low back pain. BMJ 2006;332:1430-4.
8. Lis AM, Black KM, Korn H, Nordin M. Association between sitting and occupational LBP. Eur Spine J 2007;16:283-98.
9. Paolucci T, Attanasi C, Cecchini W, Marazzi A, Capobianco SV, Santilli V. Chronic low back pain and postural rehabilitation exercise: A literature review. J Pain Res 2019;12:95-107.
10. Jancuska JM, Spivak JM, Bendo JA. A review of symptomatic lumbosacral transitional vertebrae: Bertolotti's syndrome. Int J Spine Surg 2015;9:42.
11. Wang C, Fan S, Liu J, Suyou L, Shan Z, Zhao F. Basivertebral foramen could be connected with intravertebral cleft: A potential risk factor of cement leakage in percutaneous kyphoplasty. Spine J 2014;14:1551-8.
12. Liao H, Skalski M, Bell D. Basivertebral nerve. Available from: Radiopaedia.org. [Last accessed on 2023 Aug 16]. [doi: 10.53347/rID-148622].
13. Tieppo Francio V, Sherwood D, Twohey E, Barndt B, Pagan-Rosado R, Eubanks J, *et al*. Developments in minimally invasive surgical options for vertebral pain: Basivertebral nerve ablation – A narrative review. J Pain Res 2021;14:1887-907.
14. Zheng J, Feng X, Xiang J, Liu F, Leung FKL, Chen B. S2-alar-iliac screw and S1 pedicle screw fixation for the treatment of non-osteoporotic sacral fractures: A finite element study. J Orthop Surg Res 2021;16:651.
15. Katsuura Y, Chang E, Sabri SA, Gardner WE, Doty JF. Anatomic parameters for instrumentation of the sacrum and pelvis: A systematic review of the literature. J Am Acad Orthop Surg Glob Res Rev 2018;2:e034.

Original Article

Morphometric Study of the Third Ventricle and Thalamus by Computerized Tomography

Abstract

Introduction: The third ventricle is a midline, slit-like cavity which is derived from the primitive forebrain vesicle, lying in the sagittal plane below the fornix and the corpus callosum. Much of the upper part of the lateral wall is occupied by the thalamus, that bulges convexly into the ventricle. The cerebral ventricular system acts as a marker of brain development and a predictor of neurodevelopmental outcomes. The thalamus is the gateway to the cerebral cortex. Virtually all sensory systems pass through the thalamus on their way to the cerebral cortex, and in turn, each part of the thalamus receives projections from the cortical area to which it projects. **Materials and Methods:** For the study, cranial computed tomography scans of 180 patients were studied. Anteroposterior diameter and transverse diameter of the third ventricle, thalamus, and intracranial cavity were measured and were compared with males and females of the studied population, and it was statistically analyzed. **Results:** The study showed an increase in the mean third ventricular anteroposterior and transverse diameter as age advances in the three age groups studied. There was no significant correlation in the anteroposterior or transverse diameter of the cranial cavity between the three age groups studied. Both anteroposterior and transverse diameters of the cranial cavity were larger in males when compared with females. **Conclusion:** The study in Indian adults is on morphometry of the third ventricle and thalamus by computerized tomography might help clinicians and radiologists to diagnose the pathologies ruling out the confronting effect of aging in third ventricular and thalamic dimensions. The study might also help in defining the age-specific third ventricular and thalamic diameters in the South Indian population.

Keywords: *Brain, computerized tomography, third ventricle, ventricular system*

Manjula Sajeev, R. Shubha[1], K. Sherin Jose

Department of Anatomy, KMCT Medical College, Manassery, Kerala, [1]Department of Anatomy, Kempegowda Institute of Medical Sciences, Bengaluru, Karnataka, India

Introduction

Structure of the human brain is complicated and not yet fully understood.[1] As the human brain ages, characteristic structural changes occur and these mainly include the gross and histopathologic changes with regression of the brain tissue that leads to the enlargement of ventricles. These changes are commonly expected and are considered normal. When these changes happen faster than expected, it may indicate the presence of a pathological process, including some neuropsychiatric diseases such as schizophrenia and Alzheimer's disease, as well as chronic alcoholism. Hence, the morphometric analysis of brain structures, such as volume, shape, and size of the ventricular system, has become the main area of interest recently in brain research. The knowledge about the normal and abnormal anatomy of the ventricular system of the brain is helpful for clinicians, neurosurgeons, and radiologists in clinical practice.[2] The cerebral ventricular system acts as a marker of the brain development and a predictor of neurodevelopment outcomes.[3] Morphometric analysis of the cerebral ventricular system is important for evaluating changes due to growth, aging, and intrinsic and extrinsic pathologies.[4] With the introduction of high-resolution cranial computed tomography (CT), it is possible to estimate ventricular area or diameter and this is one of the revolutionary means for morphologic study of the brain *in vivo* models and provides images of transverse slices of the brain without the use of contrast media in plain study.[5] In the present study, morphometry analysis of normal third ventricle and diencephalon in various age groups of by the South Indian population subjects was carried out to define the age-specific third ventricular and thalamic diameter variation seen across both genders [Table 1]. This study might help clinicians and radiologists to diagnose the pathologies

How to cite this article: Sajeev M, Shubha R, Jose KS. Morphometric study of the third ventricle and thalamus by computerized tomography. J Anat Soc India 2023;72:222-8.

Article Info

Received: 28 April 2022
Revised: 13 August 2023
Accepted: 13 August 2023
Available online: 28 September 2023

Address for correspondence:
Dr. Manjula Sajeev, Department of Anatomy, KMCT Medical College, Manassery - 673 602, Kerala, India.
E-mail: manjula.sajeev123@gmail.com

Access this article online

Website: https://journals.lww.com/joai
DOI: 10.4103/jasi.jasi_73_22
Quick Response Code:

Table 1: Demographic profile of the study groups depicting height and weight of the individuals expressed in terms of mean±standard deviation based on their age and gender as actual numbers

Variable	Group 1	Group 2	Group 3
Age (years)	18–40	41–60	61 and above
Gender (*n*)			
Male	30	30	30
Female	30	30	30
Height (cm)	157.45±5	159.61±8.57	160.35±10.25
Weight (kg)	61.48±10.1	64.53±9.78	63.32±10.61

ruling out the confronting effect of aging in third ventricular and thalamic dimensions.

Materials and Methods

Subject recruitment and sample collection

The study was carried out at the Department of Anatomy in association with the Department of RadioDiagnosis, KIMS Hospital, Bengaluru. During the period of study, written informed consent for the purposive sampling technique was collected from the subjects through the Department of Radiodiagnosis, KIMS Hospital, Bengaluru, and all normal cranial CT scans of patients aged above 18 years of either sex were chosen for the study. It encompasses three groups mainly consisting of 30 males and 30 females aged between 18 and 40 years, 30 males and 30 females aged above 61 years above, and 30 males and 30 females aged between 41 and 60 years were chosen to assess the cranial CT scans of 180 patients in total.

Measurements of the thalamus and third ventricle diameter

The anteroposterior diameter of the third ventricle was measured in mm from the column of the fornix to the pineal gland. Similarly, for the thalamus, it was from the anterior pole of the thalamus to the pulvinar. The transverse diameter of the third ventricle and thalamus was measured, assessing the maximum transverse diameter in mm along the horizontal axis.

Measurements of intracranial diameter

The intracranial anteroposterior diameter was measured in the midline of the cranial cavity and the maximum intracranial transverse diameter was also measured.

From the measured data, the anteroposterior diameter and transverse diameter of the third ventricle, thalamus, and intracranial cavity were compared with males and females of the studied population.

Statistical analysis

Descriptive statistical analysis was carried out, and results of continuous data were described in terms of mean ± standard deviation, and the results of categorical data were presented in proportions (%). Statistical significance was assessed at $P > 0.05$ for not statistically significant groups, $0.01< P \leq 0.05$ levels for moderately statistically significant outcomes, and $P \leq 0.01$ was taken up for highly statistically significant data. Student's *t*-test (two-tailed, independent) has been used to find the significance of study parameters on a continuous scale between three groups. The Pearson correlation has been used to assess the correlations between the three groups. ANOVA test has been used to find out the variability of different parameters in three groups.

Results and Discussion

The majority of patients in the age group of 18–40 years who underwent CT brain [Figure 1] gave a history of fall (33%) and headache (32%). The majority of patients in the age group of 41–60 years who underwent CT brain gave a history of fall (35%), loss of consciousness (27%), and dizziness (20%). The majority of patients in the age group of 60 years and above who underwent CT brain gave a history of fall (40%) and dizziness (32%) [Figure 2].

Third ventricular measurements

The mean anteroposterior diameter and transverse diameter of the third ventricle in the age group of 18–40 years are 24.01 ± 1.56 mm and 7.04 ± 1.88 mm, respectively. The mean anteroposterior diameter and transverse diameter of the third ventricle in the age group of 41–60 years are 24.39 ± 2.43 mm and 7.42 ± 1.24 mm, respectively. The mean anteroposterior diameter and transverse diameter of the third ventricle in the age group of 61 years and above are 25.31 ± 4.14 mm and 8.16 ± 1.96 mm, respectively. From the above values, we observed an increase in the mean third ventricular anteroposterior and transverse diameter as age advances in the three age groups studied. The anteroposterior diameter of the third ventricle in the Mumbai population of age <60 years was found to be 24.1 mm in females and 24.2 mm in males by Meshram and Hattangdi[1] In our study, we found that the mean anteroposterior diameters were 23.67 ± 1.37 mm and 24.28 ± 1.68 mm in females and males, respectively, in the 18–40-year age group. In the 41–60-year age group, the values are 24.27 ± 2.72 mm and 24.50 ± 2.15 mm. We did not find any statistically significant difference between male and female values, and all these values are in accordance with the previously published studies. The mean anteroposterior diameter is 25.18 ± 3.81 mm and 25.43 ± 4.51 mm in females and males, respectively, and the difference was not statistically significant in the age group of 61 years and above [Figure 3]. Meshram and Hattangdi observed the same (25.1 mm and 25.3 mm, respectively, with statistical significance not commented on in specific age groups by the authors).[1]

The transverse diameter of the third ventricle in the Mumbai population of age <60 years was found to be 5.73 mm in

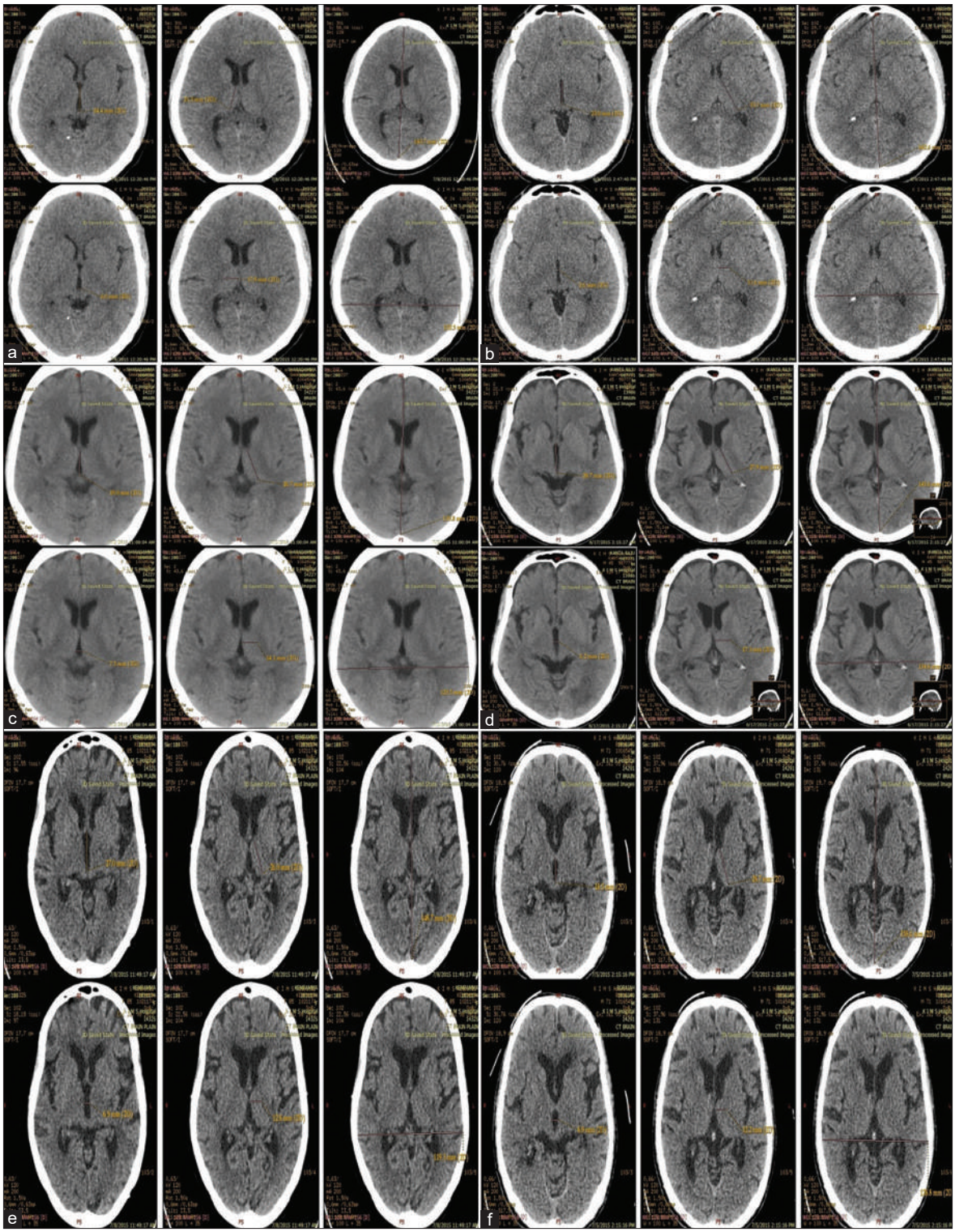

Figure 1: Computed tomography images of third ventricular and thalamic dimensions of three different age groups (a) between 18 and 40 years – males, (b) between 18 and 40 years – females, (c) between 41 and 60 years – males, (d) between 41 and 60 years – females, (e) above 60 years of age – males, (f) above 60 years of age – females segregated into male and female subjects

females and 7.26 mm in males by Meshram and Hattangdi. In our study, we found that the mean transverse diameters were 6.50 ± 1.63 mm and 7.47 ± 1.97 mm in females and males, respectively, in the 18–40-year age group. In the 41–60-year age group, the values are 7.10 ± 1.13 mm and 7.74 ± 1.29 mm. We found a statistically significant difference between male and female values, and all these values are in accordance with the previously published studies of Meshram and Hattangdi.[1] In the age group of 61 years and above, the mean third ventricular transverse

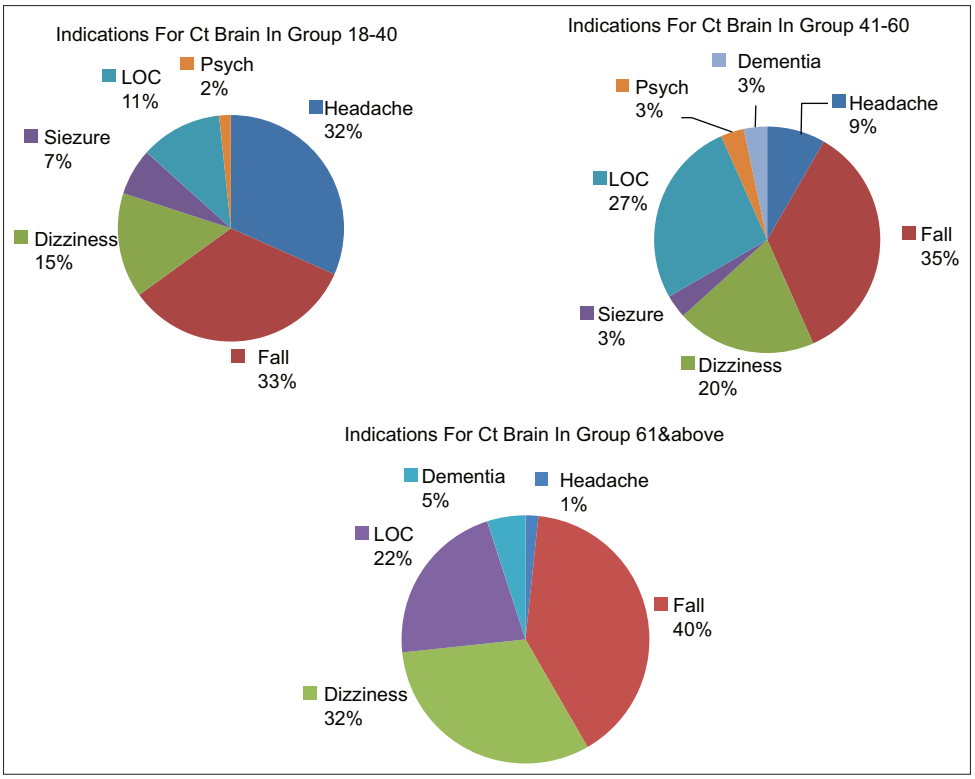

Figure 2: Pie diagram showing the distribution of indications for taking CT among the three age groups. CT: Computed tomography, LOC: Loss of consciousness

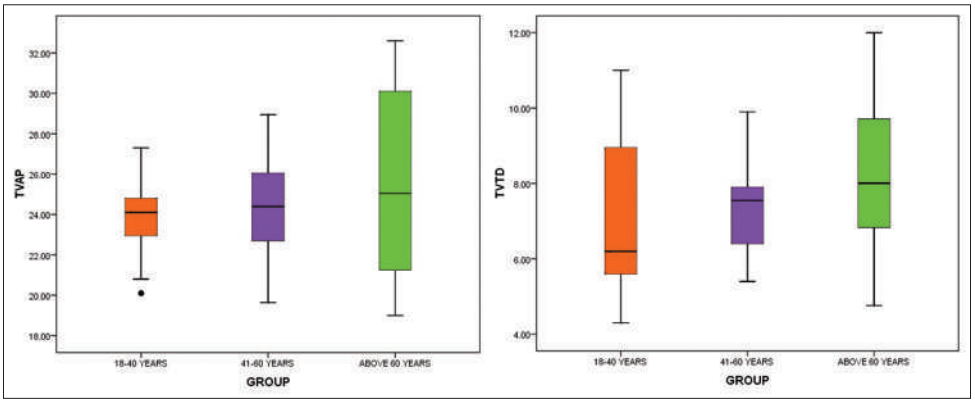

Figure 3: Third ventricular dimensions in three age groups depicting the TVAP diameter. TVTD: Third ventricular transverse diameter, TVAP: Third ventricular anteroposterior

diameter is 7.87 ± 2.22 mm and 8.45 ± 1.65 mm in females and males, respectively, and the difference was not statistically significant in our study. Meshram and Hattangdi observed the same (7.99 mm and 8.43 mm, respectively, a statistical significance not commented on in specific age groups by the authors).[1] This similarity in the values noted in our study when compared with Meshram and Hattangdi's study may be due to the similarity in the total number of the population studied and the studied population in both were Indian.

The values studied in males remained larger than females may be explained in this way. The Ideas of differences in male and female brains, circulated during time of ancient and Greek philosopher. In 1854, Emil Huschke discovered that the frontal lobe of the male is all of 1% larger than that of the females. As the 19th century progressed, scientists began researching sexual dimorphisms in the brain significantly more. Many studies attributed these changes to sexual selection and mate preference throughout evolution. There are many other factors, like sex hormones, that play an important role in the differences between male and female brain anatomy. Alteration in cerebral white matter and subcortical neurological loss may be the predominant effect of age-related atrophy. The causes of sex differences in brain atrophy are still unclear and may be attributed to internal and external factors. Sex

hormones may be involved in the former, whereas natural environment, family circumstances, education, and habits such as smoking and alcohol may be involved in the latter. Compared with external factors, levels of sex hormones on brain structures may be more important. Testosterone administration enhances spatial cognition in older men, which suggests a relationship between testosterone, brain volume, and spatial cognition.[6] This explains the larger dimensions of the third ventricle in males.

Thalamic measurements

In the present study, the mean anteroposterior diameter and transverse diameter of the thalamus in the age group of 18–40 years are 31.9 ± 2.34 mm and 14.35 ± 1.86 mm, respectively. The mean anteroposterior diameter and transverse diameter of the thalamus in the age group of 41–60 years are 30.75 ± 4.27 mm and 14.14 ± 1.68 mm, respectively. The mean anteroposterior diameter and transverse diameter of the thalamus in the age group of 61 years and above are 29.24 ± 3.02 mm and 13.92 ± 1.72 mm, respectively. From the above values, we observed a decrease in mean thalamic anteroposterior and transverse diameter as age advances in the three age groups studied.

The anteroposterior diameter of the thalamus in the Mumbai population of age < 60 years was found to be 30.18 mm in females and 31.05 mm in males by Meshram and Hattangdi.[1] In our study, we found that the mean anteroposterior diameters were 31.11 ± 2.29 mm and 32.53 ± 2.21 mm in females and males, respectively, in 18–40-year age group. In 41–60-year age group, the values are 29.99 ± 3.04 mm and 31.50 ± 5.16 mm, respectively. We did not find any statistically significant difference between male and female values in the age group of 41–60 years, but it is statistically significant in the 18–40-year age group [Figure 4]. All these values are in accordance with the previously published studies.

In our study 61 years and above, the mean anteroposterior diameter is 28.90 ± 3.65 mm and 29.58 ± 2.25 mm in females and males, respectively, and the difference was statistically not significant. Meshram and Hattangdi observed the same (28.90 and 29.60 mm, respectively, with statistical significance not commented on in specific age groups by the authors).[1]

The transverse diameter of the thalamus in the Mumbai population of age <60 years was found to be 14.22 mm in females and 14.15 mm in males by Meshram and Hattangdi.[1] In our study, we found that the mean transverse diameters were 14.19 ± 1.84 mm and 14.47 ± 1.90 mm in females and males, respectively, in the 18–40-year age group. In the 41–60-year age group, the values are

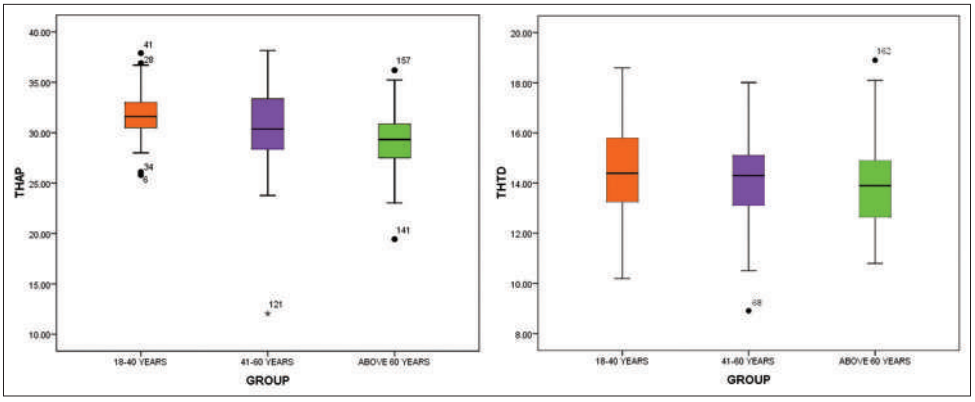

Figure 4: Thalamic dimensions in three age groups depicting THAP – Anteroposterior diameter of the thalamus. THTD: Transverse diameter of the thalamus

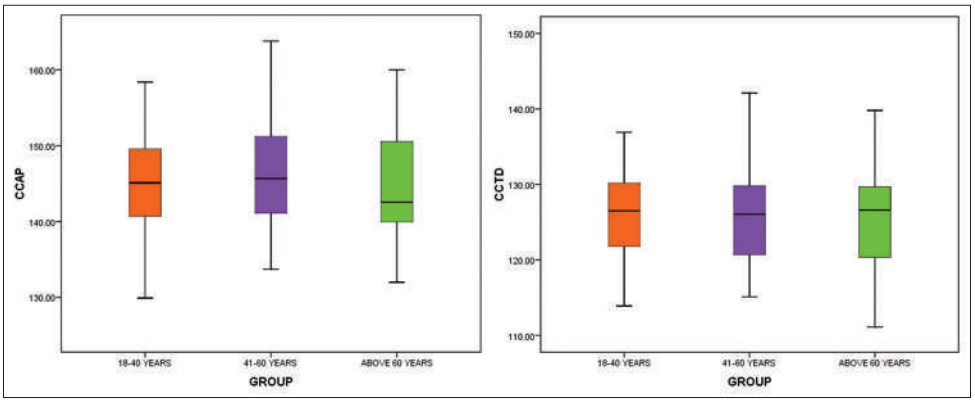

Figure 5: Cranial cavity measurements in three age groups depicting the CCAP diameter CCTD: Cranial cavity transverse diameter, CCAP: Cranial cavity anteroposterior

13.91 ± 1.88 mm and 14.38 ± 1.44 mm. We did not find a statistically significant difference between male and female values, and all these values are in accordance with the previously published studies of Meshram and Hattangdi.[1]

In the present study of the age group of 61 years and above, the mean transverse diameter of the thalamus is 13.63 ± 1.53 mm and 14.21 ± 1.86 mm in females and males, respectively, and the difference was not statistically significant. Meshram and Hattangdi observed the same (13.60 and 14.21 mm, respectively, with statistical significance not commented on in specific age groups by the authors).[1] The similarity between our study and the study conducted by Meshram and Hattangdi may be due to the similarity in the number of population studied and the studied population in both were the Indian population.

Cranial cavity measurements

In our study, the mean anteroposterior diameter and transverse diameter of the cranial cavity in the age group of 18–40 years are 144.81 ± 7.21 mm and 126.05 ± 5.58 mm, respectively. The mean anteroposterior diameter and transverse diameter of the cranial cavity in the age group of 41–60 years are 146.48 ± 7.29 mm and 126.19 ± 6.20 mm, respectively. The mean anteroposterior diameter and transverse diameter of the cranial cavity in the age group of 61 years and above are 144.78 ± 7.12 mm and 125.62 ± 6.29 mm, respectively [Figure 5]. We observed that there is no significant correlation

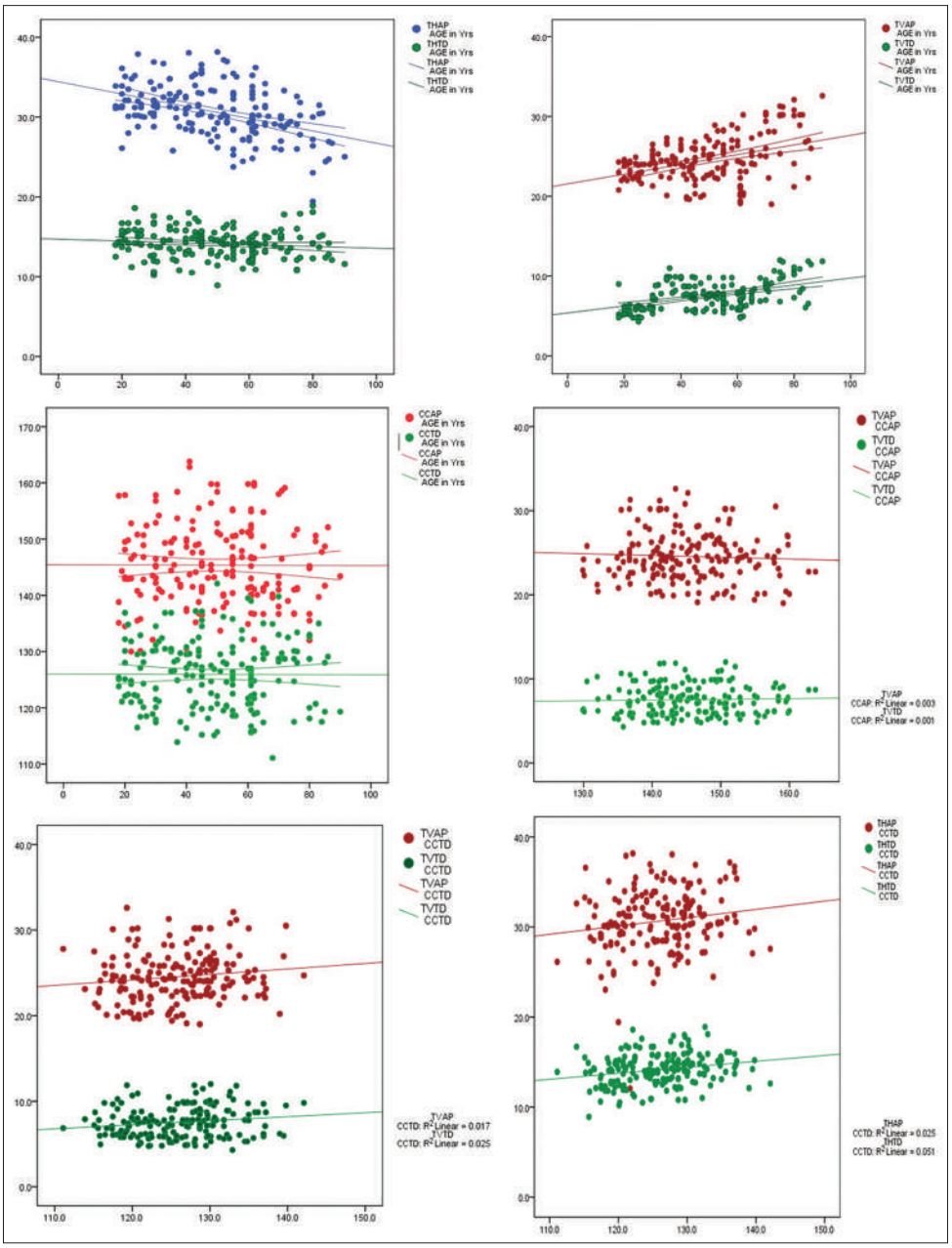

Figure 6: Correlation between various parametric measurements with age- and gender-based characteristics

with age in anteroposterior or transverse diameter of the cranial cavity in the three age groups [Figure 6].

Conclusion

This study in Indian adults is on morphometry of the third ventricle and thalamus by computerized tomography. This study might help clinicians and radiologists to diagnose the pathologies ruling out the confronting effect of aging in third ventricular and thalamic dimensions. The study might also help in defining the age-specific third ventricular and thalamic diameters in the South Indian population.

Acknowledgement

The authors sincerely thank those who were included in the study so that the research could be performed. These results from such research can potentially increase the overall knowledge to the clinicians and will be beneficial for the society too.

Financial support and sponsorship

Nil.

Conflicts of interest

There are no conflicts of interest.

References

1. Meshram P, Hattangdi S. The morphometric study of third ventricle and diencephelon by computerised tomography. Indian J Appl Basic Med Sci 2012;14 B: 8-13.
2. Srijit D, Shipra P. Anatomical study of anomalous posterior horn of lateral ventricle of brain and its clinical significance. Bratisl Lek Listy 2007;108:422-4.
3. Roza SJ, Govaert PP, Vrooman HA, Lequin MH, Hofman A, Steegers EA, *et al.* Foetal growth determines cerebral ventricular volume in infants the generation R study. Neuroimage 2008;39:1491-8.
4. Aziz A, Hu Q, Nowinski WL. Morphometric analysis of cerebral ventricular system from MR images. Med Image 2004;5369:574-82.
5. Gawler J, Bull JD, Du Boulay GH, Marshall J. Computerized axial tomography: The normal EMI scan. J Neurol Neurosurg Psychiatry 1975;38:935-47.
6. Bayat PD, Ghanbari A, Moradi M, Raoofi A. The effects of age and sex on brain volume. Int J Morphol 2014;32:1477-83.

Original Article

Psychosocial Stress and Fertility: The Preventive Potentials of Vitamin E

Raphael Eguono Uwejigho, Kingsley Afoke Iteire, Felix U. Enemali

Department of Anatomy, Faculty of Basic Medical Sciences, University of Medical Sciences, Ondo, Nigeria

Abstract

Background: Chronic exposure to psychosocial stressor could lead to various side effects, such as maladaptation by various physiological and immunological systems. **Objective:** This study investigated psychosocial stress-induced damage on the testes and epididymis using animal models and the effects of Vitamin E. **Materials and Methods:** A total 40 adult Wistar rats were divided into 2 groups (S and L) representing 52 and 104 days of experimentation. The 2 groups were subdivided into 4 groups each (S = A–D and L = E–H, n = 5 each). Groups A and E served as control, B and F were psychosocially stressed, C and G were administered 50 mg/kg of Vitamin E, while D and H were psychosocially stressed and administered 50 mg/kg of Vitamin E for 52 and 104 days, respectively. Psychosocial stress was induced on the rats using cats as predator. The weight, blood parameters, and tissue samples were obtained on days 53 and 105 and analyzed. Statistical analysis was carried out using GraphPad Prism Version 8 (San Diego, CA, USA). **Results:** Psychosocial stress resulted in a significant reduction in weight and negatively affected oxidative stress markers and sperm parameters of the animals ($P < 0.05$). Histological analysis showed that stress arrested spermatogenesis and disorganized the seminiferous tubular epithelium and reduced the semen quality. There was scanty sperm in the epididymis of stressed groups. However, Vitamin E reversed these changes and improved the quality of semen compared to the negative control group. **Conclusion:** Vitamin E was potent at ameliorating the deleterious effects of psychosocially induced stress.

Keywords: *Infertility, male fertility, posttraumatic stress disorder, psychosocial stress, Vitamin E*

Introduction

Psychosocial stress is seen as a result of the ineptness to appropriately manage day-to-day demands when they go beyond coping resources.[1] Some of these stressors include thinking of how to provide for the family, especially in a jobless society; a backwash of vulnerability to hash, adverse or tragic life occurrences in the convivial environment; the anxiousness to cater for the children's school fees or the "Coronaphobia" of COVID-19.[2] Irrespective of the diversity between the psychosocial stress which vary with populations, chronic exposure to psychosocial stressor could lead to various side effects, such as maladaptation by various physiological and immunological systems.[1]

Several researchers have divulged the connection between stress and infertility in male animals.[3-5] These reports show that chronic psychological and physical stress reduces rat's sperm population, motility, and fertilization capacity. Chronic stress can induce erectile dysfunction, possibly resulting from neuronal changes in various erectile tissues.[6] Available research within reach divulge that stress exposure upregulates the exertion of the hypothalamic–pituitary–adrenal (HPA) axis and with a consequent lowering of the hypothalamic–pituitary–gonadal (HPG) axis activities.[7] There is inhibition of testosterone (TESTO) secretion in male animals open to chronic stress.[8] Exposure of males to chronic stress can also result in suppression of spermatogenesis,[9,10] reduction in fertility, and sexual behavior of animals.[11,12] This is elucidated by the actuality of the stress system and reproductive system *modus operandi* being directly linked.[13]

Vitamin E is an organic fat-soluble compound found predominantly in the membrane of cells.[14] It is a potent antioxidant and stops free radicals (hydroxyl) and superoxide, thereby diminishing the peroxidation of lipids created by reactive oxygen species (ROS) at

How to cite this article: Uwejigho RE, Iteire KA, Enemali FU. Psychosocial stress and fertility: The preventive potentials of Vitamin E. J Anat Soc India 2023;72:229-38.

Article Info

Received: 04 April 2022
Accepted: 13 August 2023
Available online: 28 September 2023

Address for correspondence:
Dr. Raphael Eguono Uwejigho, Department of Anatomy, Faculty of Basic Medical Sciences, University of Medical Sciences, P.M.B. 536, Laje Campus, Ondo, Nigeria.
E-mail: ruwejigho@unimed.edu.ng

Access this article online

Website: https://journals.lww.com/joai
DOI: 10.4103/jasi.jasi_54_22
Quick Response Code:

the plasma membrane level.[14] Various researches on Vitamin E supplementation have revealed significant benefit on semen parameters, especially its effect on sperm motility.[15-17] Others, however, have indicated its inefficiency in providing any significant effect on semen parameters.[18]

Studies have reported the decline in male fertility rate of 15% worldwide which affects approximately 8%–12% of couples who wants to conceive.[19,20] Male infertility is the sole contributing factor in roughly 40%–50% of infertility cases, of which 25% is idiopathic[20,21] The prevalence of infertility in Sub-Saharan Africa affects approximately 20%–40% of its population. In Nigeria, 40% to 50% is attributed to male causes, varying from region to region and reported to be on the increase.[22] Myriad of challenges encountered in these regions could be a predisposing factor in emotional trauma and psychosocial stress, thus, increasing the prevalence of infertility.[22] To access this demeanor of individuals, the focus is directed toward psychosocial stress where the provenance of the stressor is neither exercise nor physical exertion related. There is fewness of data on the eventuality of psychosocial stress on the testes and epididymis and its management using Vitamin E; therefore, it is increasingly important that researchers focus on pharmacological compounds with stress ameliorating capacity, in order to reduce the growing menace which severely affect male fertility.

This study investigated the effect of Vitamin E on psychosocial stress-induced damage on the testis and epididymis by evaluating the effects of Vitamin E on the body weight and organ weight, parameters of oxidative stress of the testis, serum concentration of gonadotropic and testicular hormones, corticosterone (cortisol), and the histology of the testis and epididymis of Wistar rats exposed to psychosocial stress.

Materials and Methods

Experimental design

A total of 40 adult Wistar rats (180–250 g) were divided into 2 groups (S – short duration and L – long duration, n = 20 each) representing 52 days and 104 days of experimentation. Each of these groups was subdivided into 4 groups (S = A–D and L = E–H, n = 5). Groups A and E served as control and were neither administered Vitamin E nor psychosocially stressed. Groups B and F were psychosocially stressed in a posttraumatic stress disorder (PTSD) animal model chamber for 3 h/exposure daily for 52 and 104 days' duration (respectively) without Vitamin E administration. Groups C and G were administered with a daily dose of 50 mg/kg/body weight of Vitamin E only for 52 and 104 days (respectively) without exposure to psychosocial stress. Groups D and H were administered with a daily dose of 50 mg/kg/body weight of Vitamin E and placed in the PTSD animal model chamber for 3 h/exposure daily for 52 and 104 days' duration (respectively), and all rats in these groups were sacrificed on the 53rd and 105th days, respectively.

Procedure for induction of psychosocial stress

Each adult Wistar rat was kept in a 20 cm × 20 cm × 10 cm metal cage restrainer (PTSD animal model chamber) and taken to the cats housing and placed on the floor of the room with the adult cats. The metal cage restrainer forestalled any physical acquaintance between the cats and the rats, but the rats were exposed to all sensory stimuli associated with the cat. Cat feed was given to the cats to heighten cat motor activity during exposure. Each rat restrainer was placed in between the predator cats at certain duration and intervals to induce a preclinical PTSD that closely portrays signs and symptoms as observed in human patients.[23,24] The animals were randomly sorted in their original cages after each stress.

Animal care and management

Adult Wistar rats were obtained from the animal holdings of the Department of Anatomy, University Benin. The rats were sheltered in well-ventilated wooden cages in the animal facility of the Department of Anatomy, University of Benin, Benin City. The rats were left to acclimatize to the environment for 2 weeks under standard laboratory conditions before the experiment commenced. The rats in each group were allowed access to standard rat chow (Premier Feed Mills Co. Ltd, a subsidiary of Flour Mills of Nigeria Plc) and water *ad libitum* throughout the experimental period. The two cats utilized for all predator exposures were obtained from Uselu market, Ugbowo, Benin City. The cats were acclimatized for 2 weeks and sheltered in an open room with access to food and water freely throughout the experimental period. The cat room was maintained on the same light/dark cycle as that of the rats. The animals were weighed twice a week using a top loader weighing scale. Care and management of animals were done in accordance with international, national, and institutional guidelines for the care and use of laboratory animals in biomedical research.[25]

Collection and management of Vitamin E

Natural synthetic pure Vitamin E, a product of Nature's field (a dietary supplement) Vitamin E 1000 IU, manufactured by Bactolac Pharmaceutical Inc., 7 Oser Avenue, Hauppauge, NY 11788, USA, NAFDAC REG NO: B4-1620, was obtained from Grace Pharmaceutical stores, Ugbowo, Benin city and stored in dark containers prior to administration.

Collection of blood samples/hormonal assay

At the end of each experimental phase, blood samples were collected in lithium heparin bottles from the inferior vena cava of each rat after sacrifice. The blood samples were then centrifuged at a speed of 5000 revolutions per minute for 15 min. The supernatant was then collected, refrigerated at −20°C, and later assayed for prolactin (PRL), estrogen (ESTROG), cortisol,

progesterone (PROG), luteinizing hormone (LH), follicle-stimulating hormone (FSH) and TESTO using enzyme-linked immunosorbent assay (ELISA) and hormone test kits (AccuBind ELISA Microwells manufactured by Monobind Inc., Lake Forest, CA 92630, USA).

Procedure for luteinizing hormone

The procedure for luteinizing hormone as described by Tietz was adopted.[26]

Procedure for prolactin and follicle-stimulating hormone

The procedure is same with LH except for the specific enzyme-labeled antibody biotinylated monoclonal mouse immunoglobulin G in buffer, dye, and preservative.[27]

Procedure for testosterone and corticosterone

The procedure for TESTO and corticosterone as described by Tietz was adopted.[26]

Procedure for progesterone and estrogen

The procedure for Progesterone and estrogen as described by Tietz was adopted. The vial of working substrate for PROG contains PROG (analog)-horseradish peroxides (HRP) conjugate in a protein stabilizing matrix with red dye and the vial working substrate for estradiol contains estradiol (analog)-HRP conjugate in protein stabilizing matrix with red dye.[26]

Tissue processing

Standard histological techniques were employed for the testis tissue processing and staining[28,29] as described below.

The testes were trimmed to about 3–5 mm thick sections and processed using the paraffin wax embedding method as follows. Sections were dehydrated for 1 h each at room temperature through ascending grades of ethanol: 70% ethanol, 90% ethanol, absolute ethanol I, and Absolute ethanol II. The dehydrated tissues were cleared in two changes of xylene for 1 h in each change followed by infiltration in two changes of molten paraffin wax at 60°C for 1 h in each change and finally embedding in paraffin wax multi-block plastic embedding molds. The paraffin-blocked tissues were trimmed and mounted on wooden chocks for sectioning on a rotary microtome.

Sections of 5 μm thickness were produced from the tissue blocks using a rotary microtome (Bright B5143, Huntington, England). The sections were transferred into water bath (40°C) to allow the spreading of the folded ribbons of sections. These sections were mounted on clean glass slides and dried at 40°C on a slide drier to enhance adherence of the sections of the slides.

Hematoxylin and eosin staining procedures

The sections were washed for 2 min in xylene twice and rinsed for four min in alcohol twice. They were subsequently hydrated by sequential passage through descending grades of alcohol with the final passage in distilled water, as indicated in Table 1.[28,29]

Photomicrography

Slides containing histological sections were examined under Olympus CX 23 research microscope with an attached digital camera manufactured by Olympus Opto Systems India Pvt. Ltd. A-5, Mohan Co-operative Industrial Estate, New Delhi - 110 044, India. Photomicrographs of the tissue sections were taken at various magnifications, and an objective micrometer gauge was used to measure the diameter of the field of view.

Table 1: Preparation and staining of tissue sections

Step	Procedure	Duration
1a	1st wash in xylene to dewax	2 min
1b	2nd wash in xylene to dewax	2 min
2a	Rehydrate in alcohol absolute grade I	2 min
2b	Rehydrate in alcohol absolute grade II	2 min
2c	Rehydrate in 95% alcohol	2 min
2d	Rehydrate in 90% alcohol	2 min
2e	Rehydrate in 70% alcohol	2 min
2f	Rehydrate in 50% alcohol	2 min
3	Rinse in distilled water	3 min
4	Stain in hematoxylin	15–20 min
5	Rinse under running water to remove excess stain	2–3 min
6	Examine section under microscope to confirm adequate staining	
7	Dip in acid alcohol (0.5% HCL in 70% ethanol)	3 s
8	Rinse under running water to remove acid alcohol	10–15 min
9	Counterstain in 1% aqueous eosin	2–4 min
10	Rinse under running water to remove excess stain	
11	Dehydrate rapidly in ascending grades of ethanol (50% through absolute ethanol)	
12	Clear in xylene and mount in a synthetic resin medium (DPX) using clean glass cover slip	

DPX: Dibutylphthalate Polystyrene Xylene, HCL: Hydrochloric acid

Statistical analysis

The data procured were analyzed using descriptive statistics and inferential statistics. Values were presented as mean ± standard error of means (SEM) on tables. All statistical analysis was done with the aid of GraphPad Prism (Version 8) software manufactured by GraphPad Software Inc., 7825 Fay Avenue, Suite 230 La Jolla, CA 92037, USA. The significance of the difference in the means of all parameters was determined using one-way analysis of variance (95% confidence interval) for more than two sets of data comparison and *t*-test for two sets of data. A *post hoc* test was carried out using Dunnett's multiple comparisons for all groups and compared with control. $P < 0.05$ was considered statistically significant.

Ethical approval

Prior to the commencement of this research, ethical clearance was obtained in the year 2018, with reference number UPH/CEREMAD/REC/MM55/012 from the University of Port Harcourt Ethics Committee, Rivers State, Nigeria.

Results

Data analysis

The results of this study are presented in bars and micrographs. Values are represented as Mean ± SEM for each group; alphabets "*" indicates a significant difference at $P < 0.05$ change in weight compared with control.

Effect of psychosocial stress, Vitamin E on body weight

Figure 1a and b shows the body weight of rats psychosocially stressed only, treated with Vitamin E only, and those stressed and treated with Vitamin E for 52 and 104 days, respectively, compared with control. A significant decrease ($P = 0.0047$) was noticed in the final body weights of rats exposed to stress for 52 days when compared with control. No significant divergence was noticed in the final body weight of rats treated with only Vitamin E ($P > 0.99$), stressed, and treated with Vitamin E ($P = 0.2334$) for 52 days when compared with control. There was a significant decrease ($P = 0.0008$) in the final body weight of rats psychosocially stressed for 104 days in comparison with the control. No significant difference was seen in the final body weights of rats treated with only Vitamin E ($P = 0.0794$), psychosocially stressed, and treated with Vitamin E ($P = 0.1169$) for 104 days when compared with control.

Effect of psychosocial stress, Vitamin E on organ weight

Figure 2a and b shows the comparison of organ weights of rats psychosocially stressed only, treated with Vitamin E only, and those stressed and treated with Vitamin E for 52 and 104 days with control. There was a significant decrease in the weights of the right testes ($P = 0.0133$), left testes ($P = 0.0148$), paired testes ($P = 0.0052$), right epididymis ($P = 0.0005$), left epididymis ($P < 0.0001$), and paired epididymis weight ($P < 0.0001$) of rats after stress for 52 days when compared with control. No significant difference ($P > 0.05$) was seen in the weights of the right testes, left testes, paired testes, right epididymis, left epididymis, and paired epididymis weight of rats treated with only Vitamin E and those treated with Vitamin E and stressed for 52 days when compared with control. However, the weight of the testes and epididymis in relativity to body weight was significantly elevated ($P = 0.0001$ and $P = 0.0440$, respectively) in the stressed group when compared with control. There was a significant decrease in the right testes ($P < 0.0001$), left testes ($P = 0.0007$), paired testes ($P = 0.0001$), right epididymis ($P = 0.0004$), left epididymis ($P = 0.0007$), and paired epididymis weight ($P = 0.0006$) of rats open to stress for 104 days when compared with control. No significant difference ($P > 0.05$) was seen in the weights of the right testes, left testes, paired testes, right epididymis, left epididymis, and paired epididymis weight of rats administered with only Vitamin E and those treated with Vitamin E and psychosocially stressed for 104 days when compared with control. However, the relative testis weight was significantly lower ($P = 0.0430$) in the stressed group only when compared with the control group as against

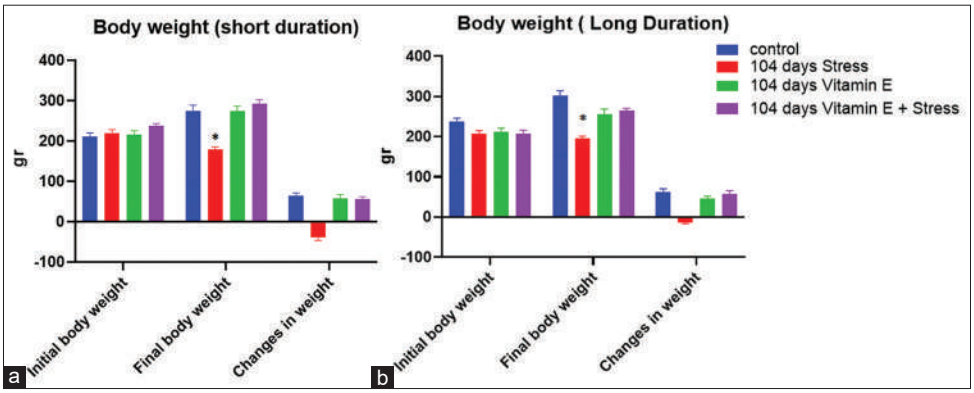

Figure 1: (a and b) Comparison of body weight of rats exposed to stress and administered with 50 mg/body weight of Vitamin E for 52 and 104 days with control [alphabet * indicate a significant difference at P < 0.05] compared with control

other groups but no significant difference ($P > 0.05$) in relative epididymis weight in all groups.

Effect of psychosocial stress, Vitamin E on hormonal profile

Figure 3a shows the comparison of hormonal levels of rats psychosocially stressed only, treated with Vitamin E only, and those stressed and treated with Vitamin E for 52 days. In groups B and F, there was significant elevation ($P = 0.0004$) in cortisol concentration, significant decrease in the concentrations of FSH ($P = 0.0130$), LH ($P = 0.0036$), PROG ($P = 0.0147$), ESTROG ($P = 0.0118$), and TESTO ($P = 0.0142$) when compared with control. However, PRL in the stressed (only) group showed no significant difference ($P > 0.05$) in concentration when compared with control. There was no significant difference ($P > 0.05$) in the concentrations of cortisol, FSH, LH, PRL, PROG, ESTROG, and TESTO of animals treated with only Vitamin E for 52 days when compared with control. No significant difference ($P > 0.05$) was seen in the concentrations of cortisol, FSH, LH, PRL, PROG, ESTROG, and TESTO of animals treated with Vitamin E and stressed for 52 days when compared with control.

Figure 3b shows the comparison of hormonal levels of rats psychosocially stressed only, treated with Vitamin E only, and those stressed and treated with Vitamin E for 104 days. There was no significant difference ($P > 0.05$) in the level of cortisol, FSH, LH, PRL, PROG, and ESTROG of rats stressed (only) for 104 days when compared with control. There was significant depletion ($P = 0.0106$) in the level of TESTO in the stressed (only) group when compared with control. There was no significant difference ($P > 0.05$) in the level of cortisol, FSH, LH, PRL, PROG, ESTROG, and TESTO of rats treated with only Vitamin E for 104 days when compared with control. No significant change ($P > 0.05$) was seen in the level of cortisol, FSH, LH, PRL, PROG, ESTROG, and TESTO of rats treated with Vitamin E and stressed for 104 days when compared with control.

Discussion of Findings

Effect of psychosocial stress on body weight and organ weight

In this research, the effect of short and long duration of psychosocial stress on animal body weight and organ weight (testes and epididymis) was significantly reduced as

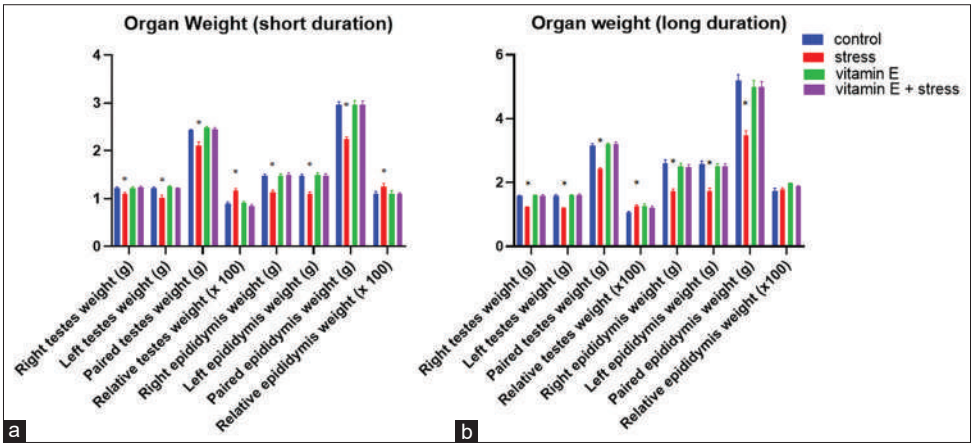

Figure 2: (a and b) Comparison of organ weight of rats stressed, administered with Vitamin E for 52 and 104 days with control [alphabet * indicate a significant difference at P < 0.05] compared with control

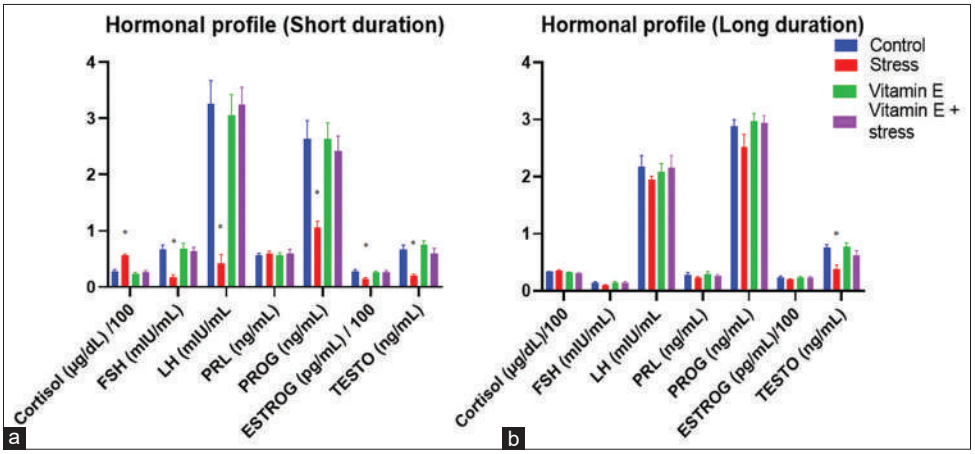

Figure 3: (a and b) Comparison of hormonal levels of rats psychosocially stressed, treated with Vitamin E for 52 and 104 days with control [alphabet * indicate a significant difference at P < 0.05] compared with control

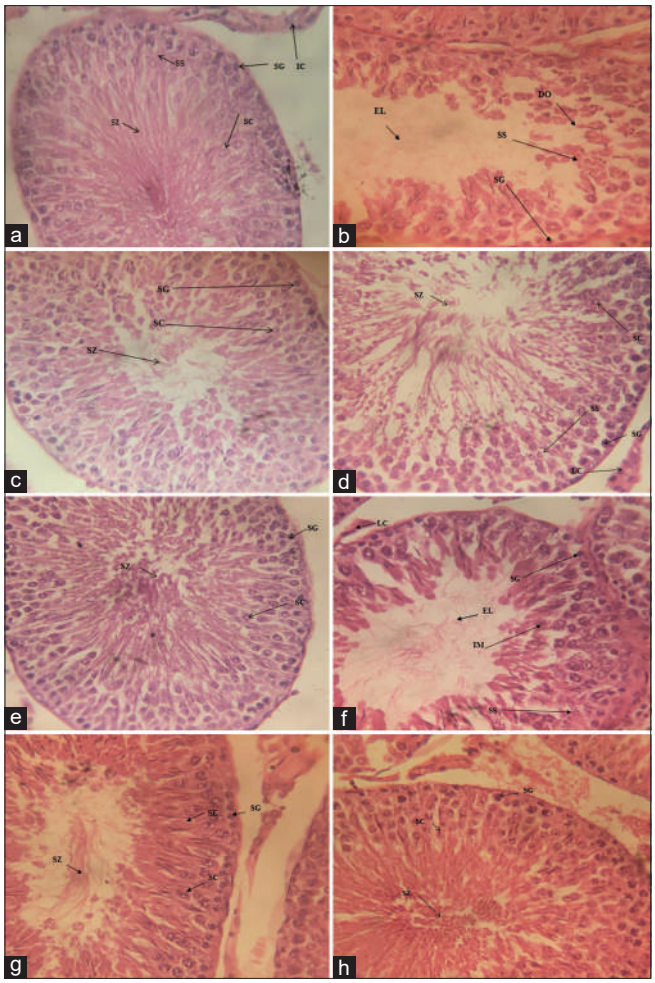

Figure 4: (a-d): Photomicrograph of the seminiferous tubule of Wistar rat sacrificed on the 53rd day showing normal seminiferous tubules lumen containing tufty tails of SZ, epithelium of the seminiferous tubules containing cells of the spermatogenic series including SG, SC, and IC of Leydig and SSs in (a). EL of the seminiferous tubules and disorganization of the epithelium of the seminiferous tubule (DO), SG, and SS in (b). Normal seminiferous tubules lumen containing tufty tails of SZ, epithelium of the seminiferous tubules containing cells of the spermatogenic series including SG and SC in (c). Normal seminiferous tubule lumen containing tufty tails of SZ, epithelium of the seminiferous tubules containing cells of the spermatogenic series including SG and SC, LC, and SS in (d) (×400, H and E). (e-h) Photomicrograph of the seminiferous tubule of Wistar rat sacrificed on the 105th day showing normal seminiferous tubule lumen containing clumps of SL, interstitial epithelium of the seminiferous tubules (SE) containing cells of the spermatogenic series including SG and SC in (e). Scanty to EL, immature cells in the lumen (IM) and SG, LC, and SS (f). Seminiferous tubules lumen containing clumps of SZ, interstitial epithelium of the seminiferous tubules (SE) containing cells of the spermatogenic series including SG and SC in (g). Lumen containing clumps of SZ, interstitial epithelium of the seminiferous tubules (SE) containing cells of the spermatogenic series including SG and SC in (h) (×400, H and E). SZ: Spermatozoa, SG: Spermatogonia, SC: Spermatocytes, SS: Sertoli cells, EL: Empty lumen, IC: Interstitial cells, LC: Leydig cells, SL: Spermatozoa, DO: Disorganized epithelium tubules, IM: immature cells in the lumen, SE: Seminiferous Epithelium

compared with control. In all groups, a decrease in weight was observed in the stressed group only, but in control and other groups, there was an increase in weight. This report showed that chronic psychosocial stress significantly decreases the body weight and organ weight of adult Wistar rats. This could have resulted from reduced food intake of the rats under stress (probably loss of appetite occasioned by corticotropin-releasing hormone [CRH] release) or exhaustion of body reserve catalyzed by increased metabolic activity.

Change in body weight and organ weight of experimental animals is an important parameter in determining the health of an animal. Stress increases adaptive functions and decreases acute vegetative, nonadaptive functions such as feeding and development.[30] Decreased body weight and organ weight have also been documented in animals open to forced swimming stress.[31] The reduced body weight and organ weight of rats beheld in this research could have been occasioned by protein catabolism and Lipolysis.[32] Contrary to this observation, some studies did not discern any significant change in weight of animals open to chronic psychosocial stress,[33] probably due to the method of psychosocial stress induction, having no effect on the animals. Reductions in organ weight have also been described in animals exposed to immobilization stress.[34]

Effect of psychosocial stress on hormonal level

Glucocorticoid synthesis and secretion in blood plasma amid stress is increased; this production is aroused by adrenocorticotropic hormone (ACTH) from the adenohypophysis. ACTH manufacture is influenced by the hypothalamic peptide and CRH, thus the HPA axis is the regulating center of stress response. The heightened production of glucocorticoid exerts a negative feedback mechanism on CRH and ACTH secretion; this action restricts the overall continuance in time of tissue exposure of the individual or organism to glucocorticoids, thereby reducing the catabolic, immunosuppressive, lipogenic, anti-growth, and anti-reproductive outcome of these hormones.[30] Nevertheless, chronic actuation of stress response can lead to a disparate package of malady as a result of protracted CRH and glucocorticoid secretion. For instance, the reproductive function of males is affected in all aspects during CPS.[30]

Cortisol

In this study, a significant elevation in the concentration of cortisol was observed when the animals were exposed to psychosocial stress for a short duration as compared with control. Research has shown that heightened blood serum concentration indicates an organisms' response to stress.[35] Studies have also confirmed an increase in cortisol level and decreased TESTO level when rats were exposed to various forms of stress.[36]

However, for long duration, no significant elevation in the concentration of cortisol was detected when the animals were exposed to CPS. Research has shown how individuals with normal HPA axis function tend to deteriorate to stress-induced HPA axis dysfunction following chronic stress.[37,38] These results show that chronic stress will ultimately prompt the HPA axis to progress from over-responsive state to

under-responsive or nonresponsive (the terms used to refer to "adrenal fatigue"/"exhaustion"). Furthermore, ACTH will signal heightened levels of cortisol and then start to de-escalate Dehydroepiandrosterone production (pregnenolone steal) amid chronic stress.

The heightened level of cortisol at long duration may lead to adaptation within the HPA axis, catalyzing dwindling cortisol production, and ultimately hypocortisolism.[39] Researchers have suggested that HPA axis adaptation is a protective mechanism to safeguard long-term survival by avoiding high level of cortisol from repressing immune function and aggrandizing catabolic pathways.[40,41] Individuals exposed to trauma may possess higher, lower, or the same level of cortisol as those who are not exposed to trauma, those with higher level are prone to increased rate of anxiety and depression, while those with low levels have adapted to the stressor and developed a high threshold for their perceived stress.[42] As a result, we proposed that the concentration of cortisol observed at long exposure duration is due to CPS physiologic adaptation.

The HPA axis has been expansively researched in people with PTSD, and reports have documented abnormally low baseline levels of cortisol in PTSD individuals.[43] This is as a result of the meliorate negative feedback inhibition of the HPA axis. Research have documented that PTSD individuals portray an elevated amount and sensitivity of glucocorticoid receptors, thus increased cortisol and ACTH suppression.[44,45] However, mixed fate has been ascertained in research on PTSD patients.[46] There have been reports on aberrantly low baseline cortisol levels[47,48] and elevated amount and sensitivity of glucocorticoid receptors.[49]

Gonadotropic hormones

In the current research, CPS caused significant abatement in the level of LH and FSH, whose effect was denoted in the depleted level of TESTO, ESTROG, and PROG when correlated with control. Chronic exposure to stressors is acknowledged to accelerate the exertion of the HPA axis and subsequently decreases the exertion of the HPG axis.[7,30] The system responsible for regulation of reproduction is directly connected to the stress system, as a result, males in chronic stress conditions display inhibition of TESTO secretion,[8] spermatogenesis,[10,12] fertility,[30] and sexual behavior.[8,13] The HPA axis hormones manufactured amid stress are accountable for the impediment of the reproductive axis, for instance, GnRH secretion is impeded by CRH.[30]

The increased glucocorticoids secreted during stress decrease the sensitivity of pituitary gonadotroph to GnRH; this action reduces the secretion of LH.[30] The gonads are also directly affected by these stress hormones which reduce the rate of Leydig cell response to LH or reduce testicular receptors to this hormone with concurrent change in sex steroid production.[50] However, glucocorticoids reduce sexual hormone receptor concentration by creating resistance in target tissues of gonadal steroids.[30] Chronic stress in rats effectuates a 90% (0.25 ng/mL) abatement in TESTO as a result of heightened stress hormones (200%, about 550 ng/mL), thereby reducing sexual incitement and fertility.[50,51]

In this study, the reduced level of serum TESTO could have been caused by the neuroendocrine effect of the psychosocial stress on the animal controlled by the hypothalamus as a result of increased stress hormone. Various researches have noted the plasma TESTO quantity in animals under various stressful conditions; however, these results have been contradicting. While some researches postulated escalation in plasma TESTO in animals subjected to physical exercise stress,[52] prolonged exposure to psychosocial stress,[53] and immobilization stress,[10] others have postulated a diminution in plasma TESTO in animals subjected to noise stress,[54,55] and restraint stress.[56] Furthermore, there have been reports of no observed significant change in the level of TESTO following chronic stress, and these were proposed to be due to the physiological adaptation of the animals to the stressor.[35] The downsized level of PROG described in this study could be due to the elevated generation of cortisol. When the body is subjected to stress, the adrenal glands produce more cortisol and adrenaline, in order to make cortisol, the adrenal glands need PROG; this could result in depleting circulating level of PROG as observed in this study, a phenomenon known as "pregnenolone steal." Contrary to this observation, there have been reports of increased levels of circulating PROG following restrain stress, these reports suggested that the production of adrenal steroid hormones (corticosterone and PROG in rats) is stimulated by ACTHs, produced from corticotrophs in the adenohypophysis. PROG is a forerunner to corticosterone, increase in corticosterone caused by stress results in high concentration of PROG.[57]

In this research, there was a decrease in testicular plasma concentration of FSH following psychosocial stress when correlated with control, probably, resulting from the escalated level of corticosterone caused by psychosocial stress, acting directly to suppress FSH secretion or indirectly via GnRH suppression. There are records of significant abatement in plasma concentration of FSH following chronic immobilization stress[57] and no observed significant change in plasma FSH after acute or chronic immobilization stress.[10] Other reports have indicated either an increase or decrease in plasma LH following stress;[58,59] these alterations could be attributed to the rat's perception, response of LH to the strength, time, duration, or adaptation of the stress stimuli.

In the current research, it was described that for longer duration, the levels of FSH, LH, PROG, and ESTROG were not significant, also probable due to physiologic adaptation.

Prolactin

In the current research, there was no significant difference in the production of PRL following psychosocial stress both for short and long duration as compared with control. Acute stress is a powerful stimulus for the secretion of PRL. Research show that its secretion peaks after 5–10 min and then decreases rapidly within 15–20 min of the stress stimulus. The surge duration usually does not last long due to the suppressive effect of concurrent rise in level of adrenal glucocorticoids.[10]

Vitamin E and the male reproductive system

Vitamin E, a powerful antioxidant, has significant benefits on semen parameters, some research has shown its beneficial role,[15-17,31,60] while others have failed to indicate any protective effect.[18] Vitamin E can reduce lipid peroxidation produced in oxidative stress, thereby enhancing the quality of sperm.[15]

Effect of Vitamin E on body weight and organ weight of animals

The effect of Vitamin E was analyzed on the body weight and organ weight of animals exposed to psychosocial stress. It was observed that the weight of animals treated daily with 50 mg/kg Vitamin E prior to the exposure of stress was statistically significant when compared with the stressed groups. The final weight of animals treated with only Vitamin E only and those treated with Vitamin E and exposed to psychosocial stress were all increased, as well as the control group; this gain in weight could have been precipitated by the antioxidant property of Vitamin E, thereupon, reducing excessive metabolic activity effectuated by stress or elevation of food consumption.

Effect of Vitamin E on hormonal level

There was a significant reduction in the concentration of cortisol when the animals were treated daily with 50 mg/kg Vitamin E prior to the exposure to stress when compared with the stressed-only groups. This result showed that the administration of Vitamin E can reduce the effect of stress on cortisol concentration.

In the present research, daily Vitamin E administration to animals prior to stress had a bulwark influence on the levels of LH, TESTO, ESTROG, PROG, and FSH when compared with animals exposed to only psychosocial stress. This protective effect could be occasioned by its antioxidant function, increasing the antioxidant protective mechanism of cells and tissues, thereby scavenging ROS and restraining lipid peroxidation of tissues. A research could not ascertain the protective effect of Vitamin E nor Vitamin C alone on LH levels following noise stress, but that combination of both vitamins has a protective effect on LH following noise stress.[54] Vitamin E administration has also been noted to ameliorate the negative effect of noise stress in raising the serum TESTO level and FSH to normal range.[15] Others have also corroborated the beneficial outcome of Vitamin E administration with regards to TESTO, LH, and FSH as a result of its potential to scavenge ROS, thereby preventing lipid peroxidation.[61]

Effect of Vitamin E and predator-induced psychosocial stress on the histology of the testis and epididymis

Testes

The features of a normal testicular histology of rats are observed in control [Figure 4a and e]. This revealed normal histo-architectural appearance, showing intact seminiferous tubules with normal seminiferous epithelial arrangements and intact basement membrane. The intertubular disposition of the Leydig cell and non-Leydig extratubular constituents are observed and reveal intact histology. Spermatogonia at the basement membrane, primary spermatocytes with enlarged nuclei, and secondary spermatocyte traversing to the adluminal section can be discerned. Tufty tails of spermatozoa are espied in the lumen of ST.

This constellation of normal testicular micro-architecture was also ascertained in animals that received 50 mg/kg body weight of Vitamin E (only) [Figure 4c and g] and those that received 50 mg/kg body weight Vitamin E prior to psychosocial stress [Figure 4d and h], both for long and short durations. This histological appearance, revealing the presence of spermatozoa in the lumen of ST indicates spermiation, an evidence of normal testicular micro-anatomy with spermatogenesis.

The histological evaluation of the effects of predator-induced psychosocial stress for short duration [Figure 4b] on the microstructure of the testes revealed scanty to empty lumen of the ST, an indication of the arrest of spermatogenesis, and a gross reduction of spermatids population. There was also distortion of the organization of the epithelium of the ST. Though, scanty number of cells appear to be undergoing spermatogenesis, indicating that few spermatogonia escaped destruction. Furthermore, long duration of exposure [Figure 4f] revealed scanty spermatozoa in the ST lumen and reduced number of interstitial cells in the interstitial space. There was also distortion of the epithelium of the ST, but the cyto-architecture of the testis remained intact.

In a similar research where animals were exposed to chronic immobilization stress, gross reduction in spermatogenesis was observed though the testis architecture was maintained. Luminal cell debris, poorly defined Leydig cell membrane, and cytoplasmic vacuolations were also described as a result of the stress.[35] A study that exposed animals to immobilization stress found that stress caused magnificent spermatogenesis suppression giving reason as the result of possible decline in LH and TESTO levels.[34]

A study on the protective result of Vitamin E on the testes showed that Vitamin E mitigated the reduction in sperm

motility, as well as morphology, count, and viability induced by nicotine, due to its antioxidant scavenging potential.[61]

Conclusion

It is obvious that psychosocial stress negatively affected male reproduction, and it has been divulged and established as documented in this research. This research has brought to knowledge the effects of psychosocial stress as it affects the testicular cadre, where its impacts have been observed and subsequently translated into changes in semen parameters, indicating reproductive dysfunction and distortion of spermatogenesis. Equally, the bulwark effects of Vitamin E in ameliorating the effects of psychosocial stress are also elucidated. This research has also described that adaptation to the stressor could be a protective mechanism against psychosocial stress.

Acknowledgments

Our sincere appreciation goes to Dr. (Mrs) E. J. Olotu, an angel in human form, full of wisdom and a heart of Gold, Dr. E.A Osunwoke, an intelligent being of exceptional quality, for their guidance during the course of this work, and Dr. O.I. Momodu (Uniben), for his positive impact and ensuring an academically and mentally sound atmosphere to complete the research.

Financial support and sponsorship

Nil.

Conflicts of interest

There are no conflicts of interest.

References

1. Von V, Nyuyki K, Sop A, Jahr I. Consequences of Chronic Psychosocial Stress in Male Wistar Rats. Dissertation of Sigillum Universitatis Ratisbonensis; 2012. p. 8-40.
2. Dubey S, Biswas P, Ghosh R, Chatterjee S, Dubey MJ, Chatterjee S, *et al.* Psychosocial impact of COVID-19. Diabetes Metab Syndr 2020;14:779-88.
3. Saleh RA, Agarwal A. Oxidative stress and male infertility: From research bench to clinical practice. J Androl 2002;23:737-52.
4. Jyoti R, Pandey SN, Srivastara RK. Testosterone hormone levels in albino rats following restrain stress of long duration. J Anat Soc India 2004;53:17-9.
5. Jalali M, Saki G, Sarkaki AR, Karami K, Nasri S. Effect of noise stress on count, progressive and non-progressive sperm motility, body and genital organ weights of adult male rats. J Hum Reprod Sci 2012;5:48-51.
6. Vijayprasad S, Bb G, Bb N. Effect of Vitamin C on male fertility in rats subjected to forced swimming stress. J Clin Diagn Res 2014;8:C05-8.
7. Selye H. The general adaptation syndrome and the diseases of adaptation. J Clin Endocrinol Metab 1946;6:117-230.
8. Retana-Márquez S, Bonilla-Jaime H, Vázquez-Palacios G, Martínez-García R, Velázquez-Moctezuma J. Changes in masculine sexual behavior, corticosterone and testosterone in response to acute and chronic stress in male rats. Horm Behav 2003;44:327-37.
9. Almeida SA, Petenusci SO, Anselmo-Franci JA, Rosa-e-Silva AA, Lamano-Carvalho TL. Decreased spermatogenic and androgenic testicular functions in adult rats submitted to immobilization-induced stress from prepuberty. Braz J Med Biol Res 1998;31:1443-8.
10. Almeida SA, Petenusci SO, Franci JA, Rosa e Silva AA, Carvalho TL. Chronic immobilization-induced stress increases plasma testosterone and delays testicular maturation in pubertal rats. Andrologia 2000;32:7-11.
11. Sapolsky RM, Lewis CK, Bruce SM. The neuroendocrinology of stress and aging: The glucocorticoid cascade hypothesis. Sci Aging Knowl Environ 2002;38:21.
12. Almeida SA, Kempinas WG, Lamano Carvalho TL. Sexual behavior and fertility of male rats submitted to prolonged immobilization-induced stress. Braz J Med Biol Res 2000;33:1105-9.
13. Tsigos C, Chrousos GP. Hypothalamic-pituitary-adrenal axis, neuroendocrine factors and stress. J Psychosom Res 2002;53:865-71.
14. Kefer JC, Agarwal A, Sabanegh E. Role of antioxidants in the treatment of male infertility. Int J Urol 2009;16:449-57.
15. Hemadi M, Saki G, Rajabzadeh A, Khodadadi A, Sarkaki A. The effects of honey and Vitamin E administration on apoptosis in testes of rat exposed to noise stress. J Hum Reprod Sci 2013;6:54-8.
16. ElSheikh MG, Hosny MB, Elshenoufy A, Elghamrawi H, Fayad A, Abdelrahman S. Combination of Vitamin E and clomiphene citrate in treating patients with idiopathic oligoasthenozoospermia: A prospective, randomized trial. Andrology 2015;3:864-7.
17. Zubair M. Effects of dietary Vitamin E on male reproductive system. Asian Pac J Reprod 2017;6:145-50.
18. Comhaire FH, Christophe AB, Zalata AA, Dhooge WS, Mahmoud AM, Depuydt CE. The effects of combined conventional treatment, oral antioxidants and essential fatty acids on sperm biology in subfertile men. Prostaglandins Leukot Essent Fatty Acids 2000;63:159-65.
19. Kumar N, Singh AK. Trends of male factor infertility, an important cause of infertility: A review of literature. J Hum Reprod Sci 2015;8:191-6.
20. Alahmar AT. Role of oxidative stress in male infertility: An updated review. J Hum Reprod Sci 2019;12:4-18.
21. Kefer JC, Argawal A, Sabanegh E. Role of antioxidants in treatment of male infertility. Int J Urol 2009;16:449-57.
22. Uadia PO, Emokpae AM. Male infertility in Nigeria: A neglected reproductive health issue requiring attention. J Basic Clin Reprod Sci 2015;4:45-7.
23. Figueiredo HF, Bodie BL, Tauchi M, Dolgas CM, Herman JP. Stress integration after acute and chronic predator stress: Differential activation of central stress circuitry and sensitization of the hypothalamo-pituitary-adrenocortical axis. Endocrinology 2003;144:5249-58.
24. Wilson CB, Ebenezer PJ, McLaughlin LD, Francis J. Predator exposure/psychosocial stress animal model of post-traumatic stress disorder modulates neurotransmitters in the rat hippocampus and prefrontal cortex. PLoS One 2014;9:e89104.
25. National Research Council. Guide for the Care and Use of Laboratory Animals. 8th ed Washington, DC 20001: National Research Council; 2011. p. 128-50.
26. Tietz NW. Textbook of Clinical Chemistry. Saunders WB, Philadelphia; 1986. p. 874-81.
27. Uotila M, Ruoslahti E, Engvall E. Two-site sandwich enzyme immunoassay with monoclonal antibodies to human alpha-fetoprotein. J Immunol Methods 1981;42:11-5.

28. Shields VD, Heinbockel T. Introductory chapter histological microtechniques. In: Histology. IntechOpen Limited, London. SW7 2QJ. United Kingdom. 2019. Available from: https://www.intechopen.com/chapters/64758. [Last accessed on 2022 Jan 20].
29. Ankul Singh S, Gowri K, Chitra V. A review on phytochemical constituents and pharmacological activities of the plant: *Aerva lanata*. Res J Pharm Technol 2020;13:1580-6.
30. Retana-Márquez S, Juárez-Rojas L, Casillas F. Interaction of adrenal and gonadal axes during stress in males. Res Rev J Zoolog Sci 2016;4:13-7.
31. Vijayprasad S, Ghongane BB, Nayak BB. An experimental study on effect of antioxidant Vitamin E in stress and alcohol induced changes in male fertility in Albino rats. Int J Med Res Health Sci 2012;1:1-6.
32. Arun S, Burawat J, Sukhorum W, Sampannang A, Maneenin C, Iamsaard S. Chronic restraint stress induces sperm acrosome reaction and changes in testicular tyrosine phosphorylated proteins in rats. Int J Reprod Biomed 2016;14:443-52.
33. Schiavone S, Morgese MG, Mhillaj E, Bove M, De Giorgi A, Cantatore FP, *et al.* Chronic psychosocial stress impairs bone homeostasis: A study in the social isolation Reared Rat. Front Pharmacol 2016;7:152.
34. Jyoti R, Pandey SN, Srivastara RK. Effect of immobilization stress on spermatogenesis of Albino rats. J Anat Soc India 2003;52:55-7.
35. Bitgul G, Tekmen I, Keles D, Oktay G. Protective effects of resveratrol against chronic immobilization stress on testis. ISRN Urol 2013;2013:278720.
36. Andersen ML, Bignotto M, Machado RB, Tufik S. Different stress modalities result in distinct steroid hormone responses by male rats. Braz J Med Biol Res 2004;37:791-7.
37. Fries E, Hesse J, Hellhammer J, Hellhammer DH. A new view on hypocortisolism. Psychoneuroendocrinology 2005;30:1010-6.
38. McEwen BS. Physiology and neurobiology of stress and adaptation: Central role of the brain. Physiol Rev 2007;87:873-904.
39. Guilliams TG, Edwards L. Chronic stress and the HPA axis: Clinical assessment and therapeutic considerations. The standard. Rev Nat Nutraceutical Ther Clin Pract 2010;9:1-5.
40. Gunnar MR, Vazquez DM. Low cortisol and a flattening of expected daytime rhythm: Potential indices of risk in human development. Dev Psychopathol 2001;13:515-38.
41. Raison CL, Miller AH. When not enough is too much: The role of insufficient glucocorticoid signaling in the pathophysiology of stress-related disorders. Am J Psychiatry 2003;160:1554-65.
42. Pfefferbaum B. Adolescent survivors of hurricane Katrina: A pilot study of hypothalamic-pituitary-adrenal axis functioning. Child Youth Care Forum 2015;44:527-47.
43. Zoladz PR, David MD. Psychosocial stress bin rats: Animal models of PTSD based on clinically relevant risk factors. In: Comprehensive Guide to Post-Traumatic Stress Disorders. Vol. 86. Switzerland: Springer International Publishing; 2016. p. 1531-52.
44. Yehuda R, Golier JA, Halligan SL, Meaney M, Bierer LM. The ACTH response to dexamethasone in PTSD. Am J Psychiatry 2004;161:1397-403.
45. Duval F, Crocq MA, Guillon MS, Mokrani MC, Monreal J, Bailey P, *et al.* Increased adrenocorticotropin suppression after dexamethasone administration in sexually abused adolescents with posttraumatic stress disorder. Ann N Y Acad Sci 2004;1032:273-5.
46. Bonne O, Brandes D, Segman R, Pitman RK, Yehuda R, Shalev AY. Prospective evaluation of plasma cortisol in recent trauma survivors with posttraumatic stress disorder. Psychiatry Res 2003;119:171-5.
47. Yehuda R. Status of glucocorticoid alterations in post-traumatic stress disorder. Ann N Y Acad Sci 2009;1179:56-69.
48. Yehuda R. Neuroendocrine aspects of PTSD. In: Handbook of Experimental Pharmacology. Vol 169. Berlin, Heidelberg: Springer; 2005. p. 371-403.
49. Rohleder N, Joksimovic L, Wolf JM, Kirschbaum C. Hypocortisolism and increased glucocorticoid sensitivity of pro-Inflammatory cytokine production in Bosnian war refugees with posttraumatic stress disorder. Biol Psychiatry 2004;55:745-51.
50. Hardy MP, Gao HB, Dong Q, Ge R, Wang Q, Chai WR, *et al.* Stress hormone and male reproductive function. Cell Tissue Res 2005;322:147-53.
51. Retana-Márquez S, Vigueras-Villaseñor RM, Juárez-Rojas L, Aragón-Martínez A, Torres GR. Sexual behavior attenuates the effects of chronic stress in body weight, testes, sexual accessory glands, and plasma testosterone in male rats. Horm Behav 2014;66:766-78.
52. Wheeler G, Cumming D, Burnham R, Maclean I, Sloley BD, Bhambhani Y, *et al.* Testosterone, cortisol and catecholamine responses to exercise stress and autonomic dysreflexia in elite quadriplegic athletes. Paraplegia 1994;32:292-9.
53. Pollard I, Bassett JR, Joss JM. Plasma testosterone levels and delta 5-3 beta-hydroxysteroid dehydrogenase activity in the testis of the rat following prolonged exposure to stress. J Reprod Fertil 1980;59:101-6.
54. Fathollahi A, Jasemi M, Saki G. Effect of noise stress on male rat fertility, and the protective effect of Vitamins C and E on its potential effect. Arab J Urol 2013;11:101-5.
55. Khavanin A, Mazaheri Z, Khajehnasiri F, Nadri F. The effect of noise stress on adult male rat sperm parameters and the protective effect of hydroalcoholic *Cinnamomum verum* extract: An experimental study. Iran Red Crescent Med J 2018;69779:1-7.
56. Rai J, Pandey SN, Srivastava RK. Testosterone hormone level in Albino rats following restraint stress of long duration. J Anat Soc India 2004;53:17-9.
57. Ren L, Li X, Weng Q, Trisomboon H, Yamamoto T, Pan L, *et al.* Effects of acute restraint stress on sperm motility and secretion of pituitary, adrenocortical and gonadal hormones in adult male rats. J Vet Med Sci 2010;72:1501-6.
58. López-Calderón A, Ariznavarreta C, González-Quijano MI, Tresguerres JA, Calderón MD. Stress induced changes in testis function. J Steroid Biochem Mol Biol 1991;40:473-9.
59. Demura R, Suzuki T, Nakamura S, Komatsu H, Odagiri E, Demura H. Effect of immobilization stress on testosterone and inhibin in male rats. J Androl 1989;10:210-3.
60. Wen JC. The role of Vitamin E in the treatment of male infertility. Nutr Bytes 2006;11:1-6.
61. Oyeyemi MO, Soetan KO, Akinpelu OB. Sperm characteristics and haemogram of male albino rats (Wistar strain) treated with saponin extract from *Vernonia amygdalina* del. *Asteraeceae* 110192. J Cell Anim Biol 2015;9:26-30.

Original Article

Morphologic and Morphometric Evaluation of Nutrient Foramina of Tibia

Mehmet Ülkir, Levend Karaçoban[1], Burcu Erçakmak Günes

Departments of Anatomy and [1]Sports Medicine, Faculty of Medicine, Hacettepe University, Ankara, Turkey

Abstract

Introduction: The aim of this study is to investigate the morphologic and morphometric characteristics of nutrient foramina on dry tibia bones, as well as the clinical implications. **Materials and Methods:** This study involved 63 tibiae (28 right and 35 left). The length of the tibia, number, direction, size, and location of nutrient foramina in relation to borders, surfaces, and soleal line, the distance between the nutrient foramina and proximal tibial end, the mediolateral, anteroposterior diameter of the tibial shaft at the level of the nutrient foramina, and the foraminal and cnemicus indexes were evaluated. The size of the nutrient foramina was classified using hypodermic needles of 14-16-18-20-22-24 gauge. Nutrient foramina with gauge sizes of 14–16, 18–20, and 22–24 were classified as large, medium, and small, respectively. **Results:** On the tibia, there is usually one nutrient foramina (92.06%), which may locate on the posterior surface (91.18%), lateral to the soleal line (95.17%), and in the upper 1/3 of the tibia (80.9%). The nutrient foramina was primarily 18–20 gauge (72.05%) and directed downward. **Discussion and Conclusion:** The morphological and morphometric features of nutrition foramina are vital to know, especially in surgical procedures and fractures of the upper 1/3 of the tibia. The sizes of NFs were evaluated detail in this study, and it was found that shorter tibiae had smaller NFs that were located more proximal than medium and large NFs. This morphological feature was described in the literature for the first time.

Keywords: *Anatomy, morphometry, nutrient foramina, Tibia*

Introduction

Tibia is one of the most stable bone in the body. People can maintain bipedal posture and walk kinematically because of its weight-bearing role. The nutrient arteries are the long bones' main blood vessels, and they enter through the nutrient foramina (NFs).[1] Because these foramina are generally found away from the growing ends of the bones;[2] the aphorism "seeks the elbow and flees the knee" is derived.[3] To determine the growing end of a bone, one must know the orientation of the nutrient canal.[4] The size of the nutrient foramina (NF) has been defined as primary (larger sized) or secondary (smaller sized) in various researches.[5,6]

The nutrient artery has a role in several clinical entities such as, including medullary bone ischemia,[7] longitudinal stress fracture,[8] fracture healing,[9] and free vascularized bone grafts.[10] Surgeons should also have detailed knowledge of the anatomy of the region to be operated on, as the success of the surgery is largely dependent on little disruption of the bone's blood flow.[11]

In forensic medicine and anthropological investigations, morphological traits of tibia may be crucial.[12,13] The distance between NF (DNF) and either the proximal or distal ends of a long bone can be used to estimate the length of a long bone from a fragment. Furthermore, the given fragment can forecast the individual's stature.[12]

Joint replacement surgery, fracture repair, bone grafts, and vascularized bone microsurgery, as well as medicolegal issues, all require knowledge about the location and morphological properties of the NF of the tibia. The aim of this study is to investigate the morphologic and morphometric characteristics of nutrient foramina on dry tibia bones, as well as the clinical implications.

Materials and Methods

Data collecting

This study was performed on 63 (28 right and 35 left) tibiae. The age and gender of the tibiae were unknown. The tibiae which had fractures, osteoporotic appearance,

How to cite this article: Ülkir M, Karaçoban L, Günes BE. Morphologic and morphometric evaluation of nutrient foramina of tibia. J Anat Soc India 2023;72:239-45.

Article Info

Received: 10 June 2022
Revised: 15 April 2023
Accepted: 14 August 2023
Available online: 28 September 2023

Address for correspondence:
Dr. Mehmet Ülkir, Department of Anatomy, Faculty of Medicine, Hacettepe University, Sihhiye, Çankaya, Ankara, Turkey.
E-mail: mehmet.ulkir@hotmail.com

Access this article online

Website: https://journals.lww.com/joai
DOI: 10.4103/jasi.jasi_87_22
Quick Response Code:

and pathological condition were not included in the study. Ethics committee approval was obtained from the Hacettepe University noninterventional clinical researches ethic committee (date: January 18, 2022 number: 2022/02-11).

Parameters

The following parameters were evaluated:

1. Length of tibia (TL)
2. Number of NF
3. Localization of the NFs on tibial surfaces or borders
4. Localization of NFs on the posterior surface according to soleal line
5. Size of NF
6. Direction of NF
7. DNF and proximal tibial end
8. Mediolateral diameter (MLD) of the tibial shaft at the level of NF
9. Anteroposterior diameter (APD) of the tibial shaft at the level of NF
10. Foraminal index (FI) = (DNF/TL) ×100
11. Cnemicus index (CI) = (MLD/APD) ×100.

The counts of the NFs were determined using a magnifying glass. Because secondary NFs are typically smaller than main NFs, all tibial surfaces and borders were thoroughly investigated. Hypodermic needles of 14, 16, 18, 20, 22, and 24 gauge were used, respectively, to determine the size of the foramina [Figure 1]. The needle that fits the foramina's diameter was used to determine the foramina's size. 14–16 gauge, 18–20 gauge, and 22–24 gauge NFs were evaluated as large-, medium-, and small-sized NF, respectively. The direction was assessed using needles of various gauges.

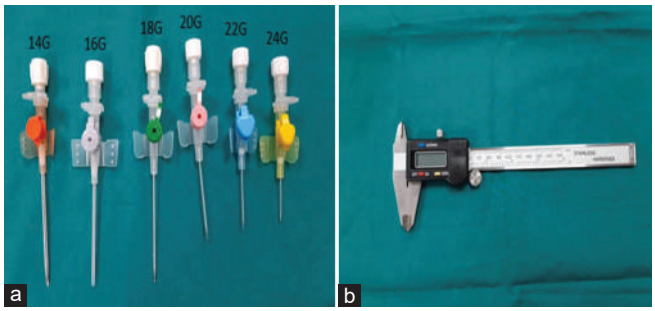

Figure 1: Hypodermic needles which were used for determination of size of nutrient foramina (a), Vernier caliper which was used for measurements on the tibia (b)

The length of the tibiae was measured using a tape measure from the medial tibial plateau to the medial malleolus. A digital caliper with 0.001 mm sensitivity was used to measure the MDL and APDs of the tibial shaft at the level of NF [Figure 2]. The foraminal and CIs were calculated after the morphometric parameters were measured.

Statistical analysis

Statistical analyses were performed using SPSS software version 22 (IBM Corporation, Armonk, NY, USA). The visual (histograms and probability plots) and analytical methods (Kolmogorov–Smirnov/Shapiro–Wilk's test) were used to determine whether or not the parameters are normally distributed. Morphologic and morphometric properties were presented using cross-tabulations. Mann–Whitney *U*-test was used to compare FI and CI between NF size groups. An overall 5% Type 1 error level was accepted to infer statistical significance.

Results

Number of NF

In total, 68 NFs were found in 63 tibiae. Only one NF was detected in 25 right tibiae and 33 left tibiae. Overall 58 of 63 (92.06%) tibiae had one NF. Besides the tibiae that had 2 NFs were detected in 3 right tibiae and 2 left tibiae. Overall 5 of 63 tibiae (7.94%) had 2 NFs.

Direction of NF

While 3 (4.41%) of NFs were directed upward, 65 (95.59%) were directed downward. One of 31 (3.23%) of the NFs on the right side was directed upward, while 30 of 31 (96.77%) were directed downward. Two of 37 (5.41%) NFs on the left side were directed upwards, while 35 of 37 (94.59%) were directed downwards.

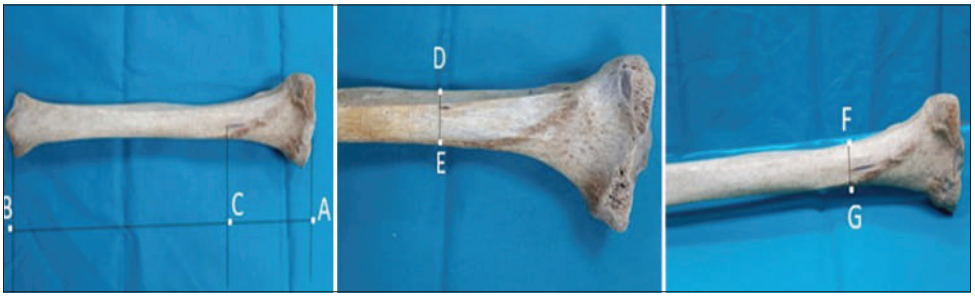

Figure 2: Demonstrations of measurements of length of tibia, distance between nutrient foramina and medial tibial plateau, anteroposterior and mediolateral diameters of the tibial shaft at the level of nutrient foramina. A: The line passes from medial tibial plateau level, B: The line passes from the most inferior part of medial malleolus, C: The line passes from level of nutrient foramina, D: The most lateral side of tibial shaft at the level of nutrient foramina, E: The most medial side of tibial shaft at the level of nutrient foramina, F: The most anterior side of tibial shaft at the level of nutrient foramina, G: The most posterior side of tibial shaft at the level of nutrient foramina

Localization of the NF on tibial surfaces or borders

Sixty-two NFs (91.18%) were found on the posterior surface, 4 (5.88%) on the anterolateral surface, and 2 of the 68 (2.94%) on the interosseous border. On the right side, NFs were found on the posterior surface in 29 of 31 (93.55%) and on the anterolateral surface in 2 of 31 (6.45%). On the left side, NFs were observed on the posterior surface in 33 of 37 (89.18%), the anterolateral surface in 2 of 37 (5.41%), and the interosseous border in 2 of 37 (5.41%).

Localization of NFs on the posterior surface according to soleal line

Fifty-nine of the 62 NFs (95.17%) were located lateral to the soleal line, one of the 62 NFs (1.61%) was found on the medial side of the soleal line, and two of the 62 (3.22%) were identified on the soleal line. Twenty-seven of 29 (93.1%) NFs were found lateral to the soleal line on the right side, while 2 of 29 (6.9%) NFs were found on the soleal line. On the left side, 32 of 33 NFs (96.96%) were found lateral to the soleal line, whereas 1 of 33 (3.04%) was found medial to the soleal line.

Size of NF

Eighth of 68 NFs were detected as small-sized (5 right and 3 left), 49 of 68 NFs were detected as medium-sized (20 right and 29 left), and 11 of 68 NFs (6 right and 5 left) were detected as large-sized.

Foraminal index and localization of NF at the tibia

Mean values of the FI were found 29.77 ± 6.2 in all tibiae, 29.49 ± 4.98 on the right side, and 30.01 ± 5.30 on the left side. Fifty-five of 68 (80.9%) NFs were located on the upper 1/3 of tibiae and 13 of 68 (19.1%) NFs were detected on the middle 1/3 of tibiae. On the right side, 26 of 31 (83.87%) NFs were detected on the upper 1/3 of tibia and 5 of 31 (16.13%) NFs were detected on the middle 1/3 of tibia. On the left side, 29 of 37 (78.37%) NFs were detected on the upper 1/3 of tibia and 8 of 37 (21.63%) NFs were detected on the middle 1/3 of tibia. No NFs were detected on the lower 1/3 of tibia. In brief, lower FI indicates proximally located NFs.

Length of tibia

The average tibia lengths were 341.79 ± 29.4 mm for all tibiae, 337.68 ± 23.73 mm for the right side, and 345.24 ± 24.43 mm for the left side.

Distance between NF and proximal tibial end

The average DNF and the proximal tibial end were 101.71 ± 22.7 mm in all tibiae, 99.59 ± 17.91 on the right side, and 103.48 ± 19.45 on the left side.

Anteroposterior diameter of the tibial shaft at the level of NF

All tibiae had mean values of APDs of the tibial shaft at the level of NF of 29.3 ± 5.0 mm, 30.16 ± 4.48 mm on the right side, and 28.58 ± 3.83 mm on the left side.

Mediolateral diameter of the tibial shaft at the level of NF

At the level of NF, the MLDs of the tibial shafts were measured to be 25.45 ± 7.0 mm in all tibiae, 26.46 ± 5.94 mm on the right side, and 24.59 ± 5.61 mm on the left side.

Cnemicus index

CI mean values were 87.57 ± 23.6 in all tibiae, 88.26 ± 17.95 on the right side, and 86.98 ± 20.91 on the left side.

Tables 1 and 2 outline the morphological and morphometric features of NFs of the tibiae.

Table 3 reveals that tibiae with small NFs had a lower FI (P = 0.016) and shorter (P = 0.009) tibial length than those with medium and large NFs. These findings suggest that smaller NFs that were located more proximal than medium and large NFs.

Figure 3 demonstrates NF morphological characteristics that are uncommon.

Table 1: Morphological properties of nutrient foramina

	Right, *n* (%)	Left, *n* (%)	Total, *n* (%)
Number of foramina			
1	25 (43.01)	33 (56.89)	58 (92.06)
2	3 (60)	2 (40)	5 (7.94)
Location			
PS	29 (93.55)	33 (89.18)	62 (91.18)
Lateral to the soleal line	27 (93.1)	32 (96.96)	59 (95.17)
Medial to the soleal line	-	1 (3.04)	1 (1.61)
On the soleal line	2 (6.9)	-	2 (3.22)
ALS	2 (6.45)	2 (5.41)	4 (5.88)
IB	-	2 (5.41)	2 (2.94)
Direction			
Downward	30 (96.77)	35 (94.59)	65 (95.59)
Upward	1 (3.23)	2 (5.41)	3 (4.41)
Placement			
Upper 1/3	26 (83.87)	29 (78.37)	55 (80.9)
Middle 1/3	5 (16.13)	8 (21.63)	13 (19.1)
Lower 1/3	-	-	-
Size			
Small	5 (62.5)	3 (37.5)	8 (11.76)
Medium	20 (40.81)	29 (59.19)	49 (72.05)
Large	6 (54.54)	5 (45.46)	11 (16.19)
Total	31 (45.58)	37 (54.42)	

PS: Posterior surface, ALS: Anterolateral surface, IB: Interosseous border

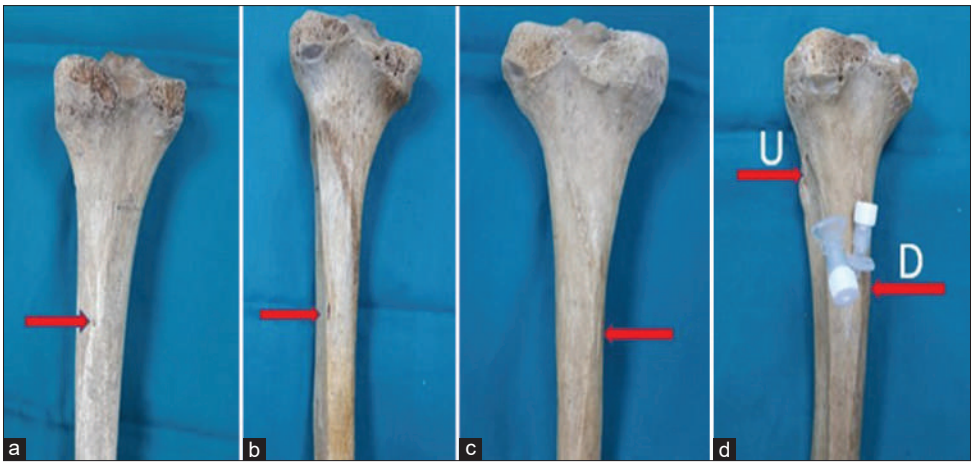

Figure 3: Demonstration of nutrient foramina (red arrow) which was located onto soleal line (a), onto interosseous border (b) at medial side of soleal line (c), and direction of the foramina (d). U: Upward, D: Downward

Table 2: Morphometric properties of nutrient foramina

	Right	Left	Total
Length of tibia (mm)	337.68±23.73	345.24±24.43	341.79±29.4
NF distance to proximal tibia (mm)	99.59±17.91	103.48±19.45	101.71±22.7
FI	29.49±4.98	30.01±5.30	29.77±6.2
AP diameter at the level of NF (mm)	30.16±4.48	28.58±3.83	29.3±5.0
ML diameter at the level of NF (mm)	26.46±5.94	24.59±5.61	25.45±7.0
CI	88.26±17.95	86.98±20.91	87.57±23.6

Data were shown as mean±SD. NF: Nutrient foramina, AP: Anteroposterior, ML: Mediolateral, SD: Standard deviation, FI: Foraminal index, CI: Cnemicus index

Table 3: Relationship between size of nutrient foramina and foraminal index and length of tibia

	Size of NF		
	Small	Middle	Large
FI	23.18±9.16*	30.56±3.94	31.05±1.73
Length of tibia (mm)	326.08±17.81**	341.69±24.37	353.63±22.6

*P=0.016 and **P=0.009. Data were shown as mean±SD. NF: Nutrient foramina, SD: Standard deviation, FI: Foraminal index

Discussion

Previous researchers had found that most tibiae only contain one NF,[5,6,14-18] that is directed downward.[5,6,17,18] It was predominantly found on the posterior surface of the tibia[5,6,14,15,17,18] lateral to the soleal line[14,15,17] with NF on the upper 1/3 of the tibia.[5,6,14,15,17,18] Two NFs[5,6,14,15] or no NFs,[5,6] distinct directions are uncommon morphologic characteristics.[5,6,17,18] In this study, one NF was found at 92.06% of tibiae, with an average of 1.08 NFs per tibia. When the foramina's direction and locations were examined, it was found that 95.59% of NFs were directed downward and 91.18% were placed on the tibia's posterior surface. 80.9% of the foramina were found on the proximal 1/3 of the tibia. Furthermore, the foramina on the posterior surface were analyzed, with 95.17% of them being on the lateral to the soleal line [Table 4].

When the mean values of the DNF and proximal tibial end,[5,6,14-16] length of tibia[5,6,14-16] and FI[5,6,14-16,18] that were measured in this study were compared to prior studies, the findings were found to be lower. The mean DNF and the proximal tibial end, the lengths of the tibia, and the FI were found to be 101.71 ± 22.7 mm, 341.79 ± 29.4 mm, and 29.77 ± 6.2, respectively, in this study [Tables 4 and 5].

The MLD of the tibial shaft at the level of NF[16,19-21] and CI[16,19-22] was found higher than the previous studies and APD of the tibial shaft at the level of NF[16,19-21] was found similar to the previous studies. The MLD and APDs of the tibial shaft at the level of NF and the CI were found to be 25.45 ± 7.0 mm, 29.3 ± 5.0 mm, and 87.57 ± 23.6, respectively, in this investigation [Table 6].

Previous researches used 20- and 24-gauge hypodermic needles to detect the size of NFs, and the majority of NFs were equivalent to or >20 gauge.[6,16] The mean diameter of NFs was reported to be 0.174 cm in a study conducted by Ertürk.[15] The size of NFs was examined in depth in this study (using 14-16-18-20-22-24-gauge hypodermic needles), with the following findings: 88.24% of NFs were equal to or larger than 20 gauge; 72.05% of NFs were medium size (18–20 gauge); and 16.19% of NFs were large size (14–16 gauge).

Table 4: Morphologic properties of nutrient foramina in this study and previous studies

Studies	Sample size	Number of NF	NF per tibia	Direction of the NF		Localization			FI
				Downward (%)	Upward (%)	According to			
						Surfaces and borders	Soleal line on PS (%)	Tibial third (%)	
Gupta and Kumari[5]	312	0: 3.2% 1: 96.5% 2: 0.3% ≥2: - Total: 302	0.97	99.01	0.09	PS: 299 AMS: - ALS: - AB: - IB: 3 MB: -		Upper: 36.1 Middle: 37.1 Lower: 26.8	Right: - Left: - Total: 32.86
Kumar *et al*.[14]	60	0: - 1: 95% 2: 5% ≥2: - Total: 63	1.05			PS: 63 AMS: - ALS: - AB: - IB: - MB: -	Lateral: 96.8 Medial: 3.2 On the line: -	Upper: 100 Middle: - Lower: -	Right: 32.48 Left: 32.26 Total: -
Ertürk[15]	206	0: - 1: 87.38% 2: 2.62% ≥2: - Total: 232	1.12	100	-	PS: 208 AMS: ALS: 8 AB: - IB: 10 MB: 6	Lateral: 98.1 Medial: 1.9 On the line: -	Upper: 75 Middle: 24.57 Lower: 0.43 On the line	Right: - Left: - Total: -
Zahra *et al*.[6]	91	0: 1.1% 1: 96.7% 2: 2.2% ≥2: - Total: 92	1.01	99	1	PS: 92 AMS: - ALS: - AB: - IB: - MB: -		Upper: 72 Middle: 28 Lower: -	Right: 32.39 Left: 32.05 Total: -
Gupta *et al*.[16]	50	0: - 1: 100% 2: - ≥2: - Total: 50	1			PS: - AMS: - ALS: - AB: - IB: - MB: -		Upper: 34 Middle: 66 Lower: -	Right: - Left: - Total: 34.75
Vadhel *et al*.[17]	188	0: - 1: 100% 2: - ≥2: - Total: 188	1	100	-	PS: 188 AMS: - ALS: - AB: - IB: - MB: -	Lateral: 95.7 Medial: - On the line: 4.3	Upper: 92.6 Middle: - Lower: 0.5 Junction of upper and middle thirds: 6.9	Right: - Left: - Total: -
Kamath *et al*.[18]	71	0: - 1: 100% 2: - ≥2: - Total: 71	1	100	-	PS: 69 AMS: 2 ALS: - AB: - IB: - MB: -		Upper: 81.82 Middle: 18.19 Lower: -	Right: - Left: - Total: 32.08
This study	63	0: - 1: 92.06%	1.08	95.59	4.41	PS: 91.18 AMS: -	Lateral: 95.17 Medial: 1.61	Upper: 80.9 Middle: 19.1	Right: 29.49

Contd...

Table 4: Contd...

Studies	Sample size	Number of NF	NF per tibia	Direction of the NF		Localization			FI
				Downward (%)	Upward (%)	According to			
						Surfaces and borders	Soleal line on PS (%)	Tibial third (%)	
		2: 7.94%				ALS: 5.88	On the line: 3.22	Lower: -	Left: 30.01
		≥2: -				AB: -			Total: 29.77
		Total: 63				IB: 2.94			
						MB: -			

NF: Nutrient foramina, PS: Posterior surface, AMS: Anteromedial surface, ALS: Anterolateral surface, AB: Anterior border, IB: Interosseous border, MB: Medial border, FI: Foraminal index

Table 5: Length of tibia and distance between nutrient foramina and proximal tibial end in this study and previous studies

Studies	Length of tibia (mm)			Distance between NF and proximal tibial end (mm)		
	Right	Left	Total	Right	Left	Total
Gupta and Kumari[5]	361	368	364.4	118	121.8	119.8
Kumar *et al*.[14]	359.2±14.73	357.28±21.15	-	116.14±7.26	116.92±6.09	-
Ertürk[15]	-	-	354.1	-	-	115
Zahra *et al*.[6]	-	-	359±27.9	-	-	116.6±17.5
Gupta *et al*.[16]	377.5±34.5	376.8±16.1	377	131.5±16.3	130.6±14.8	131.1
This study	337.68±23.73	345.24±24.43	341.79±29.4	99.59±17.91	103.48±19.45	101.71±22.7

NF: Nutrient foramina

Table 6: Anteroposterior, mediolateral diameter of the tibial shaft at the level of nutrient foramina and cnemicus index in this study and previous studies

Studies	AP diameter of the tibial shaft at the level of NF (mm)			ML diameter of the tibial shaft at the level of NF (mm)			CI		
	Right	Left	Total	Right	Left	Total	Right	Left	Total
Gupta *et al*.[16]	31.8±04.7	32.6±02.9	32.2	21.3±02.9	23±2.7	22.1	70.55	66.98	68.63
Bokariya *et al*.[19]	275.1±27.8	282.6±22.9	-	18.2±3.9	18.9±2.2	-	66.17±10.68	67.31±7.35	-
Basu *et al*.[20]	28.2±03.3	29.8±04.6	-	22.5±2.65	22.2±2.3	-	80.43±8.69	75.59±10.25	-
Nazir *et al*.[21]	315.5±28.3	331.3±0.4.7	-	21.4±1.8	22.5±2.5	-	68.19±5.23	68.02±7.48	
Tiwari *et al*.[22]	-	-	-	-	-	-	78.4±13.19	70.84±11.38	-
This study	30.16±4.48	28.58±3.83	29.3±5.0	26.46±5.94	24.59±5.61	25.45±7.0	88.26±17.95	86.98±20.91	87.57±23.6

AP: Anteroposterior, ML: Mediolateral, NF: Nutrient foramina, CI: Cnemicus index

According to this and prior researches, the tibia usually has only one NF, which is located on the posterior surface, lateral to the soleal line, and on the upper 1/3 of the tibia. The NF is usually 18–20 gauge in size and is directed downward.

Conclusion

Knowledge of the morphological and morphometric features of NFs is significant for orthopedic surgeons, especially in fractures involving the upper 1/3 of the tibia and in surgical treatments in this region. The sizes of NFs were evaluated detail in this study, and it was found that shorter tibiae had smaller NFs that were located more proximal than medium and large NFs. This morphological trait was described in the literature for the first time.

Limitations

The age and gender of the bones used in the study were unknown. For this reason, age and gender differences could not be revealed. The sample size was also limited to 63 dry tibiae in this study.

Financial support and sponsorship

Nil.

Conflicts of interest

There are no conflicts of interest.

References

1. Lewis OJ. The blood supply of developing long bones with special reference to the metaphyses. J Bone Joint Surg Br 1956;38-B: 928-33.
2. Mysorekar VR, Nandedkar AN. Diaphysial nutrient foramina in human phalanges. J Anat 1979;128:315-22.
3. Patake SM, Mysorekar VR. Diaphysial nutrient foramina in human metacarpals and metatarsals. J Anat 1977;124:299-304.
4. Lutken P. Investigation into the position of the nutrient foramina and the direction of the vessel canals in the shafts of the humerus and femur in man. Acta Anat (Basel) 1950;9:57-68.
5. Gupta RK, Kumari GA. A study of diaphyseal nutrient foramina

in human tibia. Natl J Med Res 2014;4:310-3.
6. Zahra SU, Kervancioğlu P, Bahşi İ. Morphological and topographical anatomy of nutrient foramen in the lower limb long bones. Eur J Ther 2018;24:36-43.
7. Forriol Campos F, Gomez Pellico L, Gianonatti Alias M, Fernandez-Valencia R. A study of the nutrient foramina in human long bones. Surg Radiol Anat 1987;9:251-5.
8. Craig JG, Widman D, van Holsbeeck M. Longitudinal stress fracture: Patterns of edema and the importance of the nutrient foramen. Skeletal Radiol 2003;32:22-7.
9. Gümüsburun E, Yücel F, Ozkan Y, Akgün Z. A study of the nutrient foramina of lower limb long bones. Surg Radiol Anat 1994;16:409-12.
10. Kirschner MH, Menck J, Hennerbichler A, Gaber O, Hofmann GO. Importance of arterial blood supply to the femur and tibia for transplantation of vascularized femoral diaphyses and knee joints. World J Surg 1998;22:845-51.
11. Laing PG. The blood supply of the femoral shaft; an anatomical study. J Bone Joint Surg Br 1953;35-B: 462-6.
12. Shamsunder Rao V, Kothapalli J. The diaphyseal nutrient foramina architecture – A study on the human upper and lower limb long bones. IOSR J Pharm Biol Sci 2014;9:36-41.
13. Longia GS, Ajmani ML, Saxena SK, Thomas RJ. Study of diaphyseal nutrient foramina in human long bones. Acta Anat (Basel) 1980;107:399-406.
14. Kumar S, Kumar A, Ratnesh R, Akhtar MJ, Kumar B, Sinha RR, *et al*. Morphometric study of nutrient foramen of tibia in population of Bihar. JMSCR 2018;6:1186-90.
15. Ertürk M. Morphometry of the Nutrient Foramina in the Shaft of the Tibia. Göztepe Tip Dergisi 2003;18:150-3.
16. Gupta C, Nayak N, Kalthur SG, D'Souza AS. A morphometric study of tibia and its nutrient foramen in South Indian population with its clinical implications. Saudi J Sports Med 2015;15:244-8.
17. Vadhel CR, Kulkarni MM, Gandotra AR. Anatomy of nutrient foramen of tibia – A study from Gujarat region. Indian J Clin Anat Physiol 2015;2:6-10.
18. Kamath V, Asif M, Bhat S, Avadhani R. Primary nutrient foramina of tibia and fibula and their surgical implications. Indian J Clin Anat Physiol 2016;3:41-4.
19. Bokariya P, Sontakke B, Waghmare J, Tarnekar A, Tirpude B, Shende M. The anthropometric measurements of tibia. J Indian Acad Forensic Med 2012;34:322-3.
20. Basu R, Pal DC, Haldar D, Sarkar J. Morphometric variation between right and left human tibia: A cross-sectional study in Bankura district of West Bengal. IOSR JDMS 2018;17:26-30.
21. Nazir F, Bhat G, Khan S. Morphometric study of tibia in North Indian population and its clinical relevance. Int J Curr Res 2017;9:49947-9.
22. Tiwari A, Mahendru A, Priya A. An anatomical study of the tibia in the North Indian population. IJHA 2019;2:1-7.

Original Article

Evaluation of the Relationship between Critical Shoulder Angle and Acromial Index Measurements with Rotator Cuff Rupture on Three-dimensional Models

Merve Sevgi Ince[1,2], Rabet Gözil[3], Ulunay Kanatli[4], Meltem Bahçelioglu[2,5,6,7]

[1]Department of Physiotherapy and Rehabilitation, Faculty of Health Sciences, Yüksek Ihtisas University, [2]Department of Anatomy, Institute of Health Sciences, Gazi University, [3]Department of Anatomy, Faculty of Medicine, Yüksek Ihtisas University, Departments of [4]Orthopedics and Traumatology and [5]Anatomy, Faculty of Medicine, Gazi University, [6]Neuropsychiatry Education, Research and Application Center, Gazi University, [7]Neuroscience and Neurotechnology Center of Excellence (NÖROM), Ankara, Turkey

Abstract

Objective: The relationship between rotator cuff tears (RCTs) and morphological features of the shoulder joint has yet to be fully explained. The earlier studies were usually done with two-dimensional radiography images, but joint positions and bone formations could not be thoroughly evaluated in two-dimensional images. This study aims to assess the relationship between RCTs and critical shoulder angle (CSA) and acromial index (AI) values in three dimensions. **Methods:** In our study, computerized tomography of 24 RCTs (RCT group) and 20 Bankart lesions, and no RCTs (control group) were examined. CSA and AI were measured on three-dimensional (3D) glenohumeral joint models obtained by 3D reconstructions of computed tomography examinations. **Results:** The RCT group's CSA was significantly higher than the control group (P = 0.002). AI values did not differ significantly (P = 0.151) between the groups. In addition, there was a moderate positive correlation between the AI and CSA values and the age of patients with RCTs (r = 0.309, r = 0.367). **Conclusion:** This study differs from earlier studies in some significant respects, such as AI values were not found to be associated with RCTs. CSA values were associated with RCTs in parallel with earlier studies. This difference may be because we performed our study on 3D models. We anticipate that our results will guide clinicians in revealing the etiology of rotator cuff degeneration and determining the surgical method for treatment.

Keywords: *Anatomy, morphology, rotator cuff tears, shoulder, three-dimensional imaging*

Introduction

Critical shoulder angle (CSA) and acromial index (AI) are variables of rotator cuff tears (RCT) have been examined the most. In two-dimensional images, most lateral part of the acromion reflected in the image is used when surgical planning is made to treat pathologies caused by morphological changes. However, this image can increase the error rate when performing a surgical procedure. To perform examination and surgery with greater accuracy, three-dimensional (3D) pictures are necessary. The study aims to determine any relationship between RCT and CSA, and AI values in 3D and how CSA and AI values impact formation of RCT.[1-16]

Methods

In this study, computed tomography scans of applicants to the Orthopedics and Traumatology Department at Gazi University Faculty of Medicine between 2016 and 2019 were retrospectively evaluated. The research comprised a total of 44 individuals, including 20 patients with verified Bankart lesions and no RCTs and 24 patients with proved RCTs by arthroscopic surgery (RCT group). The study excluded those with inflammatory diseases and a history of trauma. Because it is not morally acceptable to do computed tomography on healthy persons in our nation, the control group was selected from individuals with Bankart lesions rather than healthy individuals. According to our research, evaluating a control group made up of individuals with Bankart lesions is not problematic. Since Rhee *et al*. discovered that patients with RCT had significantly different CSA and AI values than those with Bankart lesions.[17]

In this study, images were captured by General Electric 14 Detector Computed Tomography. The images obtained were transferred to MIMICS software (Mimics

How to cite this article: Ince MS, Gözil R, Kanatli U, Bahçelioglu M. Evaluation of the relationship between critical shoulder angle and acromial index measurements with rotator cuff rupture on three-dimensional models. J Anat Soc India 2023;72:246-51.

Article Info

Received: 27 February 2023
Revised: 05 May 2023
Accepted: 14 August 2023
Available online: 28 September 2023

Address for correspondence:
Dr. Merve Sevgi Ince, Oguzlar Mahallesi, 1375, Sokak, No: 8, Çankaya, Ankara 06420, Turkey.
E-mail: msevgii94@gmail.com

Access this article online

Website: https://journals.lww.com/joai
DOI: 10.4103/jasi.jasi_20_23
Quick Response Code:

Innovation Suite, Materialize, Leuven, Belgium), and their 3D reconstructions were obtained.[18,19]

Image analysis and measurements

In our investigation, computed tomography scans from the RCT and the control groups were 3D reconstructed to build models of the glenohumeral joint. CSA and AI measurements were made on these. Two observers measured the CSA and AI in each patient. To verify interobserver reproducibility, the results acquired by these two observers were compared. To assess intra observer repeatability, one of the observers repeated the measurements after a 3-week gap. The same researcher took three measurements, and their average was calculated and assessed.

Critical shoulder angle measurement

The glenoid cavity's upper and lower edges are connected by a line. Following that, a line is produced by connecting the lower border of the glenoid cavity with the acromion's outermost point (which is thought to be the extreme point where the acromion's medial and lateral borders meet). The CSA is situated between these two lines [Figure 1].[9]

Acromial index measurement

A line connecting the top and bottom borders of the glenoid cavity (Glenoid plane [GP]). The distance between the GP and the acromion's most lateral point was recorded (a) The width between the GP and the most lateral point of the proximal epiphysis of the humerus was then measured, (b) The gleno-acromial distance (a) is compared to the gleno-humeral distance (b) to determine the AI [Figure 2].[13]

Ethical statement

This study received ethics committee approval with the decision of the Yüksek İhtisas University Non-Invasive Research Ethics Committee numbered 2019/05/02 and September 13, 2019 dated. This research on humans was carried out by the "Helsinki Declaration."

Statistical analysis

Data from the research were statistically analyzed using the software program Statistical Package for Social Sciences (SPSS) 22.0 (SPSS Inc. Chicago, IL, USA). Although continuous variables are displayed using the mean, standard deviation, and median, categorical variables are presented in the descriptive statistics section using numbers and percentages (minimum–maximum). Using both analytical (Kolmogorov–Smirnov/Shapiro–Wilk tests) and visual (histogram and probability charts) techniques, the conformity of continuous variables to the normal distribution was assessed. Separate samples the *t*-test was used to compare the data that fit the normal distribution between the two groups. In order to assess data that didn't conform to the normal distribution, the Mann–Whitney *U*-test was applied. The Pearson correlation test was used to assess the association between a few continuous data. The comparative research employed the Chi-square test. The Chi-square test was used in a comparative study for categorical variables among independent groups. The threshold for statistical significance in this study was established at $P < 0.05$.

Results

In our study, a total of 44 people, 22 women and 22 men, were evaluated. The participants' average age was 41.41, and the age range was 17–78. The study examined 21 right and 23 left shoulders [Table 1].

The control group's mean age was significantly younger than the RCT group's ($P = 0.004$). Compared to the control group, the RCT group had a significantly greater percentage of individuals over the age of 40 ($P = 0.001$) [Table 2].

The CSA in the RCT group was signficantly greater than in the control group ($P = 0.002$). The two group's AI values did not significantly differ from one another ($P = 0.151$) [Table 3].

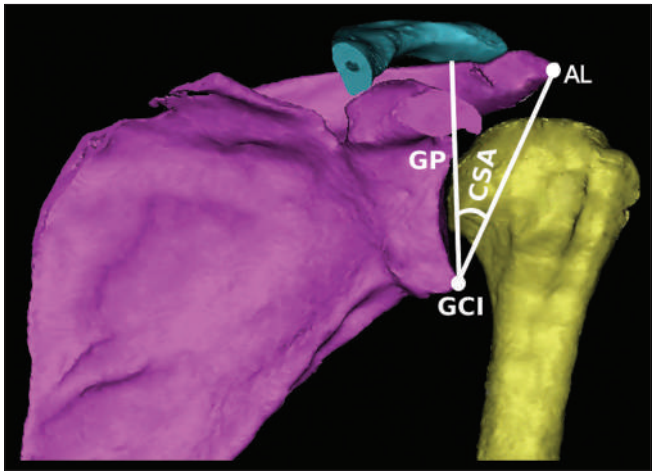

Figure 1: Measurement of critical shoulder angle. GP: Glenoid plane, CSA: critical shoulder angle, GCI: Inferior point of the glenoid cavity, AL: Most lateral point of the acromion

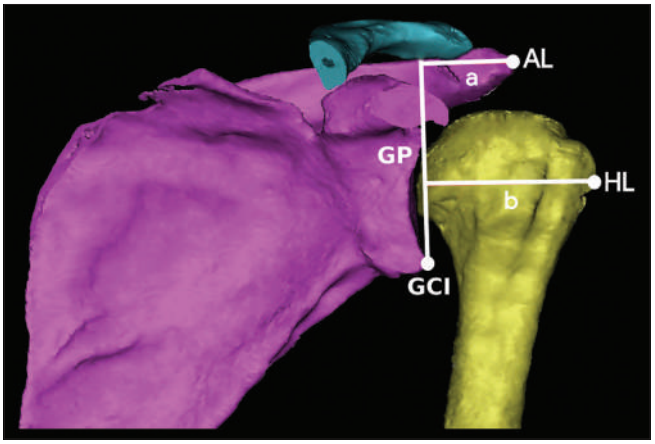

Figure 2: Measurement of the acromial index. (a) distance between AL-GP, (b) distance between HL-GP. GP: Glenoid plane, GCI: Inferior point of glenoid cavity, AL: Most lateral point of acromion, HL: Most lateral point of proximal epiphysis of humerus

There was no correlation between AI and CSA scores in the RCT group (P = 0.543). Moreover, there was no statistically significant association between CSA scores and age (P = 0.142). No correlation between age and AI levels was found (P = 0.078) [Table 4].

In the control group, there was no significant correlation between the CSA and AI scores (P = 0.913). Furthermore, there was no correlation between CSA scores and age that could be considered significant (P = 0.262). Moreover, there was no distinct correlation between age and AI scores (P = 0.168) [Table 5].

The mean CSA and AI in women in the RCT group were found to be 39.35° ± 7.82° and 0.68 ± 0.10, respectively. CSA and AI averages in men were 43.70° ± 8.96° and 0.56 ± 0.08, respectively. Women's AI measures were significantly higher than men's in the RCT group (P = 0.012) [Table 6].

The mean CSA and AI in women in the control group were found to be 34.70° ± 4.00° and 0.63 ± 0.05, respectively. The mean CSA and AI in men were found to be 33.80° ± 5.34° and 0.58 ± 0.14, respectively. The control group demonstrated no significant correlation between gender, CSA, and AI (P = 0.827, P = 0.238).

Table 1: Distribution of the rotator cuff tears group's and the control group's demographic features (*n*=44)

Parameters	*n* (%)
Gender*	
Female	22 (50.0)
Male	22 (50.0)
Age (years)	
Mean±SD	41.41±16.70
Median (minimum–maximum)	40.0 (17.0–78.0)
Age groups	
Under 40 years	22 (50.0)
40 years and older	22 (50.0)
Group	
RCT group	24 (54.5)
Control group	20 (45.5)
Side	
Right	21 (47.7)
Left	23 (52.3)

*Column percentage. SD: Standard deviation, RCT: Rotator cuff tear

Discussion

Many researchers have studied subjects such as RCT, the etiology of tears, and the biomechanics of rotator cuff muscles. Neer conducted early studies on RCT, subacromial space, and tendon lesions due to reduced subacromial space.[20] Studies have shown that many biomechanical factors, glenoid cavity, and morphometric properties of the proximal extremity of the humerus play a role in the etiology of RCT. AI and CSA measurements are the most frequently used to define these morphometric properties.

Table 2: Comparison of the rotator cuff tears group's and the control group's demographic features (*n*=44)

	RCT group (*n*=24), *n* (%)	Control group (*n*=20), *n* (%)	*P*
Gender*			
Female	17 (70.8)	5 (25.0)	0.006[a]
Male	7 (29.2)	15 (75.0)	
Age (years)			
Mean±SD	52.92±12.97	27.60±7.71	0.004[b]
Median (minimum–maximum)	55.00 (21.00–78.00)	28.50 (17.00–47.00)	
Age groups			
Under 40 years	3 (12.5)	19 (95.0)	0.001[a]
40 years and older	21 (87.5)	1 (5.0)	
Side			
Right	16 (66.70)	5 (25.0)	0.014[a]
Left	8 (33.30)	15 (75.0)	

*Column percentage, [a]Continuity correction, [b]Independent samples *t*-test. SD: Standard deviation, RCT: Rotator cuff tear

Table 3: Comparison of critical shoulder angle and acromial index measurements of rotator cuff tears and control group (*n*=44)

	RCT group (*n*=24)	Control group (*n*=20)	*P*
CSA			
Mean±SD	40.62±8.22	34.02±4.95	0.002[a]
Median (minimum–maximum)	41.00 (27.80–53.80)	34.90 (25.90–40.75)	
AI			
Mean±SD	0.65±0.11	0.60±0.13	0.151[a]
Median (minimum–maximum)	0.64 (0.44–0.88)	0.60 (0.41–0.83)	

[a]Independent samples *t*-test. SD: Standard deviation, AI: Acromial index, CSA: Critical shoulder angle, RCT: Rotator cuff tear

Table 4: Relationship between critical shoulder angle and acromial index and age values in rotator cuff tears group

	r (*P*)	
	CSA (*n*=24)	**AI (*n*=24)**
AI	−0.130 (0.543)	-
Age	0.309 (0.142)	0.367 (0.078)

r: Pearson correlations coefficient, AI: Acromial index, CSA: Critical shoulder angle

Table 5: Relationship between critical shoulder angle and acromial index and age values in the control group

	r (*P*)	
	CSA (*n*=20)	**AI (*n*=20)**
AI	0.026 (0.913)	-
Age	−0.263 (0.262)	−0.321 (0.168)

r: Pearson correlations coefficient, AI: Acromial index, CSA: Critical shoulder angle

Table 6: Evaluation of rotator cuff tears group according to gender (*n*=24)

	Female (*n*=17)	**Male (*n*=7)**	***P***
CSA			
Mean±SD	39.35±7.82	43.70±8.96	0.227[a]
Median (minimum–maximum)	38.50 (27.80–53.50)	45.30 (31.10–53.80)	
AI			
Mean±SD	0.68±0.10	0.56±0.08	0.012[a]
Median (minimum–maximum)	0.66 (0.55–0.88)	0.5 (0.44–0.66)	

[a]Mann–Whitney *U*-test. SD: Standard deviation, AI: Acromial index, CSA: Critical shoulder angle

Nyffeler *et al*. provided the first description of the AI and claimed that it was connected to RCT.[13] The CSA was discovered for the first time by Moor *et al*. and has been associated to diseases such shoulder instability, rotator cuff injuries, and osteoarthritis.[9] The full-thickness RCT patient group in our study had considerably higher CSA scores than the control group. The AI values did not, nevertheless, demonstrate any significant difference.

Ames *et al*. investigated the connection between the AI and full-thickness RCT. They used standard anteroposterior radiographs. The study's findings revealed that the size of the AI and the size of the full-thickness RCT had no correlation.[21]

Hamid *et al*. prospectively evaluated acromion morphology on 216 patients. As a result of their studies, they could not find a relationship between RCT and AI values.[22] According to our research, there was no significant difference in the AI scores between the two groups. Using anteroposterior radiographs, Moor *et al*. analysed the AI, lateral acromial angle, and CSA in the patient population having RCT and the comparison group. They discovered a significant difference between the study group and the control group's mean AI, lateral acromial angle, and CSA values.[11] In our investigation, there was no significant different in the 3D assessment between the two groups. These current findings result from the use of radiography and 3D imaging techniques.

Moor *et al*. examined the relationship between age, trauma, and CSA with RCT. They evaluated the CSA on standard radiographs of 599 patients. As a result of their studies, the mean age and CSA values of patients with full-thickness RCT were found to be significantly greater than those with intact rotator cuffs.[10] The full-thickness RCT group in our study had a mean age that was significantly older than the control group.

Cherchi *et al*. in their study, aim to evaluate the relationship between CSA and RCT and measured the CSA using goniometers on standard radiographs. They reported that the CSA was significantly greater in RCT group.[3]

Gomide *et al*. measured the CSA on the radiographic images of two patient groups with full-thickness RCT and asymptomatic patients. They found that the patient group having RCT had mean CSA scores that were substantially greater than those of the control group.[23] In our investigation, the full-thickness RCT patient group's CSA values were considerably greater than those of the control group.

Pandey *et al*. studied patients with full-thickness RCT, partial RCT, and the healthy control group. Their research evaluated the CSA and AI using standard radiography and ultrasonography images. As a result of the study, high CSA and AI values were associated with full-thickness RCT. In addition, investigators reported that the CSA and AI values were not associated with partial RCT.[14] Our study's RCT group consists of patients who underwent full-thickness RCT. According to our research, there is a relationship between CSA scores and full-thickness RCT. In contrast, no correlation was identified between AI scores. This difference is due to our measurements on 3D models.

Heuberer *et al*. evaluated radiographic images of five different shoulder pathologies with several variables in a retrospective study conducted on 1000 patients. The study's findings revealed that the CSA is a more reliable general measure than the AI for predicting and identifying various pathologies. Also, researchers noted that the CSA was highest in RCT participants and lowest in osteoarthritis patients.[5] In our study, the CSA values in the patient group with RCT and the control group differed significantly. Yet, there was no distinction in the AI values.

When the studies are examined since the CSA and AI parameters were defined, it is seen that the studies were primarily performed using radiographic examinations. Since it is difficult to accurately determine the position of the glenoid cavity of the scapula in two-dimensional

radiographic images, the need for 3D images is increasing. For this reason, recent studies have turned to 3D imaging techniques.

In addition, unlike the CSA, the evaluation of the AI was not significant in the 3D measurements in our study. Therefore, more studies are needed to evaluate the AI measurement on 3D images.

Gerber *et al*. created a model of a shoulder with a supraspinatus tear and a normal shoulder in a biomechanical study they performed by creating a mechanical shoulder simulation. As a result of their research, they found that a high CSA may cause excessive load on the supraspinatus, especially during an active abduction at low degrees.[24]

Conclusion

As a result, the measurements we made on 3D glenohumeral joint models were compared with the results of two-dimensional radiographic evaluation found in the literature. Unlike most two-dimensional radiographic assessments, AI values were not associated with RCT. In contrast, it was discovered that CSA scores were related to RCT in parallel with two-dimensional radiographic evaluation. We think this difference may be because we performed our study on models obtained by 3D computed tomography reconstruction. However, we recommend that these factors be considered in future studies, as we cannot determine whether the RCT we evaluated within the scope of the study are degenerative or traumatic due to the age difference between the groups. We anticipate our results will guide clinicians in revealing the etiology of rotator cuff degeneration and determining the surgical method for repair.

Financial support and sponsorship

Nil.

Conflicts of interest

There are no conflicts of interest.

References

1. Balke M, Schmidt C, Dedy N, Banerjee M, Bouillon B, Liem D. Correlation of acromial morphology with impingement syndrome and rotator cuff tears. Acta Orthop 2013;84:178-83.
2. Blonna D, Giani A, Bellato E, Mattei L, Caló M, Rossi R, *et al.* Predominance of the critical shoulder angle in the pathogenesis of degenerative diseases of the shoulder. J Shoulder Elbow Surg 2016;25:1328-36.
3. Cherchi L, Ciornohac JF, Godet J, Clavert P, Kempf JF. Critical shoulder angle: Measurement reproducibility and correlation with rotator cuff tendon tears. Orthop Traumatol Surg Res 2016;102:559-62.
4. Hanciau FA, da Silva MA, Martins FS, Ogliari A. Association clinical-radiographic of the acromion índex and the lateral acromion angle. Rev Bras Ortop 2012;47:730-5.
5. Heuberer PR, Plachel F, Willinger L, Moroder P, Laky B, Pauzenberger L, *et al.* Critical shoulder angle combined with age predict five shoulder pathologies: A retrospective analysis of 1000 cases. BMC Musculoskelet Disord 2017;18:259.
6. Logvinov A, Ilyin D, Kadantsev P, Makar'yeva O, Burtsev M, Riazantsev M, *et al.* Radiographic characteristics of the acromion process as a predictive factor of partial rotator cuff tears. Genij Ortop 2019;25:71-8.
7. Mantell MT, Nelson R, Lowe JT, Endrizzi DP, Jawa A. Critical shoulder angle is associated with full-thickness rotator cuff tears in patients with glenohumeral osteoarthritis. J Shoulder Elbow Surg 2017;26:e376-81.
8. Miyazaki AN, Fregoneze M, Santos PD, Silva LA, Martel ÉM, Debom LG, *et al.* Radiographic analysis of the acromion index and its association with rotator cuff tears. J Rev Bras Ortop 2010;45:151-4.
9. Moor BK, Bouaicha S, Rothenfluh DA, Sukthankar A, Gerber C. Is there an association between the individual anatomy of the scapula and the development of rotator cuff tears or osteoarthritis of the glenohumeral joint? A radiological study of the critical shoulder angle. Bone Joint J 2013;95-B: 935-41.
10. Moor BK, Röthlisberger M, Müller DA, Zumstein MA, Bouaicha S, Ehlinger M, *et al.* Age, trauma and the critical shoulder angle accurately predict supraspinatus tendon tears. Orthop Traumatol Surg Res 2014;100:489-94.
11. Moor BK, Wieser K, Slankamenac K, Gerber C, Bouaicha S. Relationship of individual scapular anatomy and degenerative rotator cuff tears. J Shoulder Elbow Surg 2014;23:536-41.
12. Musil D, Sadovský P, Rost M, Stehlík J, Filip L. Relationship of acromial morphology and rotator cuff tears. Acta Chir Orthop Traumatol Cech 2012;79:238-42.
13. Nyffeler RW, Werner CM, Sukthankar A, Schmid MR, Gerber C. Association of a large lateral extension of the acromion with rotator cuff tears. J Bone Joint Surg Am 2006;88:800-5.
14. Pandey V, Vijayan D, Tapashetti S, Agarwal L, Kamath A, Acharya K, *et al.* Does scapular morphology affect the integrity of the rotator cuff? J Shoulder Elbow Surg 2016;25:413-21.
15. Sukthankar A, Werner C, Brucker P, Nyffeler R, Gerber C. Lateral extension of the acromion and rotator cuff tears – A prospective study. Orthop Proc Br Ed Soc Bone Joint Surg 2009;91:123.
16. Watanabe A, Ono Q, Nishigami T, Hirooka T, Machida H. Association between the critical shoulder angle and rotator cuff tears in Japan. Acta Med Okayama 2018;72:547-51.
17. Rhee SM, Kim JY, Kim JY, Cho SJ, Kim JH, Rhee YG. The critical shoulder angle: Can it be sufficient to reflect the shoulder joint without the humeral head? J Shoulder Elbow Surg 2019;28:731-41.
18. Chen D, Chen CH, Tang L, Wang K, Li YZ, Phan K, *et al.* Three-dimensional reconstructions in spine and screw trajectory simulation on 3D digital images: A step by step approach by using mimics software. J Spine Surg 2017;3:650-6.
19. Yavuz MS, Buyukkurt MC, Tozoglu S, Dagsuyu IM, Kantarci M. Evaluation of volumetry and density of mandibular symphysis bone grafts by three-dimensional computed tomography. Dent Traumatol 2009;25:475-9.
20. Neer CS 2nd. Anterior acromioplasty for the chronic impingement syndrome in the shoulder: A preliminary report. J Bone Joint Surg Am 1972;54:41-50.
21. Ames JB, Horan MP, Van der Meijden OA, Leake MJ, Millett PJ. Association between acromial index and outcomes following arthroscopic repair of full-thickness rotator cuff tears. J Bone Joint Surg Am 2012;94:1862-9.

22. Hamid N, Omid R, Yamaguchi K, Steger-May K, Stobbs G, Keener JD. Relationship of radiographic acromial characteristics and rotator cuff disease: A prospective investigation of clinical, radiographic, and sonographic findings. J Shoulder Elbow Surg 2012;21:1289-98.
23. Gomide LC, Carmo TC, Bergo GH, Oliveira GA, Macedo IS. Relationship between the critical shoulder angle and the development of rotator cuff lesions: A retrospective epidemiological study. Rev Bras Ortop 2017;52:423-7.
24. Gerber C, Snedeker JG, Baumgartner D, Viehöfer AF. Supraspinatus tendon load during abduction is dependent on the size of the critical shoulder angle: A biomechanical analysis. J Orthop Res 2014;32:952-7.

Original Article

Technical Xylene Induces Maternal Toxicity Associated with Organ Inflammation during Preimplantation Stage in Pregnant Sprague-Dawley Rats

Noor Asyikin Suaidi, Mohammed Abdullah Alshawsh[1,2], See-Ziau Hoe[3], Mohd Helmy Mokhtar[4], Siti Rosmani Md. Zin[4]

Departments of Anatomy, [1]Pharmacology and [3]Physiology, Faculty of Medicine, Universiti Malaya, [4]Department of Physiology, Faculty of Medicine, Universiti Kebangsaan Malaysia, Kuala Lumpur, Malaysia, [2]Department of Paediatrics, Faculty of Medicine, Nursing and Health Sciences, School of Clinical Sciences, Monash University, Clayton, Victoria, Australia

Abstract

Introduction: Toxicity data that focus on the exposure within the range of allowable human limits of technical xylene (dimethylbenzene) on the female reproductive system and prenatal development are rarely updated. Therefore, this study aimed to investigate the outcomes of maternal exposure to technical xylene during the preimplantation period in pregnant rats. **Materials and Methods:** Timed-pregnant Sprague-Dawley rats (n = 36) were exposed to 0 (0 mg/kg), 100 (0.172 mg/kg), 500 (0.86 mg/kg), and 1000 (1.72 mg/kg) parts per million (ppm) of technical xylene via intraperitoneal injection from gestational day (GD) 1 to GD3. Clinical signs, maternal weight gain, and food intake were monitored daily. On GD5, the females were sacrificed to assess the early implantations and other reproductive parameters. **Results:** Technical xylene caused significant decreases in the number of implantation sites, maternal body weight gain, and food intake at a concentration of 1000 ppm. Significant increases in the serum total protein and potassium were also observed. Although there was no difference in the relative organ weights, increases in the uterus and liver weights were observed. Histological examination revealed systemic inflammatory changes in the uterus, liver, lungs, and kidney from all treated groups. **Discussion and Conclusion:** This study suggested that technical xylene causes maternal and prenatal toxicities associated with organ inflammation when exposed at the early gestational phase. Further studies of xylene toxicity at different stages of pregnancy are required to improve safety guidelines for technical xylene exposure.

Keywords: *Gestation, inflammation, maternal toxicity, preimplantation, reproductive toxicity, technical xylene*

Introduction

Dimethylbenzene, or technical xylene, is an organic solvent containing three major isomers: meta-xylene, para-xylene, and ortho-xylene (m-, p-, and o-xylene). Although the accurate composition of technical xylene varies due to its source, m-xylene is the major component, accounting for 44%–70% of the mixture. Approximately 20% of ethylbenzene is also present in the blend of technical xylene.[1,2] Technical xylene is extensively used in the petrochemical industries, paint manufacturing, and medical laboratories.[3,4] Xylene is one of the year's most massively synthesized chemicals and is considered a safe alternative to benzene.[5] In healthcare settings, xylene is one of the major chemicals used in histology laboratories for tissue sample processing, slide staining, mounting, and preserving the histological architecture for a histopathological examination. It acts as a clearing agent to make the tissue sample transparent after being embedded in the paraffin wax.[6] In the histology laboratory setting, xylene is one of the core chemical hazards with a long-term effect apart from formalin with its allowable time-weighted average of 100 ppm.[7]

Exposure to xylene mainly occurs by inhalation (occupational) or ingestion (accidental).[8] Unconventionally, humans are also exposed to mixed xylene by applying feminine hygiene products like sanitary pads, vaginal douches, and diapers.[9,10] Once exposed, xylene is rapidly absorbed throughout the body, where the liver is the primary site of metabolism. It predominantly accumulates in the adipose tissues or brain due to its high affinity for lipid-rich tissues.[2,11] Humans are likely to be exposed to xylene by breathing in

How to cite this article: Suaidi NA, Alshawsh MA, Hoe SZ, Mokhtar MH, Zin SR. Technical xylene induces maternal toxicity associated with organ inflammation during preimplantation stage in pregnant Sprague-Dawley rats. J Anat Soc India 2023;72:252-61.

Article Info

Received: 23 March 2023
Accepted: 15 August 2023
Available online: 28 September 2023

Address for correspondence:
Dr. Siti Rosmani Md. Zin, Department of Anatomy, Faculty of Medicine, Universiti Malaya, Kuala Lumpur 50603, Malaysia. E-mail: siti_rosmani@um.edu.my

Access this article online

Website: https://journals.lww.com/joai
DOI: 10.4103/jasi.jasi_26_23
Quick Response Code:

the xylene-contaminated air. Xylene is released into the environment mainly from industrial sources.[12] When exposed to living organisms, more than 95% of the absorbed xylene is excreted as the glycine-conjugated metabolite called methyl-hippuric acid (MHA). Although limited data is available regarding the metabolism of xylene in humans, studies on volunteers showed that 72% of retained xylene is excreted as urinary MHA. Therefore, measuring the concentration of this metabolite in human urine may indicate an exposure level to xylene.[13]

Studies on the adverse effects of xylene have been conducted on humans and animals. Occupational exposure to xylene has been associated with menstrual disturbances, skin irritation, coughing, and shortness of breath.[14,15] Menstrual irregularities have also been reported as oligomenorrhea, a menstrual dysfunction characterized by more than six cycles of more than 35 days or no menstrual bleeding for three successive months.[16,17] In healthcare facilities, xylene has been reported as one of the air contaminants that poses many health risks such as allergies, asthma, rhinitis, and contact dermatitis, although most workers recognized their workplace as having good indoor air quality.[18] Xylene studied as a mixture of benzene, toluene, ethylbenzene, and xylene (BTEX) compounds, was linked to anencephaly when exposed at an ambient level. The relationship with xylene, however, was not significant. The association was found to be stronger with benzene.[19] In addition, females exposed to BTEX from occupational exposure showed a decline in preovulatory luteinizing hormone, follicle-stimulating hormone, and prostaglandin levels.[20,21] The adverse effects of xylene as a BTEX counterpart on the female reproductive system have been investigated from various aspects, such as ovarian regulation, embryo development, and oviduct functions. However, the cellular mechanisms of its toxicity are still poorly understood.[21] Therefore, this study was conducted to investigate the toxicities of technical xylene exposed to pregnant rats during the preimplantation period of gestation and thus, to assess the findings related to the current occupational safety guidelines.

Materials and Methods

Chemicals

Xylene (CAS 1330–20–7, purity >99.5%) was purchased from Fischer Scientific, USA. Ammonium sulfide (CAS 12135–76–1, 40–48 wt. % in H2O) was obtained from Sigma Aldrich, USA. Hematoxylin, eosin, and absolute ethanol for routine histological staining were purchased from Thermo Scientific, USA.

Animals

Experiments were performed on 36 outbred virgin mature female Sprague-Dawley (SD) rats (8 weeks old), weighing between 180 and 200 g. The animals were supplied by the Animal Experimental Unit (AEU), Faculty of Medicine, University of Malaya. The females were housed in individually ventilated cages lined with corn cob bedding under regulated environmental conditions (12:12 light/dark cycle, 22°C ± 2°C). A standard diet and water were supplied *ad libitum*. Male rats of similar strains were used for the mating purpose. All experimental animal procedures were carried out under the faculty's standard guidelines. The animal use protocol was approved by the University of Malaya's Institutional Animal Care and Use Committee (IACUC) with the IACUC approval number 2020–220109/ANAT/R/SRZ (2019356).

Timed pregnancy and xylene administration

The oestrus cycles of the female rats (n = 36) were examined daily through a vaginal smear in the morning around 0930. Using a sterile pipette, a few drops of normal saline were drawn. The tip of the saline-containing pipette was inserted into the vagina of the examined females. The saline was flushed gently into the vagina and drawn back into the pipette a few times. The vaginal fluid was smeared evenly on a clean glass slide and examined under a light microscope. Females in the proestrus phase were then caged with a male overnight for mating. On the following day, the pregnancy was confirmed by the presence of sperms in the females' vaginal smear. Confirmation of sperm-positive smear indicated the gestational day 0 (GD0) of the pregnant females. The timed-pregnant female rats were then randomly arranged into four groups (n = 9) and assigned to the daily administration of technical xylene (100, 500, and 1000 ppm) or vehicle only (control) from GD1 to GD3.

The duration of the oestrus cycle was four to 5 days, with the diestrus phase being the longest period of each cycle. Determination of the oestrus cycle in the female rats was made by assessing the proportion of the epithelial cells, cornified cells, and leucocytes in the unstained vaginal smears.[22-24] Epithelial cells were identified as round or oval-nucleated cells. Anucleated, irregular-shaped cells are the cornified cells, and the round, small cells are the leucocytes. A vaginal smear of a female rat during the proestrus phase consists of predominantly epithelial cells. A smear that consisting primarily of cornified cells is an estrus smear. Metestrus is identified as an equal proportion of epithelial cells, cornified cells, and leucocytes. A smear with predominantly leucocytes is of the diestrus phase. The dose range selection for the experimental rats was based on a previous study investigating the maternal and developmental toxicity of mixed xylene and its isomers in pregnant SD rats.[25] Parts of the experimental design concerning the compound administration, duration of treatment, and the selection of the lowest and highest concentrations were adapted from previous guidelines.[2,26,27] Technical xylene in corn oil was administered by intraperitoneal (IP) injection with a volume of 0.1 mL/100 g of body weight, as described previously.[28,29] In relation to xylene's route of administration,

Kaneko *et al*.[30] demonstrated that the IP administration of xylene is more similar to inhalation exposure compared to the oral route.[30] Results from rat studies also suggested that orally administered xylenes are subject to a first-pass metabolic effect that limits the absorption of xylene compounds reaching the circulation.[2,30] Administration of technical xylene was once daily in the morning from GD1 until GD3.

Maternal assessment

Maternal clinical signs, body weight, and food consumption were recorded daily. On GD5, the pregnant females were sacrificed for data and sample collections. Pregnant animals were anesthetized using an intramuscular injection of ketamine (50 mg/kg body weight) and xylazine (5 mg/kg body weight) drug cocktail prepared by the attending veterinarian of the AEU, Universiti Malaya. The animals were later euthanized by exsanguination of the aorta. The gravid uterus, ovaries, and other internal organs i.e. liver, lungs, kidneys, spleen, and adrenal glands, were weighed and examined. Visualization of the implantation sites was not achievable using the naked eyes during the preimplantation stage. Therefore, the implantation sites were detected using a few drops of 10% ammonium sulfide solution on the gravid uteri.[31,32] Collected maternal organs were processed for histological examinations. Serum samples were obtained and stored at −80°C for endocrine, liver, and renal profile analyses.

Histological examinations

After the gross examination, the internal organs (ovaries, uteri, liver, lungs, and kidneys) were fixed using 10% neutral buffered formalin prior to tissue processing. All tissues were subjected to a series of dehydration, clearing, and paraffin wax blocking. The tissue-embedded paraffin blocks were cut using a rotary microtome at a thickness of 2.5 μm. Routine hematoxylin and eosin staining was conducted to examine the tissue sections microscopically. Microscopic evaluation of stained tissues was conducted using an Olympus light microscope installed with ImageJ software developed by the National Institute of Health. Histopathological assessment of the stained tissues was conducted under a blind condition by two independent experienced histopathologists from different institutions.

Statistical analysis

The numerical data was analyzed using IBM® SPSS® software version 26 (Chicago, United States). Values are expressed as mean ± standard error of mean. All findings were significant when the ($P < 0.05$). One-way ANOVA (with *post-hoc* Bonferroni) was applied to analyze and compare the means between groups for the normally distributed data, while Kruskal–Wallis, a nonparametric test, was used for nonhomogeneous data.

Results

Thirty-six timed-pregnant SD rats were assigned to different treatment groups in this study. There was a high probability of mating when the females were introduced to a sexually matured male at their proestrus phase. Pregnancy was confirmed 100% after the sperm was detected in the females' vaginal smears [Figure 1].

Maternal parameters

Immediately after IP injection of technical xylene, a temporary decrease in motor activity was observed in the females treated with 1000 ppm of the compound. No maternal deaths occurred in this study. Table 1 summarizes maternal toxicity of technical xylene exposed during the preimplantation period. From GD0 to GD5, maternal body weight increased in all groups of pregnant rats. However, the maternal body weight gain was significantly decreased with 1000 ppm of technical xylene administration. In addition, there was a significant decline in the maternal body weight gain during the treatment period (GD1 to GD3) and after the treatment ceased (GD4 to GD5) in the 1000 ppm treated group.

A significant decline in maternal food consumption was observed in the pregnant females treated with 1000 ppm of technical xylene. In addition, a drop in the food intake was seen throughout the preimplantation period, during, and after the treatment period.

The gravid uterine weight did not differ among the groups. However, the number of implantations was significantly decreased in the pregnant females treated with the highest concentration of technical xylene [Figure 2]. Furthermore, there was no significant difference in the counts of corpora lutea in the ovaries among the groups.

There was no significant difference in the relative organ weights of the pregnant rats treated with the technical xylene compared to those of the control group [Table 2].

Serum biochemistry showed significant increases in serum total protein and potassium levels [Table 3]. However,

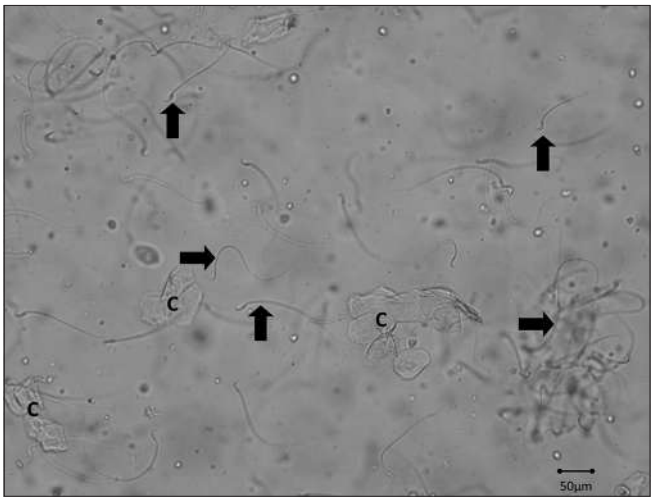

Figure 1: Sperm-positive vaginal smear of a female rat after an overnight mating. Sperms are marked by black arrows. C: Cornified cells. Wet smear, ×10 magnification

Table 1: Maternal parameters of pregnant Sprague Dawley rats exposed to technical xylene during preimplantation period

	Technical xylene (ppm)			
	0 (control)	**100**	**500**	**1000**
Number of assigned female rats (*n*)	9	9	9	9
Number of sperm-positive females	9	9	9	9
Pregnancy index (%)	100	100	100	100
Number of treated females	9	9	9	9
Number of death occurred	0	0	0	0
Maternal body weight (g)				
GD0	248.8±6.4	255.3±9.8	232.6±11.0	204±6.1
GD5	273.3±5.3	281.3±9.7	256.0±10.8	234.4±6.5
Corrected weight gain GD0–GD5	27.6±2.8	26.0±1.3	23.3±1.7	19.6±1.9*
Maternal daily weight gain (g)				
GD0–GD5	5.5±0.6	5.2±0.3	4.7±0.3	3.9±0.4*
Before treatment	8.0±2.9	5.4±2.3	7.8±1.8	8.4±1.2
During treatment†	4.6±0.5	4.4±0.7	4.0±0.6	2.3±0.5§
After treatment‡	5.8±1.0	7.0±2.2	4.2±1.3	2.4±1.3§
Maternal daily food intake (g)				
GD0–GD5	21.1±0.6	20.1±0.3	20.7±0.5	17.9±0.5*
Before treatment	19.1±0.8	20.4±0.8	20.7±0.5	19.3±0.6
During treatment†	20.9±0.7	19.7±0.5	20.5±0.8	16.6±0.5§
After treatment‡	23.6±0.9	20.9±0.5	20.7±0.4	20.1±0.9*
Reproductive organs (g)				
Relative weight of gravid uterus	0.19±0.01	0.17±0.01	0.10±0.01	0.22±0.01
Number of implantations	16.4±0.65	16.0±0.44	15.4±0.44	13.8±0.49*
Number of corpora lutea	38.9±2.5	31.2±3.9	37.8±3.4	32.9±4.0

*P<0.05 pairwise comparison to control, §P<0.01 pairwise comparison to control, †GD1–GD3, ‡GD4–GD5. Corrected weight gain= (GD5 weight−GD0 weight) − weight of the gravid uterus. Data are presented as mean±SEM. GD: Gestational day, SEM: Standard error of mean, SD: Sprague Dawley, GD: Gestational day

Table 2: Relative organ weight of pregnant Sprague Dawley rats exposed to technical xylene during preimplantation period

	Technical xylene (ppm)			
	0 (control)	**100**	**500**	**1000**
Number of assigned females	9	9	9	9
Number of treated females	9	9	9	9
Maternal organs (g)				
Gravid uterus	0.19±0.01	0.17±0.01	0.10±0.01	0.22±0.01
Right ovary	0.02±0.001	0.02±0.002	0.02±0.001	0.03±0.001
Left ovary	0.02±0.001	0.02±0.001	0.02±0.002	0.02±0.002
Liver	4.29±0.10	4.25±0.13	4.50±0.12	4.67±0.07
Lungs	0.49±0.02	0.56±0.03	0.51±0.02	0.49±0.01
Right kidney	0.37±0.02	0.38±0.01	0.36±0.01	0.38±0.01
Left kidney	0.36±0.01	0.37±0.01	0.38±0.01	0.38±0.01
Right adrenal	0.02±0.003	0.02±0.002	0.02±0.002	0.02±0.003
Left adrenal	0.02±0.002	0.02±0.003	0.02±0.003	0.02±0.002
Spleen	0.23±0.01	0.24±0.01	0.23±0.02	0.23±0.01
Heart	0.34±0.02	0.35±0.01	0.35±0.01	0.37±0.01

Data are presented as mean±SEM. SD: Sprague Dawley, SEM: Standard error of mean

there was no difference in the serum endocrine parameters i.e. estradiol, progesterone.

Histological examination

Histological examinations revealed tissue inflammation in the liver, kidney, lungs, and uterus among the xylene-treated groups regardless of the concentrations administered to the pregnant rats. The number of tissues affected is summarized in Table 4. Liver histology [Figure 3] shows degenerative changes in hepatocytes manifested by hydropobic degenerations. A classic 'salt and pepper' appearance of the hepatocytes was characterized by the finely dispersed chromatin and indistinct nucleoli.[33,34] In addition, interstitial hemorrhage with multinucleated hepatocytes and scattering pyknotic cells were also noted.

Kidney tissues from the rats treated with 1000 ppm of xylene showed congestion of the renal corpuscles (glomeruli). Interstitial hemorrhage was also noted [Figure 4]. In contrast to the control group, the kidney of rats treated with 500 and 1000 ppm of xylene revealed a diminished brush border of renal tubules. Degeneration of renal tubules was marked by nuclear shrinkage. A few inflammatory cells were also present.

Table 3: Serum biochemistry of technical xylene-treated pregnant Sprague Dawley rats

	Technical xylene (ppm)			
	0 (control)	**100**	**500**	**1000**
Number of assigned females	9	9	9	9
Number of treated females	9	9	9	9
Endocrine profile				
Luteinizing hormone (IU/L)	0.13±0.02	0.17±0.03	0.15±0.02	0.13±0.02
Follicle-stimulating hormone (IU/L)	0.88±0.12	0.83±0.15	0.83±0.14	0.88±0.12
Estradiol (pmol/L)	42.00±0.00	54.33±8.05	45.00±3.0	47.33±3.71
Progesterone (nmol/L)	190.55±1.45	180.23±7.71	187.27±4.54	176.15±8.88
Liver profile				
Total protein (g/L)	32.67±2.11	36.83±5.09	50.17±7.39	54.33±4.12*
Alkaline phosphatase (U/L)	108.17±14.36	103.67±19.05	153.17±25.86	190.00±23.96
Aspartate aminotransferase (U/L)	88.5±12.72	188.83±76.67	218.33±62.22	196.50±34.50
Alanine aminotransferase (U/L)	32.33±4.19	59.17±12.72	73.33±13.66	71.33±11.38
Renal profile				
Sodium (mmol/L)	94.50±4.81	97.83±12.98	130.33±16.78	142.50±10.40
Potassium (mmol/L)	3.02±0.21	3.87±0.66	4.78±0.80	6.00±0.88*
Chloride (mmol/L)	67.33±3.84	70.67±9.69	79.83±10.75	103.50±8.20
Urea (mmol/L)	3.68±0.45	4.35±0.57	4.90±0.77	5.92±0.43
Creatinine (μmol/L)	15.50±1.26	18.67±2.47	25.33±3.29	24.83±2.06

*P<0.05 pairwise comparison to control. Data are presented as mean±SEM. SD: Sprague Dawley, SEM: Standard error of mean

Table 4: Inflammatory changes in the organs of pregnant Sprague Dawley rats exposed to technical xylene during preimplantation period

	Technical xylene (ppm)			
	0 (control)	**100**	**500**	**1000**
Number of assigned females (*n*)	9	9	9	9
Number of treated females	9	9	9	9
Number of death occurred	0	0	0	0
Organs involved	**Number of organs affected**			
Liver (cytoplasmic and nuclear degenerations, congested vessels, pyknosis, and inflammatory cell infiltrations)	1/9	3/9	6/9	7/9
Kidney (degeneration of renal tubules, diminishing brush border, and interstitial hemorrhage)	1/9	2/9	6/9	6/9
Lungs (congestion, hypertrophy, and inflammatory cell infiltration)	1/9	3/9	6/9	7/9
Uterus (cytoplasmic degeneration, and eosinophilia)	0/9	0/9	2/9	3/9

Data are presented as number of animals displaying the organ's involvement. SD: Sprague Dawley

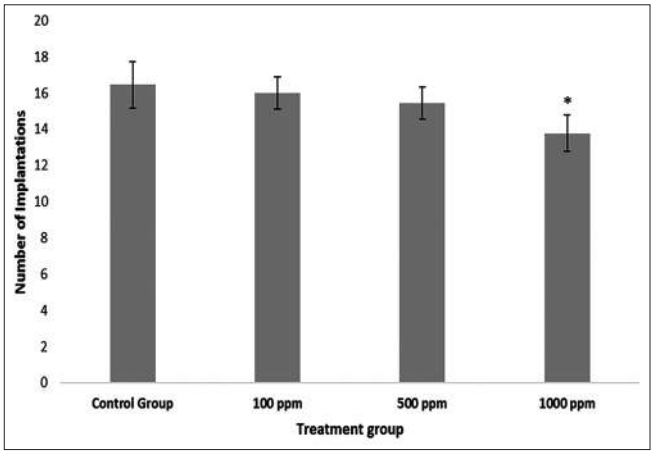

Figure 2: Effects of 100, 500, and 1000 ppm of technical xylene on the number of implantations in Sprague-Dawley Rats on GD5, data are presented as mean ± standard error of the mean, *P < 0.05 as compared to the control group, n = 9 per treatment group

Histological examination of the lungs showed congested pulmonary tissues with smooth muscle hypertrophy around the blood vessel and inflammatory cell infiltration [Figure 5]. There was also an increased occurrence of eosinophils surrounding the pulmonary tissues. These findings are consistent with acute inflammatory changes in response to foreign substances.

Uterine tissues were seen with a higher number of eosinophils (≥5 eosinophils per high power field) in the 500 and 1000 ppm treated groups. Simple glands are nonelongated and less tortuous, indicative of the proliferative phase of the endometrium. Cytoplasmic degeneration of the endometrial tissues was prominent in the 500 ppm and 1000 ppm groups compared to the control group [Figure 6].

Discussion

This study was conducted to evaluate the maternal toxicity and prenatal outcome in pregnant rats exposed to technical xylene during the preimplantation period. This study provides some knowledge regarding the impact of technical xylene exposure during the early phase of pregnancy. Many studies have been conducted to investigate the toxic effects of xylene in humans and animals before the initiation of

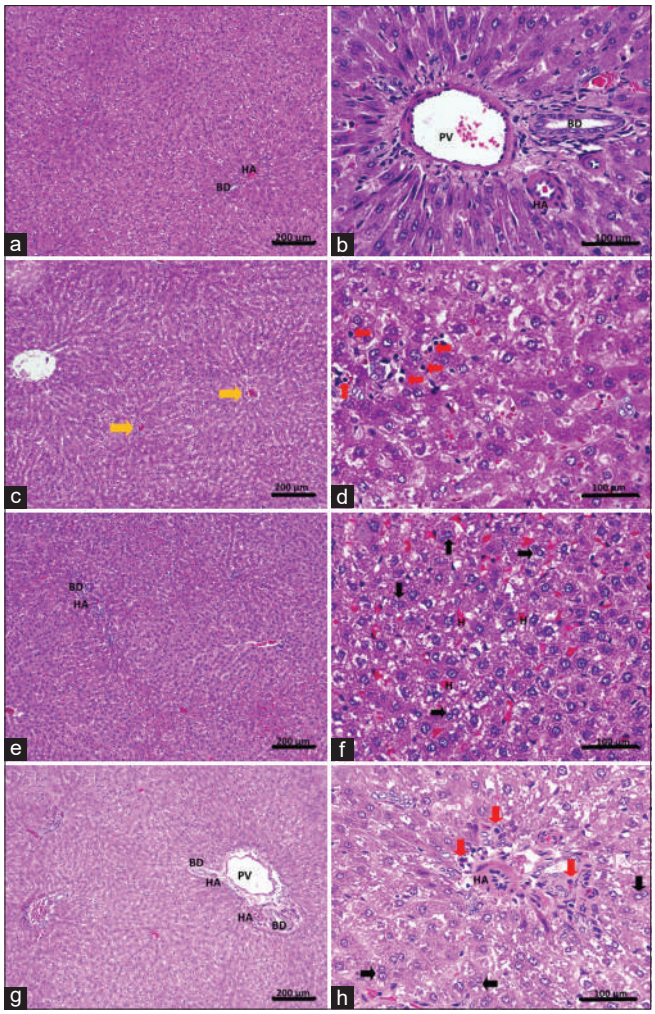

Figure 3: Photomicrographs of liver of Sprague-Dawley rats exposed to technical xylene (H and E, ×10: Scale bar 200 µm, ×40: Scale bar 100 µm). (a and b) control group; (c and d) 100 ppm; (e and f) 500 ppm; (g and h), 1000 ppm. HA: Hepatic artery, BD: Bile duct, PV: Portal vein, H: Hemorrhage, Black arrows: Multinucleated hepatocytes, Red arrows: Pyknotic cells, Yellow arrows: Congested vessels

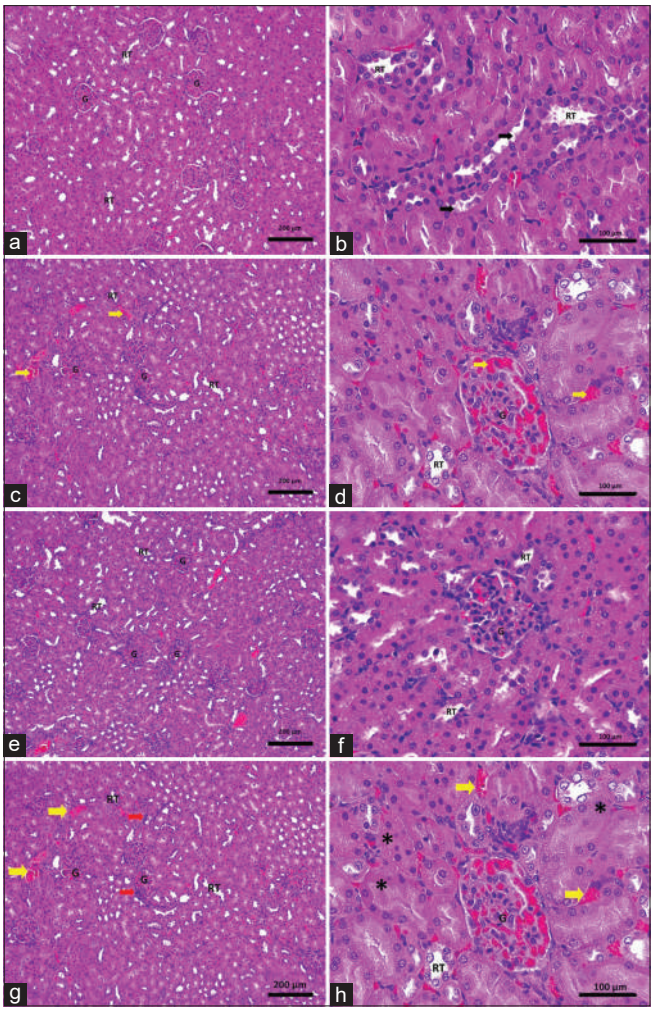

Figure 4: Photomicrographs of kidney of Sprague-Dawley rats exposed to technical xylene (H and E, ×10: Scale bar 200 µm, ×40: Scale bar 100 µm). (a and b) Control group; (c and d) 100 ppm; (e and f) 500 ppm; (g and h), 1000 ppm. G: Glomerulus, RT: Renal tubule, Black arrows: Brush border, Yellow arrows: Interstitial hemorrhage, Red arrows: Inflammatory cells, Asterisk: Nuclear shrinkage

this study. In the most recent studies, the reproductive and developmental toxicities of the xylene-containing compounds were evaluated based on exposure during the organogenesis period i.e. GD6 to GD20.[25,35-38] Nevertheless, maternal reproductive toxicity studies on technical xylene that encompass the preimplantation phase of gestation, including the histological assessment, have never been conducted. In relation to exposure levels and their effects on the population at risk, insufficient data is available on mixed xylene or its specific isomers *per se*.[5]

In this study, maternal clinical signs of toxicity in pregnant rats exposed to technical xylene were observed as a short-term decrease in motor activity, a significant loss in maternal weight gain, and a marked reduction in food intake. Similar findings were established in a study by Saillenfait *et al*.[25] when mixed xylene was exposed daily to pregnant rats from GD6 to GD20. In our study, hysterectomy on GD5 revealed that the number of implantations declined substantially in the 1000 ppm treated group as compared to the control group. The finding suggested that technical xylene adversely affects the preimplantation embryos or the implantation process, e.g. a delay in the implantation or an alteration in the uterine receptivity. Previous studies have indicated that certain compounds like herbicide mixtures and nonsteroidal anti-estrogen caused a decline in the rodents' implantations.[39,40] However, the present study was based on findings from a short period of gestational exposure. Therefore, further investigations should be conducted to determine the toxic effects of technical xylene when exposed at different gestational phases, such as the organogenesis period, with the inclusion of fetal and placental assessments.

There was a significant increase in the serum total protein and serum potassium levels of the pregnant rats treated with 1000 ppm of technical xylene. Endocrine profiles, however, did not show any significant difference among the groups.

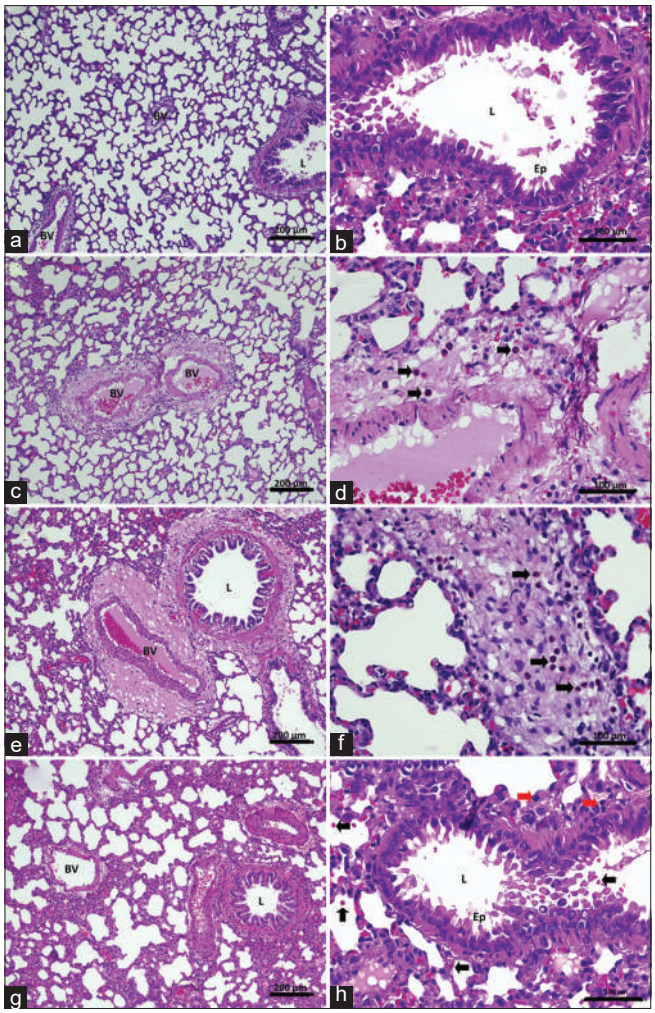

Figure 5: Photomicrographs of lungs of Sprague-Dawley rats exposed to technical xylene (H and E, ×10: Scale bar 200 µm, ×40: Scale bar 100 µm). (a and b) Control group; (c and d) 1000 ppm; (e and f) 500 ppm; (g and h), 100 ppm. BV: Blood vessel, L: Lumen, Ep: Epithelium, Black arrows: Eosinophils, Red arrows: Lymphocytes

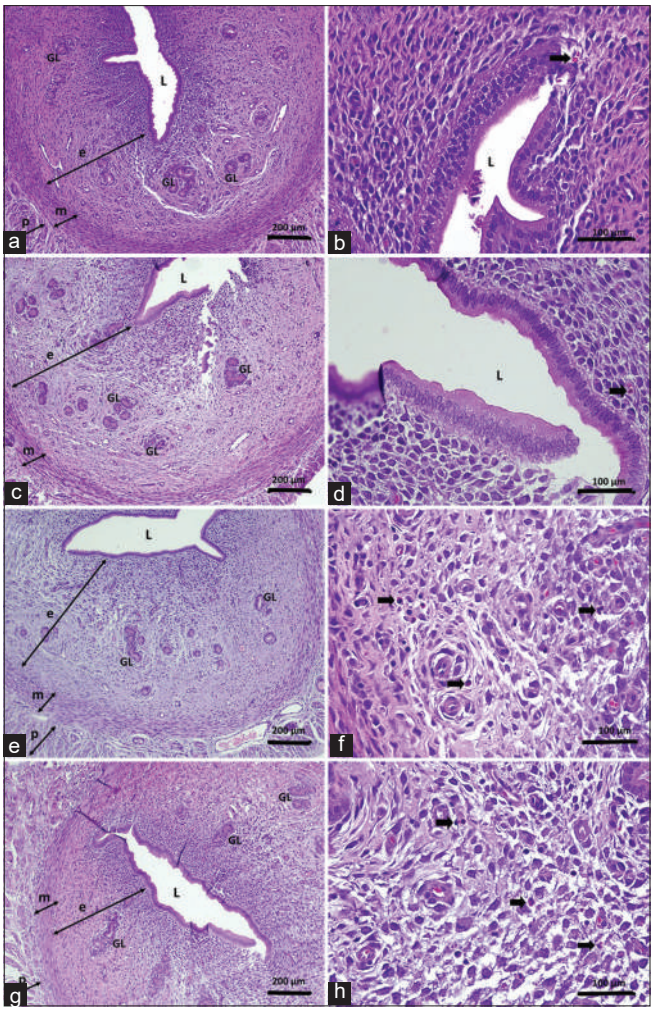

Figure 6: Photomicrographs of the uterus of Sprague-Dawley rats exposed to technical xylene (H and E, ×10: Scale bar 200 µm, ×40: Scale bar 100 µm). (a and b) Control group; (c and d) 100 ppm; (e and f) 500 ppm; (g and h), 1000 ppm; L: Uterine lumen, GL: Simple gland, p: Perimetrium, m: Myometrium, e: Endometrium, Black arrows: Eosinophils

It has been reported and supported by liver histology that an increase in serum total protein is associated with liver injury.[41] In addition, marked hyperkalemia in the 1000 ppm treated pregnant rats suggested an association with cardiac toxicity.[42] However, data on heart histological findings are not shown in the present study.

Histological findings of tissues collected from the pregnant SD rats confirmed that technical xylene caused liver, kidney, and lung injuries, possibly due to its lipophilic characteristics and a half-life of 1–6 days within the tissues.[6] Variations in the biological half-life and elimination of xylene were found to be dependent on the body constitution, i.e. rapid in a thin individual and slow in an obese person.[43] In hepatotoxicity, toxic chemicals may cause liver injury directly or indirectly. The liver cells demonstrate an inflammatory response to harmful toxic chemicals via conversion of the reactive metabolites by the liver metabolic enzymes such as cytochrome P450.[44] Histologically, degenerative changes in hepatocytes were manifested by hydropobic degenerations and cytoplasmic vacuolation. The focal area of necrosis was indicated by the infiltration of inflammatory cells around the tissues, such as the portal areas and hepatocytes.[45] It was also suggested that xylene exposure induced liver damage in adult rats via the formation of reactive oxygen species, which are the major contributors to hepatotoxicity, with the females being more vulnerable than males.[46]

Histological assessment of the lungs revealed an inflammatory response to foreign toxicants characterized by mucus plug production and inflammatory cell infiltration, particularly the eosinophils. Generally, the histological evaluation of pulmonary tissue inflammation is based on several criteria, such as relative congestion, interstitial hemorrhage, inflammatory cell infiltration, and the proportion of airspace area.[47] These inflammatory changes are strongly associated with the chemotactic effects of harmful chemicals like technical xylene.[48] The histological

findings were consistent with a previous study by Moradi *et al*. where exposure to xylene and BTEX compounds caused coughing as well as nose and skin irritation among beauty salon workers in Tehran.[15] In addition, BTEX was found to have a strong correlation with respiratory disorders such as asthma, inflammation, disturbances in lung function, and malignancies in humans.[49]

Abnormal histological findings of the treated rats' kidneys indicate an acute inflammatory response due to toxic insult. Due to the active secretion and reabsorption of chemical metabolites, kidney tubules are prone to cellular injuries.[50] Histological evaluation of rats' kidneys with toxic responses to certain chemicals, however, must be performed cautiously. The renal functions of rats and mice may hugely vary due to kidney pathologies as a result of spontaneous age-related or species-specific natural conditions.[51] Furthermore, the differences between humans' and rats' kidney anatomy and physiology must be considered when interpreting kidney-associated changes to specific test compounds.[51] Uterine tissues showed an increase in the number of eosinophils suggesting that it could be caused by both inflammatory reactions and the physiological immune reaction of pregnancy.[52] This is supported by the lowest number of implantations in the gravid uteri of the pregnant rats treated with 1000 ppm of technical xylene. In addition, an increased number of eosinophils in the endometrium has been associated with endometritis.[53]

The histological evaluation suggested that the reproductive toxicity of technical xylene occurred as a toxic insult that caused tissue inflammation. Prenatal exposure to technical xylene may have affected the pregnancy directly, as shown by a significant decline in the number of implantations and other maternal reproductive parameters such as maternal food intake and maternal body weight gain. In addition, maternal abnormal inflammation has been demonstrated to cause pregnancy failure due to the higher intensity of inflammatory hypoxia in the uterine tissues of the inflammation-induced pregnant rats.[54]

Although the threshold limit value (TLV) of xylene has been set at 100 ppm (434 g/m^3) on a weighted average of daily eight working hours,[6,55] concerns have been raised about the health risks of xylene exposure below the permissible limit.[14] Furthermore, the TLV doesn't apply to pregnant women. Maintaining the exposure below the maximum allowable limit may seem a critical safety measure, but it does not reflect the xylene level entering and accumulating in the workers' bodies.[6] In agreement, a safe level of a hazardous chemical may not apply when its permissible amount is present in an ambient space for an extended period, such as in a tissue processing laboratory.[11] A study showed that occupational exposure to BTEX mixtures at the sub-threshold limit from unleaded petrol caused early, prepathological changes in hepatotoxicity and nephrotoxicity in humans.[56]

Concerning the female reproductive system, the aftermath of occupational exposure to toxic chemicals is less known compared to that of the male reproductive system due to the complexity of the female reproductive regulations, such as hormonal control and germ-cell development. Besides, many confounding factors are attributable to the hazardous effect's extent, such as age, diet, alcohol consumption, and smoking.[57] Although it has been claimed that animal studies provide uncompelling proof of the reproductive effects of xylene, due to their limitations on interspecies function and physiology, they have identified and raised many concerns that contributed to the safety regulations and guidelines to protect workers' reproductive health.[55,57] Since the female reproductive health and functions are at risk from technical xylene and other toxicants, the adverse effects could be evident at any prenatal and developmental stages. The findings from the present study shall justify more in-depth research to scrutinize the adverse effects of technical xylene at different stages of prenatal development. Perhaps, removing the pregnant workers temporarily from the xylene-exposed workspace could be implemented as one of the safety measures to protect their reproductive well-being.

Conclusion

Maternal exposure to technical xylene during the preimplantation phase of gestation in female SD rats caused reproductive toxicity manifested by significant declines in maternal body weight, maternal food consumption, and total implantations. An increase in the relative organ weights, supported by the histological findings, indicated systemic toxicity affecting several organs of pregnant female rats exposed to technical xylene during the preimplantation stage. From the findings of this study, it could be inferred that technical xylene affects female reproduction compounded by other organs' inflammation from prenatal exposure at the preimplantation stage of pregnancy. Although significant adverse effects are found evident between the pregnant rats and the concentrations of technical xylene being studied, their mechanism of toxicity remains inconclusive. More studies are warranted to precisely establish the mechanism of toxic action of technical xylene.

Acknowledgment

The authors thank the histopathologists Dr. Rohayu Shahar Adnan (Ministry of Health) and Associate Professor Dr. Noor Kaslina Mohd Kornain (MARA University of Technology) for their expertise in histopathological examinations.

Financial support and sponsorship

Ministry of Higher Education, Malaysia under the Fundamental Research Grant Scheme (FRGS/1/2020/SKK06/UM/03/1).

Conflicts of interest

There are no conflicts of interest.

References

1. Fishbein L. Xylenes: Uses, occurrence and exposure. IARC Sci Publ 1988;85:109-20.
2. United States Environmental Protection Agency. Toxicological Review of Xylenes. 2003.
3. Rajan TS, Malathi N. Health hazards of xylene: A literature review. J Clin Diagn Res 2014;8:271-4.
4. Ikeda M. Public health problems of organic solvents. Toxicol Lett 1992;64-5:191-201.
5. Fishbein L. An overview of environmental and toxicological aspects of aromatic hydrocarbons. III. Xylene. Sci Total Environ 1985;43:165-83.
6. Buesa RJ, Peshkov MV. Histology without xylene. Ann Diagn Pathol 2009;13:246-56.
7. Buesa RJ. Histology safety: Now and then. Ann Diagn Pathol 2007;11:334-9.
8. Andrejčáková Z, Vlčková R, Sopková D, Kozioł K, Koziorowski M, Fabián D, *et al.* Dietary flaxseed's protective effects on body tissues of mice after oral exposure to xylene. Saudi J Biol Sci 2021;28:3789-98.
9. Ding N, Batterman S, Park SK. Exposure to volatile organic compounds and use of feminine hygiene products among reproductive-aged women in the United States. J Womens Health (Larchmt) 2020;29:65-73.
10. Park CJ, Barakat R, Ulanov A, Li Z, Lin PC, Chiu K, *et al.* Sanitary pads and diapers contain higher phthalate contents than those in common commercial plastic products. Reprod Toxicol 2019;84:114-21.
11. Davidson CJ, Hannigan JH, Bowen SE. Effects of inhaled combined benzene, toluene, ethylbenzene, and xylenes (BTEX): Toward an environmental exposure model. Environ Toxicol Pharmacol 2021;81:103518.
12. Fay M, Risher J, Wilson JD. Toxicological profile for xylene. Atlanta, Georgia: US Department of Health and Human Services; 2007.
13. Sedivec V, Flek J. The absorption, metabolism, and excretion of xylenes in man. Int Arch Occup Environ Health 1976;37:205-17.
14. Bolden AL, Kwiatkowski CF, Colborn T. New look at BTEX: Are ambient levels a problem? Environ Sci Technol 2015;49:5261-76.
15. Moradi M, Hopke P, Hadei M, Eslami A, Rastkari N, Naghdali Z, *et al.* Exposure to BTEX in beauty salons: Biomonitoring, urinary excretion, clinical symptoms, and health risk assessments. Environ Monit Assess 2019;191:286.
16. Asunción M, Calvo RM, San Millán JL, Sancho J, Avila S, Escobar-Morreale HF. A prospective study of the prevalence of the polycystic ovary syndrome in unselected Caucasian women from Spain. J Clin Endocrinol Metab 2000;85:2434-8.
17. Cho SI, Damokosh AI, Ryan LM, Chen D, Hu YA, Smith TJ, *et al.* Effects of exposure to organic solvents on menstrual cycle length. J Occup Environ Med 2001;43:567-75.
18. Bessonneau V, Mosqueron L, Berrubé A, Mukensturm G, Buffet-Bataillon S, Gangneux JP, *et al.* VOC contamination in hospital, from stationary sampling of a large panel of compounds, in view of healthcare workers and patients exposure assessment. PLoS One 2013;8:e55535.
19. Lupo PJ, Symanski E, Waller DK, Chan W, Langlois PH, Canfield MA, *et al.* Maternal exposure to ambient levels of benzene and neural tube defects among offspring: Texas, 1999-2004. Environ Health Perspect 2011;119:397-402.
20. Reutman SR, LeMasters GK, Knecht EA, Shukla R, Lockey JE, Burroughs GE, *et al.* Evidence of reproductive endocrine effects in women with occupational fuel and solvent exposures. Environ Health Perspect 2002;110:805-11.
21. Sirotkin AV, Harrath AH. Influence of oil-related environmental pollutants on female reproduction. Reprod Toxicol 2017;71:142-5.
22. Ajayi AF, Akhigbe RE. Staging of the estrous cycle and induction of estrus in experimental rodents: An update. Fertil Res Pract 2020;6:5.
23. Goldman JM, Murr AS, Cooper RL. The rodent estrous cycle: Characterization of vaginal cytology and its utility in toxicological studies. Birth Defects Res B Dev Reprod Toxicol 2007;80:84-97.
24. Paccola C, Resende C, Stumpp T, Miraglia S, Cipriano I. The rat estrous cycle revisited: A quantitative and qualitative analysis. Anim Reprod AR 2013;10:677-83.
25. Saillenfait A, Gallissot F, Morel G, Bonnet P. Developmental toxicities of ethylbenzene, ortho-, meta-, para-xylene and technical xylene in rats following inhalation exposure. Food Chem Toxicol 2003;41:415-29.
26. United States Food and Drug Administration. General guidelines for designing and conducting toxicity studies. In: Guidance for Industry and Other Stakeholders, Toxicological Principles for the Safety Assessment of Food Ingredients. Vol. 2000. United States: Redbook; 2003.
27. US EPA. "Methods for Derivation of Inhalation Reference Concentration and Application of Inhalation Dosimetry," EPA/600/8-90066F. Washington, DC: Office of Health and Environment; 1994.
28. Coria-Avila GA, Gavrila AM, Ménard S, Ismail N, Pfaus JG. Cecum location in rats and the implications for intraperitoneal injections. Lab Anim (NY) 2007;36:25-30.
29. Turner PV, Brabb T, Pekow C, Vasbinder MA. Administration of substances to laboratory animals: Routes of administration and factors to consider. J Am Assoc Lab Anim Sci 2011;50:600-13.
30. Kaneko T, Wang PY, Tsukada H, Sato A. m-Xylene toxicokinetics in phenobarbital-treated rats: Comparison among inhalation exposure, oral administration, and intraperitoneal administration. Toxicol Appl Pharmacol 1995;131:13-20.
31. Suckow MA, Weisbroth SH, Franklin CL. The Laboratory Rat. United States: Elsevier; 2005.
32. Hasnan J, Siti Amirah S, Paumgartten F, Hussin M, Zakiah I. Evaluation on the reproductive performance and spontaneous malformations amongst SD rats in the institute for medical research colony. Malays J Vet Res Malaysia 2014;5:53-63.
33. Jezequel AM, Orlandi F, Tenconi LT. Changes of the smooth endoplasmic reticulum induced by rifampicin in human and guinea-pig hepatocytes. Gut 1971;12:984-7.
34. Minhas K, Arshad S. Histopathology of the liver, gall bladder and pancreas. In: Atlas of Diagnostic and Predictive Histopathology. Singapore: Springer; 2020. p. 307-34.
35. Faber WD, Roberts LS, Stump DG, Beck M, Kirkpatrick D, Regan KS*, et al.* Inhalation developmental neurotoxicity study of ethylbenzene in Crl-CD rats. Birth Defects Res Part B Dev Reprod Toxicol 2007;80:34-48.
36. Faber WD, Roberts LS, Stump DG, Tardif R, Krishnan K, Tort M*, et al.* Two generation reproduction study of ethylbenzene by inhalation in Crl-CD rats. Birth Defects Res Part B Dev Reprod Toxicol 2006;77:10-21.
37. Saillenfait AM, Gallissot F, Sabaté JP, Bourges-Abella N, Cadot R, Morel G, *et al.* Developmental toxicity of combined ethylbenzene and methylethylketone administered by inhalation

to rats. Food Chem Toxicol 2006;44:1287-98.
38. Saillenfait AM, Gallissot F, Sabaté JP, Bourges-Abella N, Muller S. Developmental toxic effects of ethylbenzene or toluene alone and in combination with butyl acetate in rats after inhalation exposure. J Appl Toxicol 2007;27:32-42.
39. Cavieres MF, Jaeger J, Porter W. Developmental toxicity of a commercial herbicide mixture in mice: I. Effects on embryo implantation and litter size. Environ Health Perspect 2002;110:1081-5.
40. Singh MM, Bhalla V, Wadhwa V, Kamboj VP. Effect of centchroman on tubal transport and preimplantation embryonic development in rats. J Reprod Fertil 1986;76:317-24.
41. Gatsing D, Aliyu R, Kuiate JR, Garba IH, Jaryum KH, Tedongmo N*, et al.* Toxicological evaluation of the aqueous extract of *Allium sativum* bulbs on laboratory mice and rats. Cameroon J Exp Biol 2005;1:39-45.
42. Dote E, Dote T, Shimizu H, Shimbo Y, Fujihara M, Kono K. Acute lethal toxicity, hyperkalemia associated with renal injury and hepatic damage after intravenous administration of cadmium nitrate in rats. J Occup Health 2007;49:17-24.
43. Engström K, Husman K, Pfäffli P, Riihimäki V. Evaluation of occupational exposure to xylene by blood, exhaled air and urine analysis. Scand J Work Environ Health 1978;4:114-21.
44. Hada N, Kuramochi M, Izawa T, Kuwamura M, Yamate J. Effects of dexamethasone on hepatic macrophages in normal livers and thioacetamide-induced acute liver lesions in rats. J Toxicol Pathol 2020;33:237-46.
45. Abousalem M, Elgerwi A, El-Mashad AB. Genotoxic and histotoxic effects of air pollutants at a benzene station on albino rats. Int J Basic Clin Pharmacol 2014;3:144-50.
46. Kum C, Kiral F, Sekkin S, Seyrek K, Boyacioglu M. Effects of xylene and formaldehyde inhalations on oxidative stress in adult and developing rats livers. Exp Anim 2007;56:35-42.
47. Wang F, Zuo Z, Chen K, Fang J, Cui H, Shu G, *et al.* Histopathological changes caused by inflammation and oxidative stress in diet-induced-obese mouse following experimental lung injury. Sci Rep 2018;8:14250.
48. Kierszenbaum AL, Tres L. Histology and Cell Biology: An Introduction to Pathology E-book. New York: Elsevier Health Sciences; 2015.
49. Chen L, Hu G, Fan R, Lv Y, Dai Y, Xu Z. Association of PAHs and BTEX exposure with lung function and respiratory symptoms among a nonoccupational population near the coal chemical industry in Northern China. Environ Int 2018;120:480-8.
50. Perera T, Ranasinghe S, Alles N, Waduge R. Experimental rat model for acute tubular injury induced by high water hardness and high water fluoride: Efficacy of primary preventive intervention by distilled water administration. BMC Nephrol 2020;21:103.
51. Radi ZA. Kidney pathophysiology, toxicology, and drug-induced injury in drug development. Int J Toxicol 2019;38:215-27.
52. Pinto CR. Impact of the corpus luteum on survival of the developing embryo and early pregnancy in mares. Theriogenology 2020;150:374-81.
53. Adegboyega PA, Pei Y, McLarty J. Relationship between eosinophils and chronic endometritis. Hum Pathol 2010;41:33-7.
54. Renaud SJ, Cotechini T, Quirt JS, Macdonald-Goodfellow SK, Othman M, Graham CH. Spontaneous pregnancy loss mediated by abnormal maternal inflammation in rats is linked to deficient uteroplacental perfusion. J Immunol 2011;186:1799-808.
55. Langman JM. Xylene: Its toxicity, measurement of exposure levels, absorption, metabolism and clearance. Pathology 1994;26:301-9.
56. Neghab M, Hosseinzadeh K, Hassanzadeh J. Early liver and kidney dysfunction associated with occupational exposure to sub-threshold limit value levels of benzene, toluene, and xylenes in unleaded petrol. Saf Health Work 2015;6:312-6.
57. Rim KT. Reproductive toxic chemicals at work and efforts to protect workers' health: A literature review. Saf Health Work 2017;8:143-50.

Original Article

Correlation of Body Mass Index with Ankle Joint Range of Motion in Young Adults

Rachna Rohatgi, Aditi Bhatnagar, Nirupma Gupta, Manjari Jain[1]

Department of Anatomy, School of Medical Sciences and Research, Sharda University, [1]School of Medical Sciences and Research, Sharda University Greater Noida, Uttar Pradesh, India

Abstract

Introduction: The body mass index (BMI) together with gender and age widely affect the movements of joints of the individual. The increments in the magnitude of weight of body have a detrimental impact on the interaction of joints and muscles which have a long-term impact on balance and posture of the individual. The posture and balance is compromised to a great extent by the reduction of joints of the lower limb. **Objectives:** To calculate the BMI, range of motion (ROM) of ankle joints in both flexed and extended knee positions bilaterally and to correlate the effects of BMI on the ROM of ankle joint. **Materials and Methods:** The Department of Anatomy, School of Medical Sciences and Research, Sharda University, Greater Noida was the place of this cross-sectional study in which 235 subjects (108 males and 127 females) in the age group of 18–25 years participated voluntarily. **Results:** One-way ANOVA analysis of bilateral values of ankle dorsiflexion with flexed and extended knee of both sides revealed a statistically significant difference with a progressive decrease in the values from normal to obese group. **Conclusion:** The findings of the present study could prove useful for designing rehabilitative interventions for the overweight and obese subjects with the aim to improve their activities of daily living and reduce the morbidity from increased body mass.

Keywords: *Ankle joint, body mass index, dorsiflexion, goniometry, range of motion*

Introduction

The act of maintaining the balance in a static or dynamic posture is crucial for the attainment of postural stability. The interaction of joints and muscles which is essential for the functional capacity and postural balance of the human body is adversely affected by increased body weight. A decreased joint range of motion (ROM), especially of the lower extremity is primarily responsible for postural instability in overweight and obese subjects. The ROM varies with various factors such as age, sex of individual, and nature of motion whether the joints are moved voluntarily or without assistance. The body mass index (BMI), occupation and recreational activities also have a major impact on the joint motion.[1-3] BMI is a simple index of weight for height that is commonly used to classify underweight, overweight, and obese individuals.

The ankle ROM in humans is affected by geographical and cultural differences in the activities of daily living.[4] The average plantar flexion is 40°–56° and dorsiflexion (DF) of the ankle is reported to be 13°–33°.[5-7] The high incidence of musculoskeletal disorders in obese subjects was reportedly due to excess mass which by altering the individual's joint motion exerts excessive joint load as enunciated by Capodaglio *et al*.[8] Anatomically, the ankle joint encompasses a complex rotation axis which varies in DF and plantar flexion. Roentgen stereophotogrammetry was used for analyzing the axis of rotation in eight healthy volunteers with 10° increments between 30° plantar flexion and 30° DF by Lundberg *et al*. and observed a continuous change in axis of rotation with major individual variations.[9] The trochlear surfaces of 152 human tali were studied by Barnett and Napier and observed that that the medial and lateral curvatures of the talus are different and concluded that the axis of rotation of the ankles changes its position during the arc of motion.[10]

Anthropometric status can influence lower limb joint ROM, but there is relatively little published research regarding structural

How to cite this article: Rohatgi R, Bhatnagar A, Gupta N, Jain M. Correlation of body mass index with ankle joint range of motion in young adults. J Anat Soc India 2023;72:262-6.

Article Info

Received: 16 August 2023
Accepted: 16 August 2023
Available online: 28 September 2023

Address for correspondence:
Dr. Rachna Rohatgi, Department of Anatomy, School of Medical Sciences and Research, Sharda University, Plot No. 32-34, Knowledge Park III, Greater Noida - 201 310, Uttar Pradesh, India.
E-mail: rachna.rohtagi@sharda.ac.in

Access this article online

Website: https://journals.lww.com/joai
DOI: 10.4103/jasi.jasi_87_23

Quick Response Code:

and functional characteristics of lower limb in overweight and obese young adults. Hence, the purpose of the present study is to establish the BMI related effects on the ROM of the ankle joints for both males and females in young adults from North India.

Aims and objectives

1. To estimate the BMI from height and weight measurement
2. To measure the ROM of ankle joints in flexed knee and extended knee positions of both sides
3. To correlate the effects of BMI on the ROM of ankle joint of both sides.

Materials and Methods

Department of Anatomy, School of Medical Sciences and Research, Greater Noida, was the place of the present cross-sectional study, in which 235 subjects (108 males and 127 females) participated, after obtaining approval of the ethical committee of the School of Medical Sciences and Research, Sharda University. The subjects were in the age group of 18–25 years and excluded those not fulfilling the inclusion criteria. The participants were subjects who volunteered for the study and were included after obtaining their written informed consent.

Inclusion criteria were healthy adults between 18 and 25 years of age of either sex, not falling into the ambit of exclusion criteria. Subjects with BMI of <19 kg/m^2 existing neurologic and lower extremity chronic conditions, appreciable leg length discrepancy, history of acute lower extremity injury or surgery within the 6 months were excluded from the study.

Methodology

BMI was calculated as follows: BMI = weight in kg/(height in meter)^2.

Based on the BMI, participants were divided into three groups: Normal (19–24.9 kg/m^2), overweight (25–29.9 kg/m^2), and obese (≥30 kg/m^2.).[11] All the measurements were performed by a single investigator. Weight of the subject was measured in light clothes and without shoes using standard apparatus, which read to the nearest 0.1 kg. Height of the subject was measured without shoes to the nearest 0.5 cm, as the vertical distance from the vertex (the highest point on the top of the head) to the floor in the mid sagittal plane with the subject standing bare foot on an even floor and the head being oriented in the Frankfurt's plane. Joint ROM measurement was done using 180° system, by the universal goniometer.[12] The measurement of DF of ankle joint was done in flexed knee and extended knee positions on both the sides. The ankle DF in the flexed knee position [Figure 1] was measured with the subject seated with the popliteal fossa at the edge of the table and the knees in 90° of flexion in the sitting position. The axis of the goniometer was centered over the lateral malleolus, the stationary (proximal) arm was placed along the shaft of the fibula (this is perpendicular to 0°), and the movable (distal) arm was placed parallel to the fifth metatarsal. The ankle DF ROM was recorded in the sagittal plane in degrees. The ankle DF ROM in the extended knee position [Figure 2] was measured with the subject seated on a table with the knees fully extended (0°) and the feet off the edge of the table. The ankle joint was in neutral, starting position (90° angle between shank and foot segment) with the foot in 0° inversion and eversion. The axis of the goniometer was centered over the lateral malleolus, the stationary (proximal) arm was placed along the shaft of the fibula (this is perpendicular to 0°) and the movable (distal) arm was placed parallel to the fifth metatarsal.

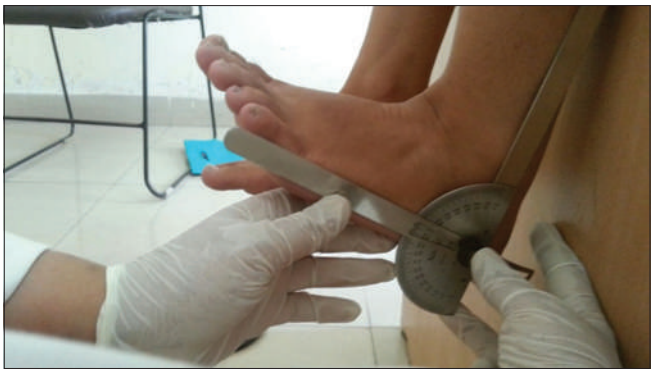

Figure 1: Ankle joint measurement in flexed knee position

Statistical analysis

Data of the three groups were combined for the standard descriptive statistics (mean ± standard deviation) which were determined for the BMI and ankle joint ROM for all the three groups. Gender and bilateral differences were tabulated and calculated for difference ($P < 0.05$) by the paired Student's *t*-test which was applied for the comparison of data among the North Indian normal weight, overweight, and obese males and females. The difference between subject groups was tested using the one-way ANOVA for multiple comparisons using a significance level of 0.05 (SPSS version 22). A 5% level of probability was used to indicate statistical significance.

Observations and Result

The anthropometric variables (height and weight) of each subject were measured to evaluate the BMI and the subjects were divided into three groups of normal (150) l, overweight (56) and obese (29). The mean values of BMI in three groups of normal, overweight, and obese subjects did not show any statistically significant gender difference, when analyzed by the Student's *t*-test [Bar Diagram 1].

The comparison of bilateral mean values of ankle joint DF in normal subjects is depicted in Table 1. The mean ankle DF with flexed knee on the left and right sides was 17.70° ± 1.93° and 17.98° ± 1.96°, respectively (1a).

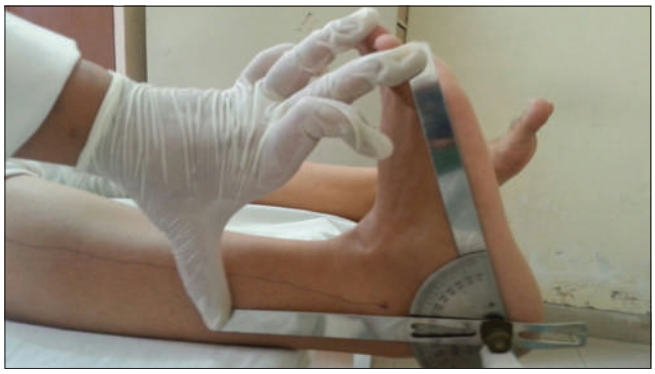

Figure 2: Ankle joint measurement in extended knee position

The values of ankle DF with extended knee were 16.28° ± 1.48° and 15.91° ± 1.69° on the left and right sides, respectively (1b). In normal subjects, on analysis of the results by Student's *t*-test, a bilateral statistically significant difference ($P < 0.05$) was observed in the values of ankle DF in both flexed and extended knee position.

The comparison of bilateral mean values of ankle joint ROM in overweight subjects is shown in Table 2. The mean values of left and right ankle DF ROM in flexed knee position were 14.68° ± 1.91° and 14.85° ± 1.53°, respectively (2a). The values of left and right ankle DF ROM in the extended knee position were recorded as 13.886° ± 1.23° and 13.70° ± 1.38° (2b). On analysis of the findings in overweight subjects by the Student's *t*-test, the comparison of bilateral mean values of ankle DF with both flexed and extended knee did not exhibit significant difference ($P > 0.05$) in overweight subjects.

Table 3 shows the comparison of mean values of ankle joint ROM in obese subjects. The ankle joint DF ROM (degrees) in the flexed knee position on the left side was 13.69° ± 1.81° and 13.10° ± 1.20° on the right side (3a). The values of left and right ankle joint DF ROM (degrees) in the extended knee position were 12.17° ± 1.16° and 12.17° ± 0.92°, respectively (3b). With flexed knee, ankle DF ROM revealed a statistically significant difference bilaterally ($P < 0.05$) while with extended knee ankle DF, ROM was not found to be statistically significant ($P > 0.05$).

One-way ANOVA analysis of values of ankle DF with flexed and extended knee of both sides revealed a statistically significant difference with a progressive decrease in the values from normal to obese group. Bar Diagrams 2 and 3 depict the gender wise comparison of ankle joint ROM in the three groups of subject. Analysis of data of male and female on both the sides by Student's *t*-test did not yield a statistically significant difference ($P > 0.05$) in the values of ankle joint ROM.

Discussion

In the present study, a statistically significant difference ($P < 0.05$) was observed between the left and right ankle DF ROM in both flexed and extended knee position in normal group, while it was not significant statistically ($P > 0.05$) in overweight subjects [Tables 1 and 2]. Obese group [Table 3] also showed a statistically significant difference ($P < 0.05$) in ankle DF ROM but only with the flexed knee position. This finding was consistent with Ferrario *et al*. who observed more than 5° difference in total ROM (DF and plantar flexion).[13] The results of the present study demonstrate that the range of ankle DF was less in the extended knee position (16.28°) than with the knee flexed (17.70°) [Table 4], which is supported by Fong *et al*. who from their study conducted on young adults of Boston university, USA, reported a mean of 14.3° ± 5.5° and 18.9° ± 5.9° ankle DF in the extended and flexed knee position, respectively, thus corroborating the observation of a decreased ROM of ankle joint with extended knee as noted in the present study.[14] The extended knee ROM measurement assesses the extensibility of both gastrocnemius and soleus

Table 1: Mean values of ankle joint range of motion in normal subjects

Parameters	Mean±SD	*t*-test	*P* and significance
Ankle DF with flexed knee (left)	17.70±1.93	2.91	*P*<0.05 (significant)
Ankle DF with flexed knee (right)	17.98±1.96		
Ankle DF with extended knee (left)	16.28±1.48	4.12	*P*<0.05 (significant)
Ankle DF with extended knee (right)	15.91±1.69		

P<0.05 indicates statistical significance. SD: Standard deviation, DF: Dorsiflexion

Table 2: Mean values of ankle joint range of motion in overweight subjects

	Parameters	Mean±SD	*t*-test	*P*
3a	Ankle DF with flexed knee (left)	14.68±1.91	1.026	0.309 (not significant)
	Ankle DF with flexed knee (right)	14.85±1.53		
3b	Ankle DF with extended knee (left)	13.88±1.23	1.526	0.133 (not significant)
	Ankle DF with extended knee (right)	13.70±1.38		

SD: Standard deviation, DF: Dorsiflexion

Table 3: Mean values of ankle joint range of motion in obese subjects

	Parameters	Mean±SD	*t*-test	*P*
3a	Ankle DF with flexed knee (left)	13.69±1.81	2.38	0.024 (significant)
	Ankle DF with flexed knee (right)	13.10±1.20		
3b	Ankle DF with extended knee (left)	12.17±1.16	0.000	1.000 (not significant)
	Ankle DF with extended knee (right)	12.17±0.92		

SD: Standard deviation, DF: Dorsiflexion

Table 4: Comparison of mean values of ankle dorsiflexion range of motion (°) in flexed and extended knee position in the three groups

Groups	Mean±SD		
	Normal	Over weight	Obese
Left ankle DF (knee flexed)	17.70±1.93	14.85±2.10	13.60±1.8
Right ankle DF (knee flexed)	17.98±1.96	15.01±1.74	13.10±1.20
Left ankle DF (knee extended)	16.28±1.48	14.01±1.39	12.17±1.16
Right ankle DF (knee extended)	15.91±1.69	13.85±1.5	12.17±0.9

P<0.05 indicates statistical significance. SD: Standard deviation, DF: Dorsiflexion

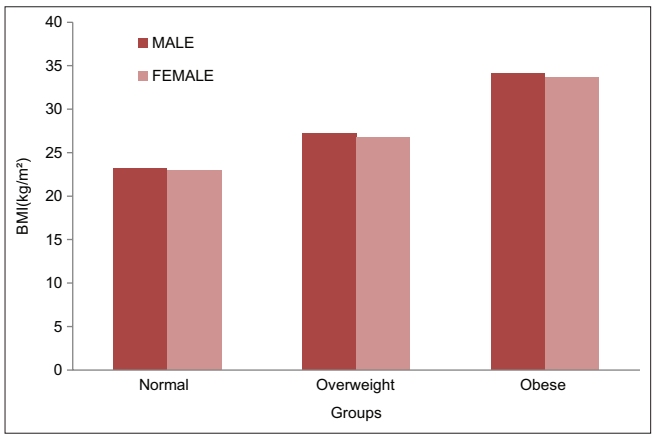

Bar Diagram 1: Representation of mean BMI in male and female subjects in the three groups. BMI: Body mass index

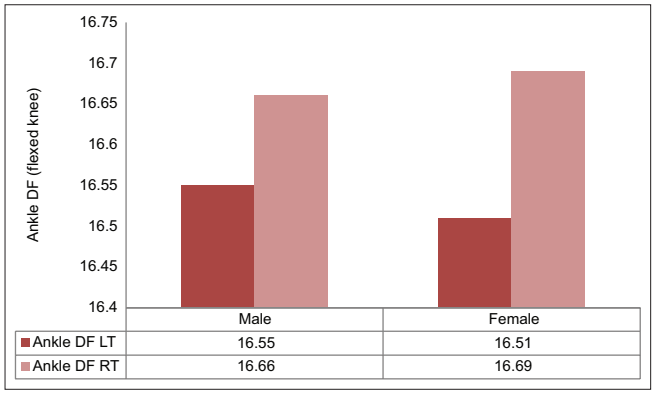

Bar Diagram 2: Gender difference of ankle dorsiflexion ROM with flexed knee. ROM: Range of motion

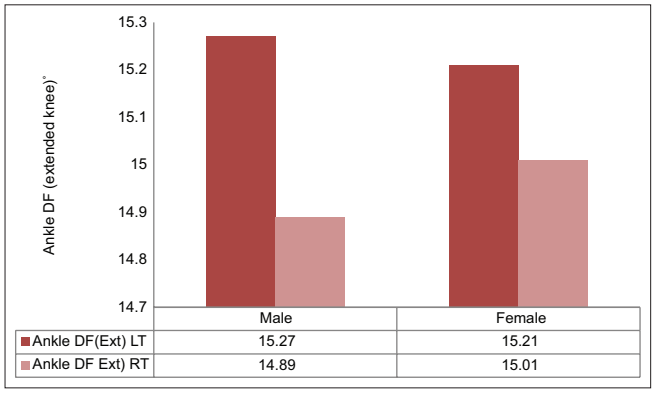

Bar Diagram 3: Gender difference of ankle dorsiflexion ROM with extended knee. ROM: Range of motion

muscles whereas the flexed knee measurement performed at 90° of knee flexion essentially isolates the soleus. Spyropoulos *et al*. studied ROM of lower limb in 12 obese and 12 nonobese men between the ages of 30–47 years and reported that obese had significantly greater DF than plantar flexion. The gastrocnemius facilitates the push off in stance phase by plantar flexion and the reduced plantar flexion in obese was to decrease energy expenditure by decreasing the height to which the body is forced up and increased DF is essential for toe clearance in the swing phase.[15] The study of alterations in ground walking patterns in obese and overweight adults by Meng *et al*., done by computing the angular displacements, ROM of bilateral hips, knees, and ankles however did not indicate significant differences among the three BMI which is not consistent with present study.[16] Jeong *et al*. from their study of preobesity and obesity impacts on passive joint ROM reported that the three categories of BMI groups did not show a significant difference in the mean ROM for ankle DF, which may be due to the soft tissues disposition of the leg. The increased BMI results in a relatively larger increase in mass and volume for the tissues in the posterior part than the anterior leading to larger resistance to passive plantar flexion from compression of the soft tissues occupying the space around the ankle joint.[17] Park and Park compared the foot arch height, plantar fascia thickness, ROM of the ankle joint, and balance between obese and normal weight young adults and concluded that obese young adults had weakened ankle eversion strength and balance problems compared with the normal weight group.[18] The results of the study could have implications in sports industry for improving ankle flexibility to improve the performance of players.

Limitations of study

The present study examined only active ROM in which the subject moves the joint unassisted. Furthermore, the study involved less number of participants of single ethnic group from a small region. Further studies could take into consideration comparison between dominant and nondominant leg and future research should aim to include a larger number of participants from wide geographical areas and a wider age group to reduce the morbidity arising from increased BMI.

Conclusion

The findings of the present study could prove useful in ergonomics for designing products and systems for the

overweight and obese individuals as they comprise a significant proportion of manpower worldwide. The effects of different levels of weight loss and its effect on the physical traits can prove useful for improving the activities of daily living of obese individuals.

Acknowledgments

We feel privileged to express our regards and sincere gratitude to the faculty and support staff of Department of Anatomy, SMS and R, Sharda University for providing their valuable support at every step of the research. We are indebted and equally privileged to express our deep gratitude to Dr. Pooja Rastogi (Associate dean, SMS and R,) for valuable advice and suggestions.

Financial support and sponsorship

Nil.

Conflicts of interest

There are no conflicts of interest.

References

1. Kejonen P, Kauranen K, Vanharanta H. The relationship between anthropometric factors and body-balancing movements in postural balance. Arch Phys Med Rehabil 2003;84:17-22.
2. Ledin T, Odkvist LM. Effects of increased inertial load in dynamic and randomized perturbed posturography. Acta Otolaryngol 1993;113:249-52.
3. McGraw B, McClenaghan BA, Williams HG, Dickerson J, Ward DS. Gait and postural stability in obese and nonobese prepubertal boys. Arch Phys Med Rehabil 2000;81:484-9.
4. Ahlberg A, Moussa M, Al-Nahdi M. On geographical variations in the normal range of joint motion. Clin Orthop Relat Res 1988;(234):229-31.
5. Stauffer RN, Chao EY, Brewster RC. Force and motion analysis of the normal, diseased, and prosthetic ankle joint. Clin Orthop Relat Res 1977;(127):189-96.
6. Lindsjö U, Danckwardt-Lilliestrom G, Sahlstedt B. Measurement of the motion range in the loaded ankle. Clin Orthop Relat Res 1985;(199):68-71.
7. Boone DC, Azen SP. Normal range of motion of joints in male subjects. J Bone Joint Surg Am 1979;61:756-9.
8. Capodaglio P, Castelnuovo G, Brunani A, Vismara L, Villa V, Capodaglio EM. Functional limitations and occupational issues in obesity: A review. Int J Occup Saf Ergon 2010;16:507-23.
9. Lundberg A, Svensson OK, Németh G, Selvik G. The axis of rotation of the ankle joint. J Bone Joint Surg Br 1989;71:94-9.
10. Barnett CH, Napier JR. The axis of rotation at the ankle joint in man; its influence upon the form of the talus and the mobility of the fibula. J Anat 1952;86:1-9.
11. WHO Expert Consultation. Appropriate body mass index for Asian population and it's implications for policy and intervention strategies. Lancet 2004;363:157-63.
12. Norkin CC, White J. Measurement of Joint Motion, a Guide to Goniometry. 3rd ed. Philadelphia: FA Davis; 2003.
13. Ferrario VF, Turci M, Lovecchio N, Shirai YF, Sforza C. Asymmetry of the active nonweightbearing foot and ankle range of motion for dorsiflexion-plantar flexion and its coupled movements in adults. Clin Anat 2007;20:834-42.
14. Fong CM, Blackburn JT, Norcross MF, McGrath M, Padua DA. Ankle-dorsiflexion range of motion and landing biomechanics. J Am Podiatr Med Assoc 2012;102:5-12.
15. Spyropoulos P, Pisciotta JC, Pavlou KN, Cairns MA, Simon SR. Biomechanical gait analysis in obese men. Arch Phys Med Rehabil 1991;72:1065-70.
16. Meng H, Connor DP, Lee BC, *et al*. Alterations in overground walking pattern in obese and overweight adults 2017;(53):145–50.
17. Jeong Y, Heo S, Lee G, Park W. Pre-obesity and obesity impacts on passive joint range of motion. Ergonomics 2018;61:1223-31.
18. Park SY, Park DJ. Comparison of foot structure, function, plantar pressure and balance ability according to the body mass index of young adults. Osong Public Health Res Perspect 2019;10:102-7.

Case Report

A Rare Anatomical Variant: Aberrant Arterial Supply of Azygoesophageal Recess Originating from the Celiac Plexus

Abstract

The aberrant arteries of the lung are very rare abnormalities. It is included in the type 1 sequestration group when it is a single finding without other sequestration features. Sequestrations account for <1% of all lung malformations. Type 1 is the least common form in this group. In 75% of these cases, the aberrant artery (AA) originates from the thoracic aorta. AA originating from the celiac plexus is very rare. Moreover, even if it originates from an abdominal vascular, AA is extended left lower lobe of the lung or the right middle lobe. Our case is atypical with its azygoesophageal recess (AOR) localization. The AOR is a special region that forms the mediobasal segment of the right lung. After the pandemic, this region has been expressed as one of the areas where COVID-19 infection shows affinity. The reason for this condition has not been definitively clarified yet. Therefore, the anatomical details of this segment need to be more probed. Furthermore, the radiological multidetector computed tomography (MDCT) appearance of our case is in the differential diagnosis, with Scimitar syndrome and, as far as we know, this differential diagnosis detail has not been mentioned so far. MDCT plays an important role in the diagnosis and planning of definitive treatment by determining the origin and course of the AA. Definitive treatment may be surgery (lobectomy or segmentectomy) or endovascular. The case of a 62-year-old patient with a lung AA is presented accompanied by radiological and clinical findings.

Keywords: *Aberrant artery, anatomic variants, radiology, thorax*

Emrah Doğan, Marwa Mouline Doğan[1], Bünyamin Güney, Özge Oral Tapan[2], Utku Tapan[2], Sabri Serhan Olcay[2]

Departments of Radiology, [1]Cardiology and [2]Pulmonology, Muğla Sıtkı Koçman University Education and Training Hospital, Muğla, Turkey

Introduction

The lung is an organ with a dual arterial supply. Except for bronchial or pulmonary arterial circulation, the supply of lung parenchyma by aberrant artery (AA) is a very rare encountered anomaly without a separate sequestered segment.[1] It is sometimes included in the type 1 sequestration group. Sequestrations account for <1% of all lung malformations. Type 1 is the least common form among the groups (types 1, 2, and 3).[2,3] In 75% of type 1 cases, the AA originates from the thoracic aorta. AA originating from the celiac plexus is a very rare variation. Moreover, even if a lung segments supply provided by an abdominal vascular, the region where abnormal vascularity is probably the left lower lobe of the lung or the right middle lobe. Our case was also atypical according to its localization.[3,4] The azygoesophageal recess (AOR) is a special region that forms the mediobasal segment of the right lung. After the pandemic, this region has been expressed as one of the areas where COVID-19 infection shows affinity. The reason for this condition has not been definitively clarified yet. Therefore, the anatomical details of this segment need to be more probed.[5,6]

Furthermore, the radiological appearance of our case in multidetector computed tomography (MDCT) is in the differential diagnosis, with Scimitar syndrome and, as far as we know, this differential diagnosis detail has not been mentioned so far.[7] MDCT plays an important role in the diagnosis and planning of definitive treatment by determining the origin and course of the AA.[8] The case of a 62-year-old patient with the AA originating from the celiac plexus, extending to the AOR, was presented accompanying by radiological and clinical findings.

Case Report

A 62-year-old male patient was referred to us with the initial diagnosis of anemia was detected in the examinations performed in an external medical center. There was a

How to cite this article: Doğan E, Doğan MM, Güney B, Tapan ÖO, Tapan U, Olcay SS. A rare anatomical variant: Aberrant arterial supply of azygoesophageal recess originating from the celiac plexus. J Anat Soc India 2023;72:267-70.

Article Info

Received: 01 September 2022
Accepted: 15 August 2023
Available online: 28 September 2023

Address for correspondence:
Prof. Emrah Doğan,
228 Sok. Obam Sitesi No: 15 Kötekli/Menteşe, Muğla, Turkey.
E-mail: emrahdogan@mu.edu.tr

Access this article online

Website: https://journals.lww.com/joai

DOI: 10.4103/jasi.jasi_117_22

Quick Response Code:

known history of medication (Saneloc 50 mg, Atacand, and oral iron use). In addition, the patient was being followed up for ascending aortic aneurysm. Abdominal, lung, heart, neurological, and systemic examinations were normal. On manual neck examination, neck lymph nodes were palpable. He had no history of hemorrhoids.

In the laboratory, iron was 74 ng/mL, total iron-binding capacity: 291 µg/dL, transferrin saturation: 25%, ferritin: 61.5 ml/ng, Vitamin B12: 458 pg/ml, and reticulocyte: 1.22%. White blood cell was 7620 × 109/L, hemoglobin: 13.3 g/dL, platelet: 278,000/µL of blood, and sedimentation: 62 mm/h. There was no evidence of anemia in the patient's laboratory results, but thrombocytosis was detected.

In the neck sonography, bilaterally big but reactive fusiform lymph nodes in the size of 22 mm × 9 mm × 8 mm in the left submandibular region (Level 1B) and 20 mm × 8 mm × 7 mm in the jugulodigastric region (Level 2A) were detected.

In the abdominal ultrasonography, there were sequela calcifications in the liver. The spleen and pancreas were normal. There were Bosniak type 1, 2, and 2F cortical parapelvic cysts in bilateral kidneys. The largest one was 8 cm. Millimetric kidney stones were detected in both kidneys.

The heart is in the normal configuration in thorax computed tomography (CT). Atherosclerotic wall calcifications were detected at the level of the aortic arch, descending aorta, brachiocephalic radix, and coronary arteries. The anteroposterior diameter of the ascending aorta is 50 mm at its widest point and is wider than normal. No effusion was detected in the pleural and pericardial spaces.

On contrast-enhanced CT images, an abnormal arterial vascular structure is incidentally observed at the entrance of the AOR on the right side. The vascular structure was extending toward the lower lobe of the right lung [Figure 1].

Vascular structure was arising from the main celiac plexus [Figure 2].

There was neither a separated lobe nor abnormal bronchial branch. All findings were compatible with Pryce type 1 sequestration and abnormal AA. The consent form was signed by the patient on April 27, 2022.

Discussion

As it is known, the lung has two separate arterial supply systems, pulmonary and bronchial.[1] In the case of sequestration, especially in the lower lobes of the lung, a focal segment is fed by the aorta or its branches. However, in this case, additional findings accompany the pathology. A systemic arterial supply with normal bronchial communication (no bronchial sequestration) and no cardiovascular or pulmonary abnormalities is a rare congenital abnormality.[2,3] Although there is no additional abnormality other than arterial variation, it should be included in the sequestration groups because of the embryological mechanism of AA of the lung. It is called type 1 according to the Pryce classification[3] [Table 1].

Although pulmonary sequestration is expressed in 0.15%–6% of all congenital pulmonary malformations in various studies, the general consensus is that it is below 1%.[3,10] However, this is the prevalence of all sequestrations. AA variant, which is considered type 1, is very rare.[8] In intralobar sequestration, the AA originates from the thoracic aorta in 74% of all cases, and 14% have more than one abnormal artery. A single artery supplies the majority of cases, and two or more arteries are seen in 21% of cases.[9] Our case is a rare case due to the presence of a single artery originating from the celiac plexus originating from the abdominal aorta. Apart from this, there are cases associated with the left subclavian artery and internal mammary artery.

In the presence of pulmonary sequestration, diaphragmatic hernia 36%, hernia with diaphragm defect 19%, diaphragm

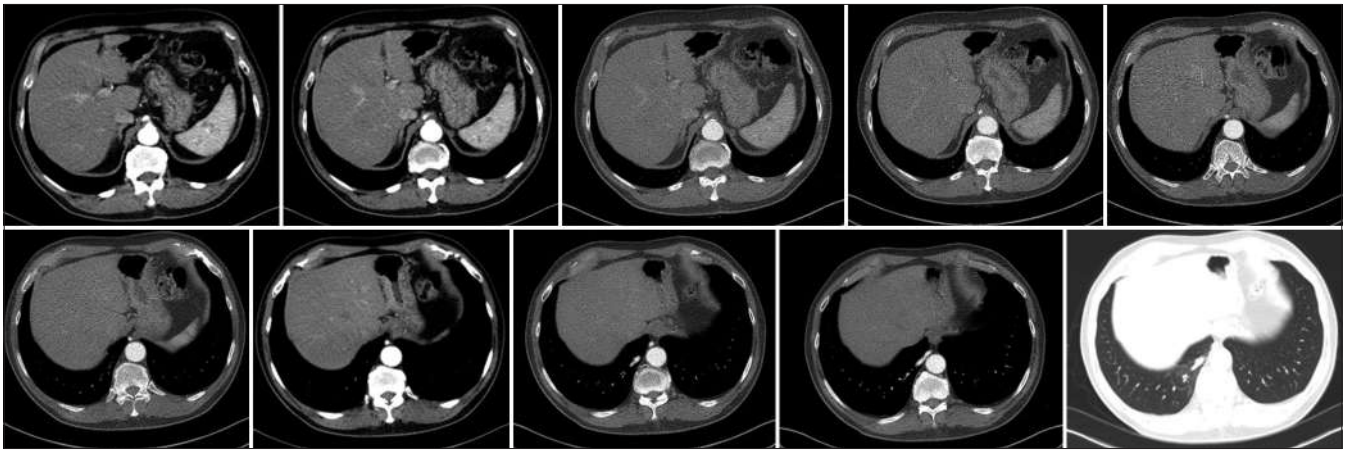

Figure 1: Axial computed tomography images showing an aberrant artery originating from the celiac plexus and vertically reaching the azygoesophageal recess of the right lung

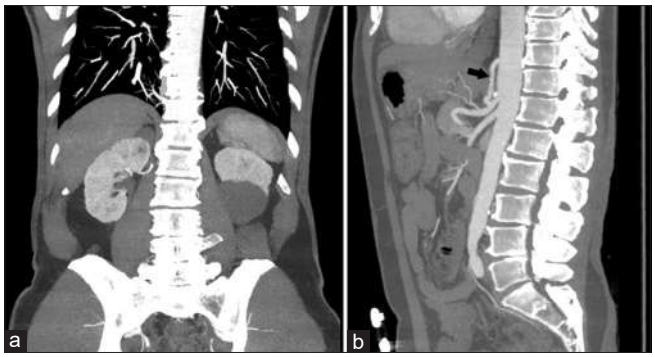

Figure 2: (a) Appearance of the aberrant artery (AA) in coronal computed tomography angiography images, (b) AA originating from the celiac main artery (arrow)

Table 1: Pryce classification

Variant type	Anomalies
Type 1	Normal lung with anomalous systemic arterial supply
Type 2	Anomalous artery supplying "disconnected lung" and adjacent normal lung
Type 3	Anomalous artery to "disconnected lung"

Our patient was compatible with type 1[9]

loosening 5%, lung anomalies 13%, tracheoesophageal fistula 2%, epiphrenic diverticulum 3%, vitium cordis 6%, pericardial anomalies 4%, funnel chest 1%, esophageal duplication 1%, megacolon 1%, and other anomalies 11% may accompany.[11] However, malformations usually accompany type 2 and 3 sequestration. Its association with the type is not expected. There was no accompanying additional anomaly in our case.[12]

The AA variant is more common in the lower lobes of the left lung and usually affects the posterior basal segment.[13] There are cases where it affects the right middle lobe. In our case, the right lower lobe AOR was affected (lower lobe mediobasal segment). It differs in this respect.

The AOR is a special region that forms the mediobasal segment of the right lung. After the pandemic, this region has been expressed as one of the areas where COVID-19 infection shows affinity. The reason for this has not been definitively clarified.[6] Therefore, the anatomical details of this segment need to be considered more.

Embryologically, the lung bud develops from the primitive aorta. When there is a migration or regression defect in this area, the feeding connection of the lung with the aorta continues. Where this is evident, there is the potential to develop focal pulmonary hypertension and high-output heart failure.[14] In our case, only thrombocytosis is present. In the systemic evaluation, there is no additional finding to explain the cause of thrombocytosis. To the best of our knowledge, there is no information on the relationship between sequestration or abnormal pulmonary artery and thrombocytosis in the literature. This topic is open to future research.

Most patients are asymptomatic in the presence of an AA. Rarely, hemoptysis is seen. In this case, contamination around the AA is expected. This is related to the higher pressure of the systemic circulation compared to the pulmonary circulation. Other symptoms include exertional dyspnea, lower chest murmur, and congestive heart failure due to left heart overload.[15]

X-ray is often insufficient to identify such lesions. Or, if it extends vertically or obliquely from the inferior, as in our case, it can stand out like the Scimitar vein. Therefore, venous pulmonary return anomaly and AA are radiologically in the differential diagnosis in the first place. This appearance becomes evident, especially when originating from the abdominal source.

CT is the most demonstrative examination. As in our case, CT angiography should be added to the examination in cases where the arterial origin cannot be determined clearly. In CT, as in direct radiography, Scimitar syndrome is in the differential diagnosis. Angiography is useful in determining the origin of the vascular structure.[16]

As in our case, follow-up is recommended in asymptomatic cases. In the presence of recurrent hemoptysis, endovascular treatment (embolization and surgical ligation) or operation (lobectomy and segmentectomy) may be considered.[8,17]

Conclusion

The presence of AA originating from the aorta is considered type 1 in the sequestration group due to embryological origin. Our case is an atypical case due to the presence of AA originating from the celiac plexus and the localization of AOR. In the absence of angiography and further examination, it mimicked Scimitar syndrome. CT angiography is important in diagnosis. Since aortic pressure is from pulmonary artery pressure, aberrant arteries may be the source of hemoptysis. If it is asymptomatic, as in our case, it should be followed up. It should be evaluated for endovascular and surgical treatment in cases of recurrent hemoptysis.

Declaration of patient consent

The authors certify that they have obtained all appropriate patient consent forms. In the form, the patient has given his consent for his images and other clinical information to be reported in the journal. The patient understands that his name and initials will not be published and due efforts will be made to conceal his identity, but anonymity cannot be guaranteed.

Financial support and sponsorship

Nil.

Conflicts of interest

There are no conflicts of interest.

References

1. Suresh K, Shimoda LA. Lung circulation. Compr Physiol 2016;6:897-943.
2. Alsumrain M, Ryu JH. Pulmonary sequestration in adults: A retrospective review of resected and unresected cases. BMC Pulm Med 2018;18:97.
3. Chakraborty RK, Modi P, Sharma S. Pulmonary sequestration. In: StatPearls. Treasure Island (FL): StatPearls Publishing; 2022.
4. Sapmaz E, İnan MŞ, Işık H, Karataş O, Çaylak H, Gürkök S. Pulmonary sequestrations: Experience of 31 patients. Chest 2019;5:21.
5. Ravenel JG, Erasmus JJ. Azygoesophageal recess. J Thorac Imaging 2002;17:219-26.
6. Zhou S, Wang Y, Zhu T, Xia L. CT features of coronavirus disease 2019 (COVID-19) pneumonia in 62 patients in Wuhan, China. AJR Am J Roentgenol 2020;214:1287-94.
7. Wang H, Kalfa D, Rosenbaum MS, Ginns JN, Lewis MJ, Glickstein JS, *et al*. Scimitar syndrome in children and adults: Natural history, outcomes, and risk analysis. Ann Thorac Surg 2018;105:592-8.
8. Peringattuthodiyil Y, Christopher DJ, Balamugesh T, Saheer S. Aberrant arterial supply to left lung. Lung India 2015;32:287-8.
9. Fabbri N, Tamburini N, Galeotti R, Quarantotto F, Maniscalco P, Rinaldi R, *et al*. A rare case of intralobar pulmonary sequestration: Combined endovascular and video-assisted thoracoscopic approach. AME Case Rep 2018;2:19.
10. Tashtoush B, Memarpour R, Gonzalez J, Gleason JB, Hadeh A. Pulmonary sequestration: A 29 patient case series and review. J Clin Diagn Res 2015;9:C05-8.
11. Lee S, Cho JS, Hoseok I, Ahn HY, Kim YD. Extralobar supradiaphragmatic pulmonary sequestration arising from the retroperitoneum through a congenital diaphragmatic defect. J Chest Surg 2021;54:224-7.
12. Mashkov AE, Mayr JM, Bobylev AV, Slesarev VV. Intralobar pulmonary sequestration with anomalous artery arising from the celiac trunk. Surgeries 2021;2:105-12.
13. Kim M, Woo JJ, An JK, Jung YY, Choi YS. A pulmonary sequestered segment with an aberrant pulmonary arterial supply: A case of unique anomaly. Korean J Radiol 2016;17:302-5.
14. Kau T, Sinzig M, Gasser J, Lesnik G, Rabitsch E, Celedin S, *et al*. Aortic development and anomalies. Semin Intervent Radiol 2007;24:141-52.
15. Hwang JH, Kim EY, Park SY. Aberrant bronchial artery to non-sequestrated left upper lobe in massive hemoptysis. Tuberc Respir Dis (Seoul) 2015;78:380-4.
16. Masrani A, McWilliams S, Bhalla S, Woodard PK. Anatomical associations and radiological characteristics of scimitar syndrome on CT and MR. J Cardiovasc Comput Tomogr 2018;12:286-9.
17. Bhalla AS, Gupta P, Mukund A, Kumar A, Gupta M. Anomalous systemic artery to a normal lung: A rare cause of hemoptysis in adults. Oman Med J 2012;27:319-22.

Case Report

Inferior Vena Cava Agenesis, Bilateral Double Renal Veins, and Left Circumaortic Renal Vein: A Rare Case and Brief Review of the Literature

Erdal Karavas[1], Sonay Aydin[1], Edhem Unver[2], Ozlem Kadirhan[1], Mecit Kantarci[1,3]

Departments of [1]Radiology and [2]Chest Disease, Erzincan University, Erzincan, [3]Department of Radiology, Atatürk University, Erzurum, Turkey

Abstract

The improper embryologic development of the inferior vena cava (IVC) is a rare congenital defect that affects about 4% of the population. IVC agenesis is one of the less common variations, with an estimated prevalence ranging from 0.005% to 1%. We present a rare instance of IVC agenesis, bilateral double renal veins, and left circumaortic renal vein that manifested as lower extremities deep vein thrombosis. While anomalies of the IVC and renal veins are exceedingly rare, they should be considered during retroperitoneal procedures to avoid major consequences, particularly venous bleeding caused by incorrect damage. Anatomical variance of the IVC and renal veins is critical for procedures such as ureteral surgery, sympathectomy, radical nephrectomy, and organ transplantation. The clinical significance of these aberrations stems from the possibility of mistakes during imaging. They play a significant role in the diagnosis and treatment of venous thromboembolic disease.

Keywords: *Agenesis, anatomical variations, deep vein thrombosis, inferior vena cava, renal veins*

Introduction

The improper embryologic development of the inferior vena cava (IVC) is a rare congenital defect that affects about 4% of the population. IVC agenesis is one of the less common variations, with an estimated prevalence ranging from 0.005% to 1%. These anomalies can be isolated or combined with other conditions such as situs inversus, dextrocardia, polysplenia, and asplenia.[1]

Except for IVC interruption, which is more common in females, they are primarily observed in males (62%), and their frequency is similar in Asiatic, European, and other Western countries, with the exception of IVC aplasia/agenesis, which is less common in Asia. More prevalent anatomical variants within the spectrum of IVC malformations are the duplicate IVC (0.2%–3%), transposition (left-sided IVC 0.2%–0.5%), the circumaortic left renal vein (1.5%–8.7%), and the retroaortic renal vein (2.1%). The absence of a portion of the IVC, azygos, and hemiazygos continuation of a double IVC, hypoplasia, or aplasia/agenesis, or interruption of the IVC, double superior vena cava (SVC), and double IVC are all rare abnormalities of the IVC.[2,3]

In most cases, IVC anatomical anomalies are identified by chance during imaging, surgery, or dissection studies. When symptomatic, persistent varicose veins, stasis dermatitis, skin ulcerations, deep vein thrombosis (DVT), and, in severe cases, venous thromboembolisms are common clinical findings of IVC agenesis.[4]

We present a rare instance of IVC agenesis and numerous venous abnormalities that manifested as lower extremities DVT.

Case Report

Two days following her initial diagnosis of lower extremity DVT, a 32-year-old female arrived with cough. The patient was first assessed with a direct chest radiogram, which revealed an abnormal convexity at the left superior mediastinum. The mediastinal abnormalities and probable pulmonary thromboembolism (PTE) were then assessed using computed tomography (CT).

The azygos vein appeared hypertrophic on CT imaging, extending the course of the SVC. The hepatic vein was directly emptied into the right atrium. The IVC was agenetic in its suprarenal region, there were two separate right renal veins (RRVs), and there was a circumaortic left renal vein (Ca-LRV) [Figures 1 and 2]. There

How to cite this article: Karavas E, Aydin S, Unver E, Kadirhan O, Kantarci M. Inferior vena cava agenesis, bilateral double renal veins, and left circumaortic renal vein: A rare case and brief review of the literature. J Anat Soc India 2023;72:271-3.

Article Info

Received: 27 March 2022
Accepted: 27 July 2023
Available online: 28 September 2023

Address for correspondence:
Dr. Ozlem Kadirhan, Department of Radiology, Erzincan University, Erzincan, Turkey.
E-mail: ozlemkkadirhan@gmail.com

Access this article online

Website: https://journals.lww.com/joai
DOI: 10.4103/jasi.jasi_50_22
Quick Response Code:

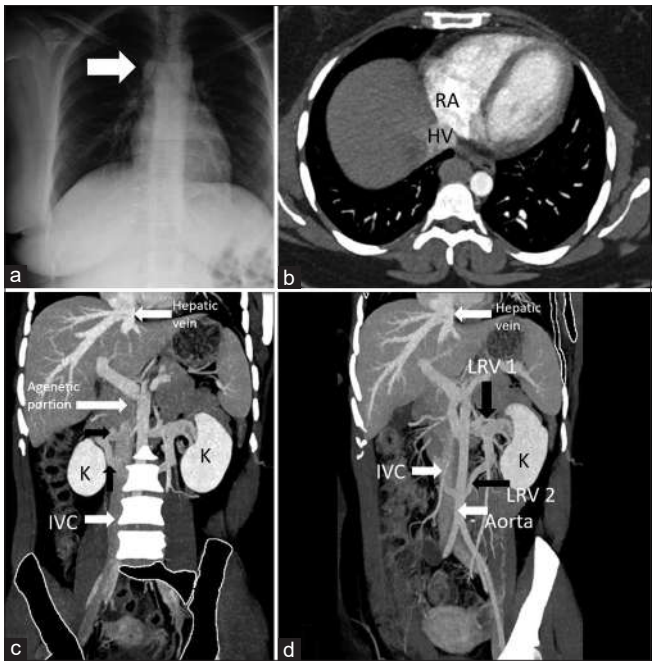

Figure 1: (a) Posteroanterior chest graphy, hypertrophic Azygos vein is seen (arrow). (b) Axial contrast-enhanced CT image, the HV directly empties into the RA. (c) Coronal maximum intensity projection, contrast-enhanced CT image; the IVC is agenetic in its suprarenal region (long arrow) and two separate right renal veins (black arrows) are seen. (d) Coronal maximum intensity projection, contrast-enhanced CT image; the HV is directly emptied into the RA (top white arrow). The IVC (bottom white arrow) is agenetic in its suprarenal region, there is a circumaortic left renal vein (black arrows). CT: Computed tomography, HV: Hepatic vein, RA: Right atrium, IVC: Inferior vena cava, LRV: Left renal vein

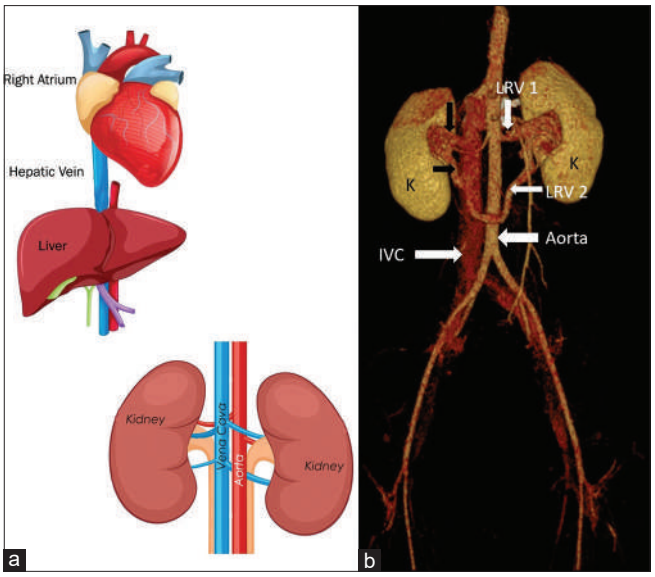

Figure 2: (a) Illustration of the presented anatomic variations. (b) 3D CT image, the IVC is agenetic in its suprarenal region, there are two separate right renal veins (black arrows), and there are two separate left renal veins (LRV1 and 2), one of them passes behind (LRV1), the other one passes ahead (LRV2) of the aorta (circumaortic left renal vein). IVC: Inferior vena cava, LRV: Left renal vein, CT: Computed tomography, 3D: Three-dimensional

was no evidence of PTE, and the patient was diagnosed with atypical viral pneumonia.

Discussion

Normal IVC has four embryological segments: hepatic, suprarenal, renal, and infrarenal. The formation of these segments, which occurs between the 4th and 8th gestational week, is a very sophisticated process that can be disrupted by a variety of circumstances, resulting in a variety of IVC defects. The vitelline vein forms the hepatic section of the IVC. There are three pairs of embryonic veins that play an important role in the development of the vena cava system: posterior cardinal veins, which arise first and then regress, subcardinal veins, and supracardinal veins. During the embryologic phase, this bilateral cardinal venous system supplies the primary venous drainage of the fetus and connects the systemic and pulmonary veins. Following that, the vena cava system develops as anastomoses between cardinal veins form and pulmonary veins connect to the left atrium. The right anterior vein generates the SVC, whereas two segments of the IVC arise from the right supracardinal vein (the infrarenal segment of IVC) and the right subcardinal vein (the suprarenal segment of IVC). The right suprasubcardinal and postsubcardinal anastomoses form the renal portion of the IVC. The postcardinal veins are gradually replaced by the supracardinal and subcardinal veins in the abdominal area, but they remain as the common iliac veins in the pelvis. The azygos and hemiazygos veins grow from the supracardinal veins in the thorax. The right brachiocephalic vein is created by the union of two vessels: the internal jugular vein and the subclavian vein. The abnormal growth of the IVC may result in an increase in intrahepatic and extrahepatic shunts between the systemic and portal veins, which should be surgically rectified.[2,5,6]

Renal vein embryogenesis is part of the complex process of IVC embryogenesis, which involves a large network of anastomoses connecting three pairs of cardinal veins that undergo a regulated process of appearance and regression until the normal IVC and renal veins are created. Anomalies of the IVC and renal veins are caused by a regression error or improper persistence of these embryonic veins. Normal renal veins form in a complicated circulatory environment dominated by the renal collar. This collar is formed ventrally by intersubcardinal anastomoses and tiny sections of the right and left subposterior anastomoses, laterally by anastomoses between supra and subcardinal veins, and dorsally by intersupracardinal anastomoses. Initially, each kidney is linked to the renal collar through a pair of veins with a dorsal and ventral limb. Later, regression of the renal collar's dorsal limb and the posterior branch will give rise to the typical renal vein.[6,7]

Regarding the embryologic mechanism, we believe that the circumaortic course of our patient's RRV could be explained by the persistence of the inter-subcardinal anastomoses, inter-supracardinal anastomoses, and left subsupracardinal anastomoses, as previously stated for a right circumaortic renal vein case.[6]

The vast majority of patients with infrarenal IVC agenesis are asymptomatic. In young male patients, the typical presentation is solitary DVT, particularly at the iliofemoral segment. Approximately 5% of DVT patients under the age of 30 had full or segmental IVC agenesis. The best therapy choice for this illness is now life-long low-molecular-weight heparin, followed by Vitamin K antagonists, however, it should be patient-tailored. Each patient's need for long-term anticoagulant medication should also be assessed.[1,4]

In general, renal vein abnormalities are clinically quiet and are most usually detected as an incidental discovery following routine tests for other reasons or during postmortem. When present, these defects have significant clinical, surgical, and therapeutic implications. Ca-LRV has tremendous clinical value when planning a nephrectomy, especially in this era of renal transplantation that we are currently witnessing. Before planning a retroperitoneal operation, a thorough study and understanding of renal vein anatomy are essential, especially when utilizing a laparoscopic method because the restricted window of vision may make it difficult to detect abnormal vessels. Even while staging for tumor lesions, radiologists should be familiar with such anomalies since aberrant renal veins can be mistaken as lymphadenopathies. The posterior limb of Ca-LRV may be crushed by the aorta in rare cases, resulting in nutcracker syndrome.[2,6,8]

Conclusion

Finally, three major findings should be emphasized. To begin, while anomalies of the IVC and renal veins are exceedingly rare, they should be considered during retroperitoneal procedures to avoid major consequences, particularly venous bleeding caused by incorrect damage. Anatomical variance of the IVC and renal veins is critical for procedures such as ureteral surgery, sympathectomy, radical nephrectomy, and organ transplantation. Second, the clinical significance of these aberrations stems from the possibility of mistakes during imaging. Third, they play a significant role in the diagnosis and treatment of venous thromboembolic disease.

Declaration of patient consent

The authors certify that they have obtained all appropriate patient consent forms. In the form, the patient(s) has/have given his/her/their consent for his/her/their images and other clinical information to be reported in the journal. The patients understand that their names and initials will not be published and due efforts will be made to conceal their identity, but anonymity cannot be guaranteed.

Financial support and sponsorship

Nil.

Conflicts of interest

There are no conflicts of interest.

References

1. Morosetti D, Picchi E, Calcagni A, Lamacchia F, Cavallo AU, Bozzi A, *et al.* Anomalous development of the inferior vena cava: Case reports of agenesis and hypoplasia. Radiol Case Rep 2018;13:895-903.
2. Hoffmann K, Piekarek A, Bieda J, Karmelita-Katulska KS, Gawrysiak D, Bryl W. Absence of the suprarenal segment of the inferior vena cava with a coexisting absence of the right brachiocephalic vein in a 22-year-old Caucasian male with arterial hypertension. Folia Morphol (Warsz) 2015;74:122-6.
3. Lambert M, Marboeuf P, Midulla M, Trillot N, Beregi JP, Mounier-Vehier C, *et al.* Inferior vena cava agenesis and deep vein thrombosis: 10 patients and review of the literature. Vasc Med 2010;15:451-9.
4. Ramos Aranda J, Ramírez Cerda C, Cohen Mussali S, Valdés Flores J. Inferior vena cava agenesis: An unusual cause of deep vein thrombosis and pulmonary embolism in young adult patients. EJVES Short Rep 2018;39:12-5.
5. Prado VE, Rey-Mendoza JP, Wakefield CJ, Aqeel SB, Kumssa A. Infrarenal inferior vena cava agenesis and recurrent deep vein thrombosis: A case report and literature review. Oxf Med Case Reports 2021;2021:omaa104.
6. Tanka M, Tuka F, Abazaj E. Circumaortic right renal vein with multiple vascular anomalies. Radiol Case Rep 2018;13:778-81.
7. Moore K, Persaud TV. The Developing Human: Clinically Orientated Embrylogy. Philadelphia: Saunders Elsevier; 2008.
8. Klimberg I, Wajsman Z. Duplicated inferior vena cava simulating retroperitoneal lymphadenopathy in a patient with embryonal cell carcinoma of the testicle. J Urol 1986;136:678-9.

The Editorial Process

A manuscript will be reviewed for possible publication with the understanding that it is being submitted to Journal of the Anatomical Society of India alone at that point in time and has not been published anywhere, simultaneously submitted, or already accepted for publication elsewhere. The journal expects that authors would authorize one of them to correspond with the Journal for all matters related to the manuscript. All manuscripts received are duly acknowledged. On submission, editors review all submitted manuscripts initially for suitability for formal review. Manuscripts with insufficient originality, serious scientific or technical flaws, or lack of a significant message are rejected before proceeding for formal peer-review. Manuscripts that are unlikely to be of interest to the Journal of the Anatomical Society of India readers are also liable to be rejected at this stage itself.

Manuscripts that are found suitable for publication in Journal of the Anatomical Society of India are sent to two or more expert reviewers. During submission, the contributor is requested to provide names of two or three qualified reviewers who have had experience in the subject of the submitted manuscript, but this is not mandatory. The reviewers should not be affiliated with the same institutes as the contributor/s. However, the selection of these reviewers is at the sole discretion of the editor. The journal follows a double-blind review process, wherein the reviewers and authors are unaware of each other's identity. Every manuscript is also assigned to a member of the editorial team, who based on the comments from the reviewers takes a final decision on the manuscript. The comments and suggestions (acceptance/ rejection/ amendments in manuscript) received from reviewers are conveyed to the corresponding author. If required, the author is requested to provide a point by point response to reviewers' comments and submit a revised version of the manuscript. This process is repeated till reviewers and editors are satisfied with the manuscript.

Manuscripts accepted for publication are copy edited for grammar, punctuation, print style, and format. Page proofs are sent to the corresponding author. The corresponding author is expected to return the corrected proofs within three days. It may not be possible to incorporate corrections received after that period. The whole process of submission of the manuscript to final decision and sending and receiving proofs is completed online. To achieve faster and greater dissemination of knowledge and information, the journal publishes articles online as 'Ahead of Print' immediately on acceptance.

Clinical trial registry

Journal of the Anatomical Society of India favors registration of clinical trials and is a signatory to the Statement on publishing clinical trials in Indian biomedical journals. Journal of the Anatomical Society of India would publish clinical trials that have been registered with a clinical trial registry that allows free online access to public. Registration in the following trial registers is acceptable: http://www.ctri.in/; http://www.actr.org.au/; http://www.clinicaltrials.gov/; http://isrctn.org/; http://www.trialregister.nl/trialreg/index.asp; and http://www.umin.ac.jp/ctr. This is applicable to clinical trials that have begun enrollment of subjects in or after June 2008. Clinical trials that have commenced enrollment of subjects prior to June 2008 would be considered for publication in Journal of the Anatomical Society of India only if they have been registered retrospectively with clinical trial registry that allows unhindered online access to public without charging any fees.

Authorship Criteria

Authorship credit should be based only on substantial contributions to each of the three components mentioned below:

1. Concept and design of study or acquisition of data or analysis and interpretation of data;
2. Drafting the article or revising it critically for important intellectual content; and
3. Final approval of the version to be published.

Participation solely in the acquisition of funding or the collection of data does not justify authorship. General supervision of the research group is not sufficient for authorship. Each contributor should have participated sufficiently in the work to take public responsibility for appropriate portions of the content of the manuscript. The order of naming the contributors should be based on the relative contribution of the contributor towards the study and writing the manuscript. Once submitted the order cannot be changed without written consent of all the contributors. The journal prescribes a maximum number of authors for manuscripts depending upon the type of manuscript, its scope and number of institutions involved (vide infra). The authors should provide a justification, if the number of authors exceeds these limits.

Contribution Details

Contributors should provide a description of contributions made by each of them towards the manuscript. Description should be divided in following categories, as applicable: concept, design, definition of intellectual content, literature search, clinical studies, experimental studies, data acquisition, data analysis, statistical analysis, manuscript preparation, manuscript editing and manuscript review. Authors' contributions will be printed along with the article. One or more author should take responsibility for the integrity of the work as a whole from inception to published article and should be designated as 'guarantor'.

Conflicts of Interest/ Competing Interests

All authors of must disclose any and all conflicts of interest they may have with publication of the manuscript or an institution or product that is mentioned in the manuscript and/or is important to the outcome of the study presented. Authors should also disclose conflict of interest with products that compete with those mentioned in their manuscript.

Submission of Manuscripts

All manuscripts must be submitted on-line through the website https://review.jow.medknow.com/jasi. First time users will have to register at this site. Registration is free but mandatory. Registered authors can keep track of their articles after logging into the site using their user name and password.

- If you experience any problems, please contact the editorial office by e-mail at editor@jasi.org.in

The submitted manuscripts that are not as per the "Instructions to Authors" would be returned to the authors for technical correction, before they undergo editorial/ peer-review. Generally, the manuscript should be submitted in the form of two separate files:

[1] Title Page/First Page File/covering letter:

This file should provide

1. The type of manuscript (original article, case report, review article, Letter to editor, Images, etc.) title of the manuscript, running title, names of all authors/ contributors (with their highest academic degrees, designation and affiliations) and name(s) of department(s) and/ or institution(s) to which the work should be credited, . All information which can reveal your identity should be here. Use text/rtf/doc files. Do not zip the files.
2. The total number of pages, total number of photographs and word counts separately for abstract and for the text (excluding the references, tables and abstract), word counts for introduction + discussion in case of an original article;
3. Source(s) of support in the form of grants, equipment, drugs, or all of these;
4. Acknowledgement, if any. One or more statements should specify 1) contributions that need acknowledging but do not justify authorship, such as general support by a departmental chair; 2) acknowledgments of technical help; and 3) acknowledgments of financial and material support, which should specify the nature of the support. This should be included in the title page of the manuscript and not in the main article file.
5. If the manuscript was presented as part at a meeting, the organization, place, and exact date on which it was read. A full statement to the editor about all submissions and previous reports that might be regarded as redundant publication of the same or very similar work. Any such work should be referred to specifically, and referenced in the new paper. Copies of such material should be included with the submitted paper, to help the editor decide how to handle the matter.
6. Registration number in case of a clinical trial and where it is registered (name of the registry and its URL)
7. Conflicts of Interest of each author/ contributor. A statement of financial or other relationships that might lead to a conflict of interest, if that information is not included in the manuscript itself or in an authors' form
8. Criteria for inclusion in the authors'/ contributors' list
9. A statement that the manuscript has been read and approved by all the authors, that the requirements for authorship as stated earlier in this document have been met, and that each author believes that the manuscript represents honest work, if that information is not provided in another form (see below); and
10. The name, address, e-mail, and telephone number of the corresponding author, who is responsible for communicating with the other authors about revisions and final approval of the proofs, if that information is not included on the manuscript itself.

[2] Blinded Article file: The main text of the article, beginning from Abstract till References (including tables) should be in this file. The file must not contain any mention of the authors' names or initials or the institution at which the study was done or acknowledgements. Page headers/ running title can include the title but not the authors' names. Manuscripts not in compliance with the Journal's blinding policy will be returned to the corresponding author. Use rtf/doc files. Do not zip the files. **Limit the file size to 1 MB.** Do not incorporate images in the file. If file size is large, graphs can be submitted as images separately without incorporating them in the article file to reduce the size of the file. The pages should be numbered consecutively, beginning with the first page of the blinded article file.

[3] Images: Submit good quality color images. **Each image should be less than 2 MB in size.** Size of the image can be reduced by decreasing the actual height and width of the images (keep up to 1600 x 1200 pixels or 5-6 inches). Images can be submitted as jpeg files. Do not zip the files. Legends for the figures/images should be included at the end of the article file.

[4] The contributors' / copyright transfer form (template provided below) has to be submitted in original with the signatures of all the contributors within two weeks of submission via courier, fax or email as a scanned image. Print ready hard copies of the images (one set) or digital images should be sent to the journal office at the time of submitting revised manuscript. High resolution images (up to 5 MB each) can be sent by email.

Contributors' form / copyright transfer form can be submitted online from the authors' area on https://review.jow.medknow.com/jasi.

Preparation of Manuscripts

Manuscripts must be prepared in accordance with "Uniform requirements for Manuscripts submitted to Biomedical Journals" developed by the International Committee of Medical Journal Editors (October 2008). The uniform requirements and specific requirement of Journal of the Anatomical Society of India are summarized below. Before submitting a manuscript, contributors are requested to check for the latest instructions available. Instructions are also available from the website of the journal (www.jasi.org.in) and from the manuscript submission site https://review.jow.medknow.com/jasi.

Journal of the Anatomical Society of India accepts manuscripts written in American English.

Copies of any permission(s)

It is the responsibility of authors/ contributors to obtain permissions for reproducing any copyrighted material. A copy of the permission obtained must accompany the manuscript. Copies of any and all published articles or other manuscripts in preparation or submitted elsewhere that are related to the manuscript must also accompany the manuscript.

Types of Manuscripts

Original articles:

These include randomized controlled trials, intervention studies, studies of screening and diagnostic test, outcome studies, cost effectiveness analyses, case-control series, and surveys with high response rate. The text of original articles amounting to up to 3000 words (excluding Abstract, references and Tables) should be divided into sections with the headings Abstract, Key-words, Introduction, Material and Methods, Results, Discussion and Conclusion, References, Tables and Figure legends.

An abstract should be in a structured format under following heads: **Introduction, Material and Methods, Results,** and **Discussion and Conclusion.**

Introduction: State the purpose and summarize the rationale for the study or observation.

Material and Methods: It should include and describe the following aspects:

Ethics: When reporting studies on human beings, indicate whether the procedures followed were in accordance with the ethical standards of the responsible committee on human experimentation (institutional or regional) and with the Helsinki Declaration of 1975, as revised in 2000 (available at http://www.wma.net/e/policy/17-c_e.html). For prospective studies involving human participants, authors are expected to mention about approval of (regional/ national/ institutional or independent Ethics Committee or Review Board, obtaining informed consent from adult research participants and obtaining assent for children aged over 7 years participating in the trial. The age beyond which assent would be required could vary as per regional and/ or national guidelines. Ensure confidentiality of subjects by desisting from mentioning participants' names, initials or hospital numbers, especially in illustrative material. When reporting experiments on animals, indicate whether the institution's or a national research council's guide for, or any national law on the care and use of laboratory animals was followed. Evidence for approval by a local Ethics Committee (for both human as well as animal studies) must be supplied by the authors on demand. Animal experimental procedures should be as humane as possible and the details of anesthetics and analgesics used should be clearly stated. The ethical standards of experiments must be in accordance with the guidelines provided by the CPCSEA and World Medical Association Declaration of Helsinki on Ethical Principles for Medical Research Involving Humans for studies involving experimental animals and human beings, respectively). The journal will not consider any paper which is ethically unacceptable. A statement on ethics committee permission and ethical practices must be included in all research articles under the 'Materials and Methods' section.

Study design:

Selection and Description of Participants: Describe your selection of the observational or experimental participants (patients or laboratory animals, including controls) clearly, including eligibility and exclusion criteria and a description of the source population. *Technical information*: Identify the methods, apparatus (give the manufacturer›s name and address in parentheses), and procedures in sufficient detail to allow other workers to reproduce the results. Give references to established methods, including statistical methods (see below); provide references and brief descriptions for methods that have been published but are not well known; describe new or substantially modified methods, give reasons for using them, and evaluate their limitations. Identify precisely all drugs and chemicals used, including generic name(s), dose(s), and route(s) of administration.

Reports of randomized clinical trials should present information on all major study elements, including the protocol, assignment of interventions (methods of randomization, concealment of allocation to treatment groups), and the method of masking (blinding), based on the CONSORT Statement (http://www.consort-statement.org).

Reporting Guidelines for Specific Study Designs

Initiative	Type of Study	Source
CONSORT	Randomized controlled trials	http://www.consort-statement.org
STARD	Studies of diagnostic accuracy	http://www.consort-statement.org/stardstatement.htm
QUOROM	Systematic reviews and meta-analyses	http://www.consort- statement.org/Initiatives/MOOSE/moose.pdf statement.org/Initiatives/MOOSE/moose.pdf
STROBE	Observational studies in epidemiology	http://www.strobe-statement.org
MOOSE	Meta-analyses of observational studies in epidemiology	http://www.consort- statement.org/Initiatives/MOOSE/moose.pdf

Statistics: Whenever possible quantify findings and present them with appropriate indicators of measurement error or uncertainty (such as confidence intervals). Authors should report losses to observation (such as, dropouts from a clinical trial). When data are summarized in the Results section, specify the statistical methods used to analyze them. Avoid non-technical uses of technical terms in statistics, such as 'random' (which implies a randomizing device), 'normal', 'significant', 'correlations', and 'sample'. Define statistical terms, abbreviations, and most symbols. Specify the computer software used. Use upper italics (*P* 0.048). For all *P* values include the exact value and not less than 0.05 or 0.001. Mean differences in continuous variables, proportions in categorical variables and relative risks including odds ratios and hazard ratios should be accompanied by their confidence intervals.

Results: Present your results in a logical sequence in the text, tables, and illustrations, giving the main or most important findings first. Do not repeat in the text all the data in the tables or illustrations; emphasize or summarize only important observations. Extra- or supplementary materials and technical detail can be placed in an appendix where it will be accessible but will not interrupt the flow of the text; alternatively, it can be published only in the electronic version of the journal.

When data are summarized in the Results section, give numeric results not only as derivatives (for example, percentages) but also as the absolute numbers from which the derivatives were calculated, and specify the statistical methods used to analyze them. Restrict tables and figures to those needed to explain the argument of the paper and to assess its support. Use graphs as an alternative to tables with many entries; do not duplicate data in graphs and tables. Where scientifically appropriate, analyses of the data by variables such as age and sex should be included.

Discussion: Include summary of *key findings* (primary outcome measures, secondary outcome measures, results as they relate to a prior hypothesis); *Strengths and limitations* of the study (study question, study design, data collection, analysis and interpretation); *Interpretation and implications* in the context of the totality of evidence (is there a systematic review to refer to, if not, could one be reasonably done here and now?, what this study adds to the available evidence, effects on patient care and health policy, possible mechanisms); *Controversies* raised by this study; and *Future research directions* (for this particular research collaboration, underlying mechanisms, clinical research).

Do not repeat in detail data or other material given in the Introduction or the Results section. In particular, contributors should avoid making statements on economic benefits and costs unless their manuscript includes economic data and analyses. Avoid claiming priority and alluding to work that has not been completed. New hypotheses may be stated if needed, however they should be clearly labeled as such. About 30 references can be included. These articles generally should not have more than six authors.

Review Articles:

These are comprehensive review articles on topics related to various fields of Anatomy. The entire manuscript should not exceed 7000 words with no more than 50 references and two authors. Following types of articles can be submitted under this category:

- Newer techniques of dissection and histology
- New methodology in Medical Education
- Review of a current concept

Please note that generally review articles are by invitation only. But unsolicited review articles will be considered for publication on merit basis.

Case reports:

New, interesting and rare cases can be reported. They should be unique, describing a great diagnostic or therapeutic challenge and providing a learning point for the readers. Cases with clinical significance or implications will be given priority. These communications could be of up to 1000 words (excluding Abstract and references) and should have the following headings: Abstract (unstructured), Key-words, Introduction, Case report, Discussion and Conclusion, Reference, Tables and Legends in that order.

The manuscript could be of up to 1000 words (excluding references and abstract) and could be supported with up to 10 references. Case Reports could be authored by up to four authors.

Letter to the Editor:

These should be short and decisive observations. They should preferably be related to articles previously published in the Journal or views expressed in the journal. They should not be preliminary observations that need a later

paper for validation. The letter could have up to 500 words and 5 references. It could be generally authored by not more than four authors.

Book Review: This consists of a critical appraisal of selected books on Anatomy. Potential authors or publishers may submit books, as well as a list of suggested reviewers, to the editorial office. The author/publisher has to pay INR 10,000 per book review.

Other:

Editorial, Guest Editorial, Commentary and Opinion are solicited by the editorial board.

References

References should be *numbered* consecutively in the order in which they are first mentioned in the text (not in alphabetic order). Identify references *in text*, tables, and legends by Arabic numerals in superscript with square bracket after the punctuation *marks. References cited only* in tables or figure legends should be numbered in accordance with the sequence established by the first identification in the text of the particular table or figure. Use the style of the examples below, which are based on the formats used by the NLM *in Index Medicus*. The titles of journals *should be abbreviated* according to the style used in Index Medicus. Use complete name of the journal for non-indexed journals. Avoid using abstracts as references. Information from manuscripts submitted but not accepted should be cited in the text as "unpublished observations" with written permission from the source. Avoid citing a "personal communication" unless it provides essential information not available from a public source, in which case the name of the person and date of communication should be cited in parentheses in the text. The commonly cited types of references are shown here, for other types of references such as newspaper items please refer to ICMJE Guidelines (http://www.icmje.org or http://www.nlm.nih.gov/bsd/uniform_requirements.html).

Articles in Journals

1. Standard journal article (for up to six authors): Parija S C, Ravinder PT, Shariff M. Detection of hydatid antigen in the fluid samples from hydatid cysts by co-agglutination. Trans. R.Soc. Trop. Med. Hyg.1996; 90:255–256.
2. Standard journal article (for more than six authors): List the first six contributors followed by *et al*.

Roddy P, Goiri J, Flevaud L, Palma PP, Morote S, Lima N. *et al*., Field Evaluation of a Rapid Immunochromatographic Assay for Detection of Trypanosoma cruzi Infection by Use of Whole Blood. J. Clin. Microbiol. 2008; 46: 2022-2027.

3. Volume with supplement: Otranto D, Capelli G, Genchi C: Changing distribution patterns of canine vector borne diseases in Italy: leishmaniosis vs. dirofilariosis. Parasites & Vectors 2009; Suppl 1:S2.

Books and Other Monographs

1. Personal author(s): Parija SC. Textbook of Medical Parasitology. 3rd ed. All India Publishers and Distributors. 2008.
2. Editor(s), compiler(s) as author: Garcia LS, Filarial Nematodes In: Garcia LS (editor) Diagnostic Medical Parasitology ASM press Washington DC 2007: pp 319-356.
3. Chapter in a book: Nesheim M C. Ascariasis and human nutrition. In Ascariasis and its prevention and control, D. W. T. Crompton, M. C. Nesbemi, and Z. S. Pawlowski (eds.). Taylor and Francis,London, U.K.1989, pp. 87–100.

Electronic Sources as reference

Journal article on the Internet: Parija SC, Khairnar K. Detection of excretory *Entamoeba histolytica* DNA in the urine, and detection of *E. histolytica* DNA and lectin antigen in the liver abscess pus for the diagnosis of amoebic liver abscess. *BMC Microbiology* 2007, **7**:41. doi:10.1186/1471-2180-7-41. http://www.biomedcentral.com/1471-2180/7/41

Tables

- Tables should be self-explanatory and should not duplicate textual material.
- Tables with more than 10 columns and 25 rows are not acceptable.
- Number tables, in Arabic numerals, consecutively in the order of their first citation in the text and supply a brief title for each.
- Place explanatory matter in footnotes, not in the heading.
- Explain in footnotes all non-standard abbreviations that are used in each table.
- Obtain permission for all fully borrowed, adapted, and modified tables and provide a credit line in the footnote.
- For footnotes use the following symbols, in this sequence: *, †, ‡, §, ‖,¶ , **, ††, ‡‡
- Tables with their legends should be provided at the end of the text after the references. The tables along with their number should be cited at the relevant place in the text

Illustrations (Figures)

- Upload the images in JPEG format. The file size should be within 1024 kb in size while uploading.
- Figures should be numbered consecutively according to the order in which they have been first cited in the text.
- Labels, numbers, and symbols should be clear and of uniform size. The lettering for figures should be large enough to be legible after reduction to fit the width of a printed column.
- Symbols, arrows, or letters used in photomicrographs

should contrast with the background and should be marked neatly with transfer type or by tissue overlay and not by pen.
- Titles and detailed explanations belong in the legends for illustrations not on the illustrations themselves.
- When graphs, scatter-grams or histograms are submitted the numerical data on which they are based should also be supplied.
- The photographs and figures should be trimmed to remove all the unwanted areas.
- If photographs of individuals are used, their pictures must be accompanied by written permission to use the photograph.
- If a figure has been published elsewhere, acknowledge the original source and submit written permission from the copyright holder to reproduce the material. A credit line should appear in the legend for such figures.
- Legends for illustrations: Type or print out legends (maximum 40 words, excluding the credit line) for illustrations using double spacing, with Arabic numerals corresponding to the illustrations. When symbols, arrows, numbers, or letters are used to identify parts of the illustrations, identify and explain each one in the legend. Explain the internal scale (magnification) and identify the method of staining in photomicrographs.
- Final figures for print production: Send sharp, glossy, un-mounted, color photographic prints, with height of 4 inches and width of 6 inches at the time of submitting the revised manuscript. Print outs of digital photographs are not acceptable. If digital images are the only source of images, ensure that the image has minimum resolution of 300 dpi or 1800 x 1600 pixels in TIFF format. Send the images on a CD. Each figure should have a label pasted (avoid use of liquid gum for pasting) on its back indicating the number of the figure, the running title, top of the figure and the legends of the figure. Do not write the contributor/s' name/s. Do not write on the back of figures, scratch, or mark them by using paper clips.
- The Journal reserves the right to crop, rotate, reduce, or enlarge the photographs to an acceptable size.

Protection of Patients' Rights to Privacy

Identifying information should not be published in written descriptions, photographs, sonograms, CT scans, etc., and pedigrees unless the information is essential for scientific purposes and the patient (or parent or guardian, wherever applicable) gives informed consent for publication. Authors should remove patients' names from figures unless they have obtained informed consent from the patients. The journal abides by ICMJE guidelines:

1. Authors, not the journals nor the publisher, need to obtain the patient consent form before the publication and have the form properly archived. The consent forms are not to be uploaded with the cover letter or sent through email to editorial or publisher offices.
2. If the manuscript contains patient images that preclude anonymity, or a description that has obvious indication to the identity of the patient, a statement about obtaining informed patient consent should be indicated in the manuscript.

Sending a revised manuscript

The revised version of the manuscript should be submitted online in a manner similar to that used for submission of the manuscript for the first time. However, there is no need to submit the "First Page" or "Covering Letter" file while submitting a revised version. When submitting a revised manuscript, contributors are requested to include, the 'referees' remarks along with point to point clarification at the beginning in the revised file itself. In addition, they are expected to mark the changes as underlined or colored text in the article.

Reprints and proofs

Journal provides no free printed reprints. Authors can purchase reprints, payment for which should be done at the time of submitting the proofs.

Publication schedule

The journal publishes articles on its website immediately on acceptance and follows a 'continuous publication' schedule. Articles are compiled in issues for 'print on demand' quarterly.

Copyrights

Checklist

Covering letter

- Signed by all contributors
- Previous publication / presentations mentioned
- Source of funding mentioned
- Conflicts of interest disclosed

Authors

- Last name and given name provided along with Middle name initials (where applicable)
- Author for correspondence, with e-mail address provided
- Number of contributors restricted as per the instructions
- Identity not revealed in paper except title page (e.g. name of the institute in Methods, citing previous study as 'our study', names on figure labels, name of institute in photographs, etc.)

Presentation and format

- Double spacing
- Margins 2.5 cm from all four sides
- Page numbers included at bottom
- Title page contains all the desired information
- Running title provided (not more than 50 characters)
- Abstract page contains the full title of the manuscript
- Abstract provided (structured abstract of 250 words for original articles, unstructured abstracts of about 150 words for all other manuscripts excluding letters to the Editor)
- Key words provided (three or more)
- Introduction of 75-100 words
- Headings in title case (not ALL CAPITALS)
- The references cited in the text should be after punctuation marks, in superscript with square bracket.
- References according to the journal's instructions, punctuation marks checked
- Send the article file without 'Track Changes'

Language and grammar

- Uniformly American English
- Write the full term for each abbreviation at its first use in the title, abstract, keywords and text separately unless it is a standard unit of measure. Numerals from 1 to 10 spelt out
- Numerals at the beginning of the sentence spelt out
- Check the manuscript for spelling, grammar and punctuation errors
- If a brand name is cited, supply the manufacturer's name and address (city and state/country).
- Species names should be in italics

Tables and figures

- No repetition of data in tables and graphs and in text
- Actual numbers from which graphs drawn, provided
- Figures necessary and of good quality (colour)
- Table and figure numbers in Arabic letters (not Roman)
- Labels pasted on back of the photographs (no names written)
- Figure legends provided (not more than 40 words)
- Patients' privacy maintained (if not permission taken)
- Credit note for borrowed figures/tables provided
- Write the full term for each abbreviation used in the table as a footnote

Journal of
The Anatomical Society of India

Salient Features:

- Publishes research articles related to all aspects of Anatomy and Allied medical/surgical sciences.
- Pre-Publication Peer Review and Post-Publication Peer Review
- Online Manuscript Submission System
- Selection of articles on the basis of MRS system
- Eminent academicians across the globe as the Editorial board members
- Electronic Table of Contents alerts
- Available in both online and print form.

The journal is registered with the following abstracting partners:
Baidu Scholar, CNKI (China National Knowledge Infrastructure), EBSCO Publishing's Electronic Databases, Ex Libris – Primo Central, Google Scholar, Hinari, Infotrieve, Netherlands ISSN center, ProQuest, TdNet, Wanfang Data

The journal is indexed with, or included in, the following:
SCOPUS, Science Citation Index Expanded, IndMed, MedInd, Scimago Journal Ranking, Emerging Sources Citation Index.

Impact Factor® as reported in the 2022 Journal Citation Reports® (Clarivate Analytics, 2023): 0.4

Editorial Office:
Dr. Vishram Singh, Editor-in-Chief, JASI
B5/3 Hahnemann Enclave, Plot No. 40, Sector 6,
Dwarka Phase – 2, New Delhi - 110 075, India.
Email: editorjasi@gmail.com
(O) | Website: www.asiindia.in

The journal is owned and run by The Anatomical Society of India